DOCTOR OF PHILOSOPHY

The electrocatalytic activity of polycrystalline copper towards the electrochemical reduction of carbon dioxide

Salimon, Jumat

Award date:
2001

Awarding institution:
Bangor University

The Electrocatalytic Activity of Polycrystalline Copper Towards the Electrochemical Reduction of Carbon Dioxide

by

Jumat Salimon
(M.Sc)

A thesis submitted for the degree of

Doctor of Philosophy

Department of Chemistry

University of Wales, Bangor

Submitted February, 2001

Acknowledgements

Acknowledgement is indeed due to the government and the Universiti Kebangsaan of Malaysia whose financial support made this work possible.

I would like to express my grateful thanks to my supervisor, Dr Maher Kalaji, for his help, guidance, encouragement and patience throughout the duration of this work.

I wish to express my deepest gratitude to my lovely wife and children, for their endurance and encouragement during the hard moments and for their love throughout all the years. Thanks for making them easygoing and everything possible.

I would like to thanks the technical and secretarial staff of the Chemistry Department of the University of Wales, Bangor, especially Kevin Spencer, John Charles, John Sambrook, Mike Lewis, Gwenda Vickers and Miss Caroline Naylor.

I am also grateful to all members of the Electrochemistry group in Bangor – those who were (Ricardo, John, Gwion, Arfon, Jason, Sue, Ana) and those who are (Robin, Ben, Eric, Duarte, Dan) - who in different ways contributed and provided a friendly working atmosphere.

Finally, I wish to acknowledge many people in Wales who offered us a warm friendship and hospitality. Thanks to all of you.

Abstract

The catalytic properties of polycrystalline copper toward the electrochemical reduction of carbon dioxide in aqueous hydrogen carbonate and buffered phosphate solution have been studied. It was found that carbon dioxide was reduced at copper in both aqueous solutions under conditions where the copper surface was polarised at high cathodic potential for prolonged time to produce carbon monoxide which adsorbed on copper in linearly and bridged bonded fashions at high negative potentials and at low temperature, 0 °C. At high temperatures, only bridge-bonded CO adsorbed on the copper surface. At low negative potentials, CO interacts with oxidised copper to form copper(I)-carbonyl which exists in both temperatures. The pH of the solution does not seem control the reduction process. Nevertheless, it has a major impact on the chemical nature of the surface and on competing Faradaic reactions. The magnitude of the applied negative potential has a remarkable impact on the quantity and the nature of the reduction products and points to the presence of a competition between the reduction of CO_2 and adsorption of anions.

Carbon monoxide was confirmed as an intermediate in the mechanism of the reduction of CO_2 on polycrystalline copper. This intermediate effectively interacts with metallic Cu inhibiting the hydrogen evolution reaction. It is found that the adsorption of CO is greatly influenced by the existence of pre-adsorbed anions such as hydroxide, phosphate and carbonate on the surface. Both adsorbed CO, linearly and bridged bonded behave differently toward the applied potentials or polarisation potential, duration of the potential polarisation and CO concentration in the solution. Both species are involved in interconversion of the binding sites under such conditions. The studies confirm that linearly bonded CO is weakly adsorbed whereas the bridge bonded CO is strongly adsorbed on the copper surface. Moreover copper(I)-carbonyl exists as a soluble species which is easily removed from the surface.

Impedance studies confirm that the presence of pre-adsorbed anions on the copper surface even at the potential near the hydrogen evolution region, which hampers the reduction of CO_2 or the adsorption of CO. Polarisation of the copper confirms that the adsorption of anions is depressed through the adsorption of CO either in one or in both linearly and bridged types. At more positive potentials the blocking process from the copper oxides is also reduced by the polarisation of the copper surface at high negative potential through the formation of soluble and insoluble copper species. Corrosion and pitting processes in turn exhibit additional problem in the reduction of CO_2.

Table of Contents

CHAPTER III: CO_2 reduction at polycrystalline copper

CHAPTER IV : Adsorption of CO at polycrystalline copper

CHAPTER V: Electrochemical Impedance Spectroscopy of CO_2 Reduction on copper

CHAPTER I

Introduction

1.1 Carbon dioxide as single carbon source

Carbon makes up only 0.087% of the weight of the earth's crust. However, it is the main component of organic life. We live in a world based on carbon, and the product of the decay of organic matter is ultimately carbon dioxide. CO_2 is ubiquitous in nature. Life itself is based on reactions of carbon dioxide. CO_2 is put to good use but also has potentially devastating effects for the human society. Starting with light and ending with carbonated water, many processes produce or use carbon dioxide [1]. CO_2 is used in the inert form in the food and beverage industries (for carbonated beverages, deep freezing, or as a protective gas for sensitive foods), in agriculture (feeding in green-house), in enhanced oil recovery and in extractions with supercritical carbon dioxide and also in used as a reagent in a number of chemical syntheses. Carbon dioxide is potentially the most abundant source for compounds containing a single carbon atom. It forms 0.036% (355 ppmv) of the air's volume [1, 2]. The total amount of carbon present as CO_2, carbonate and hydrogen carbonate in the atmosphere, hydrosphere and lithosphere has been estimated at 10^{16} tons [2]. CO_2 in the atmosphere accounts for 10^{12} tons of carbon while in the hydrosphere and the lithosphere, carbonates and hydrogen carbonates contain about 10^{16} tons of carbon. CO_2 enters the carbon cycle as a major intermediate from the combustion processes of fossil fuels and organic compounds whereas its conversion to biomass occurs *via* photosynthesis. Modern civilisation has led to an increase in CO_2 emission into in the environment, which in turns can affect the world's climate. To reduce the negative impact of an increasing CO_2 concentration in the environment, exploiting an alternative energy form is necessary. Certainly, an artificial method of reducing CO_2 to its non-polluting products is unlikely to function as a major sink of CO_2, however, it may provide a loop to recycle it.

Carbon dioxide is known as a cheap carbon source in the synthetic materials industry. It provides cheap, simple and ubiquitous, if dilute source of carbon, which can be used for producing fuels, chemicals, and other materials. Large scale industrial chemical processes utilising CO_2 as a carbon feedstock are well developed, such as in urea based

synthetic materials (80 Mt/year) using Zn catalysts, which can then be used in making resins, polyurethane and thermosetting materials [2]. CO_2 is used in methanol production (10 Mt/year), which is produced either from synthesis gas ($CO + H_2$) or by the direct reduction of CO_2 using Cu-based catalysts at moderate temperatures and high pressure (250 °C and 80 atm). Synthesis of salicylic acid (25,000 t/year) following Kolbe-Schmitt reaction and synthesis of cyclic carbonates and polycarbonates compounds; are examples of manufacturing materials using CO_2 as a carbon source. From an electrochemical point of view however, the use of CO_2 as a carbon source provides an alternative path for producing small organic molecules with relatively high conversion efficiency. However, direct utilisation of carbon dioxide has some disadvantages. These include the relative inertness of CO_2, relatively low water solubility and low yields and selectivity. To overcome these factors, it is necessary to use better catalysts, increase the solubility of CO_2 and use economical hydrogen sources. CO_2 is thermodynamically stable with a standard formation energy, $\Delta G^{\theta} = -394.4$ kJmol^{-1} whereas carbon monoxide, CO is less stable with $\Delta G^{\theta} = -137$ kJmol^{-1}. The C-O bond strength which represents by bond dissociation energy (D) in CO is the largest with 1076 kJmol^{-1} whereas in CO_2, D is measured at 532 kJmol^{-1} [3]. Despite being a fairly inert gas, CO_2 can undergo a reduction process to produce related products whose distribution depends on the condition of the starting reaction. To activate such an inert gas, a significant amount of energy is required.

Most of the chemical processes involved in utilising CO_2 as a carbon base require some form of activation; either through the provision of an external source of energy or the use of catalysts. Generally these processes are included within one of the following categories [3]:

i. Reduction *via* water gas shift reaction and technologies like the Fischer-Tropsch process.

   $CO_2 + H_2 \leftrightharpoons CO + H_2O \leftrightharpoons$ Methanol, higher alcohol, hydrocarbons, etc.

   Fisher-Tropsch reaction requires a ratio of 1:2 (CO to H_2) to produce CH_3OH.

ii. Carboxylation of active hydrogen compounds; for example, CO_2 reacts with alkynes to produce pyrrones; with 1,3-butadienes and allenes to produce esters and lactones; with methylcyclopropane to produce lactones and with epoxides to produce organic carbonates.

iii. Reactions with phenolates in the Kolbe-Schmitt Reaction.

   $$2C_6H_5OK + CO_2 + H_2 \longrightarrow C_6H_5COOK + C_6H_5OH + KOH$$

iv. The reaction of CO_2 with amines or ammonia to produce carbamates and urea.

$$R_2NH + CO_2 \leftrightharpoons R_2NCOOH$$

$$2NH_3 + CO_2 \leftrightharpoons H_2NCONH_2 + H_2O$$

The development of new catalysts used in CO_2 reduction processes has become a topic of major interest. For example CO has been identified both as an intermediate and as a product during the reduction of CO_2. Therefore, the study and modification of catalysts favouring the production of CO may provide a promising area to begin the research for new CO_2 reduction catalysts. Today there is still a considerable interest in understanding the phenomenon of CO adsorption on metal surfaces and clusters because of its implications on currently used catalytic processes. For example, methanol synthesis has been postulated to occur at copper cationic sites in a Cu/ZnO matrix from CO and H_2O (syn-gas) as starting reactant [4]. However, catalysts used in the synthesis of methanol do not work well for the reduction of CO_2 as they do for CO from syn-gas.

1.2 The chemistry of carbon dioxide

Carbon dioxide is relatively an inert molecule with a linear structure for which its canonical structures can be drawn as follows,

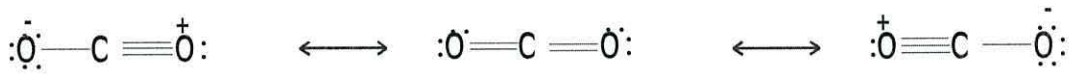

Despite the linear symmetry and overall nonpolar nature of the molecule, it can be activated either through the π-electron system of the double bonds and the lone pairs of electrons on the oxygen atoms, or through the electrophilic carbon atom. Figure 1.1 shows the qualitative molecular orbital energy level diagram of CO_2, which can assist to visualize these predictions. The energy of the lowest unoccupied anti-bonding orbital π_x^* (ca.3.8 eV) indicates a comparatively high electron affinity associated with the central carbon atom [3]. The first ionisation potential is high (13.7 eV); thus, the electrophilicity of the central carbon must be anticipated as the site of predominant reactivity. In interaction with a low oxidation state electron-rich metal centre, it acts as a Lewis acid and the bonding is dominated by electron donation from the metal atom into the anti-bonding π orbital of CO_2.

1.2.1 Dissolution of CO_2 in H_2O

The solubility of carbon dioxide in aqueous solutions is, as expected, lower than that in non-aqueous solutions. Under standard conditions, solubility in water is estimated at

0.033 mol dm^{-3} [5] compared to 0.28 mol dm^{-3} in acetonitrile [6]. Even though CO_2 has a low solubility in water, a rapid equilibrium to its aqueous form occurs, followed by a slow

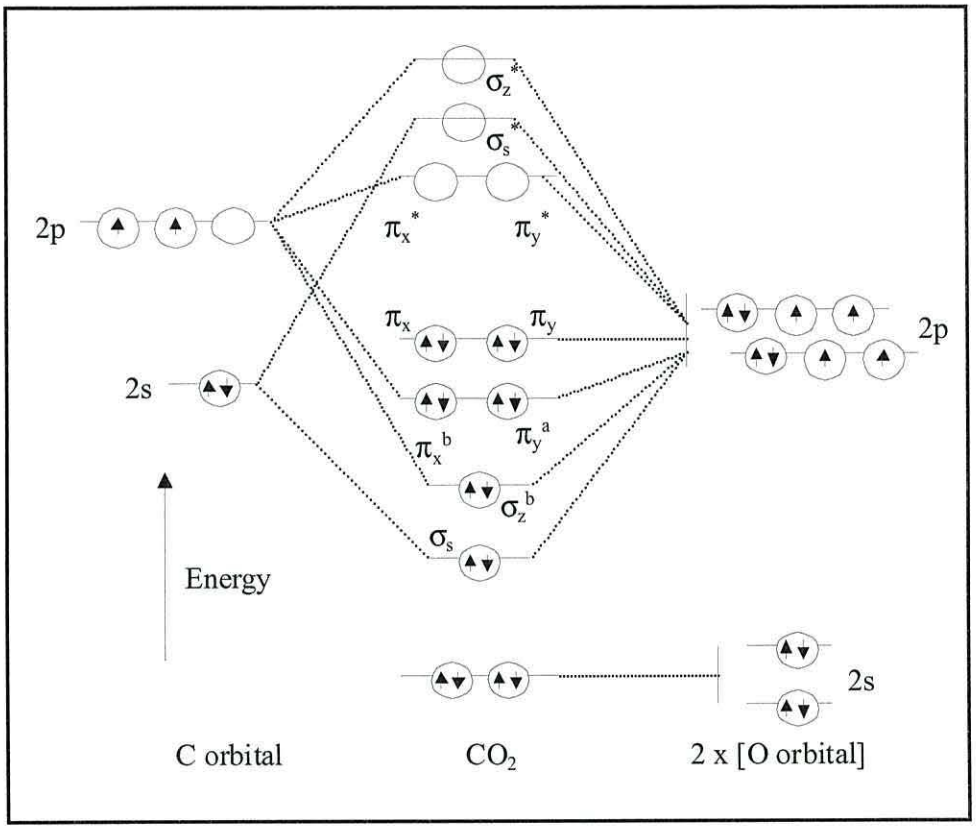

Figure 1.1: Molecular orbital diagram of carbon dioxide [3]

equilibrium between hydrated $CO_{2(aq)}$ and carbonic acid.

$$CO_{2\,(g)} \rightleftharpoons CO_{2\,(aq)} + H_2O \underset{k_2}{\overset{k_1}{\rightleftharpoons}} H_2CO_3 \qquad (K_H)$$

The equilibrium constant, K_H, is 2.6×10^{-3} at 25 ^{0}C [5]. Average values of k_1 and k_2 are 6.2×10^{-2} s^{-1} and 23.7 s^{-1} respectively under the same conditions. The dissociation constant of carbonic acid, K_0, is 1.7×10^{-4} mol dm^{-3} at 25 ^{0}C [7].

$$H_2CO_3 \rightleftharpoons H^+ + HCO_3^- \qquad (K_0)$$

The first dissociation of carbonic acid to produce bicarbonate ions with the "apparent" acid dissociation, K_1 has a value of 4.4×10^{-7} mol dm^{-3}.

$$CO_{2\,(aq)} + H_2O \rightleftharpoons H^+ + HCO_3^- \qquad (K_1)$$

At higher pH, dissolved carbon dioxide may react with hydroxide ions to form bicarbonate ion with a reaction constant, $K_{1'} = 3.3 \times 10^{7}$ mol^{-1} dm^3.

$$CO_{2\,(aq)} + OH^- \rightleftharpoons HCO_3^- \qquad (K_{1'})$$

Carbonic acid is a diprotic acid and the second dissociation constant; K_2 is 4.7×10^{-11} mol dm^{-3} at 25 °C [8].

$$HCO_3^- \rightleftharpoons H^+ + CO_3^{2-} \qquad (K_2)$$

A further equilibrium reaction, which is called carbonate catalysis reaction, may occur in the presence of carbonate in solution,

$$CO_{2\,(aq)} + CO_3^{2-} + H_2O \rightleftharpoons 2HCO_3^-$$

From the above, it is clear that the pH of a carbonic acid solution is a function of CO_2 concentration and *vice versa*. The distribution of the different species involved (as a fraction) in the dissolution of CO_2 in H_2O is shown in Figure 1.2 as function of pH [9]. From the figure it is expected that bicarbonate ions will be the prominent species near neutral pH whereas carbonate ions become prominent at higher pH value.

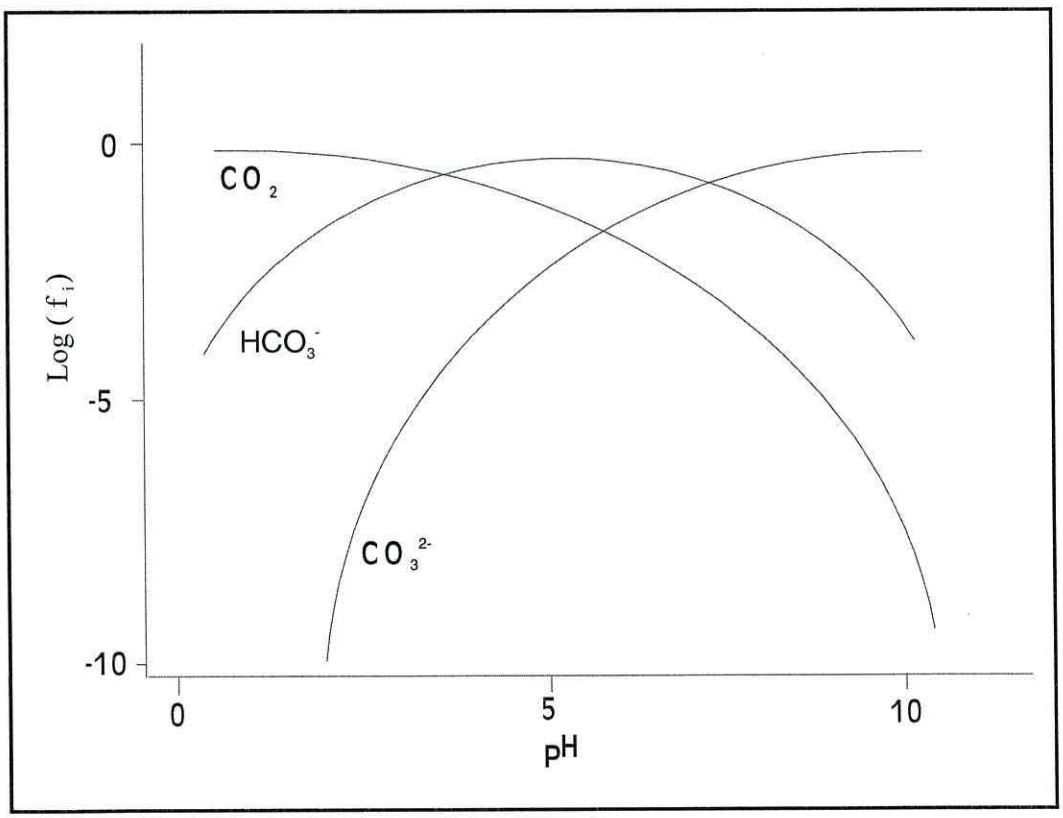

Figure 1.2: Distribution of species involved in CO_2 equilibrium in aqueous solution at 25 °C as a function of pH. f_i is the fraction of a given species present, e.g., $f_{CO2} = [CO_2]/\{[CO_2] + [HCO_3^-] + [CO_3^{2-}]\}$ [9]

1.2.2 Spectroscopic properties of gases and adsorbed carbon dioxide

The gaseous form of CO_2 has at least three fundamental vibrational modes: ν_1, the symmetric C-O stretch at 1340 cm^{-1}, ν_2 the degenerate C-O deformation at 667 cm^{-1} and ν_3 the asymmetric C-O stretch at 2345 cm^{-1} [10]; there are shown in Figure 1.3. CO_2 can undergo a one-electron reduction process to $CO_2^{\cdot -}$ (formate radical ion) and two-electrons reduction to formic acid resulting in a bent CO_2 moiety.

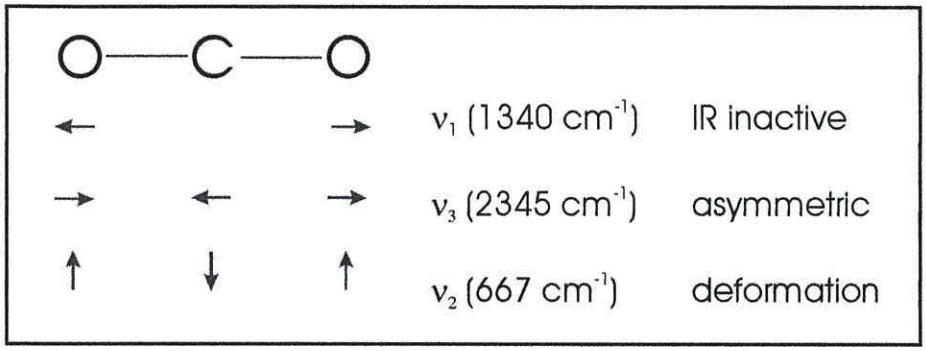

Figure 1.3: Fundamental vibrationals mode of CO_2

It has been known that CO_2 is a comparatively poor electron donor but a good electron acceptor due to vacant orbital of its lower energy [11]. Upon interaction with metals, CO_2 has at least three major potential modes of coordination, which are "side-on" (η^2-CO_2) or bonding through carbon and oxygen through the formation of π–complex *via* the C=O double bond as shown in Figure 1.4. The "end-on" (η^1-OCO) or monodentate coordination occurs *via* the donation the lone *p*-electron pair of oxygen to the vacant orbital of the metal. The "C-coordination" (η^1-CO_2) or "metallo-carboxylate" or "molecular ion" forms by overlap of the filled metal σd orbital with the CO_2 π^* orbital to form the metallo-acid derivative [12].

It is expected that upon excitation of the CO_2 molecule to the lowest excited states, or upon reduction, its configuration would change from linear to bent. Furthermore a distortion of the CO_2 molecule occurs when it is involved in bonding with any ligands or metals to form a coordination complex [13]. This is due to the large outer-space electron transfer barrier and the extremely large inner-shell rearrangements [14, 15]. The differences in structure between linear and bent CO_2 can be understood by plotting the potential energy as a function of C-O bond distance and O-C-O bond angle as suggested by Wambach and Freund [16] as shown in Figure 1.5. The ground energy level

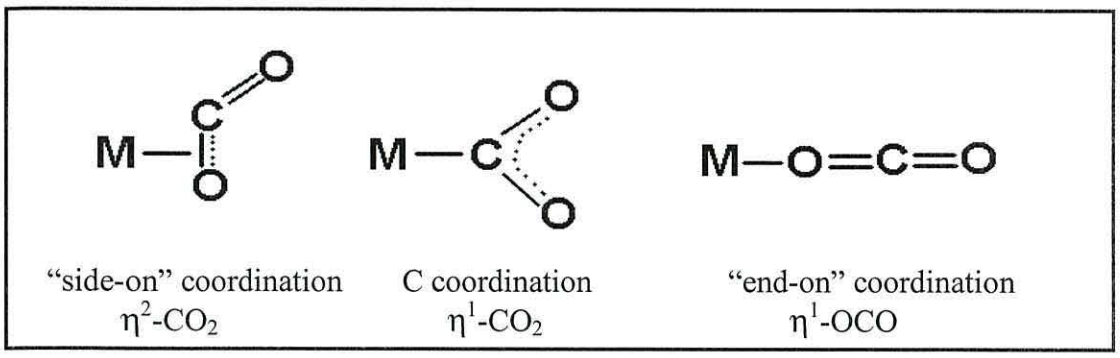

Figure 1.4: Three possible CO_2 coordination modes to metal [16]

is represented by a linear system with an enthalpy of formation of 1598 kJ/mol and double-well ground level of the CO_2^- is represented by a bent geometry with elongated C-O bonds with an enthalpy of formation of 1644 kJ/mol, about 0.5 eV higher than for linear CO_2 [17]. The $CO_2^{\angle}$ molecule in its equilibrium geometry is metastable with a lifetime of 60-90 ms and kinetically stabilised by a barrier of 41.8 kJ/mol (0.41 eV), thus it can be experimentally observed [18].

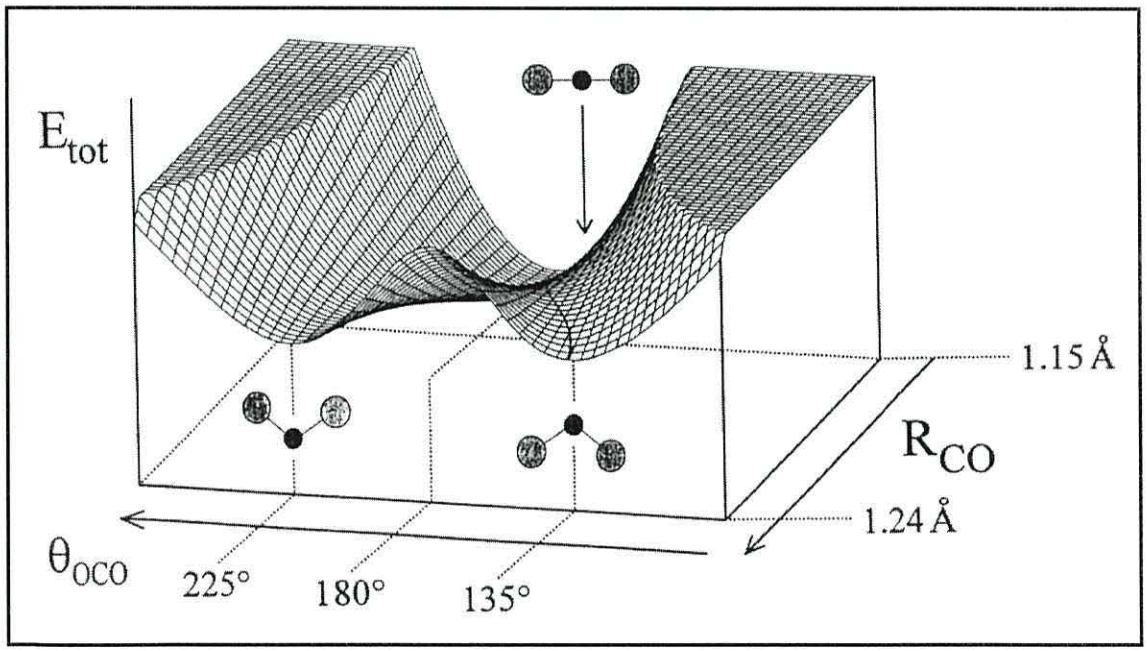

Figure 1.5: Schematic potential energy diagram for CO_2 and CO_2^- [16]

The formation of metal-CO_2 bond has been considered through the Born-Haber cycle [19]. First the ionisation of metal atom, then transfer the detached electron onto a CO_2 molecule and finally bind the CO_2^- anion to the metal cation. However in the case of electrochemically generated CO_2^-, the first step can be excluded. It has been reported that two states of molecular associative adsorption may be observed for CO_2 on the clean single

crystal metal surfaces; a physisorbed linear CO_2 and a bent chemisorbed CO_2 [20]. Moreover it is generally accepted that the electron transfer drives the formation of the chemisorbed bent species but it is not clear where this process happens at the surface. However there are indications that a metal with a low work function in conjunction with appropriate surface sites, such as steps or atomic roughness [21] are important in this respect [22]. However there are surfaces without high step density where CO_2 chemisorption take places [23].

The IR spectroscopy of chemisorbed CO_2 has been reported and the vibrational frequencies were found to depend on the metal used. The symmetric vibrational, ν_s, is in the range of 1130 - 1353 cm^{-1} and the asymmetric vibrational, ν_{as} is between 1530-1630 cm^{-1} at Ni(110), Re(0001), Fe(100), Pt(111) and Pd(110) [24, 25]. It is worth to note that the absence of the asymmetric CO_2 stretching frequency on Ni(110) for instance indicates that the molecular plane is oriented perpendicular to the surface and the symmetry of the species is in C_{2v} [16]. Using HEELS, Wambach and Freund verified and showed that the adsorption of bent CO_2 occurred through oxygen atoms binding toward the metal surfaces and not from carbon atom.

It has been reported that upon the reduction, the asymmetric stretching frequency of CO_2 is reduced from 2345 cm^{-1} [26] to 1670 cm^{-1} [27]. This is due to since the formation of CO_2^- will break one set of double bonds, the force constant for the C-O bond, after resonating the two valence-bond structures is reduced, leading to a reduced stretching frequency. Upon the adsorption of CO_2^- at metal surfaces, a reduction about 100 cm^{-1} in ν_{as} C-O is observed toward 1570 cm^{-1} [27].

It is worth to note that the formation of CO_2 anion upon adsorption on metal surfaces had been proposed very early by Eichen and Pliskin [28] based on the analysis of vibrational spectra. The adsorption of CO_2 at Ni surface for example, will produce two bands depending on the type of bonding involved. They observed a band at 1530 cm^{-1} for Ni-COO and 1390 cm^{-1} for Ni-OCO. Mascetti and Tranquille reported that the coordination complexes of CO_2 with Fe exhibits the bands at 1565 cm^{-1} (ν_{as}COO) and 1210 cm^{-1} (ν_sCOO) for Fe-COO type whereas coordinated with Cu exhibits the bands at 1716 cm^{-1} (νC=O) and 1215 cm^{-1} (νC-O) for Cu-OCO [29]. By comparing the bands position, it is worth to note that the chemisorbed CO_2 bands are close with the bands for carbonate, bicarbonate and carboxylate, which they are attached to the metal surface through monodentate or bidentate coordination. Table 1.1 shows the summary of the approximate

range of the most prominent bands that appear below 1800 cm^{-1} in the spectra of carbonates and carboxylates that arise from the structures shown in Figure 1.6.

Species	Type	Frequency / cm^{-1}				
Carboxylate (CO_2^-)	I	1630-1560 ν_{AS} OCO	1420-1350 ν_S OCO	-	-	-
Carbonate ion	II	1470-1400 ν_{AS} OCO	-	1090-1020 ν C-O*	890-820 δ OCO	750-680 δ OCO
Monodentate carbonate	III	1530-1470 ν_{AS} OCO	1370-1300 ν_S OCO	1080-1040 ν C-O	880-850 δ OCO	820-750 δ OCO
Bidentate carbonate	IVa	1620-1530 ν C=O	1270-1260 ν_{AS} OCO	1030-1020 ν_S OCO	840-830 δ OCO	760-740 δ OCO
Bidentate carbonate	IVb	1670-1620 ν C=O	1270-1220 ν_{AS} OCO	1020-980 ν_S OCO	-	-
Organic carbonate		1870-1750 ν C=O	1280-1250 ν_{AS} OCO	1020-970 ν_S OCO	790-770 δ OCO	-
$NaHCO_3$		1660-1630 ν C=O	1295 ν C-O-H	1000 ν_{AS} OCO	838 δ OCO	698 δ OCO
Hydrogen carbonate		1660-1620 ν_{AS} OCO	1410-1290 ν C-O-H	1050-990 ν_S OCO	840-830 δ OCO	705-698 δ OCO

Table 1.1: IR bands for carbonates and carboxylates showing vibrational frequencies below 1800 cm^{-1} [5, 10, 30]. (*) = IR inactive.

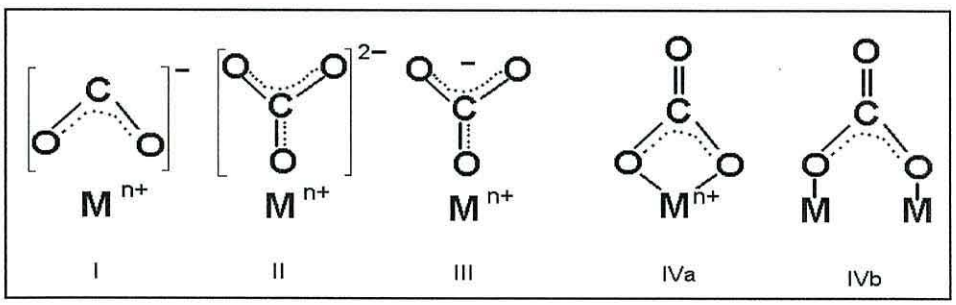

Figure 1.6: The various modes of bonding of carbonate and carboxylate to metal surfaces [30].

1.3 Reduction of carbon dioxide

1.3.1 Thermodynamic consideration

As mentioned previously CO_2 is thermodynamically very stable. Therefore, the conversion of CO_2 to more useful carbon products requires an input of energy, either from the sun, thermal, photoelectric or electric. The difference in Gibbs free energy, which represents the heat evolved or absorbed by the system between the reactants and products, must take into account whether the conversion process will occur spontaneously and to what extent. For a reaction to be spontaneous, either heat has to be evolved from the

system (negative ΔH), or enough entropy has to increase within the system (large positive ΔS) to overcome any heat adsorbed by the system (positive ΔH). Unfortunately, both terms of the Gibbs free energy do not favour the conversion of CO_2 to other products [3]. The ΔH term in Gibbs free energy term can be thought of as an indication of the relative bond strengths of the reactants and products. The two C-O double bonds in the CO_2 molecule are quite stable, and heat must be applied for their dissociation to occur. For example, to reduce CO_2 to CO under standard conditions yields a fairly large ΔH^θ.

$$CO_2 \longrightarrow CO + 1/2O_2\,(g) \qquad \Delta H^\theta = 293 \text{ kJ/mol } CO_2.$$

However if less stable reactants and more stable products are added to the reaction, ΔH is considerably lower.

$$H_2(g) + CO_2\,(g) \longrightarrow CO\,(g) + H_2O\,(g)$$

where $\Delta H^\theta = 51$ kJ/mol CO_2, $-T\Delta S^\theta = -22.6$ kJ/mol CO_2 and $\Delta G^\theta = 28.6$ kJ/mol CO_2. This reaction is known as the reverse water-gas shift reaction, which is slightly more favourable thermodynamically.

1.3.2 Chemical reduction of CO_2

Reactions involving molecular hydrogen are instructive in terms of the thermodynamics of CO_2 reactivity. The free energies for the reduction of gaseous CO_2 by H_2 are shown in Table 1.2. Clearly the thermodynamic stabilities of CO_2 and H_2O molecules are very important when considering the reaction of CO_2 with molecular hydrogen [31]. Thus in the cases where H_2O acts as an oxygen sink, the chance of favourable reactions are higher. However molecular hydrogen is produced industrially by involvement of the water-gas shift reaction, where the CO_2 itself is the ultimate oxygen sink. Other thermodynamic parameters of the reduction of gaseous CO_2 by H_2 have also been tabulated and are shown in the Table 1.2. Therefore the reduction of CO_2 to its reduced forms such as CH_3OH or CH_4 requires external activation energy such as chemical reductants and catalysts.

1.3.3 Electrochemical reduction of CO_2

Instead of using the chemical reductants, CO_2 can be electrochemically converted to methane or other carbon products. The equations for CO_2 conversion by reduction with hydrogen can be expressed as an electrochemical reduction potential by adding the electrochemical half-cell reactions for the reduction of protons to hydrogen [32].

Reaction	ΔG^θ	ΔH^θ	$-T\Delta S^\theta$
$CO_2 + H_2 \rightarrow CO + H_2O$	19.9	-2.8	22.8
$CO_2 + H_2 \rightarrow CO_{(g)} + H_2O_{(g)}$	28.6	51.2	-22.6
$CO_2 + H_2 \rightarrow HCOOH_{(g)}$	48.4		
$CO_2 + H_2 \rightarrow HCOOH_{(l)}$	33	-31.2	64.2
$CO_2 + 2H_2 \rightarrow HCHO_{(g)} + H_2O$	47.2	-9	55
$CO_2 + 3H_2 \rightarrow CH_3OH_{(l)} + H_2O$	-9.2	-131.3	122.1
$2CO_2 + H_2 \rightarrow (COOH)_{2(l)}$	90.9		
$CO_2 + 4H_2 \rightarrow CH_{4(g)} + 2H_2O$	-130.8	-252.9	122.1
$2CO_2 + 6H_2 \rightarrow CH_3OCH_3 + 3H_2O$	-36.8		

Table 1.2: The free energies, enthalpies and entropies (kJ/mol) of the reactions of CO_2 with hydrogen at 298 K [31, 33].

$$H_{2\,(g)} + CO_{2(g)} \rightarrow CO_{(g)} + H_2O_{(g)} \qquad E^\theta = -0.104 \text{ V } vs. \text{ NHE}$$

$$2H^+_{(aq)} + 2e^- \rightarrow H_{2(g)} \qquad E^\theta = 0.000 \text{ V } vs. \text{ NHE}$$

Therefore the overall reaction can be illustrated as:

$$CO_{2\,(g)} + 2H^+_{(aq)} + 2e^- \rightarrow CO_{(g)} + H_2O_{(g)} \qquad E^\theta = -0.104 \text{ V } vs. \text{ NHE}$$

Most of the half-cell reaction potentials for the reduction of CO_2 involve more than one electron for the most common products as shown in Table 1.3. The table shows that with reference to H^+/H_2 potential, the negative potentials represent the voltages required to reduce CO_2 at a cathode if 1 atmosphere of hydrogen is being oxidised at the anode. If water is being oxidised at the anode, an additional -1.229 V must be added to the half-cell potentials to obtain the overall cell potentials [33].

$$H_2O_{(l)} \rightarrow 2H^+_{(aq)} + 1/2O_{2\,(g)} + 2e^- \qquad E^\theta = -1.229 \text{ V}$$

Thus a more realistic estimate of the voltages necessary to convert CO_2 into more reduced carbon products ranges from –1.40 V (for the production of formic acid) to –1.060 V (for the production of methane). However if the first step of the reduction

Reaction	ΔG^θ (kJ/mole)	E^θ (V *vs.* NHE)
$CO_{2(g)} + 2H^+ + 2e^- \rightarrow CO + H_2O$	19.9	-0.104
$2CO_{2\,(g)} + 2H^+ + 2e^- \rightarrow H_2C_2O_4$	91.8	-0.475
$CO_{2\,(g)} + 2H^+ + 2e^- \rightarrow HCOOH$	38.4	-0.199
$CO_{2\,(g)} + 4H^+ + 4e^- \rightarrow HCHO + H_2O$	27.5	-0.071
$CO_{2\,(g)} + 6H^+ + 6e^- \rightarrow CH_3OH + H_2O$	-17.3	0.016
$CO_{2\,(g)} + 8H^+ + 8e^- \rightarrow CH_4 + 2H_2O$	-130.8	0.169

Table 1.3: Thermodynamic values of ΔG^θ and E^θ for half-reaction of the reduction of CO_2 and H^+ to various reduced carbon products in aqueous (25°C) [34]

consists of adding an electron to CO_2 to form a radical anion, the overall reaction requires a more negative potential. In aprotic solvents, for instant, the additional voltage is –1.9 V as in the reaction shown below [32];

$$CO_2 + e^- \rightarrow CO_2^- \qquad E^\theta = -1.9 \text{ V } vs. \text{ NHE}$$

In protic solvents, depending on the electrode used, if the adsorbed H is formed during the reduction process, a more negative potential is required. Therefore to optimise the conversion efficiency of the reduction process, all these initial steps should be avoided. One way of doing this is to create an intermediate with low potential energy by binding CO_2 with an electron rich metal species or complex [33].

Electrochemical reduction at electrodes such as Pt, Ag, Au, Cu, Fe, Ni, Zn, Cd, Hg, Pb or Ru in aqueous electrolytes produces mainly hydrocarbons (CH_4, C_2H_4), as major products, and alcohols (C_2H_5OH, CH_3OH), aldehyde (CH_3CHO, C_2H_5CHO), carboxylic acids, CO and CO_3^{2-} as others products [35]. Hori *et al.* [36] reported that the standard potential for the reduction of CO_2 depends upon the products (*vs.* NHE at pH 7 and 25°C) as shown in Table 1.4.

Product	E^θ / V
CO	-1.52
CH_4	-1.25
C_2H_4	-1.34
$HCOO^-$	-1.43

Table 1.4: The standard reduction potential of CO_2 to various products [36]

The ability of metals used to act as an electron rich source varies significantly due to their different electrochemical properties. Table 1.5 shows the electrode potential used for the CO_2 reduction to produce various products [37]. In general, the electrochemical reduction of CO_2 usually requires a large overvoltage and competes with hydrogen evolution, resulting in low conversion efficiencies. CO_2, however, is actually reduced electrochemically at high negative potentials, -2.0 V (*vs.* SCE). Thus the reaction should be carried out at metal electrodes with high hydrogen overvoltage such as Hg (-1.52 V) and Tl (-1.5 V) *vs.* SCE). However, product selectivity depends on the metal used. Pb, for example, produces $HCOO^-$ with high faradaic efficiency (97.4%) and CH_4 (0.1%) at an electrode potential of about -1.63 V (Table 1.5). Cu electrodes, on the other hand, produce $HCOO^-$ with low faradaic efficiency (9.4%) and high faradaic efficiency for CH_4 (33.3 %) at an electrode potential of about -1.44 V [37, 38].

Electrode	E / V *vs.*NHE	Current density / $mAcm^{-2}$	Faradaic efficiency / %							
			CH_4	C_2H_4	EtOH	PrOH	CO	$HCOO^-$	H_2	Total
Cu	-1.44	5.0	33.3	25.5	5.7	3.0	1.3	9.4	20.5	100
Pd	-1.20	5.0	2.9	-	-	-	28.3	2.8	26.2	60.2
Cd	-1.63	5.0	1.3	-	-	-	13.9	78.4	9.4	100
Ni	-1.48	5.0	1.8	0.1	-	-	0.5	1.4	88.9	92.4
Au	-1.14	5.0	-	-	-	-	87.1	0.7	10.2	98
Ag	-1.37	5.0	-	-	-	-	81.5	0.8	12.4	95
Zn	-1.54	5.0	-	-	-	-	79.4	6.1	9.9	95
Ga	-1.24	5.0	-	-	-	-	23.2	-	79	100
Pb	-1.63	5.0	0.1	-	-	-	-	97.3	5	102.4
Hg	-1.51	5.0	-	-	-	-	-	99.5	-	99.5
Sn	-1.48	5.0	-	-	-	-	7.1	88.4	4.6	100.1
Pt	-1.07	5.0	-	-	-	-	-	0.1	95.7	95.8
Fe	-0.91	5.0	-	-	-	-	-	-	94.8	94.8

Table 1.5: Products distribution for CO_2 electroreduction on various metal electrodes [37]

1.3.4 General mechanism of the electroreduction of CO_2

It has been proposed that CO_2 is initially reduced by an electron transfer process to produce a radical anion and an anion [3]:

$$\underset{\text{linear}}{CO_2} + e^- \rightarrow \underset{\text{bent}}{CO_2^{\cdot -}} \qquad E^\theta = -1.90 \text{ V } vs. \text{ NHE}$$

$$CO_2^{\cdot -} + e^- \leftrightharpoons \underset{\text{bent}}{CO_2^{2-}} \qquad E^\theta = -1.2 \text{ V } vs. \text{ NHE}$$

Upon transfer of an electron, the CO_2 structure changes from linear to bent [39].

Following this initial electron transfer reaction, one of the following competing reactions can take place:

i. Self-coupling of radical anions to form oxalate

$$2\ CO_2^{\cdot -} \rightarrow C_2O_4^{2-}$$

ii. Reaction with water to form formate

$$CO_2^{\cdot -} + H_2O \rightarrow HCO_2^- + OH^\cdot$$

iii. Carbon-oxygen coupling leading to disproportionation leading to carbon monoxide or carbonate:

$$CO_2^{\cdot -} + CO_2 \rightarrow [O{=}^{\cdot}C\text{-}O\text{-}C(O^-){=}O + e^- \rightarrow O{=}^{-}C\text{-}O\text{-}C(O^-){=}O] \rightarrow CO + CO_3^{2-}$$

$$\text{or} \quad OH^\cdot + CO_2^{\cdot -} \rightarrow HCO_3^-$$

During the electrochemical reduction, a CO_2 molecule may undergo multi-electron reduction processes [4] to produce related products depending on the number of electrons involved as was shown in Table 1.3. In general, methane is the highly reduced CO_2 form

from the reduction reaction as shown in the following equation:

$$CO_2 + 8H^+ + 8e^- \rightarrow CH_4 + 2H_2O$$

In non-aqueous solutions the reduction process may terminates in the radical anion ($CO_2^{\cdot -}$), which dimerises to form oxalate, $(CO_2)_2^{2-}$ [40].

1.3.5 Product selectivity and distribution

The electrochemical reduction of CO_2 at transition metal electrodes provides both the means for activating the inert molecule of CO_2, and simultaneously rendering a source of hydrogen. Most electrochemical reductions of CO_2 using metal electrodes indicate that the reduction products depend on [41]:

a) CO_2 solubility

Increasing CO_2 solubility in the electrolyte used for the reduction is important as it increases the surface coverage and the availability of CO_2 to be reduced at the electrode surface. The solubility of CO_2 in widely used solvents for electrochemistry is largely dependent on the type of solvent and temperature. In many cases, the solubility decreases with increasing temperature. For most organic solvents, the solubility is much higher than in aqueous solvents. As a comparison, the solubility of CO_2 in dimethyl sulfoxide and acetonitrile is 4 times higher, in propylene carbonate it is 8 times higher, and in dimethylformamide it is 20 times higher than in water.

b) Solvent

The electrochemical reduction of CO_2 is very solvent dependent. The chemical property of the solvent is important for determining the course and yield of the reaction. In protophilic solvents, such as dimethyl sulfoxide or dimethylformamide, hydrogen evolution will decrease in the course of the competition between CO_2 and H^+ for the electrons. Whereas in protophobic solvents, such as propylene carbonate or acetonitrile, hydrogen evolution during the reaction is more favoured, thus decreasing the products' yields and quantities. In water, the main product is formic acid, in solvents with lower proton availability such as dimethylformamide and dimethyl sulfoxide, oxalic acid and carbon monoxide are formed [37]. The addition of small amounts of water or in the presence of adventitious water in dipolar aprotic solvents will favour the formation of formic acid and promote the further reduction of oxalic acid to glycol acid, $HOCH_2\text{-}CO_2H$. In dimethyl sulfoxide, DMSO, for example both CO and carbonate will be produced [42].

c) Electrode material

Hori *et al.* [43] found that the potential of CO_2 reduction is correlated to the heat of fusion of the metal (Figure 1.7). CO formation takes place at low negative potentials on metal electrodes with high heat of fusion, such as Pt. $HCOO^-$ formation on the other hand takes place at high negative potential on metal electrodes with low heat of fusion, such as Hg. The later groups of metals are clearly separated from the former. The heat of fusion of metals is related to the extent of *d* electron contribution to metallic bond [44], and may be

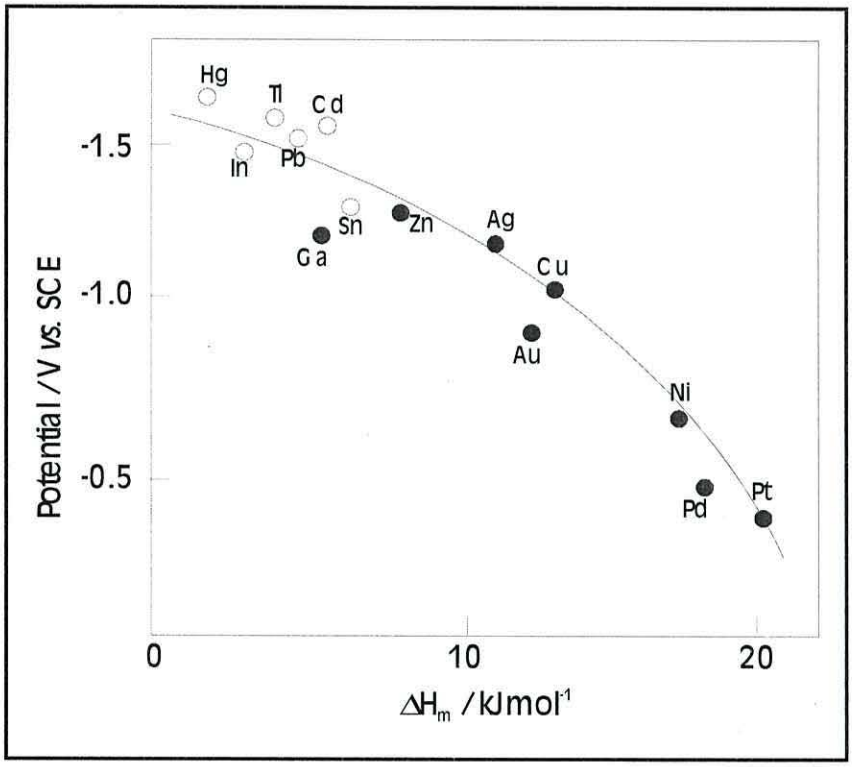

Figure 1.7: The correlation between the potential of CO_2 reduction and the heat of fusion of various metals: ● -CO forming metals; and ○ - $HCOO^-$ forming metals [43]

taken as a measure of *d*-electron availability. The *d*-electron availability effects the back donation of electrons and determines the extent of the stabilization of adsorbed $CO_2^{\cdot -}$. Stabilized $CO_2^{\cdot -}$ will have the extra negative charge on O atoms, which facilitates in reaction with H_2O that may be leading to adsorbed CO formation [36, 43]. Cu, with a heat of fusion of about 13.5 $kJmol^{-1}$, is found to have the ability to form CO in the CO_2 reduction with medium negative potential of about –1.0 V.

Pre-treatment in the early stages of the electrode preparation is crucial, and this influences the distribution of the products. Cleaning the copper electrode with HCl for example results in better conversion of methane yield than cleaning with HNO_3 [43].

d). Supporting electrolyte

The choice of supporting electrolyte influences both the solubility and the mechanism of the carbon dioxide reduction. Even though the solubility of CO_2 depends on the polarity of the solvent and the temperature, the exact mechanism of CO_2 dissolution is not fully understood. The effect of solutes on the solubility of CO_2 is well known, but their effect as catalysts is not known. Nevertheless, Taguchi *et al.* [45] have shown that ammonium ions have a catalytic effect on the reduction of CO_2 at semiconductor electrodes. It was also shown that alkali carbonates favoured the formation of formate and also tetraethylammonium perchlorate suppressed H_2 evolution better than tetraalkyl-ammonium perchlorate and alkali carbonates, phosphates or sulphates. Moreover, electrolyte composition has been found to exhibit a strong effect on the product distribution as shown in Table 1.6. Hydrogen containing anions such as HCO_3^- and HPO_4^{2-}, led to lower C_2 and C_3 yields due to hydrogen availability in the solution. Hori *et al.* [43] suggested that this could be a consequence of the hydrogen evolution reaction.

Electrolyte	pH	C_2H_4	C_2H_5OH	C_3H_7OH	H_2
KCl	5.9	47.8	21.9	36.6	3.9
$KClO_4$	5.9	48.1	15.5	4.2	6.7
K_2SO_4	5.8	46	18.2	4	8.7
$KHCO_3$	6.8	30.1	6.9	3	10.9
K_2HPO_4	6.5	1.8	0.7	Traces	72.4

Table 1.6: Effect of the electrolyte composition on the product distribution [46]

The correlation of the potential of CO_2 reduction and hydrogen evolution is shown in Figure 1.8. The good correlation shown in Figure 1.8 might be due to one of two possibilities. Firstly, adsorbed hydrogen atoms initially formed at the electrode surface are involved in CO_2 reduction to CO. However if the M-H bond strength of adsorbed hydrogen is stabilised to a medium extent, it will show high electrocatalytic activity of hydrogen evolution. The magnitude of M-H bond may depend upon the availability of electrons in the metal, which is closely connected with the back donation of *d* electrons. Another possibility is that the fashion of interaction of $CO_2^{\cdot-}$ to the electrode surface is similar to that of hydrogen atom. The good correlation in Figure 1.8 might suggest a probable similarity in chemical bonds of both intermediate species at metal surfaces.

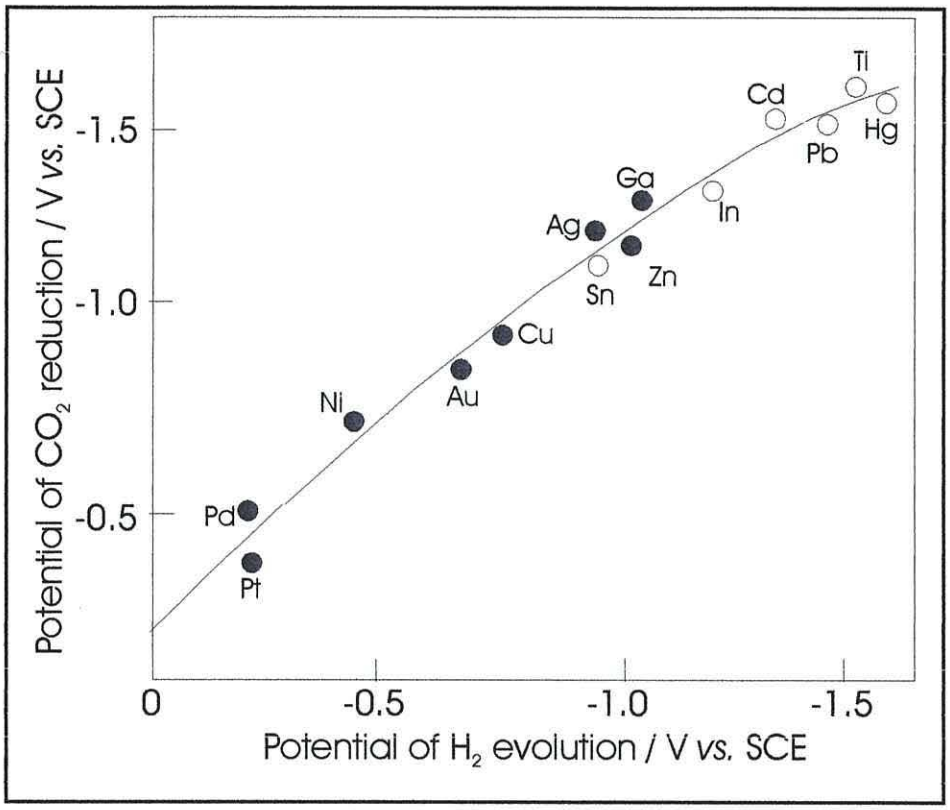

Figure 1.8: Correlation between the potential of CO_2 reduction and that of H_2 evolution: ●- CO forming metals, and ○- $HCOO^-$ forming metals [43].

e) pH

Electrochemical reduction of CO_2 to CH_4 can occur at pH values as high as 9.1 with modest rates and faradaic efficiencies [43]. This might indicate that direct reduction of CO_2 occurs even at alkaline pH as a significant partial pressure of CO_2 is present. However, CH_4 can be formed at pH values below 1. Thus the rate of CH_4 formation does depend on pH. In the pH region 9 to 3, the rate increases. This effect is rationalised as occurring either because of an increase in surface hydride coverage will increase the rate of hydrogenation of CO_2 reduction intermediates, or an increase rate of oxygen removal from the surface, which favours the oxygenation of CO_2 or other intermediates. The increase could also be related to the increasing fraction of soluble carbon in the electrochemical active CO_2 forms such as $CO_{2(aq)}$.

f) Temperature

Hori *et al.* [46] reported that the distribution of electrochemical reduction products at Cu surfaces is temperature dependent. They found that the faradaic efficiency for the formation of CH_4 at 0 °C was about 65% but drops significantly with temperature, whereas

for C_2H_4, the faradaic efficiency rose slowly with temperature as shown in Figure 1.9. Therefore depending on the product desired the electrolyte solution temperature could be programmed either to increase or to decrease the less preferred products.

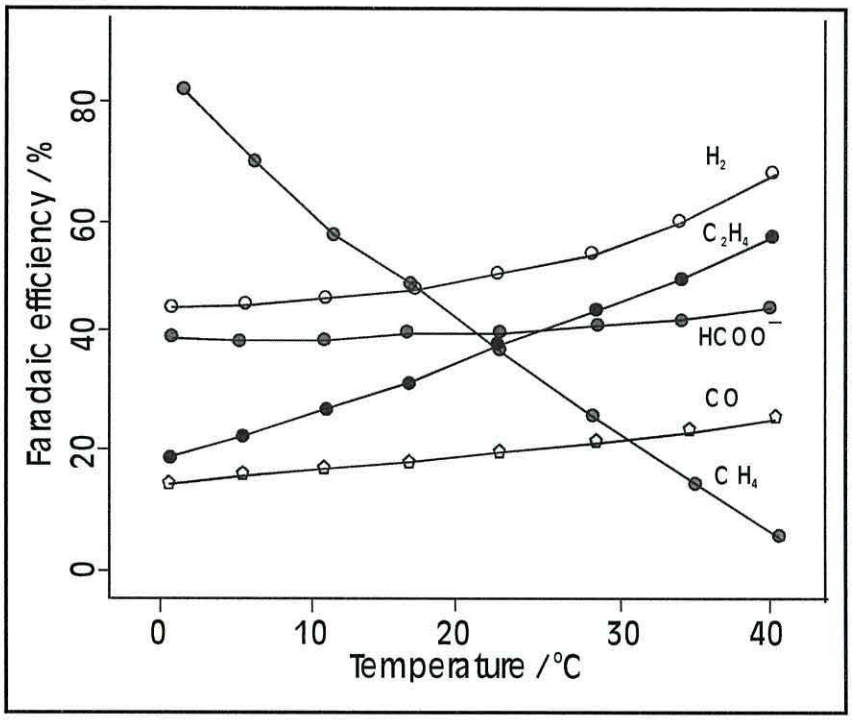

Figure 1.9: Dependence of product distribution on temperature during the electrochemical reduction of CO_2 in aqueous solution [43].

However at Ru, an exceptional is due where the effect of temperature on the rate of CH_4 formation is manifested by the reduction of the faradaic efficiencies if the reduction was carried out at a temperature greater than 80 °C, but no reduction occurs if the electrode is used at 60 °C [47]. This is due to high activation energy change for the competing hydrogen evolution in Ru.

1.4 CO_2 activation on transition metal catalyst

Transition metals are often used in CO_2 reduction reactions although the rôle of the metal in the promotion of the reactivity of CO_2 is not always understood. Undoubtedly the production of carbon monoxide (especially in association with water reduction to molecular hydrogen) is a desirable aim, since the technology of the utilisation of "synthesis gas" is well established. However, direct conversion of CO_2 to more highly reduced products is tantalising, not only from the point of view of the utility of the resultant products but also because the thermodynamics of such reactions are increasingly favourable [3].

The presence of transition metal species substantially reduces the potential associated with the electrochemical reduction of carbon dioxide, to an extent dependent on the electrocatalyst, electrode and solvent used. The mediation by transition metal centres of the chemical or electrochemical reduction of CO_2 has been extensively reviewed and has been discussed in term of [41, 48]:

a. Reaction of CO_2 with oxophilic centres, where the conversion of CO_2 to CO is achieved by transfer of the oxygen atom to a metal centre, or to an associated ligand, which has a high oxygen affinity, e.g., a phosphine.
b. Activation of CO_2 by direct coordination to the metal centre, or
c. Activation of reagents that may react with CO_2.

The latter two are clearly more general in their scope and applicability to carbon dioxide activation.

One of the possible means of activation of carbon dioxide is by modification of the properties of the CO_2 molecules by direct coordination to a metal centre. As mentioned earlier, Ito and Yamamoto [49] reported that CO_2 attaches to a metal centre *via* "end on", "side on" to C-O bond and *via* the central carbon atom of coordination bond as well as a number of less favourable modes. From molecular orbital calculation of the relative stability of these legating, Sasaki *et al.* [50] have concluded that there were two predominant interactions of π back-donation which stabilise the "side-on" coordination mode (which is generally the most favourable), and electrostatic interaction or σ-donation, which favours the "end-on" coordination and will be favoured when the metal centre is positively charged. C coordination on the other hand, is generally less favourable than side-on bonding, and would only be expected when the latter is inhibited by some effects as coordination numbers.

Much of the interest in the involvement of metals in the reactivity of carbon dioxide has been in the so-called "insertion" reaction of the general form shown below [3];

$$\text{M-L} + CO_2 \longrightarrow \text{M-O-C(O)-L}$$

$$\text{M-L} + CO_2 \longrightarrow \text{M[(O)(O)C]-L}$$

$$\text{M-L} + CO_2 \longrightarrow \text{M-C(O)-OL}$$

Where

L = H, giving rise to coordinated formated or hydroxycarbonyl ion

L = a ligand with a C ligating atom, giving rise to a carboxylated product

L = a ligand with a N ligating atom, giving rise to a carbamated product and

L = a ligand with an O ligating atom, giving rise to a carbonated product.

Since there is a lone pair of electrons on each oxygen atom of CO_2 whilst the central carbon atom is relatively electron deficient, it would be expected that a positive metal atom (or M-L bond polarised in that manner), might prefer insertion to give O-bound products. The former case would be regarded as the more likely possibility and is often referred to as the "normal" insertion mode. Therefore, it is clear that the means by which metal complexes may mediate in the CO_2 to CO conversion may arise primarily from two paths [3]:

i. Activation of CO_2 by coordination to a metal centre, including promotion of reductive disproportionation:

$$2CO_2 + 2e^- \longrightarrow CO + CO_3^{2-}$$

ii. Insertion of CO_2 into a metal-hydride bond, with subsequent formation and decomposition of a formate or hydroxycarbonyl (carboxylate) transient species.

$$\begin{array}{ccccc} CO_2 + M\text{-}H & \longrightarrow & [M\text{-}O\text{-}C(O)\text{-}H] & \longrightarrow & CO + M\text{-}OH \\ & \searrow & & \nearrow & \\ & & [M\text{-}C(O)\text{-}OH] & & \end{array}$$

The use of metal electrocatalysts in CO_2 electrochemical reduction with high current density (> 100 mA/cm^2) is required for commercial processes [3]. Therefore to improve the specific current density of the electrodes used, the kinetics of the reaction process especially in the rate limiting step reaction such as the adsorption of the CO_2 or other intermediates at the surface and the CO_2 mass transfer to the electrode must be examined. The adsorption of the species at the electrode surface is dependent on the potential of zero charge (pzc) of the various cathode materials [51]. The potential where the surface changes from being positively to negatively charge, the pzc value determines the net charge on the cathode at various applied potentials. The net charge on the electrode in turn determines the adsorption of CO_2 and reduces intermediates. In general, on a cathode surface at negative potentials one can expect that an inner Helmholtz layer of positive ions. At some applied potential the pzc is reached where the charge density of cations and ions absorbed on the surface of the metal is equal. At the pzc (–0.54 V for Cu) it is plausible to consider the surface to be electrically neutral. The pzc can therefore be used as a reference potential to determine whether an anion intermediate is adsorbed on the surface. If anion intermediates are important in the CO_2 reduction, the metal electrode with most negative pzc is preferred. Otherwise, the pzc will be exceeded under bias potential and the surface will take on a net negative charge, which will repulse the anion intermediates from the surface and reduce the reaction rate. If the current efficiency is decreased with higher current density, a more negative bias potential is needed. As the pzc is exceeded, CO_2 or

radical anions intermediates adsorption is decreased therefore favouring hydrogen evolution. Ito and Yamamoto examined the rate of formic acid formation for a variety of metals as a function of current density and found that for most metals the reaction rate decreased with higher current density [49]; whereas Frese examined the current density dependence of methane formation on copper where the rate did decrease with increasing current density [40].

1.5 Electrochemical reduction of CO_2 at metallic electrodes

Adsorbed formate has been reported appears as an intermediate species for CO_2 reduction in aqueous solution. In general it has been suggested that at least three options for the initial CO_2 electrochemical reduction step at electrocatalyst sites in aqueous solution involving adsorbed formate [52-54]. These options are as follow:

i. Initial adsorption of CO_2 onto the surface followed by electron transfer and reaction with H_2O as follow:

$$CO_2 \rightarrow CO_{2ads}$$

$$CO_{2\,ads} + e^- \rightarrow CO_2^-{}_{ads}$$

$$CO_2^-{}_{ads} + H_2O \rightarrow COOH_{ads} + OH^-$$

ii Electron transfer to CO_2 present in the electrode / electrolyte double layer region followed by the adsorption onto the electrocatalyst surface and subsequent reaction with water as follow:

$$CO_2 + e^- \rightarrow CO_2^-$$

$$CO_2^- \rightarrow CO_2^-{}_{ads}$$

$$CO_2^-{}_{ads} + H_2O \rightarrow COOH_{ads}$$

iii. Electron transfer to CO_2 in the electrode/electrolyte double layer region followed by reaction of CO_2^- with H_2O and adsorption of the resulting neutral radical onto the electrode surface as follow:

$$CO_2 + e^- \rightarrow CO_2^-$$

$$CO_2^- + H_2O \rightarrow COOH + OH^-$$

$$COOH \rightarrow COOH_{ads}$$

Ryu *et al.* [55] discussed in detail the reduction of CO_2 at mercury based on the analysis of polarisation curves obtained in aqueous solution. They proposed CO_2 is first adsorbed on the electrode before another electron transfer to adsorbed formate occurred. They suggested that this step is the rate determination step of the reaction which occur as follow:

$$CO_2 + e^- \rightarrow CO_2^-{}_{ads} \text{ (slow)}$$

$$CO_2^-{}_{ads} + H_2O \rightarrow HCO_{2ads} + OH^-$$

$$HCO_{2ads} + e^- \rightarrow HCO_2^- \text{ (slow)}$$

The overall reaction was

$$CO_2 + H_2O + 2e^- \rightarrow HCO_2^- + OH^-$$

Kudo *et al.* [56] studied the high-pressure CO_2 electroreduction on high purity Ni cathodes in $KHCO_3$ supporting electrolyte. They found that the increase of CO_2 pressure favoured the CO_2 reduction to hydrocarbon and diminished the hydrogen evolution. A possible scenario of the hydrocarbon formation at Ni surface may involve the following steps:

$$CO_2 + e^- + H_2 \rightarrow CO_{ads} + H_2O$$

$$H_2O + e^- \rightarrow H_{ads} + OH^-$$

$$CO_{ads} + 4H_{ads} \rightarrow (=CH_2)_{ads} + H_2O$$

$$(=CH_2)_{ads} \rightarrow \text{Hydrocarbons}$$

Hori *et al.* [57] used *in situ* IR spectroscopy to observe adsorbed CO at Ni electrode. Both linear and bridged adsorbed CO molecules were detected. The linear CO disappeared at -0.8 V *vs.* NHE and since the reduction of adsorbed CO proceeded at cathode potentials less then -1.0 V *vs.* NHE, the bridged type CO was presumed to be the electroactive species. Ni cathodes had favourable electrocatalytic properties for C_1 - C_4 paraffin formation (CH_4, C_2H_6, C_3H_8, *n*- and *i*-butane) and by contrast, Cu cathodes selectively produced CH_4 and C_2H_4.

1.6 Electrochemical reduction of CO_2 at copper electrode

A turning point in the use of metallic electrodes occurred with the introduction of Cu or Cu-coated electrodes for the reduction of CO_2 to hydrocarbons especially to methane. Hori and co-workers reported the use of Cu electrodes for the reduction of CO_2 to hydrocarbons in aqueous media at low temperatures with high current densities [46, 52, 53]. Since then, Cu has been extensively used for the electrochemical reduction of CO_2 due to its catalytic properties with high faradaic efficiency for the production of hydrocarbons. It is known that Cu supported on ZnO and Al_2O_3 catalyses the reduction of gaseous CO_2 by hydrogen to methanol. It is also well known that partially oxidised metallic Cu reacts with CO_2 to produce copper carbonates. Copper compounds have also been widely used as adsorbents for CO in classical methods of gas analysis; although the stability of such complex is quite low and can easily decompose to produce CO.

Beside methane, the formation of ethylene and alcohol was observed at ambient temperature and pressure. Faradaic efficiencies were high for the formation of such hydrocarbons and alcohols. Products observed were CH_4 (17%), C_2H_4 (38%), C_2H_5OH (22%), n-C_3H_7OH (4%), CO (3%), and $HCOO^-$ (10%) [51, 58]. CO is electrochemically reduced to give a similar distribution of products and thus it is expected that the reduction of carbon dioxide *via* CO will proceed with the same reaction pathway as that CO. Several mechanisms have been proposed for such a reaction to produce hydrocarbons, which involve CO_{ads} as an important intermediate. Hori and Murata [59] proposed that the molecular reaction pathway for the formation of hydrocarbons and alcohols from CO involves the formation of surface carbon. The elementary step of surface carbon formation is the decomposition of CO_{ads} to C atom and O^- ion when an electron is transferred to the CO_{ads} at the electrode surface, suggesting that the reduction of CO to $=CH_2$ occurs in the adsorbed state as illustrated by the general reaction as follows:

$$CO_{ads} + H_2O \xrightarrow{e^-} C_{ads} + OH_{ads} + OH^-_{aq} \rightarrow \rightarrow CH_{2(ads)} \rightarrow \rightarrow CH_4, C_2H_4$$

This reaction can be expanded in the proposed schematic pathway as shown in Figure 1.10. The scheme shows that the formation of CH_4 and C_2H_4 are separated at an early stage of CO reduction, where the insertion of CO to $CH_{2(ads)}$, will produce CH_2-CO_{ads}. This intermediate plays a major role in the production of C_2H_4, either *via* a hydrogenation or dimerisation process.

Wasmus *et al.* [60] and Aurian *et al.* [61], proposed that the reaction steps occur *via* a Cu-carbene to form CH_4 and C_2H_4 as follow:

$$CO_2 \rightarrow \rightarrow (CO_2^-)_{ads} \rightarrow \rightarrow Cu{=}CH_2 \rightarrow \rightarrow CH_4, C_2H_4$$

CO_2 is adsorbed on the electrode surface by a nucleophilic attack on the partially positive C atom. This so-called molecular ion undergoes further reduction steps to form a carbene-like compound where the *d*-orbital of the Cu surface forms a bond with two *p*-orbital of each carbon atom. This carbene is either further protonated to form a methane molecule or recombines with another carbene to ethylene. Friebe *et al.* [62] proposed the reaction pathway scheme of the electrochemical CO_2 reduction at Cu as follow:

$$CO_2 \xrightarrow{e^-} \rightarrow (CO_2^-)_{ads} \xrightarrow{e^-, H^+, -H_2O} Cu{=}CH_2 \xrightarrow{e^-, H^+} CH_4, C_2H_4$$

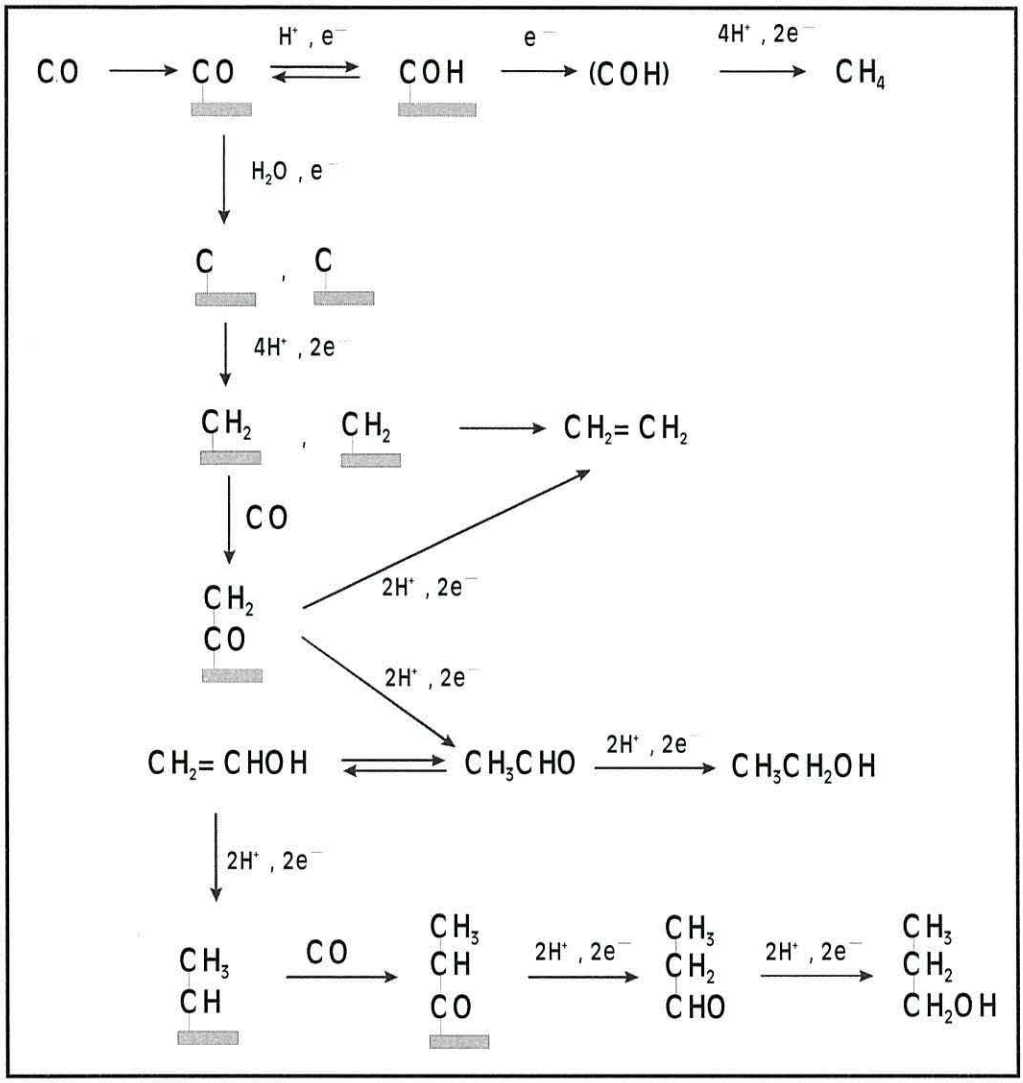

Figure 1.10: Schematic pathways of the reduction of CO. CO is adsorbed CO on metal surface [60].

Numerous reaction mechanisms were suggested for the electrochemical reduction of CO_2 in aqueous media to produce formic acid. Most of these mechanisms accept the steps shown in Figure 1.11. Jitaru *et al.* [35] proposed that the CO_2 reduction mechanism on *sp* group metals (including Cu) in aqueous solutions leading to the formation of formate ions occurs as followed. Initially the neutral hydrated CO_2 molecule (a) undergoes reduction to yield in adsorbed $CO_2^{\cdot-}$ radicals. The latter reacts with an adsorbed water molecule to form adsorbed $HCO_2^{\cdot}$ radical and OH^- ions (b). $HCO_2^{\cdot}$ radical remains adsorbed at the electrode surface and undergo further reduction to formate ions (c). Finally the negatively charged $HCOO^-$ ions diffuse away from the electrode surface (d).

In alkaline aqueous media, CO_2 adsorbed on the electrode surface (Au, Ag, Cu, Zn) is suggested [61] as the first step to occur after the electron transfer process and then

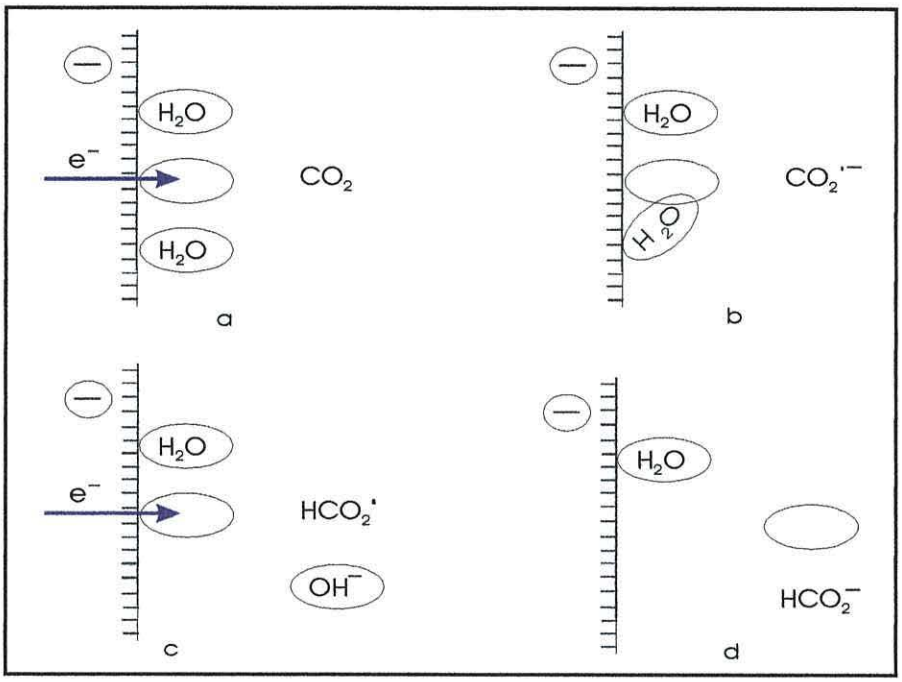

Figure 1.11: Schematic representation of the formation of formate during CO_2 reduction in aqueous solutions [35]

the production of CO_{ads} as shown in Figure 1.12:

DeWulf *et al.* [63] studied the electrolysis of possible intermediates (CO, formic acid, formaldehyde and methanol) that might be formed in the electroreduction of CO_2.

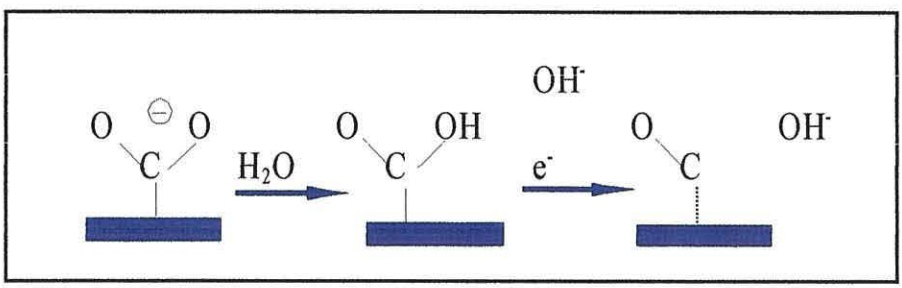

Figure 1.12: Schematic diagram for the formation of $CO_{2(ads)}$ and CO_{ads} [61]

The authors proposed that the formation of formic acid/formate would lead to the electrode-poisoning route in which graphite serves as the poisoning species. However CO and formaldehyde did not show any black deposit at the electrode surface. The authors proposed the reaction scheme shown in Figure 1.13. A year latter Wasmus *et al.* [60] proposed an additional pathway and reaction (in dotted line) in the below reaction scheme.

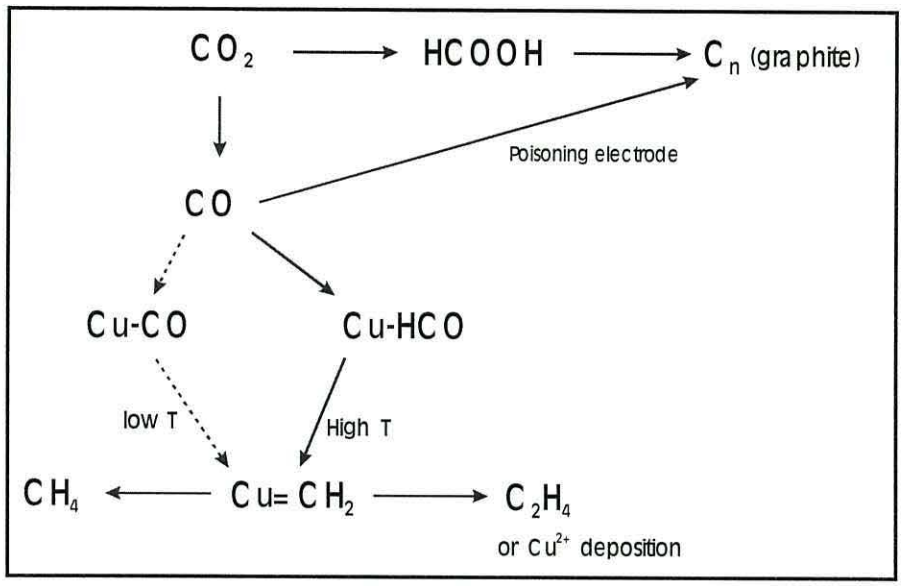

Figure 1.13: Reaction scheme that leading to the formation of poison species [60, 63]

1.7 CO as CO_2 electrochemical reduction product

At this stage it is important to highlight the importance of CO as an intermediate in the complex process. Carbon monoxide has been recognised as a product of electrochemical reduction of carbon dioxide on several metal cathodes, especially on copper. The adsorption of CO onto copper surfaces and onto copper supported on alumina or silica, using spectroscopic and thermodesorption techniques has been largely investigated. The results showed that CO could be adsorbed onto copper in a very complex manner, giving at least three vibrational bands: 2120, 2100 and 2070 cm^{-1} [64]. The resolution of these bands is only possible at low temperatures. At higher temperatures these bands are broadened and overlap, so that only a simple band is observed. Hollins and Pritchard [65] discussed in detail the adsorption of CO on polycrystalline and single crystal copper electrode surfaces. They showed a band in the infrared spectrum of CO on an evaporated Cu film in the range 2102 - 2107 cm^{-1}. On the other hand, low index crystal surfaces give bands as low as 2076 cm^{-1} for Cu (111) and 2080 cm^{-1} for Cu (100) and for high index surfaces [(110), (311), (211), (755)] the adsorption give bands in the range 2096 – 2110 cm^{-1}. According to their results, polycrystalline copper electrode surfaces contain mostly high index sites.

Hori *et al.* [66] reported that C-O stretch for adsorbed CO shows a band at 2089 cm^{-1} at rather high negative potentials; from -0.6 V to –1.0 V (*vs.* NHE), with increasing adsorption as the potential is increased negatively. On the other hand, two kinds of

linearly bonded CO have been observed by Oda *et al.* [67], at 2100 cm^{-1} and 2000 cm^{-1} on copper electrodes during the electroreduction of CO_2. Westerhoff and Holze [68] also detected CO adsorbed on polycrystalline copper electrodes at 2100 cm^{-1} in $KClO_4$ at a potential positive relative to the potential at zero charge, and this band did not show any potential dependence.

CO has also been observed adsorbed at metal surfaces during CO_2 electroreduction on Pt [69, 70] and Ni [38]. The adsorption of CO on metal surface has been proposed to occur through two bond interactions of 5σ orbital of CO to *sp* hybridised or $3d\sigma$ orbital of metal (σ component) and the interaction of metal $3d\pi$ electrons to $2\pi^*$ CO (π component) [25]. Figure 1.14 shows a scheme of the molecular orbital energy level diagram of CO (Fig. 1.14a) in addition to a representation of the interactions between the energy levels of Cu and those of CO. It is known that metal-CO interaction or bonding involves both σ and π component as suggested by Blyholder [71]. The initial σ interaction between the CO 5σ and metal valance electrons is repulsive (Figure 1.14b,c). Polarisation of the metal valance electrons away from the CO reduces this repulsion. The π interaction is attractive with metal to $2\pi^*$ donation leading to significant bonding. This metal to CO $2\pi^*$ donation leads to a positive charge on the metal and hence stabilises the metal-5σ interaction. For a single metal atom it is known that the metal to CO $2\pi^*$ donation involves the metal $3d\pi$ electrons (dz^2). For one Cu atom it has been found that the Cu 4s – CO 5σ repulsion is decreased by Cu 4s4p hybridisation and bending of the Cu-CO bond. This repulsion leads to a small binding energy of about 0.26 eV [72, 73].

1.8 The aim of the present work

The development of an effective catalyst is required for the reduction of CO_2. Any research into this area would lead to an insight into the activation of stable molecules and the rôle played by intermediates. The aim of this work is the elucidation of the processes occurring at copper electrodes and the electrochemical diffuse layer at the onset of the electroreduction of CO_2. Methods used involve electrochemical techniques [Cyclic Voltammetry (CV) and Electrochemical Impedance Spectroscopy (EIS)] and spectroelectrochemical [Subtractively Normalised Interfacial Fourier Transform Infra Red Spectroscopy (SNIFTIRS)]. The main objective consists in the identification of the species involved during the early stages of this electrochemical reaction. Most of the effort in this work has been directed towards investigating the processes occurring at

copper electrodes in aqueous phosphate buffered solutions, since copper has the adequate electrocatalytic properties for the electrochemical reduction of CO_2 to hydrocarbons

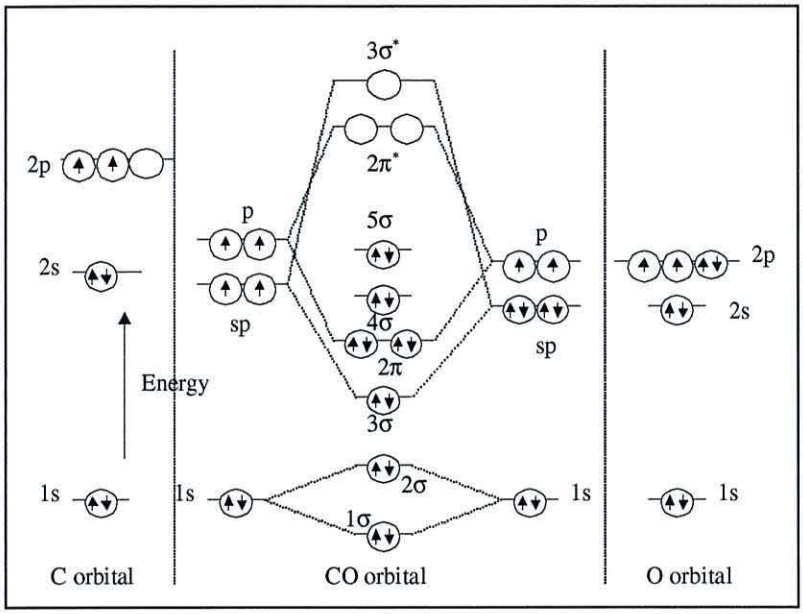

(a)

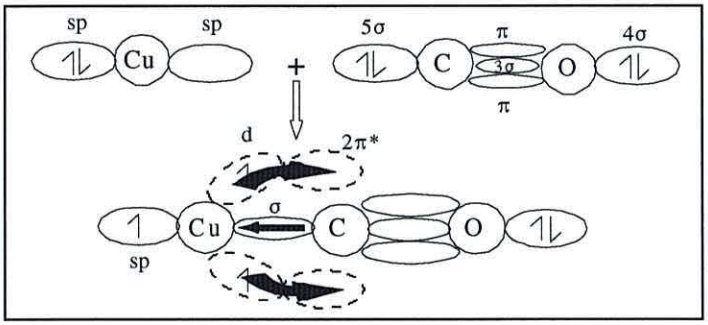

(b)

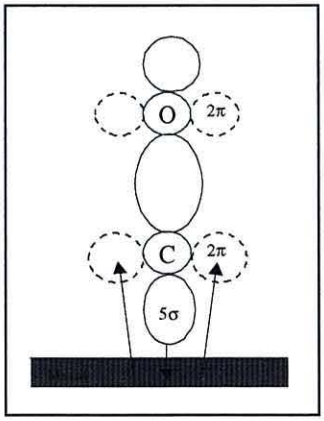

(c)

Figure 1.14: The molecular orbital energy level of carbon monoxide and metal-carbon monoxide [9, 30]

(methane, ethylene) and oxygenated hydrocarbons, such as alcohols and aldehydes. Chemicals that might be directly involved, as intermediates will be used and their electrochemical behaviour, oxidation and reduction will be assessed. A major part of this work has been dedicated to examining the behaviour of CO at copper electrodes. A novel technique, 2D-IR spectroscopy is also used to analyse the reduction step as a function of time and applied potential.

1.9 References

1 I. Taniguchi, "*Electrochemical and Photoelectrochemical reduction of carbon dioxide*" In *"Modern Aspects of Electrochemistry*", J. O'M. Bockris, R.E. White and B.E. Conway, (Eds.), Plenum (New York), Chp. 5 (1989)

2 B.P. Sulivan (Ed.), "*Electrochemical and Electrocatalytic Reactions of Carbon Dioxide*", Elsever Science Publishers, (1993)

3 F.R. Keene, "*Thermodynamic and Product Considerations in Carbon Dioxide Reactivity*" in "*Electrochemical and Electrocatalytic Reactions of Carbon Dioxide*", Chp. 1, B. Sullivan (Ed.), Elsever Science Publishers, (1993)

4 Benedict Aurian-Blajeni, "*Electrochemical Reduction of Carbon Dioxide*", Chapter 22 in "*Electrochemistry in Transition*", Oliver J. Murphy *et al.,* (Eds.) Plenum Press, New York, (1992)

5 D.A. Palmer and R.V. Eldik, *Chem. Rev.*, 83 (1983) 651

6 E. Fujita, D.J. Szalda, C. Creutz and N. Sutin, *J. Am. Chem. Soc.*, 110 (1988) 4870

7 K.F. Wissbrun, D.M. French and A.Petterson, *J. Phys. Chem.*, 58 (1953) 5197

8 M.J. Welch, J.F. Lifton and J.A. Seck., *J. Phys. Chem.*, 73 (1969) 3351

9 C.Creutz, "*Carbon Dioxide Binding to Transition-Metal Centers*" in "*Electrochemical and Electrocatalytic Reactions of Carbon Dioxide*", Chp. 1, B. Sullivan (Ed.), Elsever Science Publishers, (1993)

10 K. Nakamoto, "*Infrared Spectra of inorganic and coordination compounds*", John Wiley & Sons, New York, 4th Edition (1986)

11 M.E. Volpin and I.S. Kolomnikov, *Pure and Appl. Chemistry.*, 33 (1973) 567

12 C. Mealli, R. Hoffmann and A. Stockis, *Inorg. Chem.*, 23 (1988) 2853

13 D.H. Gibson, *Chem. Rev.,* 96 (1996) 2063

14 H.A. Schwarz, C. Creutz and N. Sutin, *Inorg. Chem.,* 24 (1985) 433

15 C. Amatore and J.M. Saveant, *J. Am. Chem. Soc.,* 103 (1981) 5021

16 J. Wambach and H.J. Freund, "*CO_2 Activation on Transition Metal Surfaces*" in "*Carbon Dioxide Chemistry: Environmental Issues*", J. Paul and C.-M. Pradier (Eds.) Proceeding of the International Symposium on CO_2 Chemistry, Sweden 1993. The Royal Society of Chemistry, Special Publication No. 153, Cambridge, (1994)

17 R.N. Compton, P.W. Reinhardt and C.D. Cooper, *J. Chem. Phys.*, 63 (1975) 3821

18 C.D. Cooper and R.N. Compton, *Chem. Phys. Letters.*, 14 (1972) 28

19 H.J. Freund and R.P. Messner, *Surf. Sci.,* 172 (1986) 1

20 S. Sasaki and A. Dedieu, *Inorg. Chem.*, 26 (1987) 3278

21 W. Akemann and A. Otta, *Surf. Sci.*, 272 (1992) 211

22 H.J. Freund, H. Behner, B. Bartos, G. Wedler, H.Kuhlenbeck and M. Neumann, *Surf. Sci.*, 180 (1987) 550

23 M. Asscher, C.T. Kao and G.A. Somarjai, *J. Phys. Chem.,* 92 (1988) 2711

24 A.R. Rossi and K.D. Jordan, *J. Chem. Phys.*, 70 (1979) 4422

25 Z.M. Liu, Y. Zhau, F. Solymosi and J.M. White, *J. Phys. Chem.*, 93 (1989) 4383

26 K.O. Hartman and I.C. Hisatsume, *J. Chem. Phys.,* 44 (1966) 1913

27 Z.H. Kafafi, R.H. Hauge, W.E. Billups and J.L. Margrave, *J. Am. Chem. Soc.,* 105 (1983) 3886

28 R.P. Eichens and W.A. Pliskin, "*Advances in Catalysis*", Vol IX, Academic Press, N. York (1957)

29 J. Mascetti and M. Tranquille, *J. Phys. Chem.,* 92 (1988) 2177

30 A.A. Davydov, "*Infrared Spectroscopy of Adsorbed Species on the Surface of Transition Metal Oxides*", C.H. Rochester (Ed.), John Wiley & Sons, New Yorks, (1990)

31 M. Schmidt. "*The thermodynamics of CO_2 conversion*" In "*Carbon dioxide chemistry: Environmental issues*", J. Paul and C.M. Pradier (Eds.), Athenacum Press (1994)

32 W.M. Ayer, "*An overview of Electrochemical Carbon Dioxide Reduction*" In "*Carbon dioxide chemistry: Environmental issues*", J. Paul and C.M. Pradier (Eds.), Athenacum Press (1994)

33 P.C. Ford, "*Catalysis of the Water Gas Shift Reaction*" in "*Electrochemical and Electrocatalytic Reactions of Carbon Dioxide*", Chp. 1, B. Sullivan (Ed.), Elsever Science Publishers, (1993)

34 A. Jimenez-Morales, J.C. Galvan, R. Rodriguez and J.J. de Damborenea, *J. Appl. Electrochem.,* 27 (1997) 550

35 M. Jitaru, D.A. Lowy, M. Toma, B.C. Toma and L. Oniciu, *J. Appl. Electrochem.*, 27 (1997) 875

36 Y. Hori, H. Wakebe, T. Tsukamoto and O. Koga, *Electrochim. Acta*, 39 (1994) 1833

37 Y. Hori, T. Tsukamoto, O. Koga and A. Murata, *Electrochim. Acta,* 39 (1994) 2495

38 Y. Hori and K.Osamu, *Electrochim. Acta*, 38 (1993) 1391

39 K.D. Jordan, *J. Phys. Chem.*, 88 (1984) 2459

40 K.W. Frese, Jr., in "*Electrochemical and Electrocatalytic Reactions of Carbon Dioxide*", Chp. 1, B. Sullivan (Ed.), Elsever Science Publishers, (1993).

41 M. P. Sanchez, M. Barrera, S. Gonzalez, R., M. Souto, R.C. Salvarezza and A.J. Arvia, *Electrochim. Acta,* 35 (1990) 1337

42 Yu.B. Vassiliev, V.S. Bagotsky, N. V. Osetrova, O. A. Kahzova and N.A. Mayolova, *J. Electroanal. Chem.*, 189 (1985) 295

43 Y. Hori, O. Koga, A. Aramata and M. Enyo, *Bull. Chem. Soc. Jpn.*, 65 (1992) 3008

44 Y.Hori, R.Takashi, Y. Yoshinami and A. Murata, *J. Phys. Chem.*, B 101 (1997) 7075

45 S. Taguchi, A. Aramata and M. Enyo, *J. Electroanal. Chem.*, 372 (1994) 161

46 Y. Hori, K. Kikuchi and A. Murata, *Chem. Lett. Chem. Soc. Jpn.,* (1986) 897

47 D.P. Summers and K.W. Fresee Jr, *Langnuir*, 4 (1988) 51

48 P. Braunstein, D. Matt and D. Nobel, *Chem. Rev.*, 88 (1988) 747

49 T. Ito and Y. Yammamoto, "*Organometallic reaction of Carbon Dioxide*" in "*Organic and Bioorganic Chemistry of Carbon Dioxide*", S. Inoue and N. Yamazaki, (Eds.), Wiley New York, (1982)

50 S. Sasaki, K. Kiraura and Morokuma, *Inorg. Chem.*, 21 (1982) 760

51 Y. Hori, O.Koga, Y. Watanabe and T. Matsuno, *Electrochim. Acta*, 44 (1998) 1389

52 Y.B. Vasiliev, V.S. Bagotzky and N.A. Maiorova, *J. Electroanal. Chem.,* 189 (1985) 271

53 J. Ryu, T. N. Anderson and H. Eyring, *J. Phys. Chem.,* 76 (1972) 3278

54 H.A. Schwartz and R.W. Dodson, *J. Phys. Chem.,* 93 (1989) 409

55. J. Ryu, T.N. Andersen and H. Eyring, *J. Phys. Chem.,* 79 (1973) 228

56 A. Kudo, S. Nakagawa, A. Suneto and T. Sakata, *J. Electrochem. Soc.,* 140 (1993) 1541

57 Y.Hori, A. Murata and Y. Yoshinami, *J. Chem. Soc., Faraday Trans.,* 87 (1991) 125

58 R.T. Carlin, T. Sullivan, J.W. Sherman and C.A. Aspinwal, *Electrochim. Acta*, 38 (1993) 927

59 Y.Hori and A. Murata, *Bull. Chem. Soc. Jpn.*, 64 (1991) 123

60 S. Wasmus, E. Cattaneo and W. Vielstich, *Electrochim. Acta*, 35 (1990) 771

61 B. Aurian-Blajini, M.H. Habib, I. Taniguchi and J. O'M Bockris, *J. Electroanal. Chem.*, 157 (1983) 399

62 P. Friebe, P.Bogdanoff, N.A. Vante and H. Tributsch, *J. Catalysis,* 168 (1997) 374

63 D.W. DeWulf, T. Jin and A.J. Bard, *J. Electrochem. Soc.,* 136 (1989) 1686

64 K. Carlin and T. Sullivan, *J. Electrochem. Soc.,* 139 (1992) 144

65 P. Hollins and J. Pritchard: in "*Vibrational Spectroscopy of Adsorbates*", chp 8 Springer Series in Chemical Physics Vol. 15. R.F. Willis (Ed.), (1980)

66 Y. Hori, O. Koga, H. Yamazuki and T. Matsuo, *Electrochim. Acta,* 40 (1995) 2617

67 I. Oda, H. Ogasawara and M. Ito, *Langmuir*, 12 (1996) 1094.

68 B. Westerhoff and R. Holze, *Ber. Busenges. Phys. Chem.,* 97 (1993) 3

69 E. Morallon, J.L. Vasquez, J.M. Perez and A. Aldaz, *J. Electroanal. Chem.,* 380 (1995) 47

70 S. Taguchi and A. Aramata, *Electrochim. Acta*, 39 (1994) 2533

71 G. Blyholder, *J. Phys. Chem.,* 68 (1964) 2772

72 C.W. Bauschlicher, *J. Chem. Phys.,* 101(1994) 3250

73 M. Moskovits and J.E. Hulse, *J. Phys. Chem.,* 81(1997) 2004

CHAPTER II

Methods and experimental details

2.1 Introduction

In this work, three major techniques were used to examine the electrochemical reduction of CO_2 and follow the electrochemical behaviour of Cu electrodes in aqueous solutions containing CO_2 and CO. These techniques are:

1) Cyclic Voltammetry (CV)
2) Electrochemical Impedance Spectroscopy (EIS)
3) Substractively Normalised Interfacial Fourier Transforms Infrared Spectroscopy (SNIFTIRS)

Cyclic voltammetry is a routinely used technique and as such only the experimental procedure will be described here. A detailed description of EIS is given in Chapter V. However, even though *in situ* spectroelectrochemical techniques for examining the electrode/electrolyte interface have been in existence for many years, there are still differences in methodologies used by various research groups. Therefore, this chapter will include an overview of *in situ* IR techniques in addition to a description of the experimental set up used in this work.

2.2 Spectroelectrochemical techniques [1, 2, 3]

Conventional electrochemical techniques, although extremely sensitive, lack the molecular selectivity and sensitivity of spectroscopic techniques, since they rely on the measurement of macroscopic quantities such as capacitance, charge, current or potential, which do not provide unequivocal identification of the electroactive molecules. In recent years there have been important efforts in attempt to characterise, by means of novel spectroscopic techniques, the electrode/electrolyte interface and the phenomena involved during redox processes. The molecular level information obtained with the use of the developing spectroscopic methods has already provided surface scientists with valuable information regarding the structure and reactivity of surfaces [4].

So far, at the present time, spectroelectrochemical techniques can be divided into two major categories; the *in situ* techniques, in which the electrode/electrolyte interface can be

studied directly, and the *ex situ* techniques which require removal of the electrode from the electrolyte and subsequent analysis. The use of the last group of techniques to study the structure of the double layer and the redox phenomena in the electrochemical cell have, however, always brought questions about the effect of the removal of the electrode from its natural environment and on the validity of the results at the moment of extrapolating them to the phenomena occurring in the electrochemical cell [5]. As it is evident, *in situ* spectroelectrochemical techniques do not give rise to the uncertainties of the *ex situ* techniques.

Several *in situ* spectroscopic techniques [6] have been developed and/or improved during the last three decades, including among others: Electron Spin Resonance Spectroscopy (ESRS), Ellipsometry, Infrared Reflection Spectroscopy, Mössbauer Spectroscopy, Scanning Tunnelling Spectroscopy, Surface Extended X-ray Absorption Fine Structure (SEXAFS), Surface Enhance Raman Spectroscopy (SERS), and UV-Visible Reflectance Spectroscopy. Reflection spectroscopic methods can provide information on atomic and/or molecular level, they are non-destructive and more importantly, they are applicable *in situ.* Among the *in situ* techniques, the specular external reflectance spectroscopy using UV-visible radiation has been successfully employed for a number of years; however, it lacks the sensitivity towards the molecular structure possessed by the vibrational spectroscopy. The first *in situ* IR spectroelectrochemical experiments used the so-called internal reflection method. This particular technique was limited severely by the need of appropriate infrared transmitting materials as electrodes. However, since the work of Bewick, Pons and Kunimatsu [7, 8] external reflection infrared spectroscopy has become very versatile; as it can be applied to a wide variety of electrode surface morphologies, ranging from single crystals to relatively rough surfaces; not only just metallic electrodes but carbon electrodes, semiconductors and polymer (conducting or not) coated electrodes. The success of the *in situ* infrared spectroscopy in this field can be easily appreciated by the number of laboratories, which are now using and improving the technique and by the growing number of articles and reviews related to its application.

2.2.1 Reflection of Infrared Radiation at Metal Surfaces.

The fundamentals and mathematical derivation related to the reflection-absorption spectroscopy is beyond the scope of this section and only a summary of the relevant concepts will be presented here; a complete treatment can be found in reference [9]. The reflection of infrared radiation at the metal surface and its interaction with a thin surface

layer has been discussed since 1959 [10]. When light is reflected at a surface both the intensity and the state of polarisation are affected. The electric field vector, E_i for the incident plane wave and E_r for the reflected plane wave, can be decomposed into two independent perpendicular components: E_p, linearly polarised in the plane of incidence, and E_s, perpendicular to the plane of incidence. For these two components there are no changes in the polarisation state upon reflection, but a change in amplitude and phase result.

The reflectivity coefficient R of the interface is defined as the ratio between the intensity of the reflected light, 'I_r' and the intensity, 'I_i', of the incident light:

$$R = \frac{I_r}{I_i} \qquad \text{..... (2.1)}$$

The expression for *p*-polarisation and *s*-polarisation can be obtained from the Fresnel coefficients as follows:

$$R_p = \frac{\tan^2(\varphi_1 - \varphi_2)}{\tan^2(\varphi_1 + \varphi_2)} \qquad \text{..... (2.2)}$$

$$R_s = \frac{\sin^2(\varphi_1 - \varphi_2)}{\sin^2(\varphi_1 + \varphi_2)} \qquad \text{.....(2.3)}$$

where φ_1 is the incidence angle and φ_2 the reflection angle. Thus, according to Equation (2.2), R_p can reach zero when $\tan(\varphi_1 + \varphi_2)$ becomes infinite in non-absorbing media. This condition corresponds to a Brewster angle of incidence. For absorbing media, R_p exhibit a minimum at the so-called pseudo-Brewster angle. The reflectivity coefficients of the two linearly polarised components are different except for $\varphi_1 = 0$ and $\varphi_1 = 90^0$, so that the state of polarisation of the incident light is changed upon reflection. The degree of polarisation of a non-polarised incident light after reflection at the interface may be defined by the ratio:

$$\Delta = \frac{I_{rs} - I_{rp}}{I_{rs} + I_{rp}} = \frac{R_s - R_p}{R_s + R_p} \qquad \text{..... (2.4)}$$

which is maximum for the pseudo-Brewster angle (since R_p is minimum). Phase angles are also changed upon reflection. The change in the phase depends on the angle of incidence and on the optical constants.

In the presence of an adsorbed layer, or a film of thickness d, the reflected light has an intensity, I(d), lower than the intensity I(o) in the absence of the adsorbed film. Therefore, the normalised reflectance change will be defined by:

$$\frac{\Delta R}{R} = \frac{R(d) - R(o)}{R(o)} = \frac{I(d) - I(o)}{I(o)} \quad \ldots\ldots\ldots\ldots\ldots\ldots \quad (2.5)$$

which usually is negative for an absorbing film.

The absorption of radiation results from interaction between the electric dipole moment and the electric field vector, $E = E_i + E_r$, which results from the simultaneous presence of both the incident electric field vector, E_i, and the reflected electric field vector, E_r. This is illustrated for *p*-polarisation in figure 2.1, where E_i, is decomposed into two components, $E_p\perp$, perpendicular to the plane of reflection, and $E_{p\|}$, parallel to the plane of reflection.

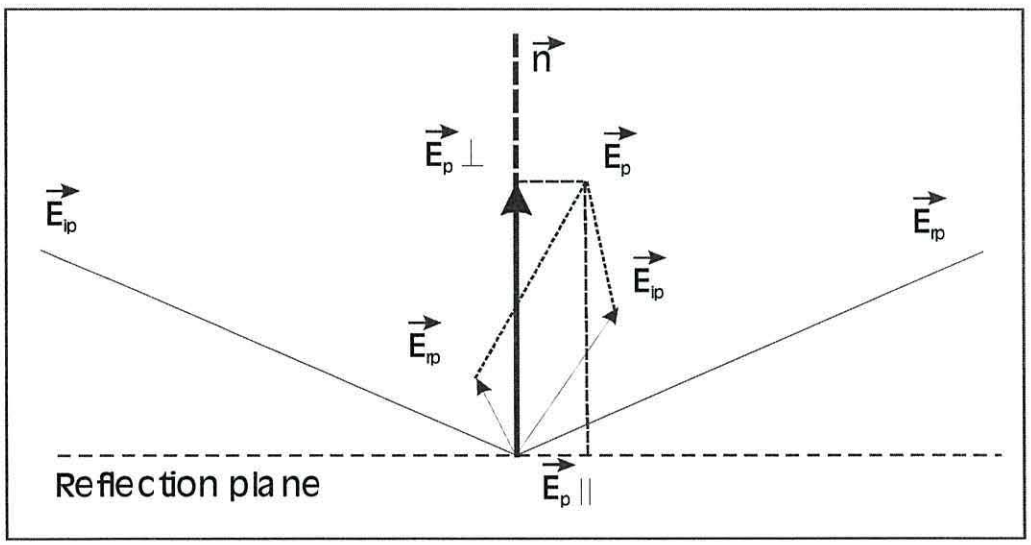

Figure 2.1: Vector E_p resulting from the sum of the incident and reflected electric field vectors E_{ip} and E_{rp}.

For angles of incidence smaller than the pseudo-Brewster angle, φ^B, both *p*- and *s*-polarisation display a change in the phase angle of π, so that the incident and reflected lights tend to be cancelled. However for angles of incidence greater than φ^B, the angle of the phase for *p*-polarisation does not change and both E_{ip} and E_{rp} add in phase. The resulting *p*-polarisation, $E_p = E_{ip} + E_{rp}$, will be maximum near the grazing incidence ($\varphi_1 \approx 90^0$) whereas the resulting *s*-polarisation will be close to zero for any angle of incidence. $E_{p\|}$ is also very small, whereas $E_p\perp$ approaches a maximum (about twice the amplitude of

the incident light, E^0_i). This is particularly true in infrared range, where most of the metals behave as highly reflective surfaces due to a very high electrical conductivity ($\sigma > 10^7\ \Omega^{-1}\ m^{-1}$). This leads to high values of extinction coefficients ($k > 10$). Thus, the interaction with the adsorbed molecules will only be important for molecules having their electric dipole moment perpendicular to the separation plane. This restriction constitutes the so-called *"surface selection rule"*, which is not in fact a true selection rule because no quantum numbers are involved. Another consequence is that the maximum adsorption of the infrared beam will occur for *p*-polarised light. This would justify the use of a polariser in reflectance spectroscopy.

Thus, in specular reflectance spectroscopy, the change in reflectivity induced by the adsorbed layer is related to the surface selection rule which cause an enhancement of the dipole moment of adsorbed molecules as described above. McIntyre and Aspnes [11] calculated the normalised reflectivity changes, $\Delta R/R$, for highly conductive metals using a three-phase model and assuming that the thickness, d, of the film (or of the adsorbed layer) is much smaller than the wavelength, λ. According to these authors the normalised change in reflectivity is given by

$$\frac{\Delta R}{R} \approx \frac{4\sin\varphi_1 \tan\varphi_1}{n_2^3} (\alpha_2 d) \quad \ldots\ldots\ldots\ldots\ldots\ldots (2.6)$$

where α_2 is the absorption coefficient of the film. For high angles of incidence, the first term of this equation can reach values greater than unity, and thus behaves as an enhancement factor for the reflectance.

Although this theory fails for a monolayer and sub-monolayer of adsorbed molecules, because a film of molecular thickness is not a continuum, it is possible to treat the monolayer (or sub-monolayer) like a film by defining the effective index of refraction (or dielectric constant) for a sub-monolayer and the effective thickness, $d = \theta d_0$; where d_0 is the thickness of a full monolayer and θ the degree of coverage of the surface by adsorbed species. Thus, for a fixed angle of incidence, the normalised change in reflectivity will be approximately proportional to the degree of coverage.

The detection of sub-monolayer quantities of species at the electrode/electrolyte interface by infrared spectroscopy requires a high level of sensitivity. Two major problems have had to be overcome to achieve such sensitivity. First, the bulk electrolyte imposes restrictions in the spectral range due to the large absorption of radiation; especially serious if the solvent is water; even trace amounts of water, which may be present in non-aqueous

solvents, might interfere. This has led to the development of thin-layer cells, which minimise the amount of radiation absorbed by the bulk electrolyte. In such thin-layer cells a flat disc electrode is positioned against the window, so that a thin layer of solution (5-50 μm) is formed between the window and the electrode.

The second problem deals with the amount of molecules under study, which is usually very small; sub-monolayer coverage with values no greater than few tenths of a nanomole. The absorbance of such species (10^{-2} to 10^{-6}) must be differentiated from the superimposed noise, background absorbance, source fluctuation and stray light. To achieve such level of sensitivity, the use of phase sensitive detectors and modulation techniques have been developed which involve either the modulation of the light polarisation or the electrode potential followed by suitable processing with microcomputer software.

Phase Sensitive Detection. - The purpose of the phase-sensitive detector (PSD) is to extract a weak signal buried in noise. The signal to be analysed is first modulated at a suitable reference frequency, ω_0 and then input to the phase sensitive detector and compared with the reference signal. Input signals, which differ in frequency, are mostly rejected whereas those with the reference frequency pass through a maximum if they are in phase with the reference signal. Thus, the phase sensitive detector allows the signals in phase and frequency to be stored and rejects the noise.

Signal Averaging. - Another way to improve the sensitivity has been well known by spectroscopists since the development of Fourier Transform Spectroscopy. It consists in using ensemble averaging and signal processing by means of a computer. As the noise is random whereas the absorption bands appear at the same frequency all time, then as the data is averaged, the net result would be to average out the effect of this noise. On the other hand, as the noise decreases, the absorption bands appear as an observable feature. If the noise is really random, then the amount of noise reduction will be proportional to the square root of the number of scans that has been averaged.

FTIR Spectroscopy. - In a grating spectrometer, the light is dispersed by the monochromator, which means that the detector receives each wavelength separately and consequently the intensity is low. In Fourier transform spectroscopy, on the other hand, all wavelengths are collected and received simultaneously by the detector. This high

throughput results in a high signal to noise ratio (S/N). FTIR is routinely used and its theoretical has been described in detail elsewhere and will not be discussed in this chapter. Fourier transform infrared spectrometer posses several advantages over conventional grating (dispersive) spectrometers as below:

i. simplicity and reliability (constant resolution),
ii. high speed and signal to noise ratio (Fellgett's or multiplex advantage),
iii. high energy throughput (Jaquinot's advantage), because no slit is used, and
iv. accuracy in frequency determination (Conne's advantage) due to the use of a subsidiary internal laser.

2.2.2 *In situ* Modulated Infrared Spectroscopy

Polarisation Modulation Infrared Spectroscopy

Infrared reflection absorption spectroscopy (IRRAS) has been used to obtain spectra of species on electrode surfaces with both grating and Fourier transform (FT-IRRAS) spectrometers. IRRAS, as applied to the metal solution interface, is not able to obtain full demarcation between surface and bulk components, since the 'surface region' which it probes extends to about 0.5 λ away from the reflecting surface (where λ is the infrared wavelength). Consequently species in the bulk solution, as well as in the double layer, will exhibit polarisation sensitive infrared absorbance. The polarisation state may be alternated between *s* and *p* (Polarisation Modulation) and the ac signal (Ip - Is) being detected by lock-in amplification. The polarisation modulation is usually achieved with a high frequency photoelastic modulator. According to the surface selection rule, only the *p*-polarised component can be absorbed by the surface species. Absorbance by randomly oriented species in the path of the beam produce no (Ip - Is) signal. The rate of modulation of polarisation is chosen to suit the detector (typically of the order of 70 kHz for solid state cooled detectors). In FT-IRRAS the frequency of polarisation modulation (fm) has to be sufficiently high, such that electronic separation of fm from the Fourier frequencies (typically 1 -10 kHz) can occur. The advantage of the polarisation modulation technique is that it gives spectra at a single potential. The potential difference spectra obtained by the potential modulation technique are sometimes more difficult to interpret.

Potential Modulation Infrared Spectroscopy.

Electrochemically Modulated Infrared Spectroscopy (EMIRS)

EMIRS instrumentation has been described in detail [12]. In this technique a grating spectrometer, designed for high throughput, is used. The spectrometer is a single beam instrument, however, the modulation of the electrode potential makes of it a virtual double beam spectrometer with perfectly matched sample and reference cells. A square wave potential modulation is applied and the fluctuating IR absorbance is detected by lock-in amplification. Further enhancement of this signal by the accumulation of data from several repeated spectral sweeps leads to a sensitivity of 10^{-6}. The choice of potential modulation frequency is a compromise. For the solid-state detectors typically used, the detector pre-amplified response is better for the higher modulation frequencies. However, this frequency must be low enough for the electrode potential to reach the applied potential after the potential step perturbation.

Subtractively Normalised Interfacial Fourier Transform Infrared Spectroscopy (SNIFTIRS).

This technique employs an FTIR spectrometer. The potential difference spectrum is produced by subtracting the spectrum obtained at each of the two potentials and ratio this by the background; this is analogous to the EMIRS spectrum. However, commercial Fourier transform infrared spectrometers are not as sensitive as their EMIRS counterparts. This is mainly due to the dynamic range available from 12 to 15 bits analogue-digital converters (ADC) installed in most instruments. If the machine is not detector noise limited, then the digitisation uncertainty of the 15-bit ADC limits the performance. In general the performance of commercially available FTIR spectrometers, as applied to the SNIFTIRS technique, depends on other several factors: as for EMIRS a high-intensity source and attention to a careful optical design are important considerations. The stability of the optical system and a good quality detector (for example narrow band cooled mercury cadmium telluride detector) are also of particular importance; evacuation of the spectrometer bench results in a significant improvement of the interferometer stability and hence on the S/N ratio. However, despite these requirements, commercially available FTIR spectrometers usually need to be only slightly modified for the SNIFTIRS technique. In contrast EMIRS technique requires specially designed spectrometers.

There are several ways to increase the sensitivity. The use of higher resolution ADC to increase the dynamic range of the instrument is always a possibility. The natural form

of the interferogram places extreme demands on the ADC, since digitalisation of both the intense centre burst and relatively small side lobes is necessary. Significant improvements in digitisation may be obtained if auto-scaling of the ADC is employed as it decreases the gain of the ADC around the centre burst, such that a greater dynamic range may be obtained in the wings of the interferogram. The interferogram can be re-scaled to its 'normal' form after the accumulation. Care must be taken when using this approach since the cooled detectors are often not linear in their outputs with respect to the optical flux at high intensity.

The most effective way to increase the sensitivity is by optical subtraction techniques that null the centre burst and all other signals unrelated to the change caused by the modulation of the potential. There are two basic timing sequences that can be used in the SNIFTIRS technique. For studies where the electrode/solution interphases are reversible with respect to the modulating electrode potential, a pulse technique similar to EMIRS is used except that modulation time scale is much longer and the interferograms are signal averaged to enhance the S/N ratio. Two sets of averaged interferograms are collected and separately Fourier transformed to produce S_1 and S_2, which correspond to the single beam spectra at potentials E_1 and E_2, respectively. If there is a significant reflection from the front surface of the window, then an additional single beam spectrum is required, S_w, which is obtained with the electrode pulled away from the window. The potential difference spectrum, which is equivalent to that obtained by EMIRS, is calculated using the following equation:

$$\frac{\Delta R}{R} = \frac{S_2 - S_1}{S_1 - S_w} \qquad \text{..... (2.7)}$$

The second timing sequence is necessary for systems, which may exhibit any kind of irreversibility. In this sequence, which is usually performed over a larger potential range, the electrode potential is simply modulated in a 'staircase mode' and the sequences of interferograms are cumulated and averaged at each potential (step). Reproducibility here is a problem since drift and other long time effects will be more important.

EMIRS *vs.* SNIFTIRS: Advantages and disadvantages

i. Sensitivity.- EMIRS is more sensitive, with detection limits of 10^{-5} -10^{-6} $\Delta R/R$ being obtainable. The detection limits for SNIFTIRS is about an order of magnitude worse

than this. Clearly this limits the SNIFTIRS technique to the study of species giving relative strong absorbance. To obtain 10^{-4} -10^{-5} sensitivity requires several hours of data collection, comparatively much longer than the EMIRS experiment. Surface contamination during such long periods may present problems. SNIFTIRS is a less sensitive technique than EMIRS since the latter employs phase sensitive detection to observe a small fluctuation in the signal, while the former relies on the subtraction of two sets of interferograms (obtained at different potentials) to observe a small difference. Large improvements in S/N are often obtained by observing a small difference as a.c. signal rather than a d.c. signal.

ii. Resolution.- This is typically better for the SNIFTIRS technique (4 to 8 cm^{-1}). EMIRS spectrometers are generally constructed for maximum throughput at the expense of resolution (10 to 15 cm^{-1}).

iii. Accessible spectral range and the multiplex advantage of FTIR-SNIFTIRS enable a wide spectral region to be studied simultaneously, without any increase in data collection time. This arises from the 'multiple' advantage of FTIR spectroscopy, all spectral frequencies being modulated simultaneously by the movement of the scanning mirror of the main interferometer. Generally individual EMIRS spectrum is recorded over a narrow region of the mid-IR.

iv. Diffraction instruments are generally unsuitable for the far-IR, since several gratings and several filters are required for order sorting. Far-IR sources are of relatively low brightness and FTIR spectrometers sample a considerably larger proportion of the source radiation (the throughput advantage of FTIR). Consequently SNIFTIRS is the only suitable *in situ* IR technique for the far-IR.

v. Other comparisons.- EMIRS spectrometers are specifically designed for the technique, while SNIFTIRS spectrometers can be commercially available FTIR spectrometers. One can significantly alter the path of the beam without critically affecting the performance.

2.3 *In situ* Infrared Measurement

Detecting an adsorbed species on highly reflecting metal surface can be carried out using polarised light. In general two phenomena associated with the optic of the reflection of the electromagnetic radiation can be understood through different properties of *p* or *s*-polarised light. For other than normal incidence, the effective intensity of the radiation very close to the surface is different for the *p*-polarised and *s*-polarised states. There is a

180^0 phase change on reflection at a metal surface at all angles of incidence for *s*-polarised radiation, which has its electric vector tangential to the surface, and since the reflection coefficients is close to unity, the resultant amplitude of the electric vector at the surface is essentially zero [1, 12, 13]. Thus *s*-polarised IR radiation does not interact with vibrating dipoles near the surface, i.e. it is inactive in the detection of adsorbed species. Consequently, only *p*-polarised radiation, which has it electric vector in the plane of incidence, is effective for studies at metal surfaces. This could lead an additional selection rule, the surface selection rule [14], defining those normal modes of a molecule sitting on a metal surface able to show IR activity, i.e. only those vibration modes having a non-zero component of the dipole derivative perpendicular to the surface are able to interact with the IR radiation. A useful consequence of this is that the relative intensities of the adsorption bands shown by an adsorbed molecule will vary as its orientation with respect to the surface is changed.

The design of the experiment method, which allows the investigation of the electrode/solution interface at the molecular level, has become critical in the last two decades. The determination of the reaction mechanisms based solely by electrical measurements on the microscopic scale such as in cyclic voltammetry will give rise numerous controversies interpretation. It has become apparent that this physicochemical method has to be used in conjunction with electrochemical spectroscopy methods in which the latter is of major importance in obtaining experimental data, which are significant for the electrochemical experiments. Furthermore the use of the spectroelectrochemical methods should be operated *in situ*, be able to provide detail information such as the properties of the electrode surfaces, the structure and the constituent of the double layer, the nature and the structure of the adsorbed species, the quantity or the coverage of the adsorbed species on the electrode surface and their nature of the interaction between themselves and with other substrates [15].

It is known that as early as 1975, infrared specular reflection spectroscopy was recognised as a powerful technique for investigating adsorbed molecule at solid-gas interfaces [16]. As mentioned earlier by using a polarisation modulation technique, high sensitivities is achieved toward 10^{-5} absorbance unit or for a strong absorption band species such as CO, detection up to sufficient 10^{-3} of a monolayer. The development method of investigating the electrode/solution interface however is more recent, since it was believed that the present of solvent (particularly water), which display strong IR absorbance, precluded the use of such techniques. However the ability of the modulation technique to

uncover a very small signals buried in the large amplitude background, makes it possible to detect a signal of the magnitude expected for infrared spectra of adsorbed molecule at electrode/electrolyte solution interfaces [12, 17].

In SNIFTIRS, a sophisticated FTIR spectrometer is normally required for work at the electrode/electrolyte solution interface. The instrument should be able to allow alternating access to several memories for coadding the interferograms at two different potential limits that are repetitively changed or at a series of potentials that are continuously increased or decreased. In conventional "block mode" approaches (Figure 2.2a) where the applied potential is repetitively switched in two different values e.g., E_1 and E_2, which are able to give enough potential perturbation to the system. This approaches is normally used for fully reversible systems. This method allows the spectra are taken only at two potentials and repeated for better signal to noise ratio. The technique consists in collecting successive series of interferograms at each of two potentials limit, E_1 and E_2. These potentials are chosen according to the electrochemical behaviour of the system studied. E_1 is the reference potential at which no reaction occurs and E_2 a potential of interest at which an electrochemical process occurs. The step between E_1 and E_2 is repeated until the desired signal-to-noise ratio is obtained (an average of 100 scans is sufficient). If the R_1 and R_2 are the reflectivity measured at E_1 and E_2, it is easily to calculate the relative change of the

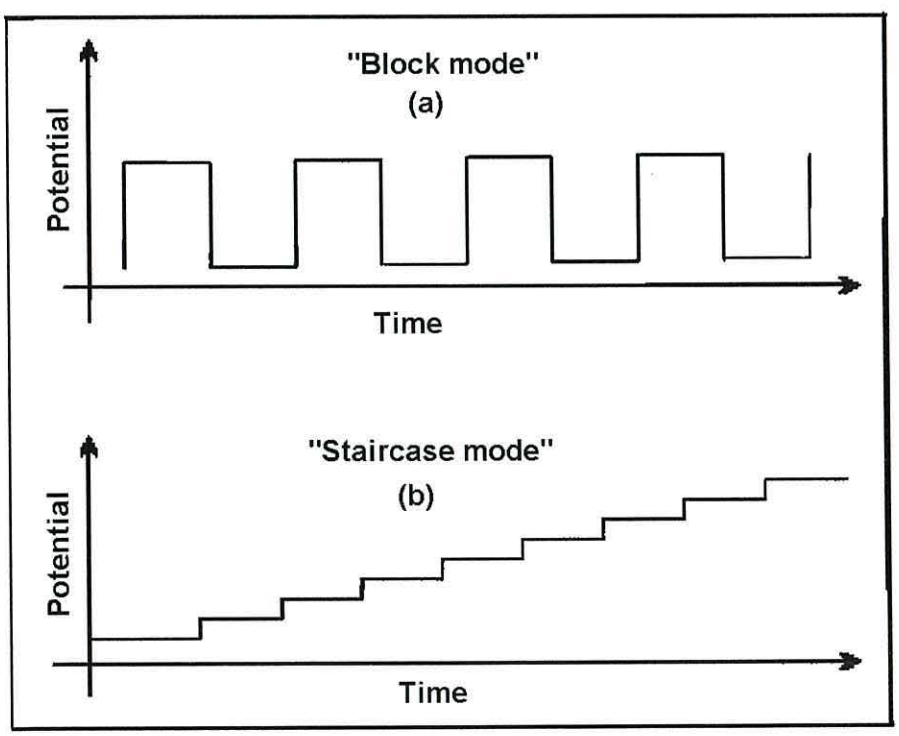

Figure 2.2: Potential transients in SNIFTIRS

reflectivity in normalised difference, $\Delta R/R$:

$$\frac{\Delta R}{R} = \frac{R_2 - R_1}{R_1} = \frac{R_2}{R_1} - 1 \quad \text{.....} \quad (2.8)$$

This normalisation is referred to the "Dynamic Reference Normalisation" (DRN).

Another approach is when the potential of the working electrode was applied in "staircase mode" which consists of successive potential steps (Figure 2.2b). In contrast to the conventional "block mode", this approach can be used in most electrochemical systems. The spectra obtained from this technique can be represented as normalised difference spectra ($\Delta R/R$) in two ways. The first method is as DRN method where it compares the spectra taken at various potentials at the previous potentials. This operation helps to distinguish between the electrochemical processes occurring after a particular potential step. It also provides an "instantaneous picture" of the system after each potential step. The second method consists of correlating successive spectra (R_n) with a single reference spectrum, usually the spectrum taken at the initial potential (R_1), which is giving the normal background without any perturbation effect. This particular normalisation is shown by the following equation:

$$\Delta R/R = [R_n - R_1] / R_1 = [R_n / R_1] - 1 \quad \text{.....} (2.9)$$

This processing method of the raw spectra resulting spectra contain the accumulation of the vibrational changes occurred since the application of the first potential spectrum; thus provides an accumulative spectrum. This would be equivalent to a successive addition of all DRN spectra up to the DRN spectra obtained at a specific potential. This type of normalisation is known as the "Static Reference Normalisation" (SRN).

As a comparison, the DRN method provides particular vibrational information from an electrochemical system when such a system is disrupted by the application of a small amplitude potential bias pulse. In fact it is a differential normalisation method, which presents the normalised vibrational changes when a differential change in potential is applied to the system being studied [18]. This method allows the observation of subtle changes, which may not visible in the SRN spectra due to the accumulation of the products after several consecutive potential bias pulses. However both normalisation techniques, the SNIFTIRS spectra will exhibit negative band for increases in spectral absorbance whereas positive bands for loses in spectral absorbance intensity.

The SNIFTIRS technique has proved to be quite suitable for the *in situ* detection of either electrochemical generated intermediates in the double layer or species adsorbed at

the electrode surfaces. The shape of the absorption band in SNIFTIRS can be either monopolar or bipolar. Various theoretical forms are to be expected for the SNIFTIRS signal, as of in the electrochemically modulated infrared reflectance spectroscopy, EMIRS. Depending on whether the species which adsorb the radiation do so only at one or at two potential limits, the signal may appear as a single band (monopolar) with either a positive or a negative sign, a bipolar band with positive and negative lobes, or even not at all if at constant coverage of the adsorbed species, the change of the potential does not sufficiently effect the force constant of the bond [3, 13]. The illustration of the schematic subtraction bands which producing either single/monopolar or bipolar bands of an adsorbed species as a function of potential are shown in Figure 2.3. The way of the species adsorb on the surface, either flat or perpendicular is also a dominant factor contributing whether the corresponding IR absorbance bands can be observed.

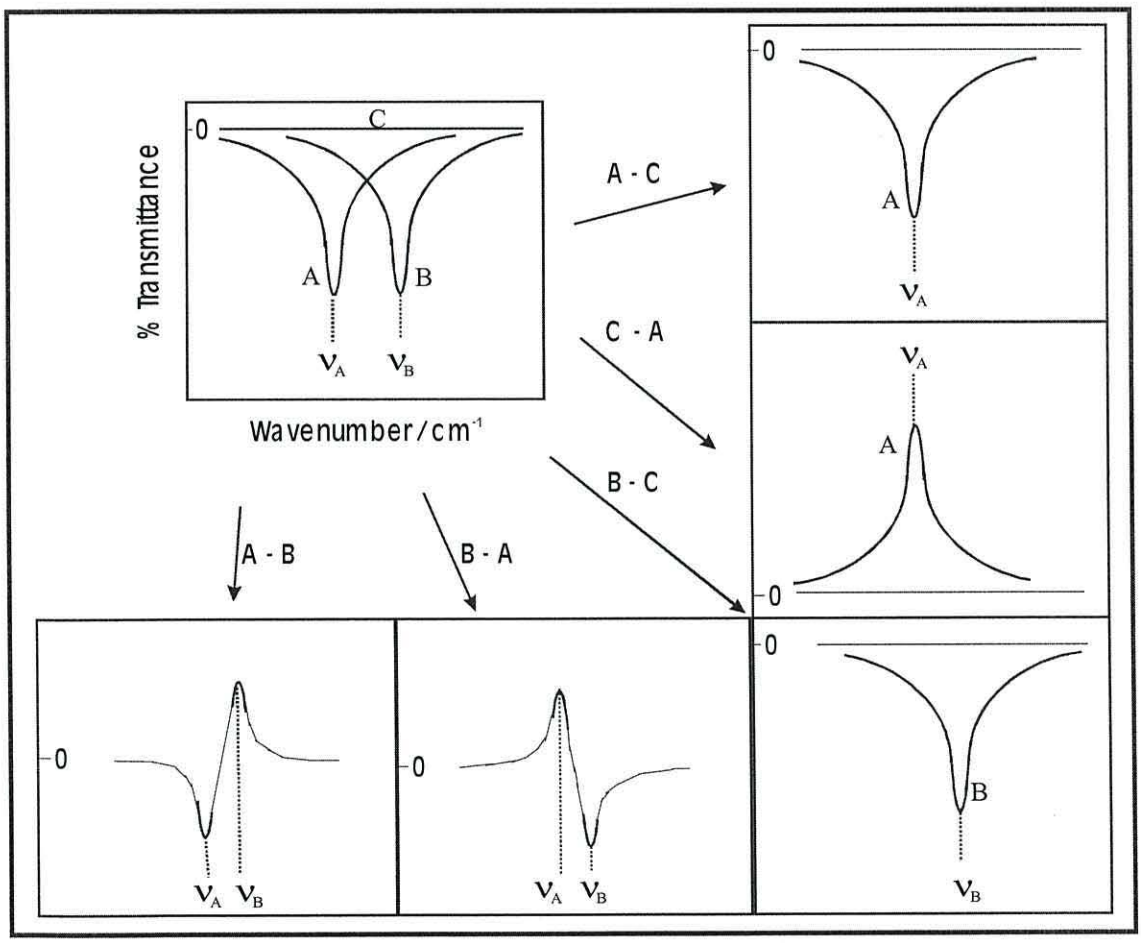

Figure 2.3: The type of SNIFTIR spectrum band shape of an adsorbed species relative to the band at reference spectrum, showing either a negative or positive band after the subtraction between two bands, A and B at different wavenumber (correlated to the applied potential) or with a background band, C [1].

2.4 Experimental

2.4.1. Electrode preparation

Copper disc electrodes (0.8 cm diameter, 99.99% purity) were either sealed in Teflon (PTFE) holders, which have been machined in such a way to allow the flexibility or sealed using epoxy glue or to a small Teflon cylinder or held with a shrinkable tube (RS Components Ltd.). A 1 cm distance between the Teflon cylinder and glass tube holder was maintain to allow the electrodes flexibility. The electrical connecting wire was attached at the back of the metal disc with silver conductive paint (RS Components Ltd.) and reinforced with epoxy glue and allow to cure overnight at room temperature. In case to construct the flow cell electrodes, a small hole was drilled in the centre of the metal disc. A small Teflon tube was tightly inserted in the middle of the hole and jointed with a medium size Teflon tube towards the end of the electrodes. Once assembled, the electrodes were flat ground with fine emery paper, then polished with successively finer grades of alumina powders ranging from 9.5 μm for very new electrodes to 0.05 μm to mirror finished. The electrode assemble is shown in Figure 2.4.

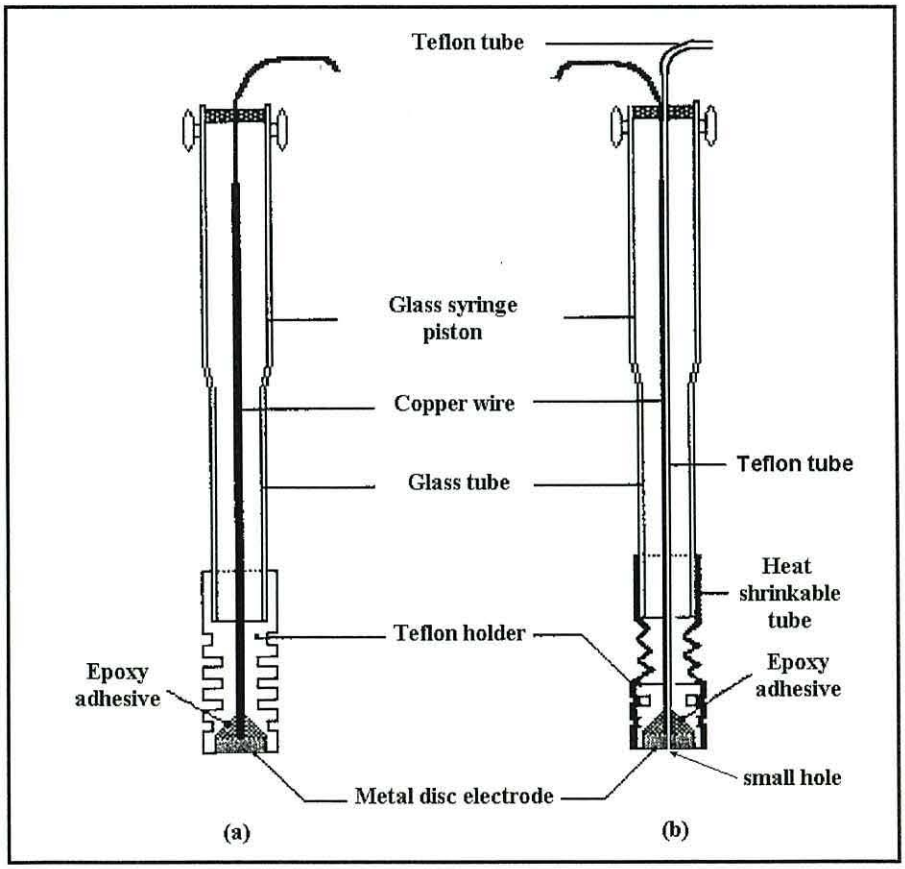

Figure 2.4: The assemble of (a) normal and (b) flow cell working electrode

Once the electrode is constructed, it has to be polished to obtain a smooth, brilliant and mirror finished surface, which is free of physical defects. The polishing material used depends on electrode material hardness, normally alumina powder and can be used on special polishing cloths. The process begins with large particles, using successively smaller particles, verifying the absence of scratches. It is worth to note that the surface of the solid electrode is not truly clean after every polish especially if particle of abrasive remain at the electrode surface. For this reason it is necessary to resort to method such as ultrasound or electrochemical cleaning.

2.4.2 Electrochemical polishing

The surface of the electrode is subjected to physical and chemical changes prior to, during or even after the electrode reactions. Therefore it is of paramount importance to bear in mind that the electrode surface conditions are very difficult to maintain to their 'original' or at a 'desired' condition each time. One significant problem with solid electrodes is the reproducibility of the electrode surface, since the state of the electrode surface can have a significant effect on the rate of electron transfer; for instant the presence of adsorbed ion or molecule or oxidized surface typically decreases the rate of electron transfer. In certain cases the electrode can be coated with a film, which is either a product of its own oxidation or product of the electrochemical process under study. However, performing routine standard polishing procedure can minimize the physical or chemical change and thus restore the 'original' condition of the working electrode. Polishing the surface using alumina or diamond polishing compound is a cleaning procedure typically adequate for certain electrochemical processes. However for reactions, which are sensitive to surface condition such as the adsorption of specific molecules or adsorbate intermediates, the state of the surface of the electrode can produce significant differences in the rate of reaction. This is due to the presence even after the finest mechanical polishing, of a rough surface (at microscopic level), consisting of scratches, cracks, holes and projections [4]. Such surface will naturally occlude particles of the abrasive (i.e. alumina polishing powder) and other foreign materials, which in some experiments can strongly affect the performance of the electrode. Therefore it is necessary to resort to methods such as ultrasonic cleaning and in severe cases extensive chemical or electrochemical pre-treatment (electrochemical cleaning) are generally recommended.

The electrochemical cleaning typically involves oxidation of the electrode surface by electrochemical or chemical means to remove any impurities and to generate an oxide

layer, which afterwards will be removed by applying an appropriate potential. The electrochemical polishing is normally carried out in acidic media such as phosphoric acid, sulphuric acid or in perchloric acid-acetic acid solutions. Methanol is sometimes used as a solvent instead of water. Tegart has tabulated possible electrolytes used in electrochemical polishing methods for several purposes [19]. During electrochemical polishing, the initial step involves a positive polarization that induces anodic current densities, which increase with potential. Dissolution in this range produces a dull surface that features preferential crystallographic attack. In this region surface kinetics (charge transfer) is rate controlling. Beyond a certain potential, the curve flattens considerably and becomes insensitive to the applied potential. In this region, the electrode brightens because the rate-limiting step is mass transfer either to or from the surface of the electrode. Figure 2.5 shows the anodic current-voltage curve for copper in 6 mol dm^{-3} H_3PO_4. The metal to be electropolished forms the anode in an electrolytic cell, and continued dissolution of the metal occurs in such a way that irregularities on the surface are removed and the surface becomes smooth and bright. As seen from the figure, depending on the conditions of operation and the solution used, a metal can be etched, polished, partially passivated or

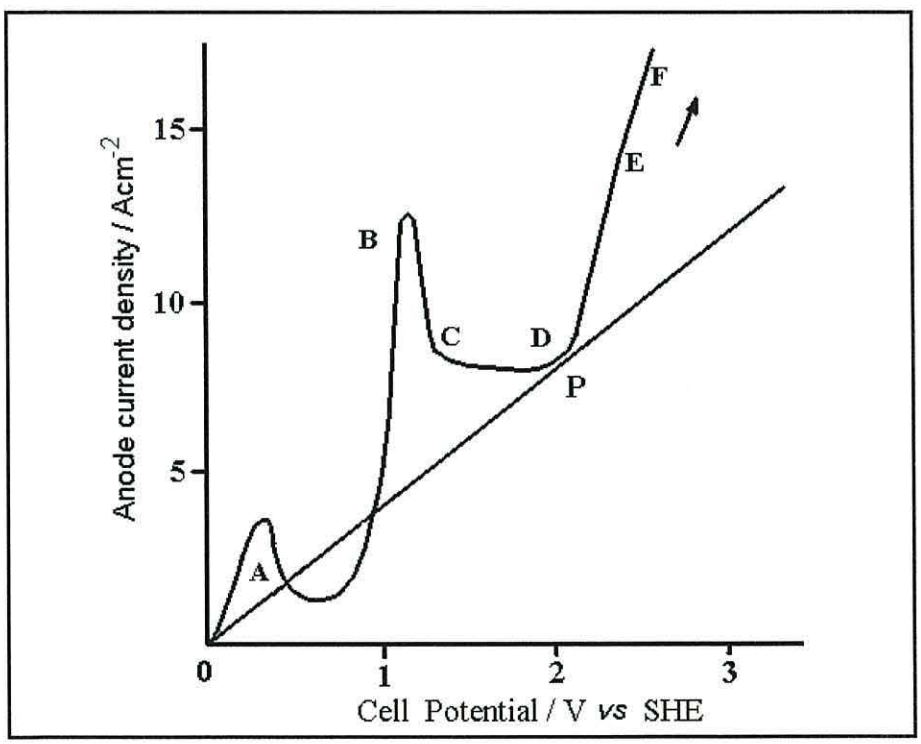

Figure 2.5: Copper in phosphoric acid; the regions on the curve are: A-B etching, B-C unstable, C-D stable plateau with polishing, D-E slow gas evolution with pitting, E-F polishing with rapid gas evolution. P indicates optimum polishing conditions [19]

completely passivated. In the etching region (A – B), considerable smoothing takes place but the surface retains a dull matt finish (or acquires one if it is initially bright). In the 'unstable region' (B – C) periodic oscillations of current density may occur. In the 'polishing plateau' (region between C and D) polishing occurs at almost constant current density (also known as 'limiting current density') with the quality of the polish increasing as the voltage is increased. Along DE gas evolution occurs and the surface becomes pitted. After this, at much higher potentials, an etched and polished surface is obtained. Temperature, stirring, concentration and viscosity of the acid affect the whole process. Thus, in the temperature range between 4 to 31 ^{0}C a good polish can be obtained; however further increases in temperature lead to an uneven surface. With regards to the concentration of phosphoric acid, the best results can be obtained with a solution containing 6 mol dm^{-3} of H_3PO_4. In general, below the optimum concentration, the lower the concentration, the higher is the etching of the surface. Above the optimal concentration, increased acid concentration results in poor brightness. The addition of copper phosphate increases the viscosity and reduces the limiting current density.

The working copper electrode was first mechanically polished by a gradual sequence of finer grades of alumina powder ranging from 9.5 μm for the very new electrodes followed by 1 μm, 0.3 μm, 0.1 μm and finally 0.05 μm to mirror finished. After each polish, the electrode was rinsed in distilled water followed by cleaning in an ultrasonic bath for about 5 minutes. In most experiments, final electrochemical polishing was performed by applying a constant current to the copper electrode when placed as an anode in the electrochemical cell. The electrode was electrochemical polished in 85 % H_3PO_4 solution at 200 mA for 5 minutes using a Pt sheet as a cathode as shown in Figure 2.6. The electrode was then successively washed with distilled water followed by buffers or electrolyte solutions, and finally with distilled water and then cleaning in an ultrasonic bath. After each electrochemical or spectroelectrochemical measurement, the electrodes were polished with a fine size; 0.05 μm or electrochemical polished before storage in clean and dry containers.

Platinum coupon/sheet was used as secondary electrode in these studies. Mixture of hot sulphuric-nitric acids was used to clean Pt electrode. After that it was thoroughly rinsed with deionised water and then red flamed. This process was repeatedly at least twice and the coupon was finally rinsed with a buffered supporting electrolyte prior to measurement. A Saturated Calomel Electrode (E = 0.249 mV *vs.* SHE) was used as a

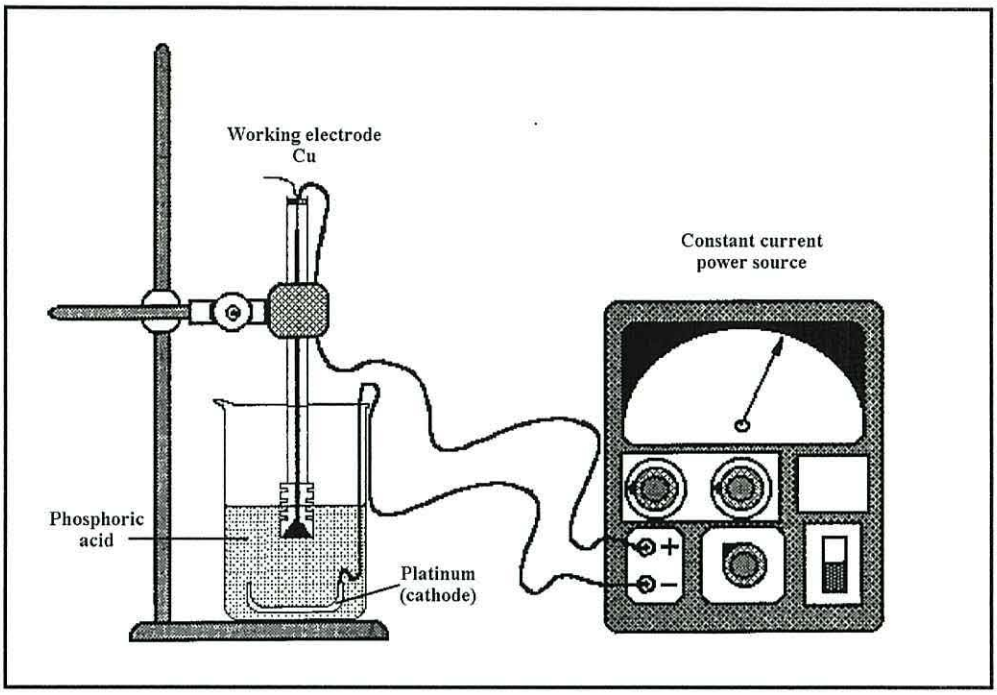

Figure 2.6: Schematic diagram set up for the electrochemical polishing

reference electrode. The electrode was rinsed thoroughly with pure water before and after each experiment. To maintain the electrode performance, the electrode was stored in a saturated potassium chloride, KCl solution when not in use.

2.4.3 Chemicals

Solutions were prepared from pure water and analytical grade chemicals. Ultra-pure deionised water (18 MΩ) was obtained by passing through purified water from Elgastat UQ system to another purification system of an Elgastat UHQII MKII. The pure water was prevented from coming into contact with any plastic container and was transferred to acid-washed flasks before used to prepare the electrolyte solution. The electrolyte solutions were prepared from Aldrich reagent grade chemicals KH_2PO_4 (>99.5%), K_2HPO_4 (>99.5%), K_3PO_4 (>99.5%), H_3PO_4 (>99.5%), $KHCO_3$ (>99.5%) without further purification.

2.4.4 Glassware and cells

Prior to any measurements, all glassware was soaked for 24 hours in a freshly prepared mixture of concentrated sulphuric and nitric acids. Afterwards the glassware was removed from the acid bath, thoroughly rinsed with deionised water (Ulgastat UHQII

MKII), and transferred to a "steam bath" for steaming for about 30 minutes. The steam bath allows steam to freely circulate around the glassware thus removing any acid traces. After steaming, the glassware was removed from the steam bath and again thoroughly rinsed with deionised water. For experiments in which deuterium oxide or deuterated chemicals were used, the glassware was dried in the oven prior to their used. Silicon infrared transmitting window and Teflon washers were treated in a similar way as the glassware in the acid bath and rinsed thoroughly with deionised water. When necessary, the silicon window was polished with very fine diamond polishing compound to remove any scratches from the silicon surface. In this case the silicon window was cleaned in an ultrasonic bath prior the immersion in the concentrated acid mixture.

2.4.4.1 Cyclic voltammetric and electrochemical impedance

The electrochemical measurements (CV and EIS) were performed using a three-electrode electrochemical cell as shown in Figure 2.7. The working electrode is pushed down from the top of the cell by sliding it through a syringe barrel attached to the cell body. The counter electrode (platinum coupon sheet welded to a platinum wire) is inserted from the cell body perpendicular and close to the working electrode to minimise the resistance between the electrodes. The body of the cell is also provided with gas inlet for

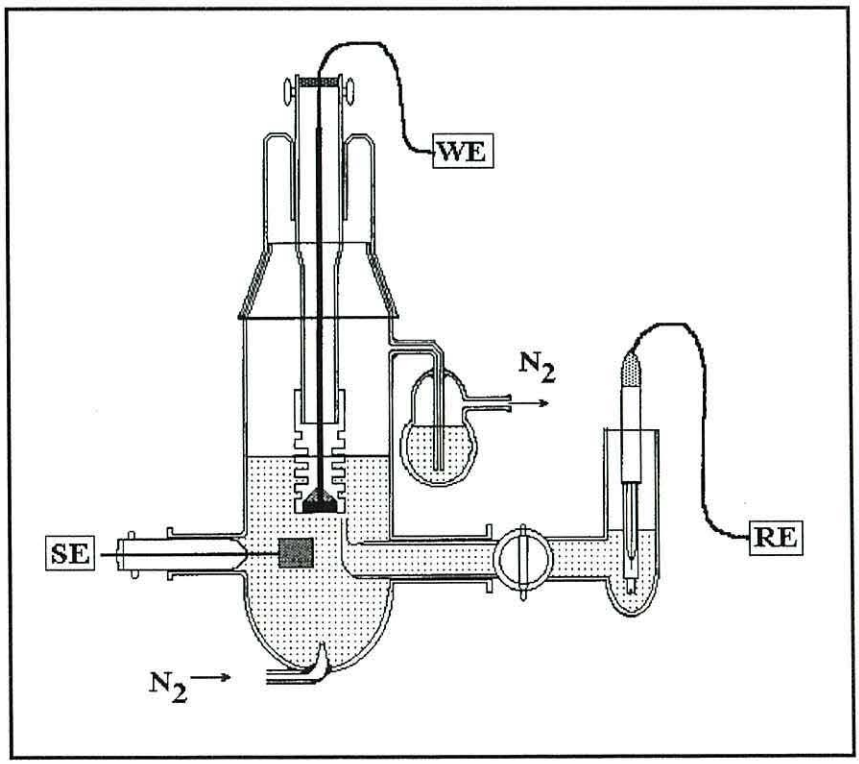

Figure 2.7: Cyclic voltammetry and impedance measurements cell

gas bubbling (degas) and gas outlet fitted with gas bubbler. When the bubbler is filled with supporting electrolyte, it acts as a one-way valve and allows the gas escape from the cell and prevents the atmospheric gases re-entering the cell. The reference electrode (SCE) is inserted from the reference compartment attached to the cell body fitted with three-way tap through a very narrow capillary tip (the Lugging Capillary).

2.4.4.2 *In situ* Infrared

Figure 2.8 shows the spectroelectrochemical cell used in this work, which was designed specifically for the *in situ* infrared experiments. The cell design enables the electrode to be pushed against the silicon window producing a thin layer of electrolyte (ca. 5-10 μm), thus minimising the absorption of the incident IR radiation by the solvent. Basically, the cell design has the same concepts for the electrodes and gas in/outlets as the electrochemical cell. This spectroelectrochemical cell body has round open end where an IR transmitting window can be placed. A flat silicon disc window is sealed to the cell by pressing it against a PTFE washer and silicon rubber seal between the cell body and the aluminium holder. The Lugging Capillary probe for the reference electrode is extended parallel to the

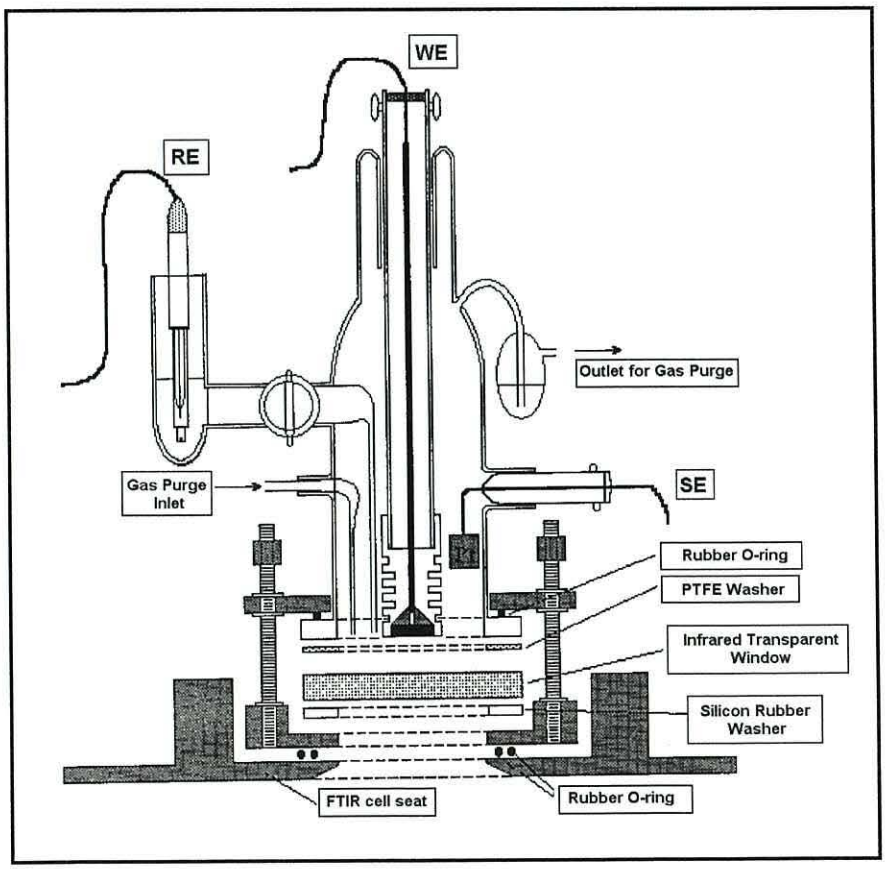

Figure 2.8: FTIR cell assemble for *in situ* measurement.

working electrode to within one millimetre of the cell window. Silicon window is an IR transparent material, which is not attacked by acid solutions and is useful for spectral measurements over a wide range of wavenumbers (4000 – 800 cm^{-1}). The experiments with variable temperature measurements (0 to 80 °C) were performed using a larger cell. A glass water jacket is inserted into the cell body. The electrolyte solution temperature can be cooled down or raised up to the desired temperature prior to the measurement. A thermostatic controlled cooling system unit with temperature range from –30 °C to 80 °C was used to control the cell temperature. The coolant used was a mixture of industrial methylated spirits and water (50:50). The silicon tubes that connected the cell to the cooling unit were fully covered with insulating hose and the IR cell body was fully covered with thick cotton wool layers to prevent and minimise the temperature losses to the environment. The temperature difference between the cooling unit and the IR cell is maintained about ± 2 °C. A cell set up for variable temperature experiments and flow channel system was shown in Figure 2.9.

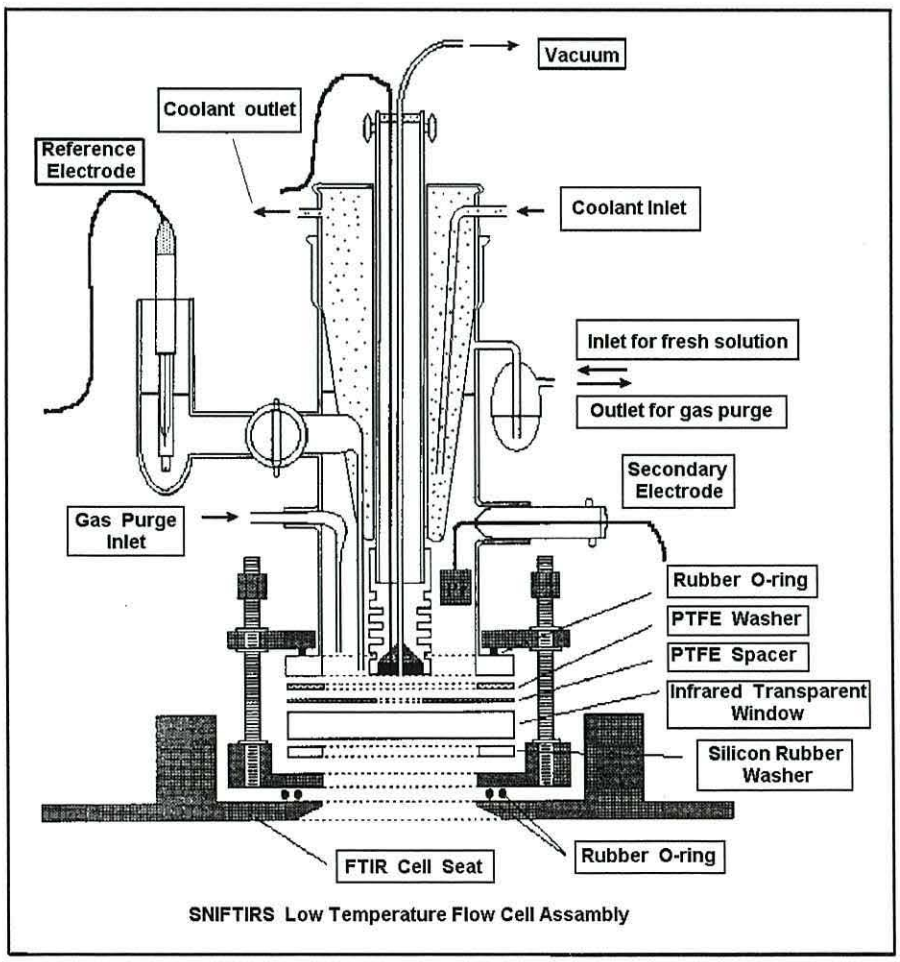

Figure 2.9: Variable temperature *in situ* FTIR measurement cell set up

As mentioned earlier a thin layer of the electrolyte is required to perform the *in situ* measurement. A typical thin layer of supporting electrolyte is formed when a flat working electrode is pushed against the IR transparent window. A thickness of 5-10 μm of thin layer will form in between them and this is considerably good thickness to minimise the absorption of the incident radiation by solvent and supporting electrolyte (Figure 2.10). To maintain the thickness of the thin layer, a good seal from the glass electrode holder and the body cell syringe barrel must be obtain by wet seal with the supporting electrolyte solution.

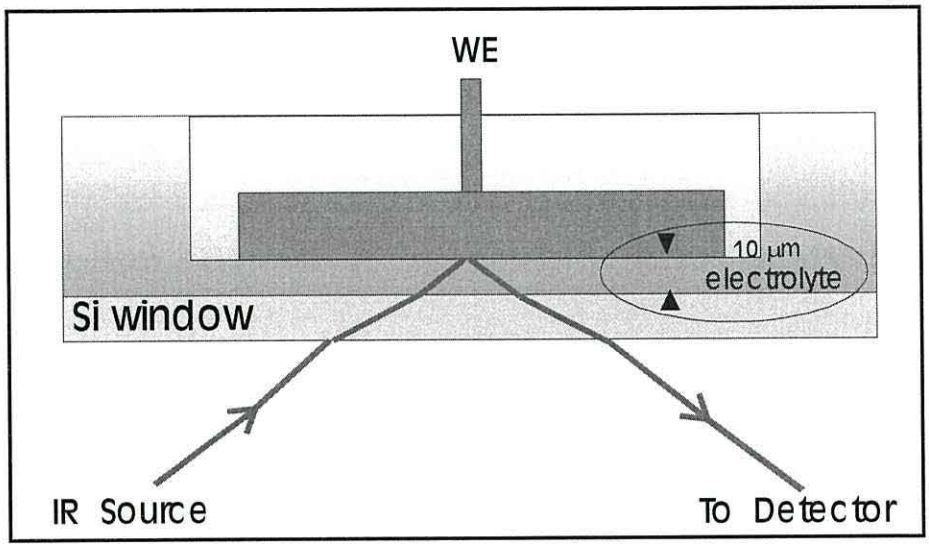

Figure 2.10: An electrolyte thin layer for the *in situ* measurement

By putting an open circle cut TPFE spacer with 0.005 mm thickness between the window and the working electrode, a thin layer flow channel can be formed. A rapid replenish of the electrolyte thin layer together with it components can be achieved by sucking them out of the cell from the centre of the flow-cell electrode using a water vacuum system.

2.5 Experimental details

2.5.1 Cyclic Voltammetry

Cyclic voltammetric runs were made at room temperature, 18 °C or at low temperature, 0 °C under an Ar or N_2 atmosphere using a Hi-Tek DT-2101 potentiostat and PP-R1 waveform generator as shown in Figure 2.11. All voltammograms were recorded onto a conventional analogue X-Y recorder. A new fresh mirror-polished disc electrode and supporting electrolytes were used for each run. For the mechanically polished electrode the pre-treatment procedure was done by the working electrode at 0.1 Vs^{-1} between applied potential of -1.1 V and -0.7 V so that oxide layer on the electrode surface is reduced.

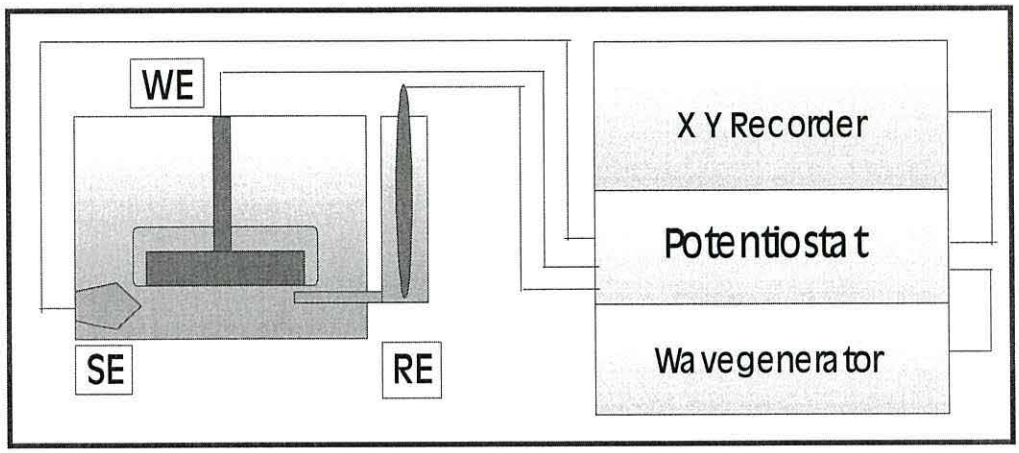

Figure 2.11: Schematic diagram for cyclic voltammetry measurements

Another advantage of doing this treatment is that the physical stress produced by the polishing technique at the electrode surface is relieved and thus it is possible to restore the physical condition of the electrode surface [20, 21]. This treatment allowed establishing a stable and reproducible starting conditions of the electrode throughout each experiment. The voltammogram was measured by applying the potential within the working range limit of the solution system at copper electrode (-1.5 V to 0 V) at different scan rate. For electrochemical polished electrode, the electrode is polarised at -1.5 V for 3 min in the electrolyte solution at current densities of 2.8 Acm^{-2} prior to the measurements as suggested by Hori *et al.* [22].

2.5.2 Electrochemical Impedance Spectroscopy

The impedance measurements were performed using the same three electrodes cell as that used for the voltammetric measurements. Both the cell and the potentiostat (home build) were placed inside a Faraday cage as shown in Figure 2.12. A Solatron 1170 frequency respond analyser (FRA) was used for all EIS measurements. The impedance spectra were measured from low to high frequency range of 0.1 Hz to 10 kHz, taking ten points per decade. The measurement is fully computer controlled. The amplitude of the superimposed ac signal was 10 mV in order to avoid non-linearity effects. The position of working, counter (Pt) and reference electrodes (SCE) were placed as close as possible to each other to avoid an increase in resistance between the electrodes during the impedance measurement. The connecting cables were as short as possible to reduce resistance. Impedance data was stored and manipulated by Microsoft Excel software. Impedance

data (Nyquist plot) were plotted using ZView software (Solatron). An additional data analysis was also performed using Boukamp's electrical circuit software [23].

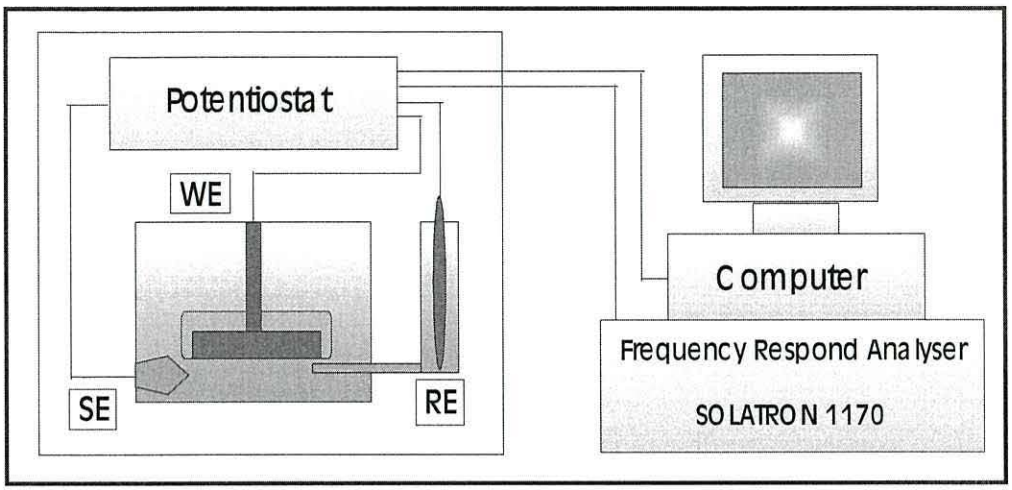

Figure 2.12: Schematic diagram for EIS measurements

2.5.3 *In situ* FTIR

Figure 2.13 shows the schematic diagram of the IR set up used in this work. All the IR measurements were performed using electrochemical polished electrode. The spectral measurements were performed in a staircase mode using a fully evacuated FTIR spectrometer (Bruker IFS-113V) fitted with a mercury-cadmium-telluride (MCT) photoconductive detector cooled at 77 °K (using liquid nitrogen), *p*-polariser and Ge/KBr beam splitter. The operation of spectrometer is computer controlled running under OPUS 3.0 software. The optics bench is fully evacuated. Removal of water vapour and CO_2 is necessary since these exhibit strong IR absorbance. The evacuation of the spectrometer

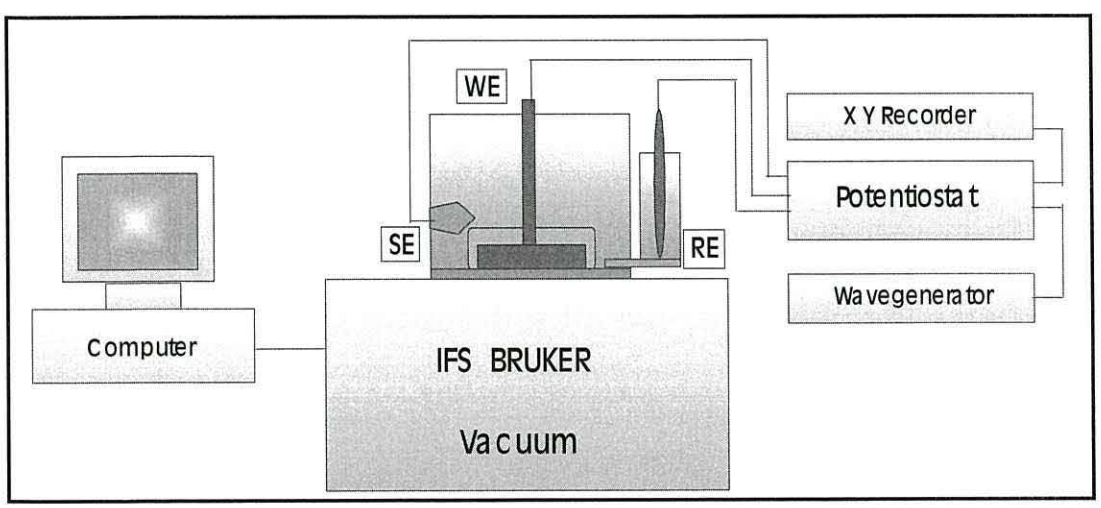

Figure 2.13: Schematic diagram of IR *in situ* measurement

bench produces a significant improvement in the interferometer stability and firmly holds the cell as well as removing atmospheric component absorption from the spectra. The spectrometer consists of four distinct modules: IR source, interferometer, sample and detector modules. The source module contains two broad bands infrared sources; silicon-carbide source (6000 –100 cm^{-1}) and a mercury lamp (700-10 cm^{-1}). A choice of four apertures is available and these can be selected under automatic control. Medium resolution (4) is sufficient for SNIFTIRS experiment and this is attainable throughout the mid-IR region, with a maximum aperture of 10 mm diameter and medium scanner speed of 6 kHz/sec. SNIFTIR spectra collection was performed at 200 scan in a staircase mode. The potential, either generated by Hi-Tek DT-2101 potentiostat and PP-R1 waveform generator, was changed by 100 or 50 mV during each step or from a custom written software for an interface digital to analogue converter, (DAC) which was run under OPUS 3.0 which enable voltage 'steps' to be programmed. The DAC conveys a programmed voltage sequence to the potentiostat (HI-TEK DT2101). A time delay can be introduced after any change in voltage and before the collection of spectra is started, in order to allow the electrochemical system to reach a stable semi-steady state.

The same cell design was used for the flow cell electrode experiment (Figure 2.9), which was performed in order to allow the replenishment of the thin layer. A thin Teflon separator was placed between the silicon window and the working electrode. A round shape with a diameter of 0.8 cm was cut from the centre of the separator (PTFE, 0.005 mm thickness). Another small vertical cross cut (1.5 cm long) was made across the centre of the circle to allow the electrolyte flow from the bulk solution to the thin layer. After the working electrode was pushed toward the silicon window, the working electrode rested on the inner circle border of the separator and thus creating two small channels of the thin layer with a fixed thickness. The electrolyte or reactant solution flowed freely through the small channel to the thin layer after the vacuum was applied through the small tube, which was attached to the centre of the working electrode. By maintaining the vacuum flow, the solution was sucked out from the cell while maintaining the thickness of the thin layer, thus maintaining the reactant concentration in the thin layer.

2.6 References

1 R.J. Gale, (Ed.) "*Spectroelectrochemistry: Theory and Practice*" Plenum Press, London (1988)

2 P.A. Christensen and A. Hamnett, "*Techniques and Mechanisms in Electrochemistry*", Blackie Academic and Professional (1994)

3 A. Bewick and S. Pons, in "*Advances in infrared and Raman Spectroscopy*" Vol. 12, Chp.1, R.J.H Clark and R.E. Hester (Eds.) Wiley-Heyden, London (1985)

4 G.A. Somorjai, "*Introduction to Surface Chemistry and Catalysis*", John Wiley & Sons Inc., New York (1998)

5 R.J. Nichols, in "*Adsorption of Molecules at Metal Electrode*", Chp. 7, Series: Frontiers in Electrochemistry, P.N. Ross and J. Lipkowski (Eds.), VCH Publication Inc. (1992)

6 M. Kalaji and R.J. Nichols, *Chemistry in Britain,* 33 (1997) 40

7 A. Bewick, K. Kunimatsu and S. Pons, *Electrochim. Acta,* 25 (1980) 465

8 A. Bewick, S. Pons and K. Kunimatsu, *Surf. Sci.*, 101 (1980) 131

9 R.S. Nicholson, *Anal. Chem.,* 37 (1965) 1351

10 R.G. Greenler, *J. Phys. Chem.,* 50 (1959) 1963

11 J.D.E. McIntyre and D.E. Aspnes, *Surf. Sci.,* 24 (1971) 417

12 A. Bewick, K. Kunimatsu, B.S. Pons and J.W. Russell, *J. Electroanal. Chem.,* 160 (1984) 47

13 C.H. Hamann, A. Hamnett and W. Vielstich, "*Electrochemistry*", Wiley-VCH, N.York (1998)

14 R.M. Hexter and M.C. Albercht, *Spectrochim. Acta*, A, 35 (1978) 233

15 T. Davidson, B.S. Pons, A. Bewick and P.P. Schmidt, *J. Electroanal. Chem.,* 125 (1981) 237

16 S. Pons, T. Davidson and A. Bewick, *J Electroanal. Chem.,* 160 (1984) 63

17 A. Bewick and J.W. Russell, *J. Electroanal. Chem.,* 132 (1982) 329

18 M. Fleischmann, "*The Investigation of Electrode-Solution Interface by in-situ Methods*" in "*Advanced in Electrochemistry*", The Robert A. Welch Foundation Conferences on Chemical Research XXX, Houston (1986)

19 W.C. Mc. Tegart, "*The Electrolytic and Chemical Polishing of Metals*", Pergaman Press, London, (1959)

20 R.N. Adams, "*Electrochemistry at Solid Electrodes*", Marcel Dekker, Inc. New York (1968)

21 R.G. Compton and G.H.W. Sanders, "*Electrode Potentials*", Oxford Science Publication, Oxford (1995)

22 Y. Hori, R. Takahashi, Y. Yoshinami and A. Murata, *J. Phys. Chem.* B, 101 (1997) 7075

23 B.A. Boukamp, "*Equivalent Circuit*" (EQUIVRT – PAS), version 4.51, University of Twente (1989)

CHAPTER III

CO_2 reduction at polycrystalline copper

3.1 Introduction

3.1.1 Copper as an electrocatalyst

In the electrochemical reduction of CO_2 to hydrocarbons, copper exhibits significantly low overpotentials and high values of faradaic efficiencies [1]. The unique properties of a Cu in comparison with others metals such as Fe and Ni have been reported with reference to the selectivity and the distribution of the reduction products [2]. Cu electrodes selectively produce CO, which can be further reduced to hydrocarbons (CH_4, C_2H_4) and alcohols (C_2H_5OH, C_3H_7OH) [3] whereas Fe and Ni produce CH_4 and C_2H_4 in a small amount, where the distribution of the products is not affected by pH at the electrode surface [4]. Products such as CH_4, C_2H_4, C_2H_5OH, C_3H_7OH, CH_3CHO and C_2H_5CHO have been produced in aqueous hydrogen carbonate electrolytes at Cu electrodes with high faradaic efficiency and high current density at low temperature [5-7]. The reduction at low temperature in 0.1M KOH-methanol electrolytes, on the other hand yields carbon monoxide, formic acid, ethylene and methane. Under these experimental conditions, 56% faradaic efficiency has been observed for carbon monoxide formation, 23% for formic acid, and 10% for methane whereas 12% has been reported for the formation of ethylene by electrolysis at -2.2 V and at 0 ^{0}C [8].

3.1.2 Electrode treatment

The chemical and physical states of the surface of the electrode are known to influence the distribution of products during the reduction of CO_2 [9]. Various ways of Cu electrodes pre-treatment such as mechanical polishing, electrochemical polishing, etching with acids, ultrasonically cleaning and oxidation in air have been reported with each method yielding a drastic different product distribution. Heavily oxidised surfaces for instance, produce H_2 predominantly, while surfaces with a relatively large amount of metallic Cu give preferential CO production [10]. A surface with metallic Cu, Cu oxide and adsorbed oxygen had an enhanced activity for hydrocarbon production. The oxide film at the surface was gradually reduced to bare Cu metal with increasing electrolysis

time, resulting in a variation of the product distribution [9]. Significant performance differences were also found between rough and smooth surfaces and between thermally and non-thermally treated electrodes. A rough surface was much more active than a smooth one in terms of current efficiency and catalytic electrode life due to the reduction in the amount of poisoning species that block a roughened electrode surface. The presence of a large number of defect sites such as of kinks, steps and dislocations does not favour the adsorption of poisoning species [9, 10].

Several reports have pointed out that the activity of copper decreases due to the formation of poisoning species at the surface. The total current efficiency for hydrocarbon production (CH_4, C_2H_4) for instance, increased with electrolysis time during the first electrolysis stage and decreased afterwards [11]. Using surface enhanced Raman scattering (SERS) and time-dependent decay of the bands, Smith *et al.* [12] attributed the decrease in the efficiency of electrolysis to the formation of a poisoning species of copper oxide patina. Surface analyses [XPS and Auger electron spectroscopy (AES)] have been also performed on Cu electrodes following electrolysis to identify surface intermediates [13]. In addition to hydrocarbon formation, a poisoning process occurred, causing a deposit of a black film on the surface of the Cu cathode. XPS and AES studies indicated that the black film was graphitic C, probably due to the result of a side reaction, e.g. the reduction of CO_2 through formate and further reduce to graphite [13]. Therefore a tentative reaction mechanism for CO_2 reduction involving the reaction pathway of CO_2 to CO then to surface-bound formyl (Cu-HCO) which then turns to surface-bound methylene (Cu:CH_2) and finally converted to hydrocarbon products has been proposed instead.

3.1.3 Electrode deactivation

Deactivation of the electrode surface through the formation of the poisonous intermediate has prompted many researchers to find alternative methods of electrochemical reduction. A potential-pulsed technique developed for the electrochemical reduction of CO_2 on copper gave another insight into the reduction mechanism. When the pulsed method was applied, the total faradaic efficiency for the generation of hydrocarbons (φHc) of CH_4 and C_2H_4 reached approximately 65% at 10 °C [14]. Also, φHc increased with increasing reduction time in strong contrast with conventional potentiostatic electrochemical reduction in which φHc decreased drastically with the reduction time due to the poisoning effect of such intermediate products. This is probably due to surface

intermediates formed through the interaction between CO_2 and the thin oxide layer on a Cu electrode leading to CH_4 and to C_2H_4; the final product depends on the anodic reactions taking place during the anodic pulse period [14]. A periodic anodic activation procedure has been shown to enable high hydrocarbon yields to be maintained over prolonged electrolysis runs [15]. In pulsed technique, copper modified silver electrodes produced larger amounts of methane with φHc of 49% compared to pure copper electrodes with highest φHc obtained of 33 % [16, 17].

3.1.4 Aqueous CO_2 electrochemical reduction

Due to the factors and variables conditions discussed so far, a concordant result on the nature of the CO_2 electrochemical reduction mechanism in aqueous solution is still unclear especially at polycrystalline copper. Many reports suggested that CO_2 is initially reduced to adsorbed CO and further reduced to hydrocarbons and alcohols [18, 19]. Abundant numbers of reports have shown the presence of CO on transition metal electrodes during the CO_2 reduction. However, the generally accepted reduction mechanism is not suitable for explaining the specific behaviour of some electrodes such as Cu deposited on glassy carbon during the formation of CH_4 and C_2H_4. The reaction at this electrode is reported to proceed *via* the formation of weakly adsorbed CO_2 which react with electrochemically generated chemisorbed H. Subsequent reduction of this reduced species probably leads to bridged CO groups with can be desorbed to give either CO or reduced further to give CH_4 and C_2H_4 [20].

Most spectroscopic studies of the reduction of CO_2 at copper carried out in aqueous hydrogen carbonate or bicarbonate solutions, show that CO is present either as the product or as the intermediate before further reduction to other products. One or both types of adsorbed CO species, linear and bridged-bonded were identified from the observation from IRRAS [21, 22] and FTIR [23] spectra. Linearly adsorbed CO (2080 cm^{-1}) was observed at Cu below the potential of the cathodic charge transfer between -0.8 and -1.0 V (*vs.* SHE) and at 2040 cm^{-1} between -0.7 and -0.8 V (*vs.* SHE) [24]. Hori *et al.* observed that the electrochemical reduction of CO_2 on a Cu electrode produced two kinds of linear CO at 2100 cm^{-1} and 2000 cm^{-1} and that the band at 2000 cm^{-1} showed a large frequency shift with potential. Recent work on the reduction of CO_2 on polycrystalline copper did not report any reduction products; the reason for this was that CO_2 is mainly lost through the carbonate route [25]. In the present study, the electrochemical reduction of CO_2 on polycrystalline copper in phosphate buffered solution is examined using *in situ* Fourier

Transform Infrared Spectroscopy. The unusual behaviour of a reduced-carbon dioxide in a phosphate buffer solution as a function of potential and polarisation time was studied.

3.2 Experimental

Electrochemically polished copper electrodes used throughout this work were cathodically protected by applying a negative potential immediately after its immersion into degas buffered phosphate solution (pH 6.8). A reducing potential close to or at the hydrogen evolution potential was applied for few minutes before the cyclic voltammetry measurements in order to remove any oxides or hydroxides from the surface. Nitrogen gas was bubbled through the solution between the experiments and passed over the electrolyte quiescently during experiments. For the reduction experiments, CO_2 was bubbled for 15 minutes to prepare CO_2-saturated solutions.

3.3 Result and discussion

3.3.1 Studies in hydrogen carbonate solutions

3.3.1.1 Cyclic voltammetry

The electrochemical behaviour of Cu, mainly at positive potentials, has been the subject of numerous investigations, and extensive lists of references to earlier studies can be found, among others, in the work of Shoesmith *et al.* [26, 27], Strehblow and Titze [28], Lenglet *et al.* [29] and Drogowska *et al.* [30 - 32]. The oxidation of metallic copper is complex as both soluble and insoluble products are involved and three different oxidation states, Cu(0), Cu(I) and Cu(II), may be produced depending upon the pH of the solution and the potential applied. The assignment of the oxidation and the reduction peaks for the electrochemically formed species was mainly based on current-potential response of voltammograms obtained. Figure 3.1 shows a voltammogram of polycrystalline copper electrode in an aqueous $KHCO_3$ solution, (0.1 mol dm^{-3}, pH 9.2) as the electrode potential is swept from negative to positive potentials and then back to the initial negative potential. The electrochemical behaviour of copper in alkaline solutions has been reported elsewhere in detail [26-35]. In general the anodic peak, A_1 is related to the formation of hydroxide and/or oxide film of Cu(I), CuOH and or Cu_2O. Further oxidation of copper at more positive potentials leads to the formation of oxide or hydroxide of Cu(II), CuO, $Cu(OH)_2$ at A_2 [36]. The standard potential, E^{θ} of copper oxide, CuO formation is 0.46 V (*vs.* SHE) and it has been suggested that the copper oxide layer has, in general, a duplex structure made up of inner Cu_2O layer followed by CuO and then a $Cu(OH)_2$ layer, depending on the

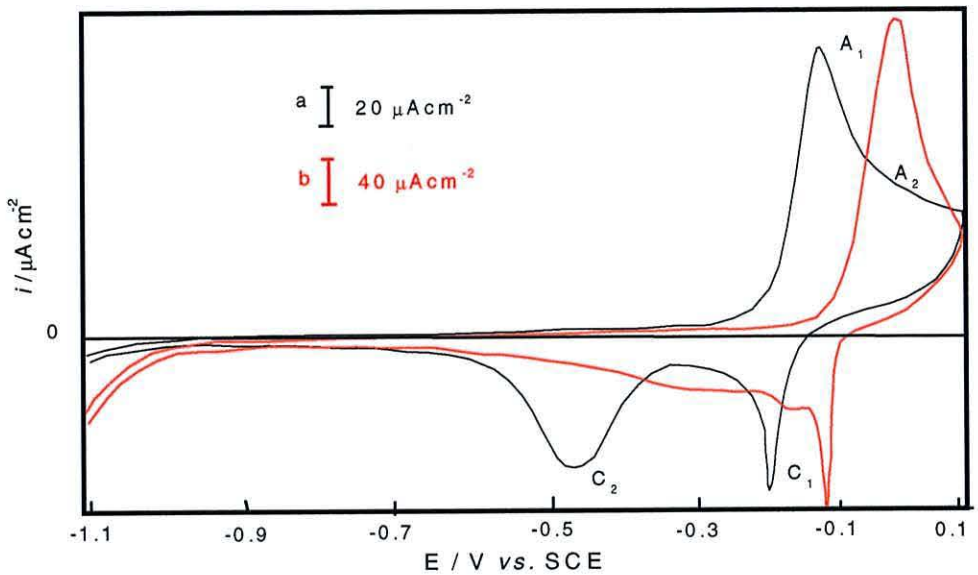

Figure 3.1: Voltammogram of copper in $KHCO_3$ (0.1 mol dm^{-3}, pH 9.2) at 18 ^0C for ν= 0.05 Vs^{-1}; (a) N_2 and (b) CO_2–saturated solution.

electrode potential [36]. However by combining cyclic voltammetry and probe beam deflection measurements, Brisard *et al.* [37] reported that in KOH solution (pH 12), $Cu(OH)_2$ is a stable species that was formed after the formation of a Cu_2O layer. In fact the authors suggested that $Cu(OH)_2$ is a film that grows continuously on the Cu_2O intermediate layer. Nevertheless, in the present study, the copper surface is possibly being passivated in hydrogen carbonate (pH 9.2) by the CuO layer. This mechanism has been proposed by Drowgoska *et al.* for the passivation of Cu surface by CuO in alkaline solution (pH 8.5) as follow [33, 35].

$$Cu_2O + 2OH^- \rightarrow 2CuO + H_2O + 2e^-$$

On the reverse sweep from 0.1 V to –1.1 V, the reduction of copper oxides occurs at about –0.21 V (C_1) and –0.48 V (C_2).

When the aqueous solution of $KHCO_3$ is saturated with CO_2 (Figure 3.1b), the same behaviour is observed. The major difference is where the oxidation and the reduction waves are positively shifted about 0.1 V. This is due to the drop in the pH of the solution (about 2.7 unit) to 6.5 after saturation with CO_2; this also leads to a positive shift in the onset of hydrogen evolution. No apparent peaks can be attributed to the reduction or adsorption of CO_2 in the voltammogram. However, this does not exclude the possibility that the reduction might occur within the hydrogen evolution region. Furthermore, the

charge of the oxidation peak is increased. This implies that the pH of the electrolyte plays an important role for the formation of oxide/or hydroxide forms of copper and thus increases the intensity of anodic peaks.

3.3.1.2 *In situ* FTIR

Figure 3.2 shows the SNIFTIR spectra obtained as the potential of the electrode, initially set at –1.1 V and held for 30 sec for current become stable, was varied in a staircase mode (0.1 V/step) towards 0 V in a N_2-saturated hydrogen carbonate solution (0.1 mole dm^{-3}) as shown in scheme A (Figure 3.3). The spectra are normalised relative to a reference potential, E_{ref} of –0.6 V. The main features in the spectral region below 2400 cm^{-1} are the evolution of the positive band at 1650 cm^{-1} and the negatives bands at 1389 and 1072 cm^{-1}. A broad positive absorbance band centred at 3220 cm^{-1} is also observed. The main features that are centred at 3220 and 1650 cm^{-1} are attributed to the OH stretching and bending modes of water respectively. The bands observed at 1389 and 1072 cm^{-1}, can be attributed to ν_s OCO and νC=O for adsorbed CO_3^{2-} [38]. The bands further disappear, as

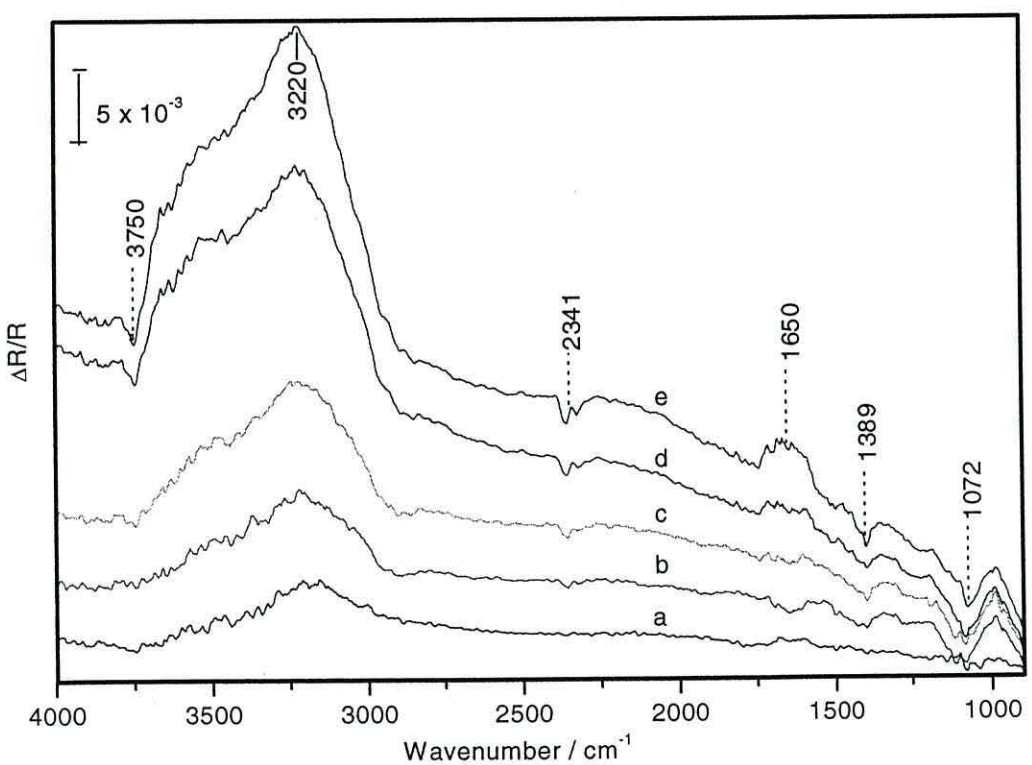

Figure 3.2: SNIFTIR spectra obtained from copper in N_2-saturated hydrogen carbonate (0.1 mol dm^{-3}) solution as the potential was varied in staircase mode. Spectra shown are from (a) –0.7 V to (e) –1.1 V in 0.1 V per step. The reference spectrum, E_{ref} was obtained at –0.6 V.

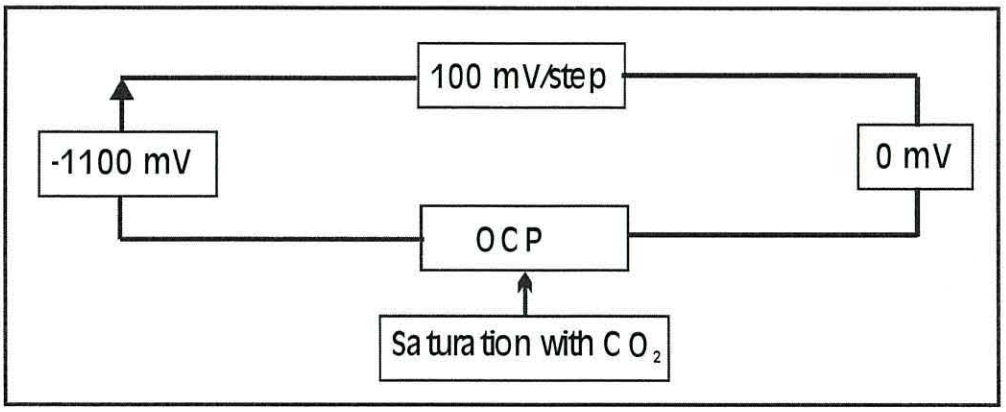

Figure 3.3: Scheme A used for evaluation of the reduction of CO_2

the potential is made more positive. It might suggest that the adsorbed monodentate CO_3^{2-} is more likely in this case due to one oxygen atom of carbonate bonded to the metal becomes less stable as the electrode surface becomes more positive. Whereas the bidentate carbonate with two oxygen atoms bonded to the surface, should show νC-O stretching at lower wavenumbers [39]. It is interesting to note that a band for dissolved CO_2 at 2341 cm^{-1} appears, as the potential is made more positive. This could imply that surface carbonate is transformed to CO_2 in very small amount at more positive potential as the electrode surface is oxidised.

Figure 3.4 shows the SNIFTIR spectra observed when the same solution is saturated with CO_2 and the same scheme A is repeated. The SNIFTIR spectra are normalised relative to E_{ref} of –0.6 V. The main features in the same spectral region are the bands at 2341, 1401, 1361, 1302 and 1116 cm^{-1}. The intensity of the positive band attributed to dissolved CO_2 (2341 cm^{-1}) increases, as the potential is made more negative. This indicates that $CO_{2(aq)}$ is being consumed at more negative potential. However it is interesting to note that the band at 1401 cm^{-1}, attributed to the asymmetric stretch, ν_{as}OCO of the free carbonate, and the bands at 1361 cm^{-1}, the symmetric stretch ν_sOCO group and at 1302 cm^{-1} (C-OH) bending of hydrogen carbonate respectively [39-41] appear and disappear with potential. The carbonate ions are formed at potentials more negative than –0.5 V. This coincides with the reduction peak C_2 in Figure 3.1. The bicarbonate ions are formed at less negative potential. As compared to the N_2-saturated bicarbonate solution, the presence of dissolved CO_2 plays a prominent role in the carbonate-bicarbonate equilibrium reaction as the pH changes. Nevertheless, according to these results, it can be assumed that hydrogen carbonate ions are transformed to carbonate ions,

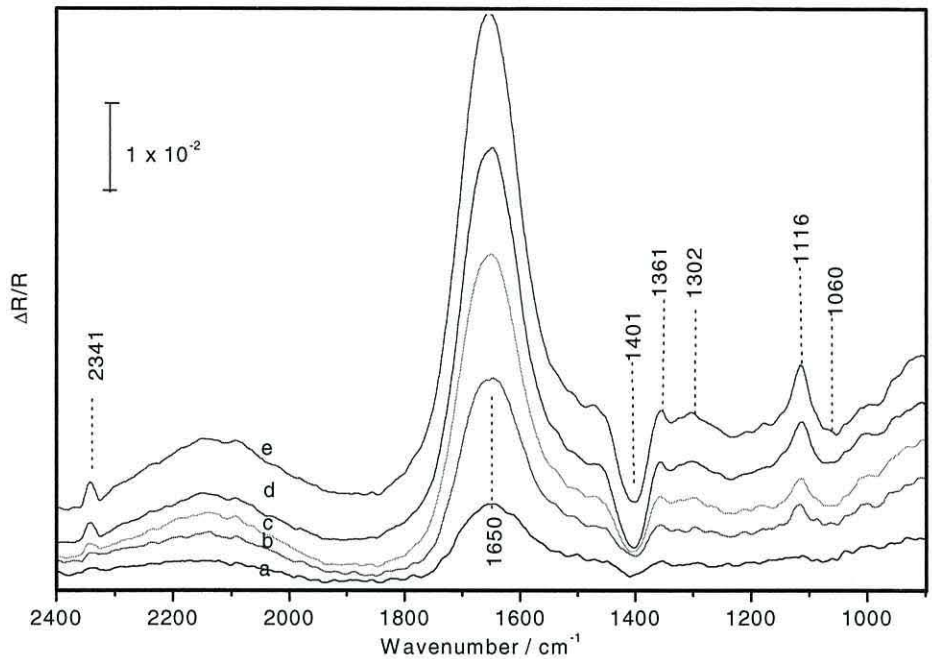

Figure 3.4: SNIFTIR spectra obtained from copper in CO_2-saturated hydrogen carbonate (0.1 mol dm^{-3}) solution as the potential was varied in staircase mode. Spectra shown are from (a) –0.7 V to (e) –1.1 V in 0.1 V per step; normalised relative to –0.6 V.

as the potential becomes more negative and carbonate ions are transformed to hydrogen carbonate ions as the potential becomes more positive. Further evidence for this interconversion has been clearly shown by experiments performed using isotopic labelled compound [25]. These results also indicate that CO_2 is transformed to carbonate and hydrogen carbonate ions rather than being involved in the reduction processes, as the potential is made more negative. This is in agreement with the CO_2-carbonate equilibrium process as follow:

$$CO_2 + H_2O \rightarrow H_2CO_3 \rightarrow H^+ + HCO_3^- \rightarrow CO_3^{2-} + H^+.$$

It is well know that as the potential approaches that of hydrogen evolution the solution in the proximity of the surface becomes more alkaline. As the pH of the solution increases, CO_2 will be converted to HCO_3^- and CO_3^{2-}. Both are inert at these potential. Therefore no reduction products are observed. This is in agreement with previous work reported by Hernandez and Kalaji [25]. The involvement of $CO_{2(aq)}$, apart from altering the pH as it enters in the acid-base equilibrium of carbonic acid-hydrogen carbonate-carbonate in other electrochemical reactions remained unclear at that stage.

The complete reduction of surface oxides and hydroxides may require negative overpotentials. Therefore, the reduction of CO_2 may not occur should the surface contain

anything else but pristine Cu. Therefore, the initial applied potential of -1.1 V for 0.5 minute could be the reason why the bands associated with the electrochemical reduction were not observed. However increasing the initial applied potential to –1.5 V (for 0.5 minute) failed to produce any spectroscopic evidence for CO_2 reduction (spectra not shown). Another possible factor that may help to ensure that the electrochemical reduction process occurs is the length of time after which the electrode is initially polarised in the presence of CO_2.

Therefore another approach was pursued in which the electrode was polarised at high negative potentials in the CO_2-saturated solution for 15 minutes whilst continuously bubbling CO_2 in the solution prior to spectral collection as shown in scheme B (Figure 3.5). It is interesting to note that a weak negative band appears at 1889 cm^{-1} and shifts with potential to 1920 cm^{-1} as shown in Figure 3.6. The SNIFTIR spectra are normalised relative to E_{ref} of –0.6 V. The shift in band frequency is an evidence for the existence of an adsorbed species [42, 43]. No such bands were observed when the same polarisation procedure was carried out in N_2-saturated solution (spectra not shown).

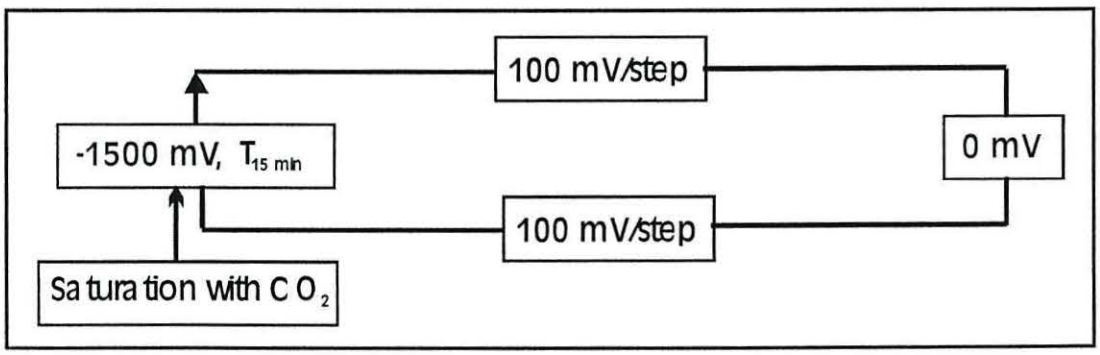

Figure 3.5: Scheme B used for evaluation of the reduction of CO_2

Adsorbed multi-bonded CO on Cu(111) has been reported by Hayden *et al.* [23] and by Raval *et al.* [41] to produce a band at 1830 cm^{-1}. However the band observed here is close to the value of bridge-bonded CO on polycrystalline platinum at 1860 cm^{-1} [42, 43] and on polycrystalline copper at 1885 cm^{-1} [44]. Therefore it can be assumed that the band at 1889 cm^{-1} in the present study is associated with the adsorbed bridge-bonded CO, $Cu\text{-}CO_B$ on polycrystalline copper. The result indicates that CO_2 is electrochemically reduced to CO in hydrogen carbonate solution. No bands can be attributed to an adsorbed CO_2 under these conditions; however, adsorbed CO_2 has been reported to be an electroactive species that is produced from the electrochemical dissociation of CO_2 on zinc oxide [45] and on Pt

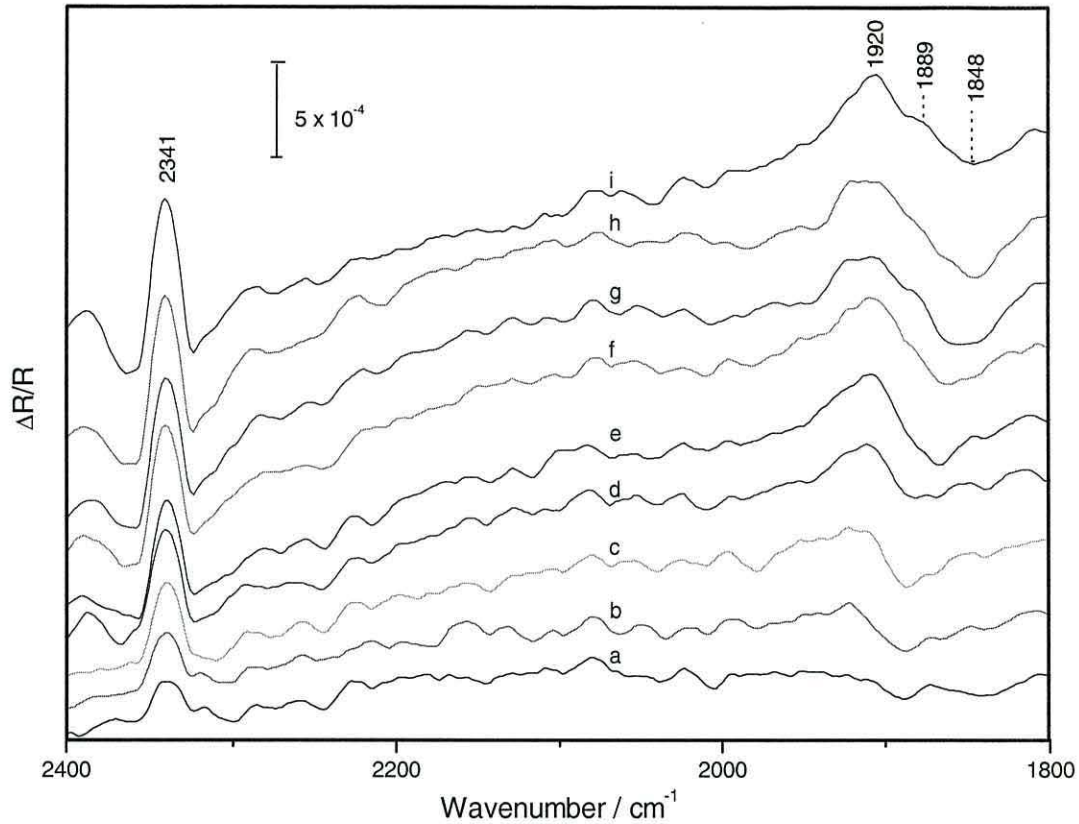

Figure 3.6: SNIFTIRS spectra obtained from a CO_2-saturated hydrogen carbonate (0.1 mol dm^{-3}) solution as the copper surface was polarised at –1.5 V for 15 minutes. Spectra shown are from (a) –0.7 V to (i) –1.5 V in 0.1 V per step; normalised relative to E_{ref} –0.6 V.

[46] as shown in the following equations:

$$CO_2 + e^- \rightarrow CO_2^{\cdot -}{}_{(ads)}$$

$$CO_2^{\cdot -}{}_{(ads)} + H_2O + e^- \rightarrow CO^{\cdot}{}_{(ads)} + 2OH^-$$

No evidence for this mechanism has been provided in the results discussed so far.

3.3.2. Studies in buffered phosphate solution

It is clear from the previous section that the control of pH is an important issue when discussing the reduction of CO_2. The loss of CO_2 through the carbonate route is a consequence of this. Two methods were used to control the pH in the thin layer: the use of a flow cell and buffering the solution. The use of buffer solution such as phosphate buffer that can maintain the pH in the thin layer during the electrochemical reduction is worth to try. Beside its better pH control, phosphate buffers do not exhibit any absorbance that may overlap with the carbonate-hydrogen carbonate system during SNIFTIRS measurements.

3.3.2.1 Voltammetry of copper in buffered phosphate solution

The electrochemical behaviour of copper in phosphate solution has been reported elsewhere [3, 25, 32, 34, 35]. In general, in N_2-nitrogen saturated buffered phosphate solution (Figure 3.7) an anodic wave corresponding to the formation of copper oxides and/or hydroxides of Cu(I) and Cu(II) is observed at about –0.12 V during the forward sweep from –1.1 V to 0 V. However there is no clear peak separation between the formation of oxide and hydroxide of Cu(I) and Cu(II) as was observed in hydrogen carbonate solution. On the reverse sweep from 0 V to –1.1 V, it is clear that the reduction of such oxides occurs at about -0.23 V. At low sweep rate, 0.005 V/s, the oxidation and the reduction peaks are much sharper than that at 0.05 V/s. The result shows that the oxidation and the reduction of copper surfaces may be a slow process. Hydrogen evolution HER commenced at potentials more negative than –1.0 V.

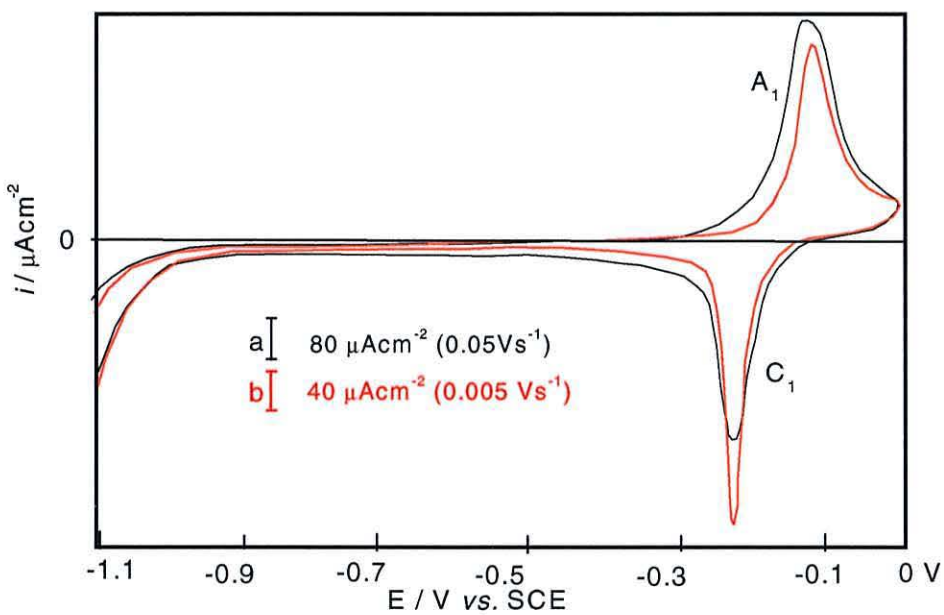

Figure 3.7: Voltammogram for copper at (a) v= 0.05 and (b) 0.005 Vs^{-1} in N_2 saturated phosphate buffered solution (pH 6.8) at 18 °C.

The effect of the anodic limit on the shape of the voltammograms is illustrated in Figure 3.8. The onset of the hydrogen evolution (not shown) was not affected by the positive potential limit. The current profiles in the positive direction (from –0.6 V) show a broad region with only one noticeable current peak, A_1 at -0.04 V, whereas during the negative sweep, one cathodic peak, C_1 at -0.16 to -0.18 V is observed. The broad anodic

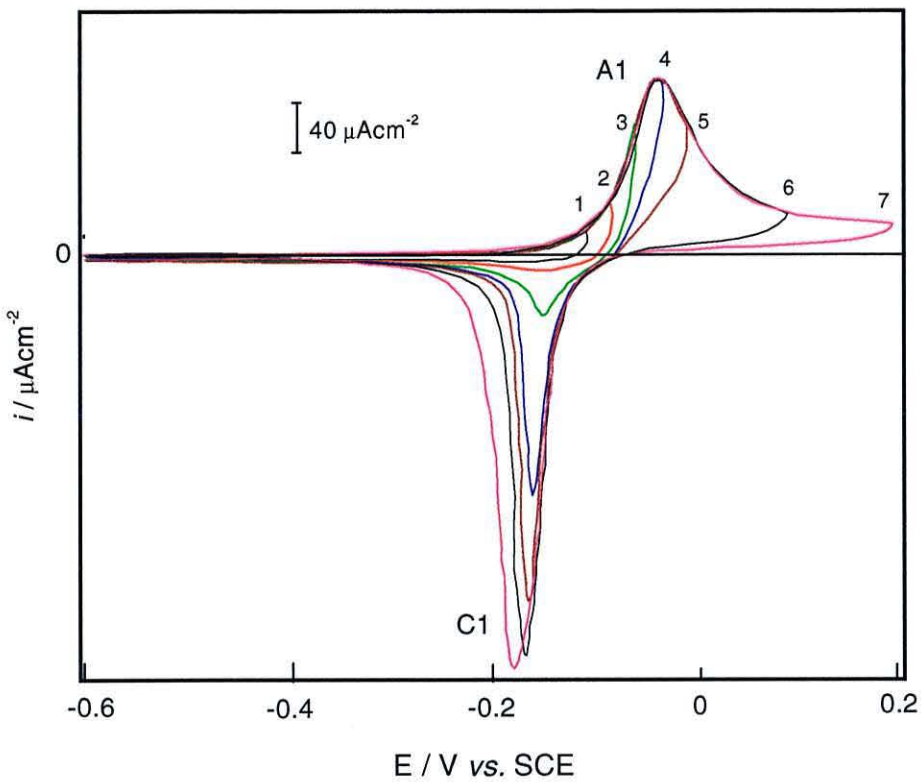

Figure 3.8: Voltammogram of copper at $\nu = 0.005\ Vs^{-1}$ in buffered phosphate solution (pH 6.8) at 18 °C. Potential range from (1) –0.6 to –0.1 V; (2) -0.6 to –0.075 V; (3) -0.6 to –0.05 V; (4) -0.6 to -0.025 V; (5) -0.6 to 0 V; (6) -0.6 to 0.1 V and (7) –0.6 to 0.2 V.

peak is due to the copper dissolution and anodic film growth [35]. The position and the charge of anodic current peak A_1 were maintained for several successive runs whereas the structure and the position of the cathodic peak depended on the positive potential limit. As the positive potential limit became more positive, the charge of the cathodic current increased, whereas the peak potentials shifted in the negative direction. The difference in shape between the anodic and cathodic peaks is most likely due to different reaction mechanisms. Therefore the oxidation is most likely to be diffusion controlled, whereas the reduction step is kinetically controlled. Such behaviour is known in electrochemical system such as the reversible conversion of Pb to $PbSO_4$ in sulphuric acid.

The charge density associated with the cathodic wave, Q_{red} was always smaller than the one associated with the anodic peak, Q_{ox}. This indicates a loss of copper species into the solution, possibly through copper species such as CuO or $CuHPO_4$. It is possible but unlikely that the difference in this value could be due to the accumulation of unreduced anodic film on the copper surface. However, since the voltammograms show a good

reproducibility on all subsequent anodic sweeps under repetitive cycling conditions, it can be concluded that any anodic film formed on the copper surface was easily reduced, possibly in quasi- reversible manner [47].

3.3.2.2 Voltammetry of CO_2 saturated phosphate buffer solution

The introduction of CO_2 into phosphate buffer solution has an impact on HER as well as the redox behaviour of copper. Figure 3.9 shows the difference in voltammetric behaviour between N_2-saturated and CO_2-saturated solution (Fig 3.9a and 3.9b respectively). It is interesting to note that HER occurs at very similar potential in the two solutions, which is in contrast to hydrogen carbonate solutions. This is due to the buffering effect of the phosphate solution, in which the pH drops by only 0.6 units upon saturation with CO_2. The oxidation of the Cu surface and the corresponding reduction of solution species and deposits is similar to that observed in hydrogen carbonate solutions; however, an asymmetry was observed here between Q_{red} and Q_{ox}; indication of a loss of soluble species to the bulk solution.

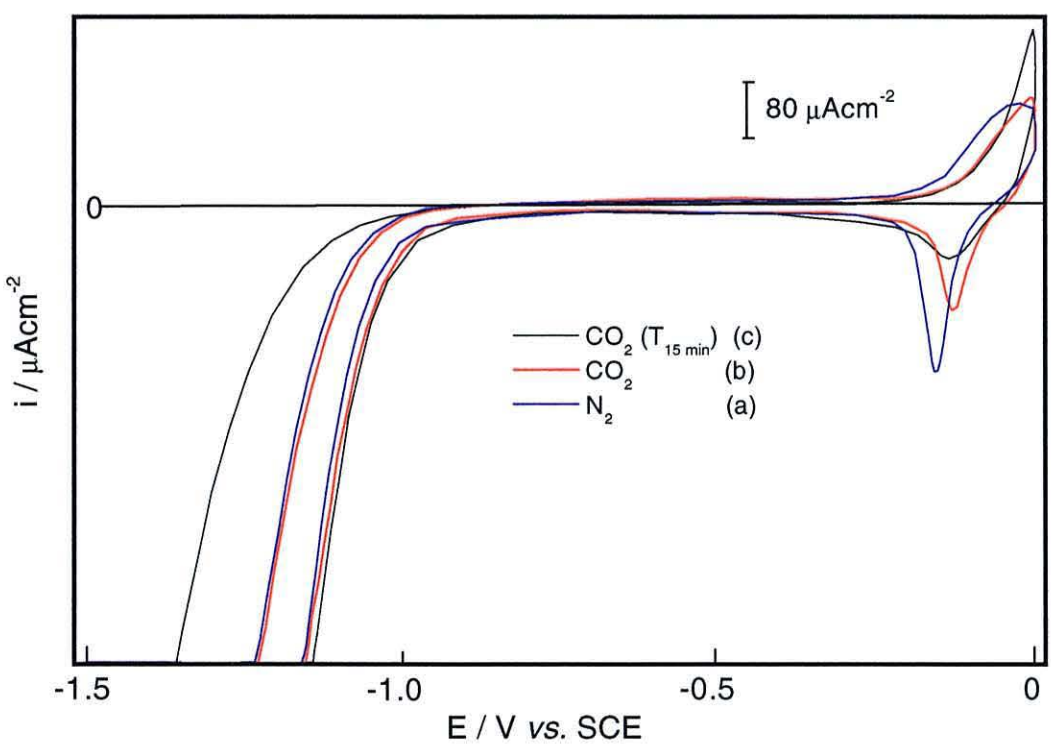

Figure 3.9: Voltammogram for copper at $\nu = 0.05\ Vs^{-1}$ in (a) N_2 saturated phosphate buffered solution, (b) CO_2 saturated without and (c) CO-saturated with polarisation at potential of –1.5 V for 15 minutes.

The average of the Q_{red}/Q_{ox} efficiency is about 70 % (Figure 3.9b). It is possible and likely that the different in this value could be due to the accumulation of unreduced anodic film on the copper surface, which is related to the formation of species that related to the oxidation of copper species at anodic potential region. The formation of oxidised copper film (oxides and/or hydroxides) and soluble copper species result from the interaction of reduced-CO_2 species such as CO with oxidised copper also believed to occur at this potential. It is interesting to highlight that once the electrode was first polarised at negative potential, E_{pol} of –1.5 V for 15 minutes prior to the voltammogram measurement, the average of the Q_{red}/Q_{ox} efficiency decreases dramatically to about 30 % (Figure 3.9c). It indicates that the formation of soluble copper species increased at anodic potential dramatically due to the polarisation of the electrode surfaces at high negative potential.

3.3.3 *In situ* FTIR

3.3.3.1 SNIFTIR spectra of N_2-saturated buffered phosphate solution

It is important to be able to distinguish the background spectrum of the electrolyte from that of the electroactive species. Therefore the SNIFTIR spectra of the phosphate solution in responses to potential changes were recorded. Figure 3.10 shows the SNIFTIR spectra

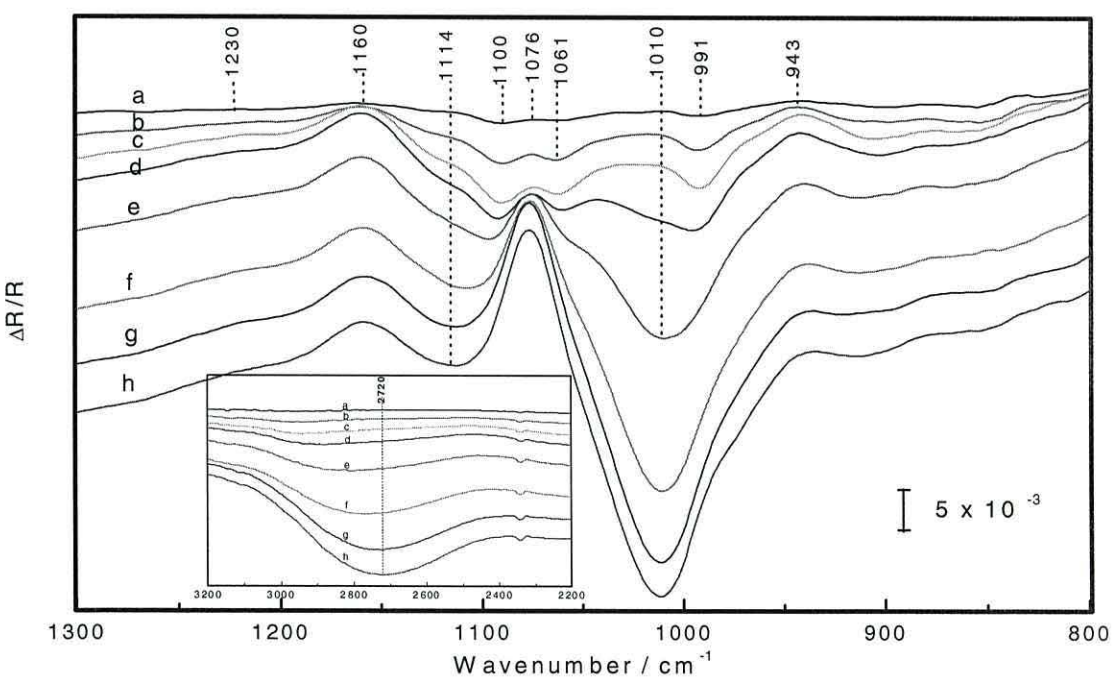

Figure 3.10: SNIFTIR spectra obtained from N_2-saturated buffered phosphate solution as the potential was varied in staircase mode. Spectra shown are from (a) –0.8 V to (h) –1.5 V in 0.1 V per step. E_{ref} = –0.7 V.

of the phosphate buffer solution in N_2-saturated. Table 3.1 shows the vibration mode and infrared frequency region for phosphate ions as comparison [48, 49, 50].

Species	Vibration mode	Wavenumber (cm^{-1})
PO_4^{3-}	$\nu P\text{-}O_3$	1004
ads. sp		1060-1083
HPO_4^{2-}	$\nu P\text{-}O_2$	1076, 988, 862
ads. sp		1000*
$H_2PO_4^-$	$\delta P\text{-}O\text{-}H$	1230, weak
	$\nu_{as}P\text{-}O_2$	1159, strong
	$\nu_sP\text{-}O_2$	1072, strong
	$\nu_{as}P\text{-}(OH)_2$	947, strong
	$\nu_sP\text{-}(OH)_2$	878, strong
ads. sp	$P\text{-}O_2$	1100 *, 1120**
	$P\text{-}(OH)_2$	980 *, 1000**

Table 3.1: Vibration mode frequency of phosphate ions; source * [48], ** [49], [50].

The positive bands at 1160 cm^{-1} (ν_{as}- PO_2), 1076 cm^{-1} (ν_s-PO_2) and 943 cm^{-1} (ν_{as}-$P(OH)_2$) correspond to the depletion of monobasic phosphate, $H_2PO_4^-$ whereas negative bands at 1061 cm^{-1} (ν_s-PO_2) and 991 cm^{-1} (ν_s-$P(OH)_2$) correspond to the formation of dibasic phosphate, HPO_4^{2-} as the potential becomes more negative [49, 50]. The main negative band at 1010 cm^{-1} (ν_s-PO_3) can be assigned to the formation of tribasic phosphate, PO_4^{3-} as HPO_4^{2-} is deprotonated, as the potential is made more negative. Consequently, a broad negative band at 2720 cm^{-1} appears as the potential becomes more negative. It is attributed to the OH stretching for the hydrogen bonding that forms between H_2O molecule and PO_4^{3-} [49].

Figure 3.11 shows scheme C at which the SNIFTIR spectra in CO_2-saturated phosphate buffered solution (Figure 3.12) were obtained as the initial potential at –1.5 V was stepped towards positive 0 V. The spectra are normalised relative to E_{ref} –0.6 V. The spectra obtained are similar to those obtained in CO_2-saturated hydrogen carbonate

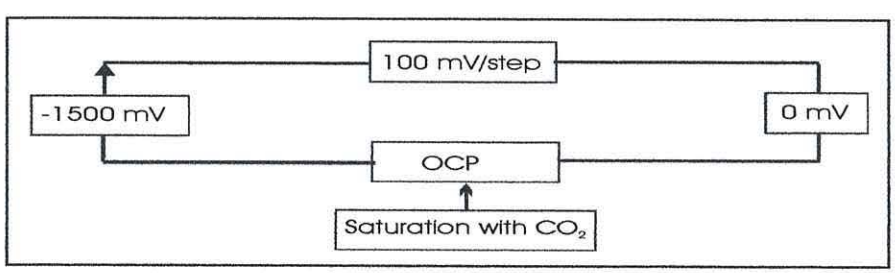

Figure 3.11: Scheme C used for evaluation of the reduction of CO_2

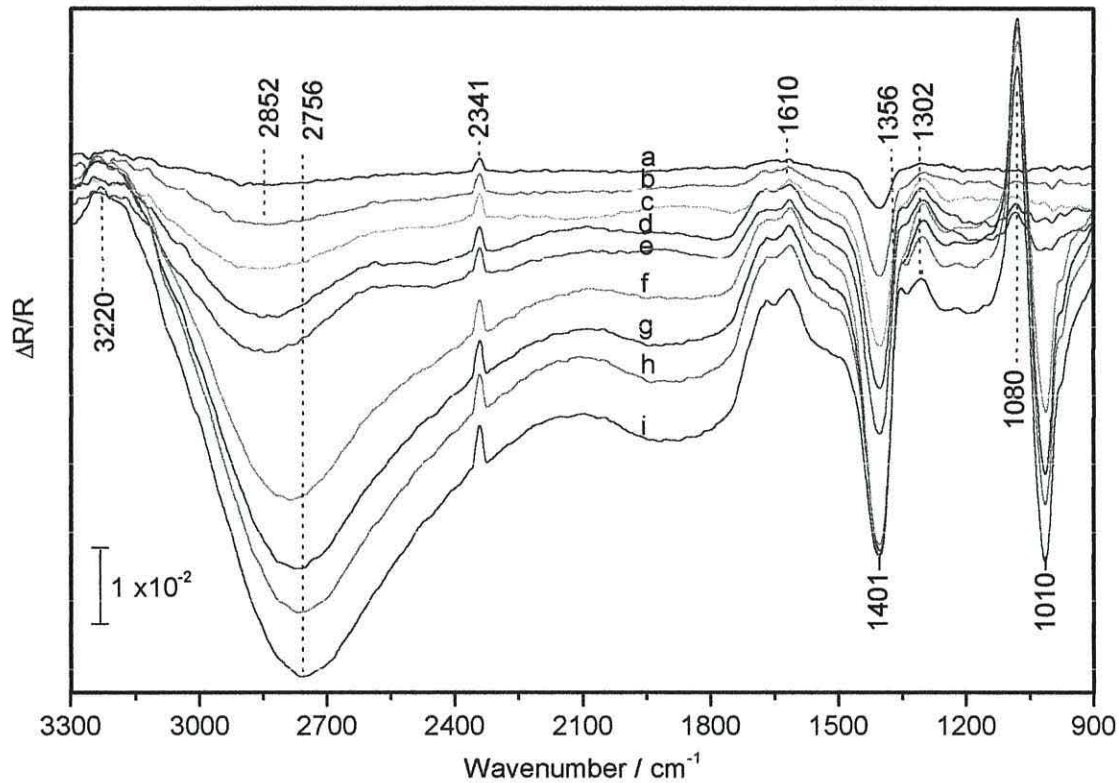

Figure 3.12: SNIFTIR spectra obtained from copper in CO_2-saturated buffered phosphate solution as the potential was varied in staircase mode. Spectra shown are from (a) –0.7 V to (i) –1.5 V in 0.1 V per step. E_{ref} = -0.6 V.

solution, except for the bands due to the phosphate species. HCO_3^- (1356 and 1302 cm^{-1}) and CO_3^{2-} (1401 cm^{-1}) bands appear with potential. Carbonate initially formed at potentials that are more negative and then converted to bicarbonate as the potential becomes less negative, as the carbonate ions involve in the protonation process. Up to this stage, the fate of CO_2 during the cathodic polarisation of the copper electrode is still unclear as the main compounds involved are those associated with the hydrogen carbonate/carbonate equilibrium. The broad band centred at 2852 cm^{-1} corresponds to OH stretch of water H-bonded to anions. At less negative potential, the orientation of water molecule at the electrode surface bounds through an oxygen atom [51]. This orientation cause the hydrogen atoms pointing away from the surface and this will induce the formation of H bonding with anion such as carbonate. As the potential becomes more negative, water bonds on the electrode surface through hydrogen atoms. An excess negative charge on water will promote oxygen atom pointing away from the surface and thus enable the formation of hydrogen bonding with surrounding anions containing

hydrogen such as phosphate. The band at 2756 cm^{-1} is consistence with the band observed for OH stretch of hydrogen bond of water-phosphate couple, as compared to that spectra in N_2-saturated solution where a broad band centred at 2720 cm^{-1} as shown by insert figure in Fig 3.10 which is associated with OH stretch of hydrogen bonded water-phosphate couple [49]. The 2852 cm^{-1} band shifts toward lower frequency as the potential becomes more negative. This may indicate that the OH stretch of hydrogen bonded in water-phosphate couple is more predominant than water-carbonate couple at more negative potentials due to the predominant water orientation [51].

3.3.3.2 Cathodic polarisation effect

Again it is interesting to highlight that when the electrode was polarised at high negative potential of –1.4 V for about 15 minutes while CO_2 was continuously bubbled in the solution (adopted scheme B in Figure 3. 5). The same band as in the case hydrogen carbonate solution was observed at 1898 cm^{-1} at –1.4 V and shifted with potential. The SNIFTIR spectra are shown in Figure 3.13, as the spectra are normalised relative to –0.7 V at 0 °C. Again, when the same procedure was repeated in N_2-saturated solution, the band was not observed. This indicates that the band is associated with the reduced-CO_2 species, which is produced during the cathodic polarisation process. This species also believed

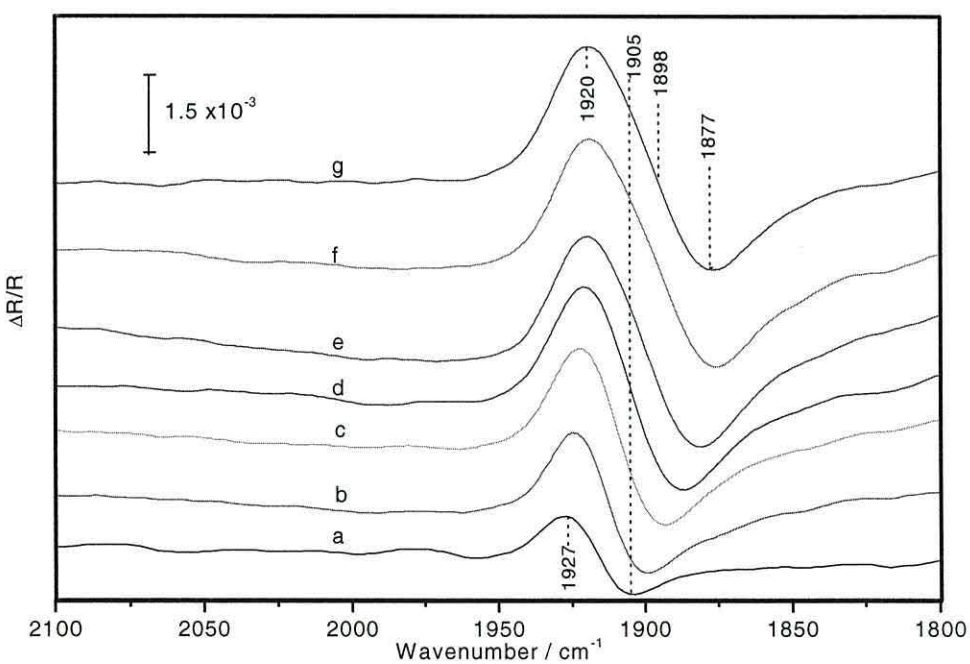

Figure 3.13: SNIFTIR spectra obtained from continuous CO_2 bubbling in buffered phosphate solution as the copper surface was polarised at –1.4 V for 15 minutes at 0 °C. Spectra shown are from (a) –0.8 V to (g) –1.4 V in 0.1 V per step. E_{ref} = –0.7 V.

responsible for the depression of the hydrogen evolution region as shown in voltammogram in Figure 3.9c, is most likely to be adsorbed carbon monoxide. The band assignment will be discussed in more detail in next section. Figure 3.14 and 3.15 show the SNIFTIR spectra for CO_2-saturated phosphate buffered solution as the electrode surface was polarised at –1.5 V at room temperature (30 minutes) and 0 ^{0}C (10 minutes) respectively (adopted scheme B in Fig 3.5). The main feature observed at high negative

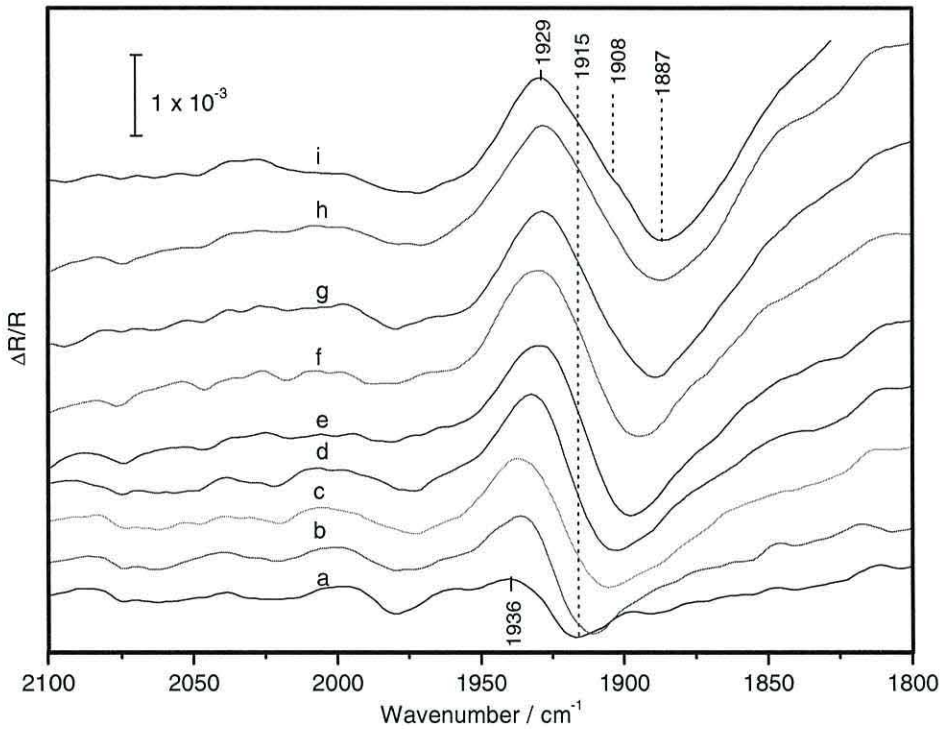

Figure 3.14: SNIFTIR spectra obtained from continuously bubbling CO_2 in buffered phosphate solution as the copper was polarised at –1.5 V for 30 minutes at room temperature. Spectra shown are from (a) –0.7 V to (i) –1.5 V in 0.1 V per step. E_{ref} = –0.6 V at cathodic sweep.

potentials is the band associated with the reduced-CO_2 species at 1908 cm^{-1} (18 ^{0}C) and 1891 cm^{-1} (0 ^{0}C). The band intensities are much higher at low temperature compared to those observed at room temperature solution. This is due to the increased solubility of CO_2 at lower temperature. This can also be observed from the transmittance values of single channel spectra for the CO_2 band at 2341 cm^{-1} which is 15 % higher at 0 ^{0}C at a potential of 0 V compared to that at 18 ^{0}C (spectra not shown). The difference in the band positions of adsorbed CO at different temperatures is related to the difference in polarisation time. This effect will be discussed in section 3.3.5. The band feature

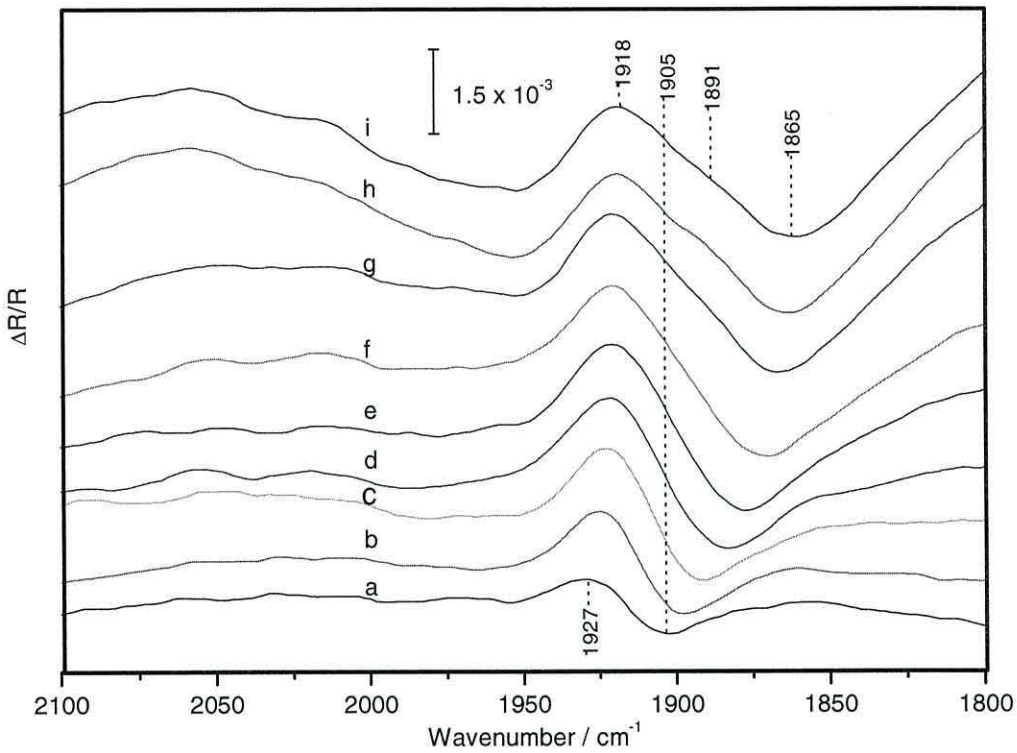

Figure 3.15: SNIFTIR spectra obtained from continuous bubbling CO_2 in buffered phosphate solution as the copper was polarised at –1.5 V for 10 minutes at 0 °C. Spectra shown are from (a) –0.7 V to (i) –1.5 V in 0.1 V per step. E_{ref} = –0.6 V.

becomes unipolar when the spectra are normalised relative to spectrum at –0.4 V of reverse sweep, which is the potential at which the surface is reduced. Figure 3.16 shows an example of such features as spectra in Fig 3.13 are normalised relative to E_{ref} = -0.4 V of reverse sweep. The adsorbed CO band position therefore can be determined accurately at 1881 cm^{-1} at –1.4 V.

3.3.4 Products of the electrochemical reduction of CO_2

3.3.4.1 Reduced-CO_2: linear-bonded adsorbed CO, Cu-CO_L

The results so far show that only one type of adsorbed CO (reduced-CO_2) is observed as bridge-bonded CO at frequencies lower than 2000 cm^{-1}. However it is known that adsorbed CO can exist at more than one binding site, namely linear-bonded and multi-bonded on the metal surface. To investigate whether CO of reduced-CO_2 can be observed at more than one binding site on polycrystalline copper, the influence of the holding time at the polarisation potential was investigated. The measurements were carried out at 0 °C to increase the solubility of CO_2. The holding time (polarisation time), $T_{hold\ min}$ at polarisation potential (E_{pol}) was varied from 0 to15 minutes in CO_2-saturated solution

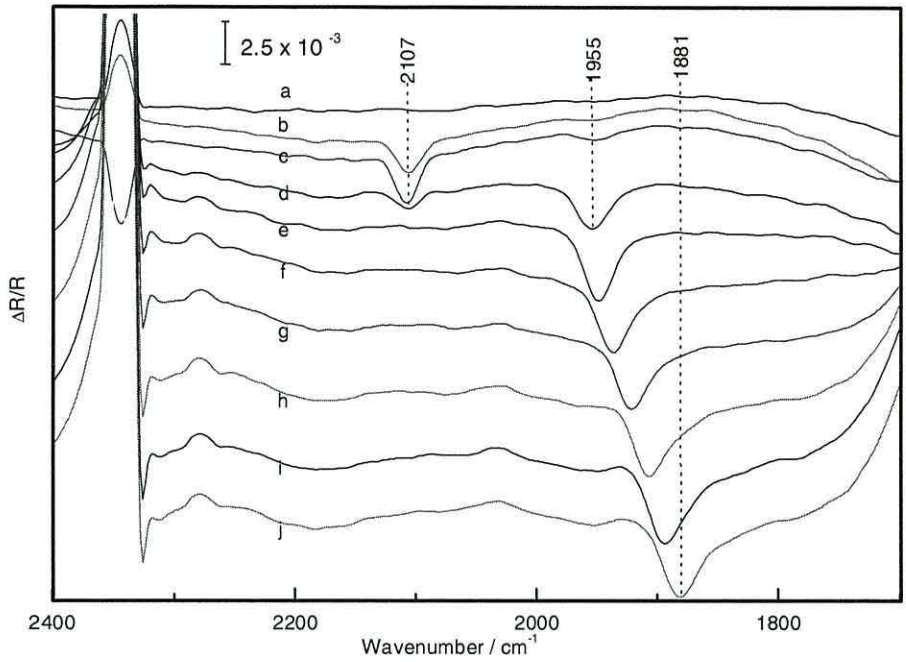

Figure 3.16: SNIFTIR spectra obtained from continuous CO_2-saturated buffered phosphate solution as the copper was polarised at –1.4 V for 15 minutes at 0 °C. Spectra shown are from (a) –0.3 V, (b) –0.1 V of reverse sweep, (c) 0 V to (j) –1.4 V of forward sweep in 0.2 V per step. E_{ref} = –0.4 V of reverse sweep.

(without further CO_2 bubbled) before the electrode was pushed against the IR window, adopted of scheme D in Figure 3.17. Figure 3.18 shows SNIFTIR spectra of the region of 2400 – 1800 cm^{-1} as the E_{pol} was held at –1.5 V for 10 minutes, $T_{10\ min}$. The main bands appear at 2341 cm^{-1}, 2082 cm^{-1} and weak band at 1860 cm^{-1} as spectra are normalised relative to –0.7 V. A positive going band at 2341 cm^{-1} of CO_2 in solution is consumed as the potential is changed to more negative potentials (spectra not shown). A negative band at 2082 cm^{-1} appears at high negative potentials of –1.5, -1.4 V and –1.3 V indicates that the band is produced at these potentials. The band shows slight frequency shifts to 2080

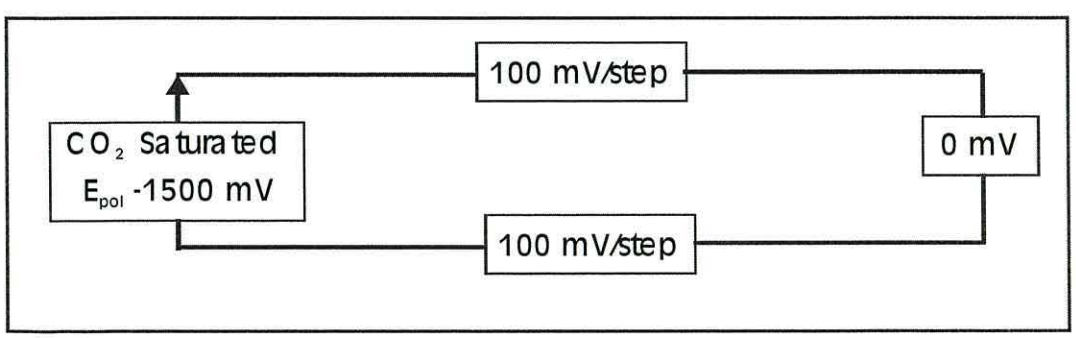

Figure 3.17: Scheme D used for evaluation of the reduction of CO_2

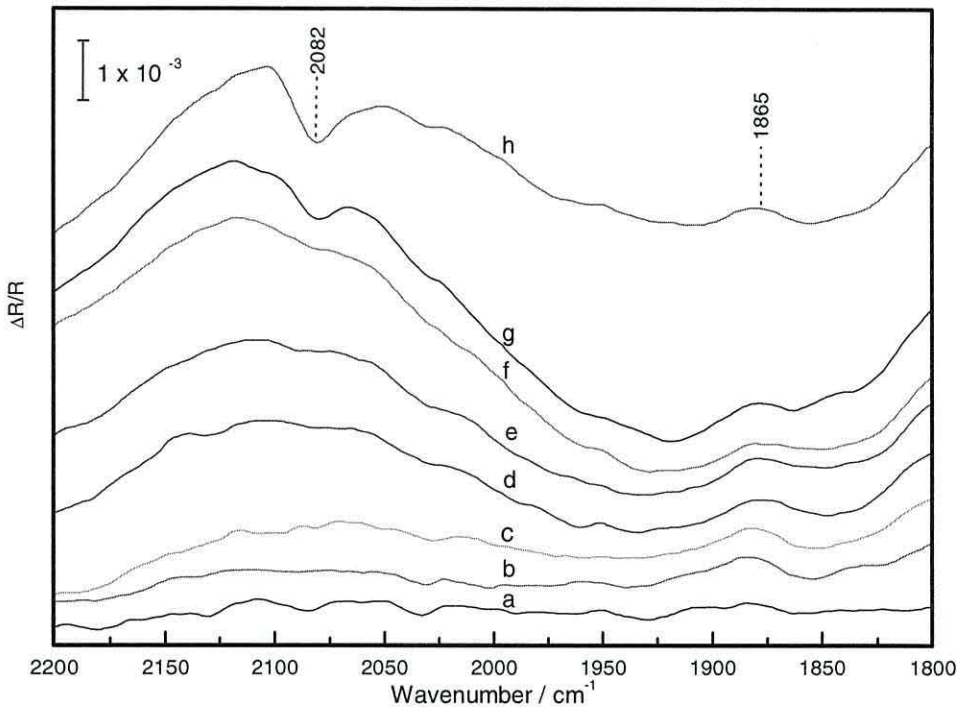

Figure 3.18: SNIFTIR spectra obtained from a CO_2-saturated buffered phosphate solution as the copper was polarised at –1.5 V for 10 minutes at 0 °C (without continuous CO_2 bubbling). Spectra shown are from (a) –0.8 V to (h) –1.5 V in 0.1 V per step. E_{ref} = –0.7 V.

cm^{-1} at –1.3 V. The unipolar feature of the band indicates that the band is present only at that potential and not at a reference spectrum. Upon measurement with *s*-polarised light, the band is not observed (spectra not shown). It indicates that the band at 2082 cm^{-1} is generated from an adsorbed species produced from the reduction of CO_2 from the solution. The band position is in agreement with linearly adsorbed CO on polycrystalline copper at 2078 cm^{-1} [52] and at 2081 cm^{-1} [53], and on copper single crystal at 2080 cm^{-1} [23, 24]. Therefore the band at 2082 cm^{-1} in the present study is assigned to linearly adsorbed CO, Cu-CO_L on polycrystalline copper, which is produced from the electrochemical reduction of CO_2 [54]. It is important to note that there was no Cu-CO_L band observed for the same E_{pol} with holding time less than 10 minutes (spectra not shown). It may indicate that the adsorption of CO on copper in CO_2-saturated phosphate buffered solution occurs in a slow process, since the adsorption of CO as linear-bonded CO, Cu-CO_L is a fast reaction at the same E_{pol} (-1.5 to –1.3 V). This will be discussed in detail in Chapter IV. A positive weak band that may associate with adsorbed multi-bonded CO since it appears at lower wavenumber, is observed at 1865 cm^{-1}. The positive sign indicates that the band is present at more positive potentials.

3.3.4.2 Reduced CO_2 – bridge bonded CO, Cu-CO_B

As mentioned earlier a weak band at 1898 cm^{-1} (Fig 3.13), 1908 cm^{-1} (Fig 3.14), 1891 cm^{-1} (Fig 3.15) and band at 1865 cm^{-1} (Fig 3.18), associates with multi bonded CO on copper surfaces when the electrode was polarised at high negative potential for several minutes. When spectra at Figure 3.18 are reploted for the overall potentials limit studies and normalised the spectra with respect to spectrum at –0.4 V of reverse sweep, the shifting band at 1868 cm^{-1} is clearly observed at –1.2 V (Figure 3.19). The band is shifting to 1937 cm^{-1} as the potential is made toward more positive. The band at 1868 cm^{-1} is close to the value of adsorbed bridge-bonded CO on polycrystalline Pt at 1860 cm^{-1} [33, 43, 55]. Therefore the bands in the present study as mentioned in the above might be assigned with the band that associates with a bridge-bonded CO, Cu-CO_B. This will be reconfirmed by the isotopic labelling ^{13}CO latter in next chapter.

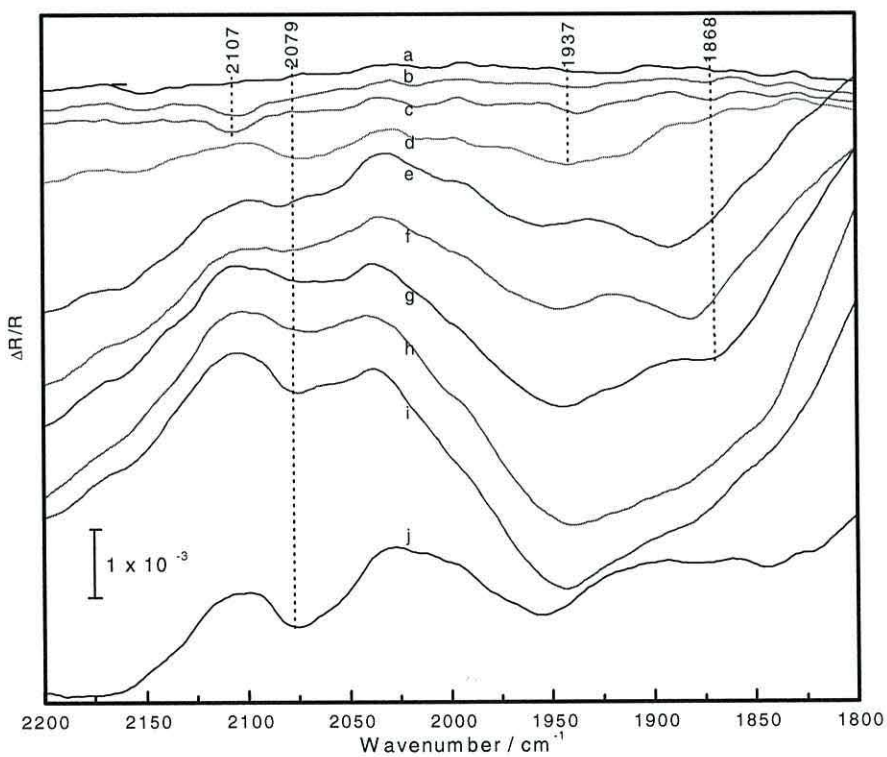

Figure 3.19: SNIFTIR spectra of CO_2-saturated buffered phosphate solution as the copper electrode was polarised at –1.5 V for 10 min. at 0 °C (without further CO_2 bubbling). Spectra shown are from (a) –0.2 V of reverse sweep, (b) 0 V, (c) –0.1 V, (d) –0.3 V, (e) –1.0 to (j) –1.5 V of forward sweep in 0.1 V per step. E_{ref} = –0.4 V (reverse sweep)

The spectra shown so far clearly indicate that the band frequencies associated with reduced-CO_2 (Cu-CO_L and Cu-CO_B) are potential dependent. Particularly for Cu-CO_B, as can be seen in Figure 3.16, the band shifts, as the potential is made more positive. It shifts

from 1881 cm^{-1} (at –1.4 V) to 1955 cm^{-1} (at –0.2 V) or in Fig. 3.19 the band shifts from 1868 cm^{-1} to 1937 cm^{-1}. This shifting band occurs in the thin layer environment. A shift in band position for adsorbed CO has been rationalised by the π-back donation process, which is well documented by Blyholder [56]. The shift to higher frequency as the potential is made more positive indicates an increase in the C-O bond order/strength. At high negative potential, π–back donation from copper dπ orbital to CO antibonding 2π* is believed to decrease the C-O bond order which consequently lower the C-O stretch frequency. On the other hand, at less negative potentials (-0.2 V), the π–back donation becomes less thus increasing the C-O bond strength. Increases in C-O bond order will therefore increase the C-O stretch frequency.

It is interesting to note that no linear-bonded adsorbed CO, Cu-CO_L is observed in the experiments where CO_2 was continuously bubbled during the electrode polarisation process. However both adsorbed CO, Cu-CO_L and Cu-CO_B can be observed forming in the stagnant solutions (without further CO_2 bubbling process during the electrode polarisation). The Cu-CO_L band shows significantly high band intensity whereas the Cu-CO_B shows a weak band as can been seen in Figure 3.18 and 3.19. It might suggest that the formation of Cu-CO_L is more favourable than Cu-CO_B in stagnant solution compared to those observed in continuously CO_2 bubbling experiments. This may be attributed to the conversion of Cu-CO_L to Cu-CO_B as the CO coverage increases. This binding site interconversion has been reported to occur as a function of CO surface coverage on single crystal copper [23] and other metals such as Pt [57], Rh [58], Pd [59] and Co [60].

3.3.5 The influence of varying the polarisation potential and its duration

To further uncover the dependency of adsorbed bridge-bonded CO, Cu-CO_B on the cathodic potential polarisation effect, the reduction of CO_2 was carried out at different E_{pol} of -0.9 to -1.6 V with the same polarisation time (15 minutes) during which CO_2 was continuously bubbled. The spectra were then collected after the electrode polarisation as the potential was stepped from –1.5 V to –0.7 V in each set of experiments as adopted of scheme E (Figure 3.20). Figure 3.21 shows the SNIFTIR spectra at a potential of –0.7 V obtained from each experiment set, normalised relative to E_{ref} = –1.3 V. The figure shows that the bipolar feature of Cu-CO_B band indicates that the band appears both during the electrode polarisation process at E_{pol} of –1.0 V to –1.6 V and at a potential of –0.7 V. The band intensities increase with high negative E_{pol} compared to that observed at less negative

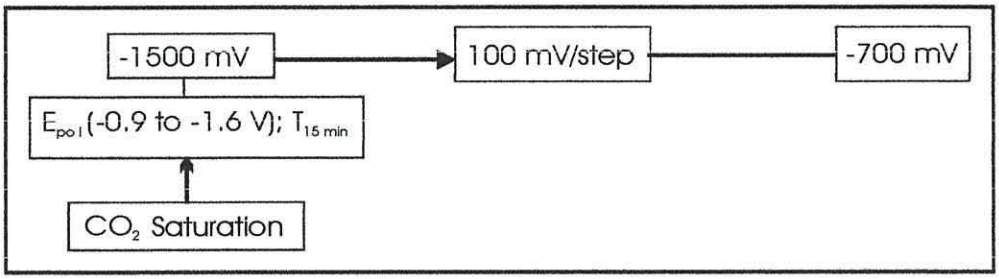

Figure 3.20: Scheme E used for evaluation of the reduction of CO_2

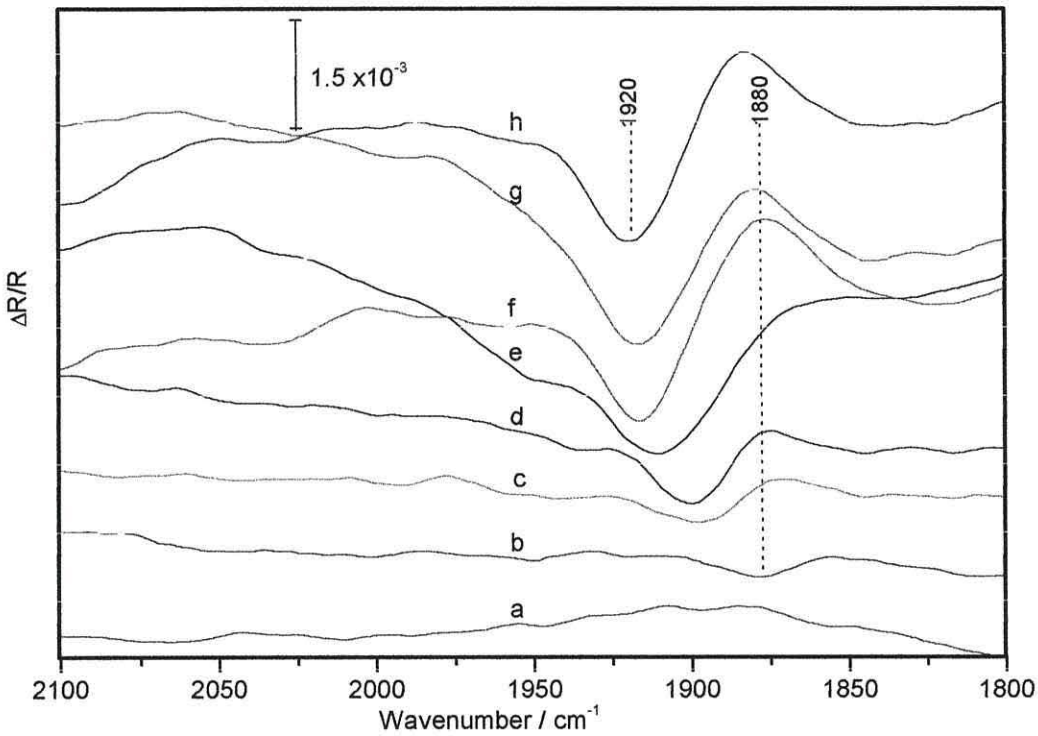

Figure 3.21: SNIFTIR spectra of Cu-CO_B at –0.7 V obtained from CO_2-saturated buffered phosphate solution as the copper was polarised at different potential (continuous bubbling); (a) E_{pol} = –0.9 V to (h) E_{pol} = –1.6 V for 15 min. at 0 °C. E_{ref} = 1.3 V at each sets.

E_{pol}. The band intensity increases about twice for E_{pol} of –1.2 V and increases about eight times for E_{pol} of –1.6 V relatively to E_{pol} of –1.1 V respectively. Increases in band intensity at high negative E_{pol} suggest that increases in amount of Cu-CO_B surface coverage, which implies that the electrochemical reduction of CO_2 to CO occurred in favour at more negative E_{pol}. It is worth noting that Cu-CO_B band shifts toward higher frequency with more negative E_{pol} as it shift from 1880 cm^{-1} (E_{pol} = –1.0 V) to 1920 cm^{-1} (E_{pol} = –1.6 V). This might due to the binding site preferences; as CO surface coverage increases the binding site should shift from bridge bonded (2-fold) site to 3-fold hollow

sites that show a band at lower frequency, if the 5σ-Cu of σ interaction is more important than 3d-2π* of π interaction in polycrystalline Cu [61]. However the result shows no band that is associated with 3-fold hollow sites at 1813 cm^{-1} [23, 61]. The result shows that at high CO coverage (E_{pol} = –1.6 V), Cu-CO_B exhibits a band at higher frequency (1920 cm^{-1}) compared to that at low CO surface coverage, which exhibits a band at 1880 cm^{-1} (E_{pol} of –1.0 V). This implies that the bond order of C-O increases as the CO coverage increases at higher negative E_{pol}, which is opposite circumstances from that shifting band in thin layer environment as the potential is changed (Figure 3.13 to 3.18). This behaviour can be explained by π back-donation process where as the CO surface coverage increases at higher negative E_{pol} (-1.6 V), the competition for d metal electron increases. Consequently it decreases the metal electron availability for donation to CO 2π* antibonding orbital and increases the C-O bond order, and in turn increases the νC-O stretch frequency [56]. At low E_{pol} of –1.0 V on the other hand, the CO surface coverage is much less than that at E_{pol} of –1.6 V, thus less competition for metal d electron. Therefore more electron will be donated to CO 2π* antibonding orbital and consequently will reduce the νC-O stretch frequency compared to that at –1.6 V. Another possibility of frequency shifts as CO coverage increases might coincide with the occupation of CO in defect binding sites such as step or terrace which exhibits higher νCO stretch frequency due to their low coordination binding site [62] and will be further discussed in Chapter IV.

The above results show that the reduced-CO_2 (CO) surface coverage on copper surfaces is dependent on E_{pol} and its duration. In order to investigate the relationship between the polarisation time and the amount of Cu-CO_B produced from the reduction of CO_2, experiments at different E_{pol} (1.6 to –1.1 V) and for different polarisation time (0 to 25 minutes) were carried out for the electrochemical reduction of CO_2. The spectra were measured after the polarisation process as the potential was stepped from a potential of –1.5 V to –0.7 V in each sets (modified scheme E at different $T_{hold\ min}$). Figure 3.22 (black curve) shows the relationship between the polarisation potential (E_{pol}) and the time required at that potential to produce the same amount of Cu-CO_B at –0.7 V (E_{ref} = -1.3 V) in each set. The amount of Cu-CO_B was calculated by integrating the area under the absorbance band (the red curve in the figure). The data clearly show that the more negative the polarisation potential (E_{pol}) is, the less time is required to produce Cu-CO_B from CO_2. However, more information that is interesting was obtained when the data was analysed for each polarisation potential as a function of time.

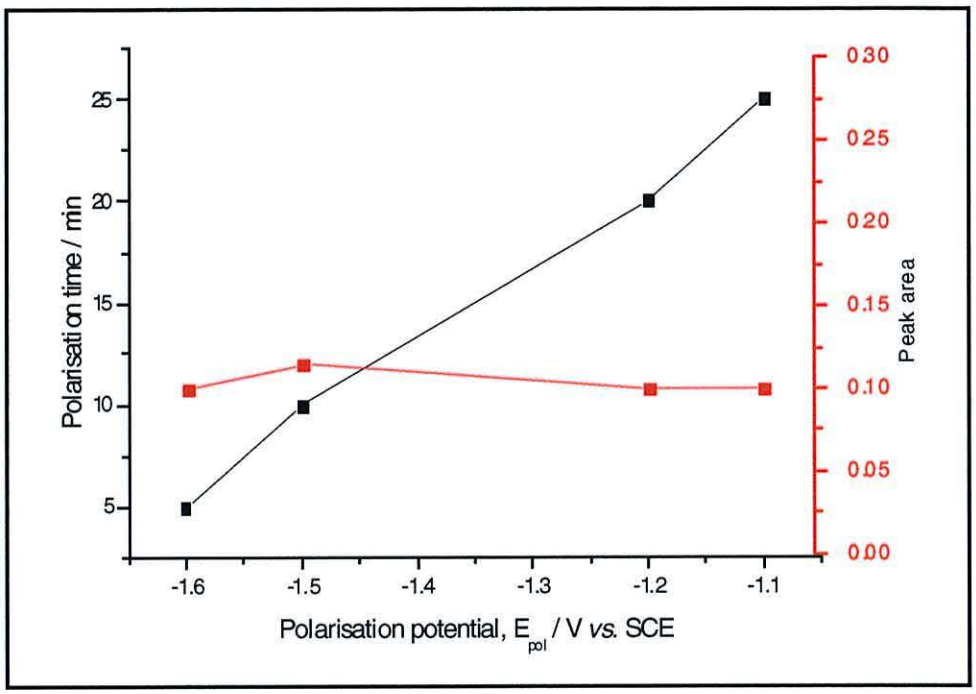

Figure 3.22: The relationship between E_{pol}, polarisation time and integrated peak area of Cu-CO_B at –0.7V. E_{ref} = -1.3 V of each set.

Figure 3.23 shows an example of such information, which was obtained when the electrode was polarised at –1.2 V for a period of time, t_1 and then spectra were collected as the potential was stepped from –1.5 V to –0.7 in 0.1 V increments (scheme E). The spectrum collected at –0.7 V was normalised against –1.3 V and the peak area and band position for Cu-CO_B were noted. The procedure was then repeated for a different polarisation time, t_2. The peak areas were normalised by the peak area of 0.12 obtained after 27 minutes polarisation (red curve). The first interesting observation is that the amount of Cu-CO_B continuous to increases with time and reaches plateau after nearly 27 minutes. This implies that the Cu-CO_B surface coverage increases with time. This could either imply that the reduction of CO_2 is a very slow process or that the surface of the electrode is covered with an oxide or hydroxide layer which is difficult to reduce and requires prolonged period of reduction [63]. It is more likely that the latter reason is more palpable as the voltammetry indicates an incomplete reduction of surface oxides or hydroxides at the time scale of the voltammetric experiments. It is also possible to preclude the slow adsorption of CO at the surface of the electrode in CO_2-saturated phosphate buffered solution as the reason for this observation due to the presence of carbonate or/and bicarbonate at the electrode surface which may also compete with the CO adsorption process. Further

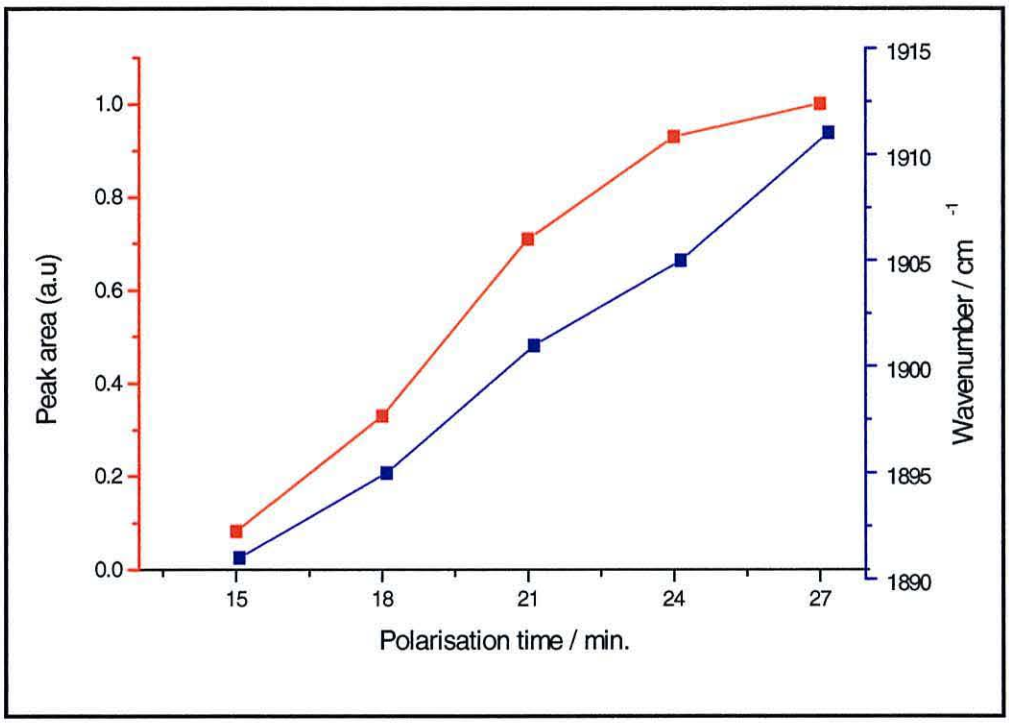

Figure 3.23: Integrated peak area of Cu-CO_B at –0.7 V for CO_2-saturated buffered phosphate solution as the copper was polarised at –1.2 V for different polarisation time at 0 °C, relative to polarisation time at 27 min. (E_{ref} = –1.3 V at each sets).

evidence for this will be provided in the next chapter. The second interesting observation from Figure 3.23 is that the frequency of Cu-CO_B undergoes a blue shift as a function of polarisation time (blue curve). This implies that the order of the C-O bonding increases as a function of polarisation time. This can be rationalised by increasing in CO surface coverage at longer polarisation time. As discussed earlier, as the CO surface coverage increases the competition for metal d electron increases and in turn decreases the π back donation to the CO molecule and thus increase the νC-O stretching frequency [56–59, 64, 65].

3.3.6 Measurement in deuterated phosphate solution

A shift in CO stretching frequency has been reported in several metal surfaces due to several factors such as changing in binding sites, surface coverage, applied potential, or coadsorption from other molecule such as water [57], NO [58, 59], the electrolyte cation such as K^+, Na^+ or Li^+ and adsorbed hydrogen/hydride and hydroxide [59]. The reduction experiments were also carried out in deuterium oxide, D_2O, in order to examine the possibility of the presence of the reduction products that exhibit IR features that are masked by the strong absorbance by H_2O. In CO_2-saturated deuterated phosphate solution

in D_2O, the electrode surface was polarised at E_{pol} of –1.5 V for 10 minutes while CO_2 was continuously bubbled before the electrode was pushed against the IR window (adopted scheme B). Figure 3.24 shows the SNIFTIR spectra from such an experiment, normalised relative to E_{ref} of –0.6 V. The general features are the same as those carried out in H_2O except for the strong absorbance centred at 2214 cm^{-1} (as shown latter in Figure 3.25) which is due to the stretching mode of D_2O isotopically shifted to lower wavenumbers compared to H_2O.

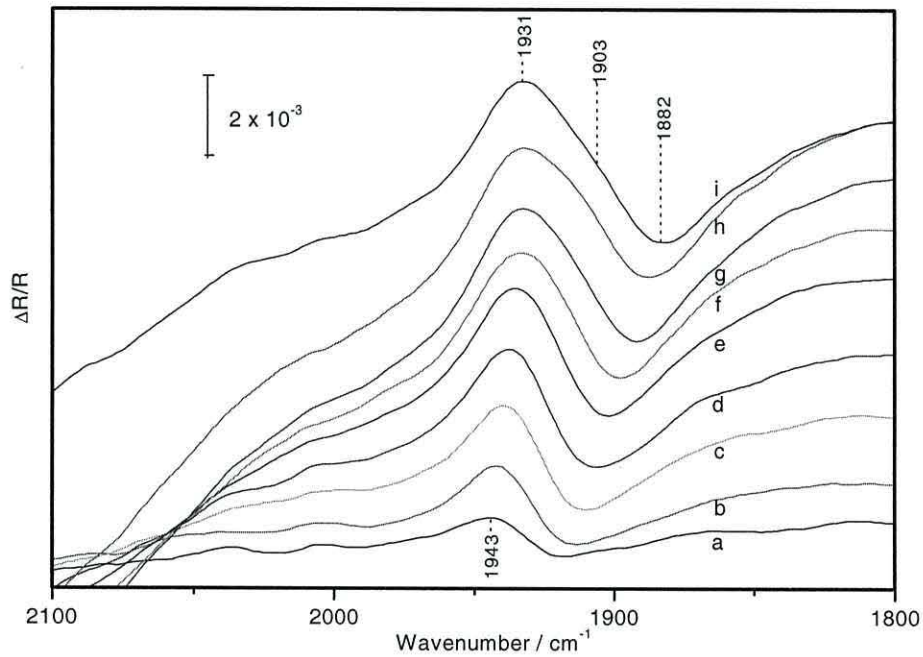

Figure 3.24: SNIFTIR spectra from of CO_2-saturated deuterated-phosphate buffered in D_2O solution as the copper was polarised at –1.5 V for 15 min. at 0 °C. Spectra shown are from (a) –0.7 V to (i) –1.5 V in 0.1 V per step. E_{ref} = –0.6 V.

The most interesting observation is the increase in all band intensities compared to measurements carried out in H_2O. For example, the intensity of the band associated with Cu-CO_B has increased by 40 % compared to studies in H_2O. Table 3.2 shows a comparison of the integrated peak area for measurements carried out in H_2O and D_2O (Fig

Potential, V	%, $[(A_D - A_H)/A_H] \times 100$
-1.3	40
-1.0	40
-0.7	45

Table 3.2: The percentage ratio of the Cu-CO_B peak area in deuterated and normal phosphate solution; [note; A_D = peak area in deuterated phosphate; A_H = peak area in normal phosphate].

3.15 and 3.24). This is in agreement with several reports where the solubility of gases such as Ar increases 10% [66] and CO_2 (35%) [67] in D_2O solution. Higher CO_2 solubility in solution will increase the amount of dissolved CO_2 that reach the electrode surface and thus increases the chance for the electrochemical reduction.

Figure 3.25 shows the SNIFTIR spectra as the spectrum obtained at the same experiments as in Figure 3.24 are normalised relative to E_{ref} = -0.4 V of reverse sweep. It is worth to note that a weak band for the linearly adsorbed CO, Cu-CO_L at 2081 cm^{-1} is also observed. A weak band of Cu-CO_L becomes less stable or conversion to Cu-CO_B occurred in this particularly experiment condition where CO_2 was continuously bubbled in the solution during the polarisation process. The stability properties of Cu-CO_L will be examined and will be discussed in detail in Chapter IV. It is worth to note that a band at 1623 cm^{-1} strongly appears in deuterated phosphate solution (spectra not shown). The band is attributed to ν_{as}OCO of bicarbonate ion where this band is strongly masked by a strong absorption of water bending mode frequency at 1640 cm^{-1}.

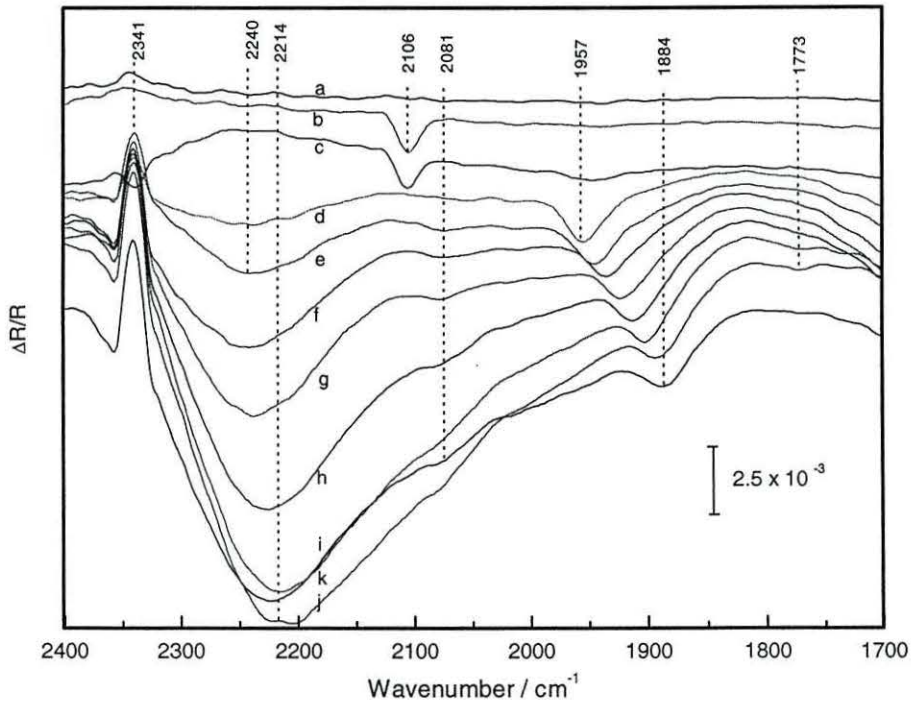

Figure 3.25: SNIFTIR spectra of CO_2-saturated deuterated-phosphate buffered in D_2O solution as the copper was polarised at –1.5 V for 10 min. at 0 °C. Spectra shown are from (a) –0.3 of reverse sweep, (b) 0, (c) –0.1 to (i) –1.3 V in 0.2 V per step, (j) –1.4 and (k) –1.5 V. E_{ref} = –0.4 V of reverse sweep.

It is interesting to note that a weak band at 1773 cm^{-1} appears at high negative potential at –1.5 to –1.1 V, the same adsorption potential as linear-bonded CO, Cu-CO_L.

The frequency value falls within the higher coordination binding sites of CO such as 3-fold hollow at metals such as Pt(111) at 1780 cm^{-1} [68]. Furthermore the translation barrier for moving from 2-fold to 3-fold binding site is suspected to be rather low [69] with an energy difference between the 2-fold and the 3-fold binding site is about 100 meV [70]; suggests that their conversion can be easily occurred. However the band value is far too low from the value reported for CO adsorption on 3-fold hollow binding site on Cu(111) at 1813 cm^{-1} [23, 41]. Furthermore the existence of the band at 1773 cm^{-1} only at high negative potential which indicates that it is less stable than the bridge bonded CO which exists at wider potential regions. Therefore the assumption that the band at 1773 cm^{-1} for the adsorbed CO at 3-fold hollow is spurious. It might be associated with the adsorbed CO_2, since inorganic copper complexes of CO_2 (O-bonded) have an IR frequency at 1716 cm^{-1} [71].

3.3.7 Reaction of reduced-CO_2 with oxidised copper

For most of the measurements described so far, it was noted that as the potential became more positive, the Cu-CO_B band shifted toward higher frequency and gradually decreased in intensity. As the potential reached at –0.1 V, the Cu-CO_B band stopped shifting, and the band disappeared and consequently a new band appeared at 2106 cm^{-1}. The same band was observed in *s*-polarised light measurements. This indicates that the band may not derive from an adsorbed species. As the copper surface is oxidised at –0.1V, a reaction of reduced-CO_2 with oxidised copper, possibly Cu(I) can occur. Hernandez and Kalaji reported that the band at 2107cm^{-1} to be associated with the formation of copper(I) carbonyl, Cu(I)-CO on copper in CO saturated solution [44]. Therefore the band at 2106 cm^{-1} in the present study which exists only at anodic potentials (from –0.1 to 0 and back to –0.2V on the reverse sweep) can be assigned to coper(I)-reduced-CO_2 species, which is the same as Cu(I)-CO.

3.3.8 The influence of pH on the reduction of CO_2

pH obviously affects the copper electrochemical behaviour as shown in voltammogram of CO_2-saturated solution. Voltammogram of CO_2 saturated phosphate buffered solution with varied electrolyte solution's pH is shown in Figure 3.26. The effect of solution pH is clearly shown by the shifting in anodic peak toward more positive and cathodic peak toward more negative potentials. The anodic peak current increases with pH due to the oxidation of copper to oxide or to hydroxide layer is pH dependent. According to

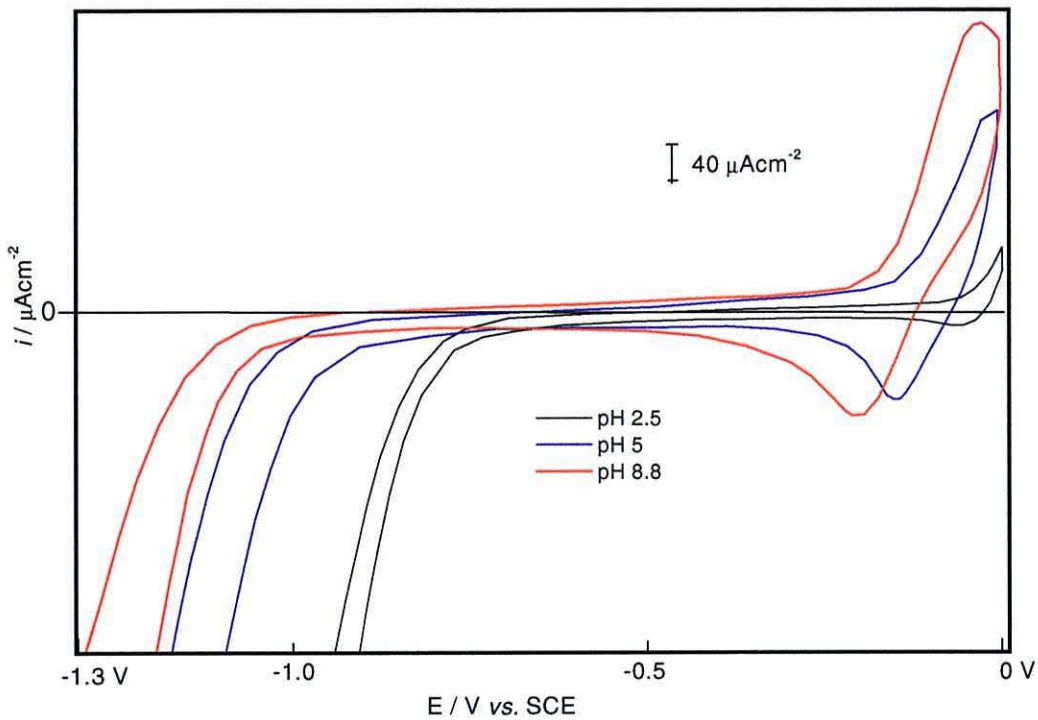

Figure 3.26: Voltammogram for copper at $\nu = 0.05\ Vs^{-1}$ in CO_2 saturated buffered phosphate solution at different solution pH.

Pourbaix diagram [36], it is established that the formation of cuprous oxides, Cu_2O is an intermediate step before dissolution at less negative potential starts. This process is described by the following equation;

$$2Cu + H_2O \leftrightarrow Cu_2O + 2H^+ + 2e^-$$

As can be seen this is a pH dependent reaction; the higher the concentration of H^+ the higher the potential is required to oxidise the copper surface.

The same pH dependent is shown for the hydrogen evolution region where hydrogen evolution favourably occurred at low pH which is observed to occur at less negative potential as expected. However no additional peaks for the adsorption or the reduction of CO_2 are observed.

The amount of dissolved CO_2 in aqueous solution that is available for the electrochemical reduction process is pH dependent. Hori *et al.* [24, 72] reported that the current response of a Cu electrode at –1.3 V in phosphate buffered solution is due to the reduction of CO_2. However, others indicated that there is no difference in this particular current response for N_2 and CO_2-saturated phosphate buffered solution [25]. The only difference is that the current response shifted cathodically by about 0.1 V due to pH

changes in solution and this is reconfirmed through the present study (Figure 3.9a and 3.9b). To get a clearer picture of these contradictory observations and to investigate the effect of pH on the CO_2 reduction, the reduction of CO_2 was investigated spectroscopically by referring to the formation of an adsorbed CO, Cu-CO_B and copper(I)-carbonyl, Cu(I)-CO as these species are the prominent CO_2 reduction and side-reaction products. The pH of the phosphate buffer solution was regulated from 1.5 to 9.2 by adding phosphoric acid or potassium phosphate solution. Figure 3.27 shows the peak areas of Cu-CO_B at –0.7 V and Cu(I)-CO at 0 V as the copper surface was polarised at –1.5 V while CO_2 was continuously bubbled into the solution (scheme E). The SNIFTIR spectra were normalised relative to –1.3 V at each set and then divided by the highest peak area at pH 6.8, 0.15 for Cu-CO_B and 0.10 for Cu(I)-CO. The figure shows that both Cu-CO_B and Cu(I)-CO are observed in the pH range 3.1 to 9.2. No Cu-CO_B or Cu(I)-CO were observed at pH values below 3.1. The amount of Cu-CO_B produced increased as the pH increased and peaked at neutral pH after which it slowly decreased.

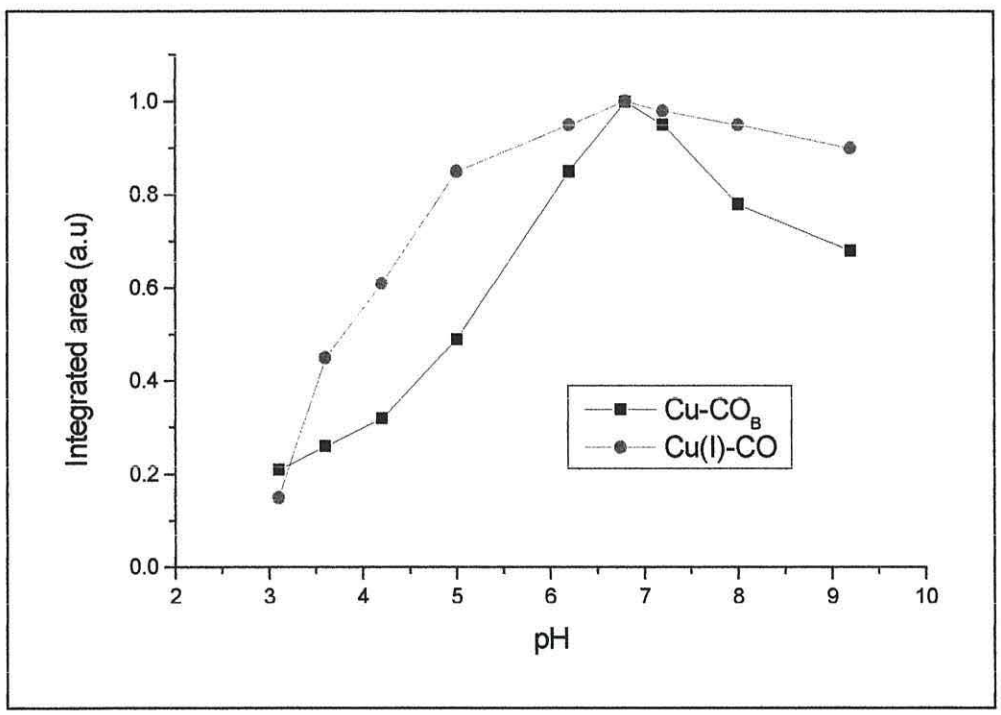

Figure 3.27: Integrated peak area of Cu-CO_B at –0.7 V and Cu(I)-CO at 0 V correspond to the electrolyte pH change, relative to values at pH 6.8 at 0 ^{0}C.

The results indicate that CO_2 is not electrochemically reduced to CO at pH values lower than 3.1. This is due to, in acidic medium, the solubility of CO_2 decreasing due to $CO_{2(aq)}$ being immediately released from solution as the pH drops. However, a weak band at 2145

cm^{-1} is observed possibly for CO in solution of pH 2.5 (Figure 3.28). The band is assigned based on the value reported in literature for CO gas in solution [38, 73-75]. CO that is produced from the CO_2 reduction is not adsorbed on the copper surface at pH 2.5. The amount of both species, Cu-CO_B and Cu(I)-CO is higher at pH value near neutral compared to those at low or high pH values. At low pH values, the electrode surface is expected become clean as the copper oxides and hydroxides are reduced at acidic media. However the HER is positively shifted and becomes predominant as the pH of the solution decreases as shown by voltammogram in Fig 3.26. Therefore, there are no big net in the reduction of CO_2 process at pH values lower than neutral pH. At pH value higher than neutral pH, the reduction of CO_2 also decreases due to the loss of dissolved CO_2 from the solution. As pH values increases, the more hydroxides presence in the solution after which it converts the CO_2 to carbonate and in turn reduces the chance of the reduction of CO_2. However in neutral pH ranges, the CO_2 reduction process can be directly carried out by controlling the high negative E_{pol}, which is directly influenced the distribution of the electrode surface charge which reduces the CO_2.

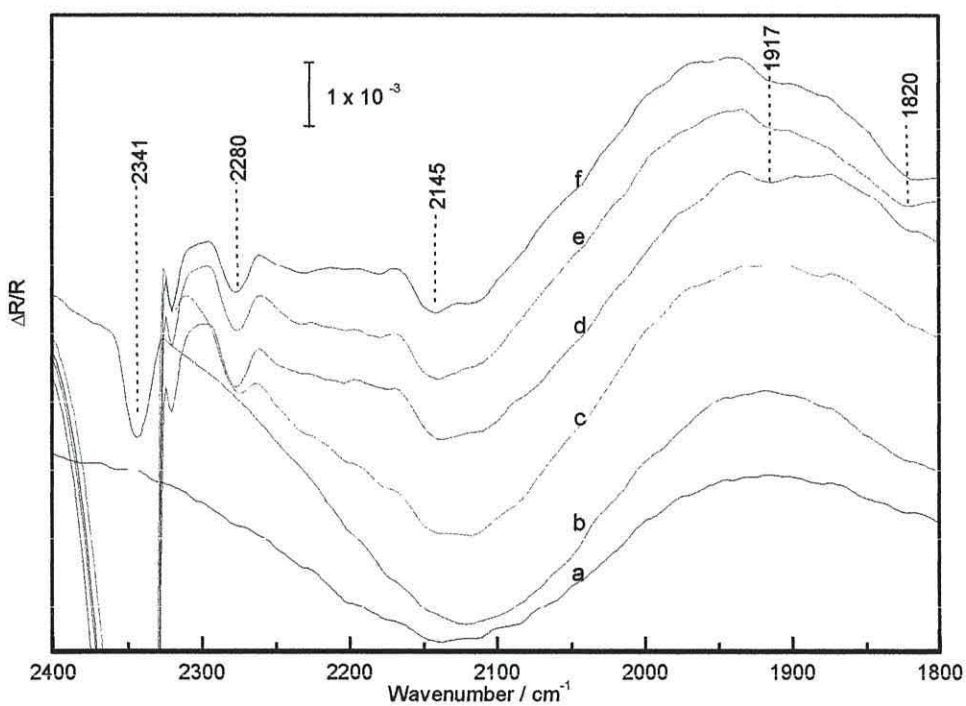

Figure 3.28: SNIFTIR spectra obtained from a CO_2-saturated buffered phosphate solution (pH 2.5) as the copper was polarised at –1.5 V for 15 min. Spectra shown are from (a) –1.0 V to (f) 0 V in 0.2 V per step. E_{ref} = –1.3 V.

The copper carbonyl, Cu(I)-CO shows the same behaviour toward pH responses. Higher band intensity is observed at pH near or at neutral (pH 6.2-6.8) whereas having low

band intensity at lower and higher pH values. As mentioned earlier the oxidation of Cu to Cu(I) either to cuprous oxide, Cu_2O or cuprous hydroxide, CuOH is pH dependent [36, 76, 77]. Therefore at low pH, at potentials where the Cu(I)-CO appears, the band intensity reduces as expected. The potential-pH relationship might be a good explanation for this observation as can be seen directly from the formal potential of the couple Cu/CuO and pH which is given by the following equation [78]:

$$E = 0.471 - 0.0591\ (pH)$$

At high pH, the potentials where Cu(I)-CO is normally observed at -0.1 V for instance, the electrode surface environment is probably more negative than – 0.1 V. Therefore the formation of Cu(I)-CO could not fully occur at this potential in alkaline condition and thus reduces its amount. It is also worth to note that the band at 2280 cm^{-1} is clearly observed at low pH. The band is associated with isotopic $^{13}CO_2$ [25, 39]. However, no bands can be attributed to the reduction products of $^{13}CO_2$ since its amount that present in the solution is far too small compared to $^{12}CO_2$.

3.3.9 The influence of temperature on the reduction of CO_2

The temperature of the solution is believed to influence the electrochemical reaction as it can control the amount of soluble CO_2. As expected the solubility of CO_2 decreases with increasing temperature. However, the effect of temperature on the reduction step may not only effect the concentration of CO_2 but also the kinetics of the reduction process in addition to the redox behaviour of Cu. Figure 3.29 shows the voltammogram of CO_2-saturated phosphate buffered solution in the temperature range 10 to 70 ^{0}C at sweep rate of 0.05 V/s. The effect of the solution temperature on the electrochemical behaviour of copper is shown by the increase of both anodic and cathodic peaks current in the same ratio as the temperature increases. However no noticeable additional peak can be attributed to the electrochemical reduction of CO_2 effect is observed. HER also is not affected by the change of solution temperature.

The chance of soluble CO_2 being involved in the electrochemical reduction depends on the amount that reaches on the copper surface, which is related to its solubility in phosphate buffered solution, which depends on the temperature. The effect of solution temperature on the reduction of CO_2 was carried out spectroscopically at a temperature range from 0 to 80 ^{0}C. The electrochemical reduction of CO_2 was evaluated by the formation of Cu-CO_B and the Cu(I)-CO as adopted of scheme E (pg. 84). Figure 3.30 shows the integrated peak area of

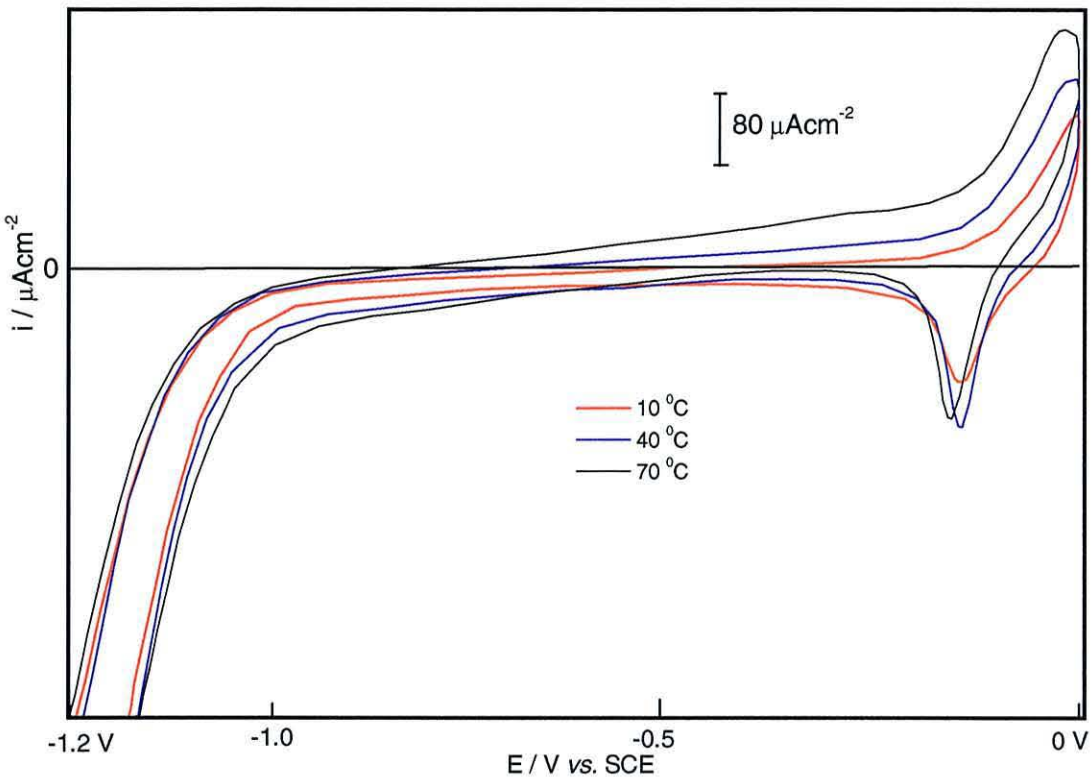

Figure 3.29: Voltammogram for copper at $\nu = 0.05\ Vs^{-1}$ in CO_2-saturated buffered phosphate solution at different solution temperature

Cu-CO_B at –0.7 V and Cu(I)-CO at 0 V at different temperature. The SNIFTIR spectra are normalised relative to –1.3 V at each set and divided to the highest values at lowest temperature of 0 °C, 0.12 for Cu-CO_B and 0.10 for Cu(I)-CO. The figure shows that the peak area for both Cu-CO_B and Cu(I)-CO show the highest value at lowest temperature, 0°C and reduces with solution temperature. A reduction about 50% of the peak area is observed for solution temperature at 60°C compared to that of at 0°C. The reduction in peak area in high temperature is due to decreased in CO_2 solubility. However no other bands appeared that may be related to other reduction products at high temperature as at high temperature should stabilise the higher coordination binding sites (expected 3-fold hollow) [79]. This may be due to the temperature under present study is far too high from the one that has been reported. Rao *et al.* reported the stabilisation of higher coordination binding site can be occurred, however their studies were carried out at lower temperatures, 80 to 270 K.

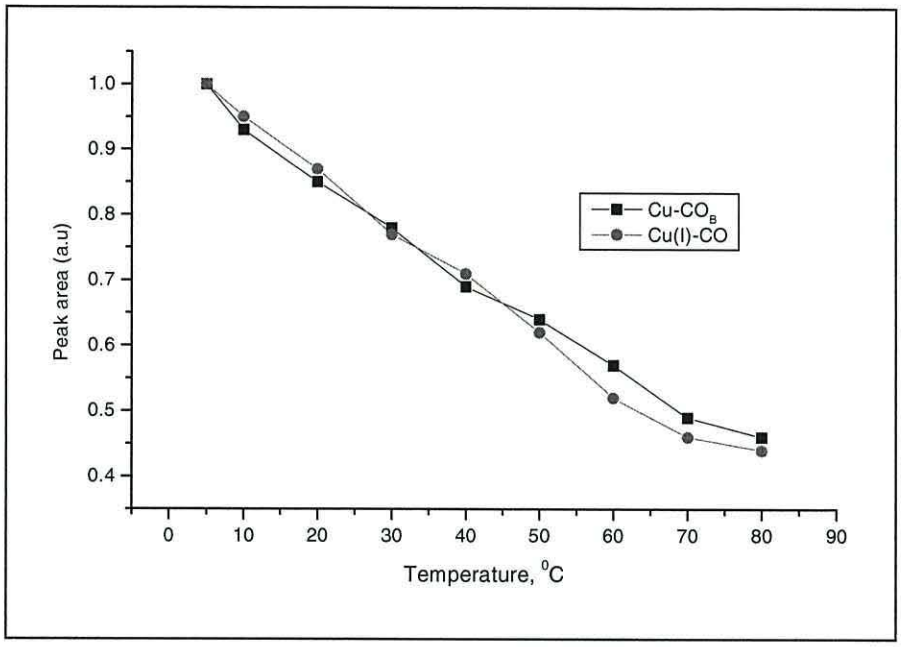

Figure 3.30: Integrated peak area of Cu-CO_B at –0.7 V and Cu(I)-CO at 0 V at different solution temperature relative to values at 0 ^{0}C. Spectra are normalised relative to E_{ref} = -1.3 V

3.3.10 Flow effect on the reduction of CO_2

It is known that one of the major problems of thin layer cells employed for *in situ* IR work is related to the restricted flow of the reactants, depletion of reactant species and accumulation of the products. As mentioned earlier, the "carbonate route" is a major obstacle in the process of the electrochemical reduction of carbon dioxide [25]. This "carbonate route" causes an almost complete depletion of the dissolved carbon dioxide through its conversion to either bicarbonate or carbonate; largely reported as non-electroactive substances. The polarisation of the working electrode in a thin layer cell leads to a large concentration of such anions in the thin layer; which in turn presents a major interference as the infrared absorption of such anions may block the detection of intermediates or products from the electrochemical reduction of the remaining traces of carbon dioxide. Thus, it is imperative to replenish the thin layer and to remove the excess of either bicarbonate, carbonate or poisoning substance if the products are to be seen. By using the flow cell system, the flow of the electrolyte will replenish the solution and in the thin layer during the course of the reaction.

As was shown in Figure 3.4 and 3.11 under static conditions, the bicarbonate (1356-1365 cm^{-1}) and carbonate (1401 cm^{-1}) are generated, as carbon dioxide (2341 cm^{-1}) is consumed when the potential is increased toward more negative values. At a potential of

–1.1 V the remaining carbon dioxide in solution is only about 6.6% compared to the concentration at a potential of -0.7 V. On the other hand, the concentration of carbonate has grown significantly. However, if the electrode is periodically lifted to refresh the thin layer after each potential step, the concentration of carbon dioxide, although still decreasing, is slightly higher about 8.3% at -1.1 V) than in the non-replenished system (spectra not shown). Similar behaviour was observed when a CO_2-saturated buffered phosphate solution (pH 6.8) was used instead. This rudimentary procedure was improved by using the channel flow cell. Figure 3.31 shows SNIFTIR spectra when the flow cell was used, as the spectra are normalised relative to the initial potential at –0.7 V (static mode). The electrode surface was initially polarised at –1.5 V for 10 minutes and then the potential was slowly stepped up to –0.7 V. After the initial spectrum at –0.7 V was collected, the flow was switched on (dynamic mode) and after the solution flow equilibrium was achieved, the first spectrum was collected (a). The flow was continuously switched on and the potential was stepped down at 0.1 V/step towards –1.5 V (dynamic

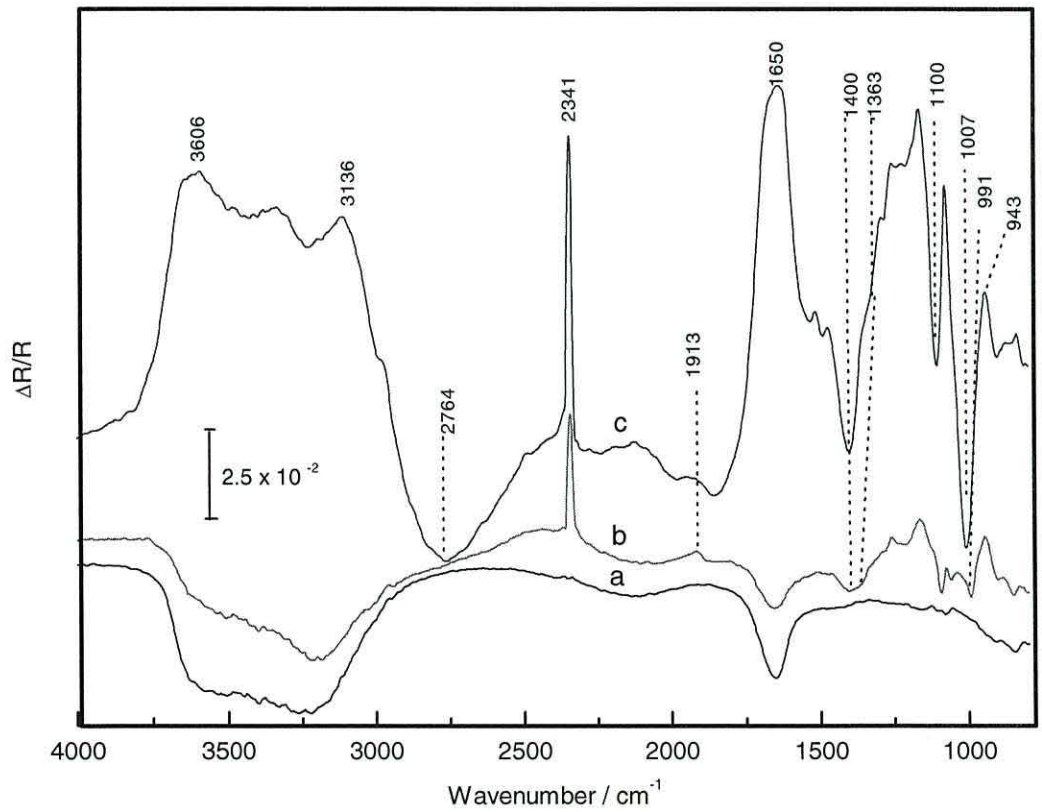

Figure 3.31: SNIFTIR spectra obtained from a CO_2-saturated phosphate buffered solution as the copper was polarised at –1.5 V for 10 minutes. Spectra shown are (a) –0.7 V with flow, (b) –1.5 V with flow and (c) –1.5 V without flow; E_{ref} = –0.7 V without flow.

mode; spectrum b). Finally, the flow was switched off and a final spectrum was collected at -1.5 V (static mode; spectrum c). As can be observed in the figure, no differences in CO_2 concentration depletion or consumption at –0.7 V in dynamic mode (spectrum a) relative to the static mode. This indicates that at this potential no significant difference in CO_2 concentration either through reduction or in carbonate-bicarbonate equilibrium is observed. However the concentration of CO_2 at –1.5 V decreases more than twice (dynamic mode; b) relative to CO_2 concentration at static mode at the same potential (spectrum c). This indicates that a rapid depletion of CO_2 concentration in the thin layer at high negative potential due to the involvement in a reduction or carbonate-bicarbonate equilibrium process. An interesting observation is that the Cu-CO_B band at 1913 cm^{-1} is clearly observed during the flow was applied as shown in spectrum b. It may indicate that the reduction of CO_2 is much favoured in flow condition as compared to the carbonate-bicarbonate equilibrium process. It may imply that the accumulation of the excessive anions on the electrode surface may prevent the reduction of CO_2 to occur. Another important feature observed is that during the dynamic mode, the carbonate band almost disappeared. It is clear that the species accumulated during the 'static' mode period were driven out from the thin layer and consequently the thin layer was refreshed. However, a weak shoulder band at 1363 cm^{-1} for hydrogen carbonate was still present suggesting that the formation of these ions is a process faster than the flow applied. In another experiment, the flow was applied from the beginning of the experiment showing that CO_2 concentration never fell more than 45% of the initial concentration and that at no time carbonate anions were accumulated. Instead, a constant concentration of bicarbonate ions was observed.

Figure 3.32 shows the SNIFTIR spectra obtained when the copper surface was polarised at –1.5 V for 10 minutes at the starting potential while the flow was switched on (adopted scheme B with flow system). The acquired spectra were then measured in the forward sweep to 0 V and back to the initial potential of –1.5 V in staircase mode in 0.1 V/step. The appearance of the band for adsorbed bridge-bonded CO, Cu-CO_B at 1922 cm^{-1} is the main feature. However reduced-CO_2 of copper(I)-carbonyl, Cu(I)-CO (2107 cm^{-1}) is not observed as the potential reaches the anodic potentials. The figure shows that Cu-CO_B can be observed at laminar flowing of the thin layer whereas the Cu(I)-CO disappears in the same flowing environment. The result indicates that again the Cu-CO_B is thermodynamically stable; adsorbs on the copper surface and is not affected by the electrolyte laminar flow. On the other hand, Cu(I)-CO is easily removed from the

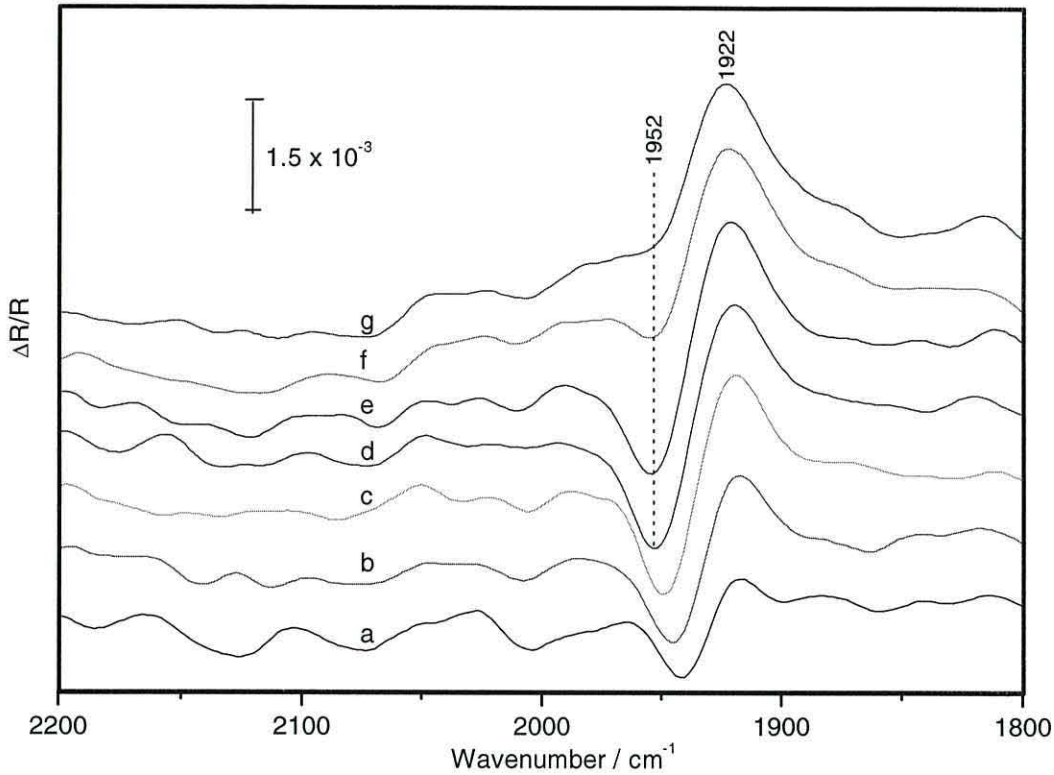

Figure 3.32: SNIFTIR spectra of CO_2-saturated buffered phosphate solution as the copper was polarised at –1.5 V for 10 min at 0 °C for flowing system. Spectra shown are from (a) –0.5 V to (f) 0 V of forward sweep and (g) –0.1 V of reverse sweep in 0.1 V per step. E_{ref} = –0.6 V.

electrode surface indicating that it is a soluble species, which is easily removed from the thin layer environment.

3.3.11 Anodic pulse technique

The reactivity of the electrode surface has been reported to decrease as the electrolysis time increases due to the formation of poisoning species during the electrochemical reduction process [13]. The active sites or the binding sites are blocked by the accumulation of the intermediate layer, thus reducing the electrode catalytic activity. No further electrochemical reduction occurs when the surface is completely covered by this layer. Sudden potential change to the opposite potential bias could be used to interrupt such reaction pathways [14, 15, 80]. To further investigate whether such potential interruption could enhance the electrochemical reduction of CO_2 at copper surface, experiments were performed by polarising the potential at –1.5 V for 10 minutes while continuously bubbling CO_2. The spectra were collected as the potential was stepped in 0.1 V increments towards

potential of 0 V and back to the initial potential of –1.5 V as adopted of scheme B. This was followed by potential steps from –1.5 V immediately to 0 V for 1 minute without lifting the electrode. The spectra were then collected back starting from the initial potential of –1.5 V to 0 V and back to –1.5 V for the second cycles.

As expected, the same bands as reported before for an adsorbed bridge-bonded CO, Cu-CO_B and Cu(I)-CO were observed in the first cycle (spectra are not shown). However the results showed no additional new bands after the anodic potential pulse (spectra are not shown). Furthermore when the potential was pulsed from –1.5 V to 0 V in the second cycle, no Cu-CO_B and on the other hand a very weak Cu(I)-CO is observed. The same observation for Cu-CO_B and Cu(I)-CO is expected in the first cycle as before for the same experimental procedure. No Cu-CO_B is observed in the second cycle after the anodic pulsed is also expected due to its formation requires E_{pol} at high negative potential with sufficient polarisation time whilst the electrode surface should be exposed to the bulk solution, which is not performed in this case. However, it is surprisingly that no Cu-CO_L is observed in the second cycle. This may be due to the Cu-CO_B is completely oxidised or converted to Cu(I)-CO or converted to HCO_3^- during the anodic pulsed, thus no CO available in the thin layer to be adsorbed at high negative potential. In anodic pulse approaches, the technique should be able to force the surface charge to redistribute across the interface or in the thin layer and allow the anions take part in charge redistribution, which in turn can affect the electrode reduction reaction-taking place during the next cathodic period [81]. However no significant effect of anodic potential pulsed in producing a reduction product in the present study. This is might due to phosphate electrolyte anion might poorly involved in surface charge redistribution, thus no further electrochemical reduction occur.

3.4 Conclusion

The electrochemical reduction of carbon dioxide on polycrystalline copper occurs in both hydrogen carbonate and phosphate buffered solutions. However, the reduced-CO_2 species produced from the electrochemical reduction process were more clearly observed in phosphate buffered solution with nearly neutral pH. The electrochemical active product of the reduction of CO_2 observed in phosphate buffered solution are adsorbed reduced-CO_2 of carbon monoxide in both forms, linearly bonded, Cu-CO_L (2082 cm^{-1}) and bridge-bonded, Cu-CO_B (1865 cm^{-1}) and side reaction product of soluble copper(I)-carbonyl (2106 cm^{-1}) species. The results also show that CO_2 is reduced electrochemically to CO as a function

of high negative E_{pol} and polarisation time to produce adsorbed CO, Cu-CO_B. Deuteration of phosphate buffered solution revealed the absence of coadsorbed species involved in a Cu-CO_B band at 1865 cm^{-1}. This indicates that the band is purely associated with an adsorbed CO, which is produced from the CO_2 reduction. In a stagnant solution, reduced-CO_2 adsorbs in both linearly bonded, Cu-CO_L and bridge-bonded, Cu-CO_B. This implies that at low CO coverage both types of adsorbed CO can be observed. However in saturated solutions, only bridge-bonded CO appears due to its preference for binding sites at high CO coverage. As the CO coverage increases by prolonging the polarisation time and by polarisation at higher negative E_{pol}, CO prefers to adsorb in bridge-bonded binding site. Under the studied experimental conditions, CO_2 is electrochemically reduced in phosphate buffered solution at wide pH range from 2.5 to 9.2 and wide range of temperature from 0 to 80 ^{0}C. This observation is based on the formation of adsorbed bridge-bonded CO, Cu-CO_B and Cu(I)-CO at chosen E_{pol} of –1.5 V with specific polarisation time of 15 minutes.

It is worth noting that the adsorbed bridge-bonded CO, Cu-CO_B exists and appears at wider potential range from –1.5 V to –0.1 V. On the other hand, the adsorbed linear-bonded CO, Cu-CO_L appears within smaller potential range from –1.5 to –1.0 V. It indicates that Cu-CO_B is the more stable form of adsorbed CO on copper surfaces. It is also interesting to note that the Cu-CO_B band formation is not affected by continuous CO_2 bubbling process where the band intensity increases with polarisation time. On the other hand, Cu-CO_L is not observed during continuous CO_2 bubbling during the cathodic potential polarisation. It only can be observed in stagnant solutions with low CO surface coverage or without further CO_2 bubbling. It disappears by further CO_2 bubbling probably through a physical diffusion process or by interfacial binding conversion from Cu-CO_L to Cu-CO_B. Furthermore, the appearance of Cu-CO_L only within narrow potential limit gives another evidences that Cu-CO_L is weakly adsorbed on the polycrystalline copper electrode, possibly as a weak chemisorbed species. Therefore, from the results obtained it might possible to imply that an intermediate reactive species involved in the CO_2 electrochemical reduction process is Cu-CO_L for a short lifetime intermediate reduction process whereas Cu-CO_B reacts as longer lifetime intermediate reduction process.

3.5 References

1 Y. Hori, K. Kikuchi and A. Murata, *Chem. Lett. Chem. Soc. Jpn.*, (1986) 897

2 Y. Hori, R. Takahashi, Y. Yoshinami and A. Murata, *J. Phys. Chem. B.,* 101 (1997) 7075

3 Y. Hori, A. Murata and Y. Yoshinami, *J. Chem. Soc. Faraday. Trans.,* 87 (1991) 125

4 Y. Hori and K. Osamu, *Electrochem. Acta,* 38 (1993) 1391

5 B. Aurian-Blajeni, "*Electrochemical reduction of carbon dioxide*", in "*Electrochemistry in Transition*", O.J. Murphy (Ed.), Plenum Press, N. York.(1992)

6 Y.Hori, H. Wakebe, T. Tsukamoto and O. Koga, *Electrochim. Acta,* 39 (1994) 1833

7 Y.Hori and A. Murata, *Bull. Chem. Soc. Jpn.,* 64 (1991) 123

8 T. Mizuno, K. Ohta and M. Kawamoto, *Energy Sources.*, 19 (1997) 249

9 G. Kyriacou and A. Anagnostopoulos, *J. Electroanal. Chem. Interfacial Electrochem.,* 322 (1992) 233

10 Y. Terunuma, A. Saitoh and Y. Momose, *J. Electroanal. Chem.,* 434 (1997) 69.

11 H. Noda, S. Ikeda, Y. Oda, K. Imai, M. Maeda and K. Ito, *Bull. Chem. Soc. Jpn.,* 63 (1990) 2459

12 B.D. Smith, D.E. Irish, P. Kedzierzawski and J. Augustynski, *Can. J. Chem.,* 144 (1997) 4288

13 D.W. DeWulf, T. Jin and A.J. Bard, *J. Electrochem. Soc.,* 136 (1989) 1686

14 G. Nogami, H. Itagaki and R. Shiratsuchi, *J. Electrochem. Soc.,* 141 (1994) 1138

15 B. Jermann and J. Augustynski, *Electrochim. Acta*, 39 (1994) 1891

16 R.S.Y. Aikoh and G. Nogami, *J. Electrochem. Soc.,* 140 (1993) 3479

17 A. Saito, T. Sato, A. Miyazaki, T. Onish, S. Yamazaki and S. Kyushu, *Daigaku Kogakubu Kenkyu Hokuku.,* 35 (1998) 99

18 Y. Hori, K. Kikuchi and S. Suzuki, *Chem. Lett. Chem. Soc. Jpn.,* (1985) 1695.

19 R.L. Cook, R.C. MacDuff and A.F. Sammells, *J. Electrochem. Soc.,* 135 (1988) 1320

20 M. Jitaru, D.A. Lowy, M. Toma and L. Oniciu, *J. App. Electrochem.,* 27 (1997) 875

21 I. Oda, H. Ogasawara and M. Ito, *Langmuir*, 12 (1996) 1094.

22 B. Westerhoff and R. Holze, *Ber. Busenges. Phys. Chem.,* 97 (1993) 3

23 B. E. Hayden, K. Kretzscmar and A.M. Bradshaw, *Surf. Sci.,* 155 (1985) 553

24 Y. Hori, O. Koga, H. Yamazaki and T. Matsuo, *Electrochim. Acta,* 40 (1995) 2617

25 R.M. Hernandez and M. Kalaji, *J. Chem. Soc., Faraday Trans.,* 92 (1996) 3957

26 D.W. Shoesmith, S. Sunder, M.G. Bailey, G.J. Wallace and F.W. Stanchell, *J. Electroanal. Chem.*, 143 (1983) 153

27 D.W. Shoesmith, T.E. Rummery, D. Owens and W. Lee, *J. Electrochem. Soc.,* 123 (1976) 790

28 H.H. Strehblow and B. Titze, *Electrochim. Acta*, 25 (1980) 839

29 M. Lenglet, K. Kartouni and D. Delahaye, *J. Appl. Electrochem.*, 21 (1991) 697

30 M. Drogowska, L. Brossard and H. Menard, *J. Electrochem. Soc.*, 139 (1992) 39.

31 M. Drogowska, L. Brossard and H. Menard, *Surf. Coating Technol.,* 34 (1988) 383

32 M. Drogowska, L. Brossard, and H. Menard., *J. Electrochem. Soc.,* 139 (1992) 2787

33 D.W. Daniel, *J. Phys. Chem.,* 92 (1988) 1389

34 S.B. Ribotta, M.E. Folquer and J.R. Vilche, *Corr. Sci.,* 51 (1995) 682

35 J.N. Alhaji and M.R. Reda, *British Corr. J.,* 31 (1996) 125

36 M. Pourbiax, in "*Atlas of Electrochemical Equilibria in Aqueous Solution*", Pergamon Press, London (1965)

37 G.M.Brisard, J.D. Rudnicki, F. McLarnonand and E.J. Cairns, *Electrochim. Acta*, 40 (1995) 859

38 A.A. Dovydov, "*Infrared Spectroscopy of Adsorbed Species on the Surface of Transition Metal Oxides*", John Wiley & Sons, N. York (1990)

39 K. Nakamoto, "*Infrared Spectra of inorganic and coordination compounds*", John Wiley & Sons, New York, 4th Edition, (1986)

40 Michael L. Hair, "*Infrared Spectroscopy in Surface Chemistry*", Marcel Dekker, Inc., New York, (1967)

41 R. Raval, S.F. Parker, M.E. Pemble, P. Hollins, J. Pritchard and M.A. Chesters, *Surf. Sci.,* 203 (1988) 353

42 A. Beden, A. Bewick, M. Razaq and J. Weber, *J. Electroanal. Chem.*, 139 (1982) 203

43 J.W. Russell, M. Severson, K. Scanlan and A. Bewick, *J. Phys. Chem.*, 87 (1983) 293

44 R.M. Hernandez and M. Kalaji, *J. Electroanal. Chem.,* (1997) 5323

45 K.W. Frese, Jr., in "*Electrochemical and Electrocatalytic Reactions of Carbon Dioxide*", Chp. 1, B. Sullivan (Ed.), Elsever Science Publishers, (1993)

46 S.Taguchi, T. Ohmori, A. Aramata and M. Enyo , *J. Electroanal. Chem.*, 369 (1994) 199

47 C.H. Pyun and S.M. Park, *J. Electrochem. Soc.,* 133 (1986) 2024

48 A.C. Chapman and L.E. Thirlwell, *Spectrochim. Acta*, 20 (1964) 937

49 M. Weber and F.C. Nart, *Electrochim. Acta*, 41 (1996) 6531

50 F. C. Nart and T. Iwasita, *Electrochim. Acta*, 37 (1992) 365

51 M.F. Toney, J.N. Howard, J. Richer, G.L. Borger, J.G. Gordan, O.R. Melroy, D.G. Wister, D.Lee and L.B. Sorensen, *Nature*, 368 (1994) 444

52 Y.Hori, O. Koga, Y. Watanabe and T. Matsuo, *Electrochim. Acta*, 44 (1998) 1389

53 O. Koga, T. Matsuo, H. Yamazaki and Y. Hori, *Studies in Surf. Sci. and Catalysis.*, 114 (1998) 569

54 J. Salimon and M. Kalaji, in preparation

55 M.I.S. Lopez, B. Beden, F. Halm, J.M. Leger and C. Lamy, *J. Electroanal. Chem.*, 313 (1991) 323

56 G. Blyholder, *J. Phys. Chem.,* 68 (1964) 2772

57 C. Tang, S.Z. Zau, S.C. Chang and M.J. Weaver, *J. Electroanal. Chem.,* 467 (1999) 92

58 C.T. Williams, C.G. Takoudis and M.J. Weaver, *J. Phys. Chem.,* 102 (1998) 406

59 S.Z. Zau, R. Gomez and M.J. Weaver, *J. Electroanal. Chem.,* 474 (1999) 155

60 Y.T. Je and A.L. Companion, *Bull. Korean. Chem. Soc.,* 16 (1995) 729

61 M. Persson, *J. Chem. Phys.,* 92 (1990) 5034

62 E. Borguet and H-L. Dai, *J. Chem. Phys.,* 101 (1994) 9080

63 S. Hartinger, B. Pettinger and K. Doblhofer, *J. Electroanal. Chem.,* 397 (1995) 335

64 G.J. Edens, A. Hamelin and M.J. Weaver, *J. Phys. Chem.,* 100 (1996) 2322

65 C. Tang, S. Zau, M.W. Severson and M.J. Weaver, *J. Phys. Chem. B*, 102 (1998) 8796

66 A.Ben-Naim., *J. Chem. Phys.,* 42 (1965) 1512

67 G.R. Anderson, *J. Phys. Chem.,* 81 (1977) 273

68 M.W. Severson, C. Stuhlmann, I. Vilegas and M.J. Weber, *J.Chem. Phys.,* 103 (1995) 9832

69 N.V. Richardson and A.M. Bradshaw, *Surf. Sci.,* 88 (1979) 255

70 B.N.J. Persson, M. Tushaus and A.M. Bradshaw, J. Chem. Phys., 92 (1990) 5034

71 J. Mascetti and M. Tranquille, *J. Phys. Chem.,* 92 (1988) 2177

72 Hori, A. Murata and S. Suzuki, *J. Chem. Soc.,* 141 (1994) 2097

73 G. Socrates, "*Infrared Characteristic Group Frequencies: Tables and Charts*", 2nd ed ., Wiley, (1994)

74 L.H. Little, "*Infrared Spectra of Adsorbed Species*", Academic Press, New York, (1966)

75 S.D. Ross and J.A. Goldsmith, *Spectrochim. Acta,* 20 (1964) 781.

76 M.P.S. Sanchez, M Barrera, S. Gonzalez, R.M. Souto, R.C. Salvarezza and A.J. Ariva, *Electrochim. Acta*, 35 (1990) 1337

77 S.B. Ribotta, M.E. Folquer and J.R. Vilche, *Corr. Sci.*, 51 (1995) 682

78 H.G.Thode, M. Shima, C.E. Rees and K.V. Krishnamurty, *Can. J. Chem.,* 43 (1965) 582

79 C.N.R. Rao. P.V. Kamath, K. Prabhakaran and M.S. Hegde, *Can. J. Chem.,* 63 (1985) 1780

80 R. Shiratsuchi, Y. Aikoh and G. Nogami, *J. Electrochem. Soc.,* 140 (1993) 3479

81 R. Shiratsuchi, S. Ishimaru and G. Nogami, *Studies in Surface Science and Catalysis*, 114 (1998) 573

CHAPTER IV

Adsorption of CO at polycrystalline copper

4.1 Introduction

It is clear from the results discussed in Chapter III that CO plays an important rôle during the reduction of CO_2. In this chapter, the adsorption of CO at Cu will be examined in order to confirm that the observations made in the previous chapter are solely due to the presence of CO.

4.1.1 Adsorption of Carbon Monoxide

Depending on the metal surface, carbon monoxide may adsorb either in a molecular form or in a dissociative fashion where in some cases both states coexist on particular surface planes and over specific ranges of temperature. On reactive surfaces of metals (the left-hand side of the periodic table, e.g. Na, Ca, Ti, rare earth metals) the adsorption is almost invariably dissociative, leading to the formation of adsorbed carbon and oxygen atoms. This reaction thereafter leads to the formation of surface oxide and oxy-carbide compounds [1]. By contrast, on surfaces of metals on the right hand side of the d-block, e.g. Cu, Ag, the interaction results in the adsorption of the molecular form. The strength of the interaction between the CO molecule and the metal is also much weaker, so that the metal-carbon monoxide, M-CO bond may be readily broken and the CO desorbed from the surface by raising the surface temperature without inducing any dissociation of the molecule. For the majority of the transition metals, however, the nature of the adsorption (CO molecular or dissociative) is very sensitive to the surface temperature and surface structure; for example the Miller crystal index plane, the presence of any lower coordination sites such as step and defects sites, and a mixture of a variety of surface structure as in polycrystalline surfaces [1, 2].

Molecularly chemisorbed CO has been found to bond in various ways to single crystal metal surfaces particularly, analogous to its behaviour in isolated metal carbonyl complexes as shown in Figure 4.1 [2, 3]. Linear or terminal binding sites (Figure 4.1a) of low coordination involve chemisorptions of a single CO molecule onto one metal substrate atom, M-CO, which has the highest energy and heat of adsorption. Bonding in high

coordination binding sites on the other hand, such as 2-fold bridge (Figure 4.1b) and 3-fold hollow (Figure 4.1c) shows high stability. Consequently, as the number of metal atoms to

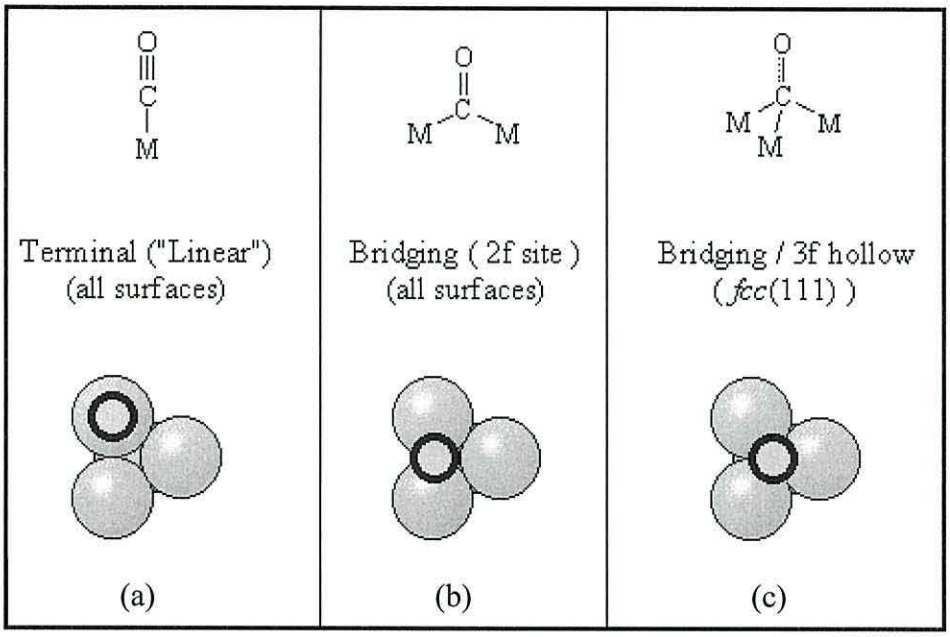

Figure 4.1: Possible structures of chemisorbed CO [2, 3].

which the carbon is coordinated increases, there is a corresponding increase in the M-CO bond order and reduction in the C-O bond order [2].

However, it must be emphasised that CO does not necessarily prefer to bind to the highest available coordination site. So, for example, the fact that there are 3-fold hollow sites on many surfaces with face cubic centred, *fcc* (111), does not mean that CO will necessarily adsorb to these sites. Moreover the preferred site may still be a terminal or 2-fold bridging site, and the site which is occupied, may change with either surface coverage or temperature. The energy difference between the various adsorption sites available for molecular CO chemisorption appears therefore to be very small [4].

Adsorbed carbon monoxide usually gives rise to strong absorption bands in both the infrared (IR) and electron energy loss (EELS) spectra in the νC≡O stretching frequency region (2200 –1800 cm^{-1}). The metal-carbon stretching mode (400 –100 cm^{-1}) is also accessible to EELS. The interpretation of spectra of CO as an adsorbed surface species draws heavily upon IR spectra from related inorganic cluster and coordination complexes with the structure of such complexes usually being available from x-ray single crystal diffraction measurements [XRD]. Nevertheless the IR spectra of νC≡O stretching

frequency can provide a good indication of the surface coordination of the molecule as a rough guideline as shown in Table 4.1.

Coordination type	$\nu(C{\equiv}O)$, cm^{-1}
CO (gas phase)	2143
Terminal CO	2100 - 1980
Bridging (2f site)	1980 - 1800
Bridging (3f / 4f site)	< 1800

Table 4.1: Vibrational frequency of adsorbed CO on metal [5]

The reduction in the stretching frequency of chemisorbed CO from the value observed for the gas phase (2143 cm^{-1}) can be explained in terms of the Dewar-Chatt or *Blyholder model* for the metal-CO bonding, which involves the π-back bonding theory.

4.1.2 Blyholder model - Chemisorbed carbon monoxide [6]

The Blyholder model is commonly used to rationalise the red shift in frequency on adsorbing CO relative to the gas phase. The subsequent increasing frequency as the coverage increases is due to a decrease in π back-bonding character. This is usually associated with donation of *d* electrons from the metal and this form can be used to explain the upward or downward chemical shift of $\nu C{\equiv}O$ on metals.

Figure 4.2 shows a typical classical Blyholder model that considers the metal-CO bonding to consist of two main components:

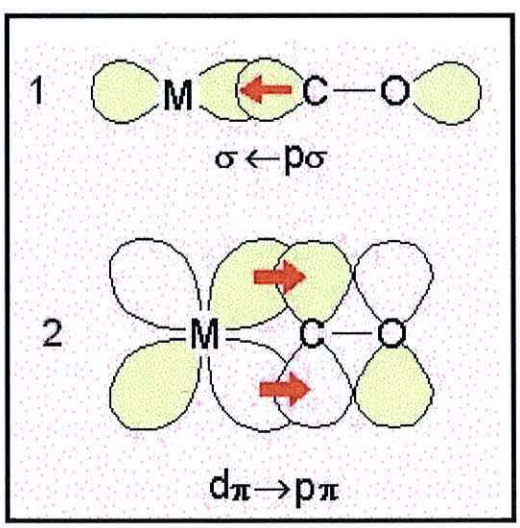

Figure 4.2: A typical classical model of metal-CO bonding [7, 8, 9]

Bonding in CO results from an sp_z-hybridised C, which combines with a p_z orbital of O to produce a σ-bond, while the p_x and p_y orbitals of C and O combine to produce 2π-bonds. This leaves a lone pair of electrons on O2s and Csp_z-hybridised orbitals free to form a coordinate bond with metal (with suitable acceptor orbital such as d-orbital) to form a complex. As illustrated in Figure 4.2, the first component involves the main bonding between CO and the metal (Fig. 4.2-1). This is a σ bonding interaction due to the overlap of a filled 5σ, "lone pair" orbital on the carbon atom with an empty metal *d*-orbital of the correct symmetry to form a dative type bond. In this classical theory, the σ–dative interaction leads to an excess electron density transfer from the CO molecule to the metal centre, thus the bond is repulsive. However polarisation of the metal valence electrons away from the CO reduces this repulsion [6, 7]. Therefore, due to the large formal negative charge on the metal, a π–back donation from a metal dπ-orbital to the antibonding 2π* molecular orbital on the CO ligand occurs to remove the excess negative charge. This is the second component of M-CO bonding and it involves balancing the excess charge (Figure 4.2-2). Donation of metal d electron forms a π bonding interaction due to the overlap of filled metal dσ (e.g. 3*d* of copper) orbital with the 2π* antibonding molecular orbital of CO, thus stabilising the σ–dative bond. The π–back donation in M-CO is in the form of a simple Hűckel molecular orbital where the wave function for the lowest orbital, Ψ_1 places most of the charge on the carbon and oxygen atoms and adds to the bond strengths for both the carbon-oxygen and metal-carbon bonds. However, the second orbital, Ψ_2 whose energy is lower than a metal d-orbital, is "bonding" for the metal-carbon bond but "antibonding" for the carbon-oxygen bond, since the wave function has a node between the carbon and oxygen atoms.

The wave function of the antibonding molecular orbital of 2π*, Ψ_2 plays an important rôle in the interpretation of the behaviour of C-O stretching frequency in M-CO. If only the lone-pair on the C atom forms the σ-bond, the C-O stretching frequency for the carbonyl would be expected to be very close to that of free CO. In fact, this frequency is shifted to somewhat lower values. This is taken as an indication that π–back bonding does occur with some charge occupying an orbital like Ψ_2, which weakens the C-O bond. If more electrons are donated to the Ψ_2-orbital (contributing directly to the π-bonds of C-O but the σ–bond remaining constant) the occupancy of Ψ_2-orbital increases and in turn lowers the

lowers the C-O stretching frequency. On the other hand, if less electrons are donated to ψ_2, the ψ_2-orbital occupancy decreases, thus increasing the C-O stretching frequency.

4.1.3 CO frequency as a function of coverage

The Blyholder model can in many cases be used to explain the chemical shifting in C-O stretch frequency of chemisorbed CO. For example:

i) An increase in CO surface coverage, θ_{CO}, results in a blue shift in $\nu C{\equiv}O$.

As θ_{CO} increases, the competition for the electrons of the metal surface increases, so that there is less charge available to be fed back into each ψ_2–orbital and thus $\nu C{\equiv}O$ increases.

ii) Shifting in binding sites can cause a band shift.

If the types of sites are distinct and if the adsorbed CO is mobile enough to find the site which results in the highest heat of adsorption, CO will adsorb on high coordination number metal atoms (lowest energy sites), thus giving the lower frequency bands, e.g. bridge sites. Eischens *et al.* [10] were the first to observe chemisorbed CO, which has $\nu C{\equiv}O$ band below 2000 cm^{-1}, which is tightly held due to its high binding energy being at the lowest energy level sites. After the site with lowest energy is filled, the next lowest energy site will be filled which gives a band at higher frequency. Therefore when θ_{CO} is large, the result will be a band with its maximum at a high frequency and one or more shoulders on the low frequency side.

iii) Coadsorption of molecules or ions on the metal, which either contribute or receive electrons from the metal surface, will alter the $\nu C{\equiv}O$ frequency region.

If an electron is removed, the occupancy of the ψ_2–orbital is reduced, thus raising $\nu C{\equiv}O$ frequency and inversely if the electron is added to the metal surface, there will be lowering in the $\nu C{\equiv}O$. Adsorbed hydrogen on the metal for example, contributes electron to the surface as shown by magnetic measurement [11] and electric resistance data [12]. Therefore adding H_2 to CO on Pt for instant will shift the $\nu C{\equiv}O$ stretch to a lower frequency. Adsorption of halogen atoms in contrast, will shift the $\nu C{\equiv}O$ band to higher frequency.

iv) High degree of well-defined crystallinity of the metal surface makes it more effective in competing for electron, leaving fewer electrons to contribute to ψ_2-orbital thus increasing the $\nu C{\equiv}O$ frequency. Sintering or annealing the electrode surface for instance, will increase and restore the degree of crystallinity (high crystalline surfaces) and thus increasing the $\nu C{\equiv}O$ frequency.

v) Evaporated metal films on specific support are usually condensed with more amorphous material/particle and less well-crystallised particles which are in turn less effective in competing for electron, thus lowering the $\nu C{\equiv}O$.

vi) Less well-crystallised surfaces (polycrystalline metal) are less effective in competing for electrons due to the surfaces consisting of less crystallographic planes rich with edge atoms, dislocations, and amorphous materials. This leaves more electrons to be donated to Ψ_2-orbital which results in lowering $\nu C{\equiv}O$.

vii) At oxidised surfaces, the electrons are removed from the metal, thus the occupancy of the Ψ_2–orbital is reduced with consequent raising of the $\nu C{\equiv}O$ frequency. For example the formation of oxides or hydroxides on the surface at less negative potentials, will remove the electrons from the surface, thus shifting the $\nu C{\equiv}O$ band to higher frequency.

The above explanations have been used to elucidate the behaviour of adsorbed CO with respect to adsorption and desorption processes from the surface, at single crystal or polycrystalline electrodes at smooth and rough surfaces in the presence of coadsorbed molecules or ions and at clean and oxidised surfaces. When chemisorbed CO is removed from the surface by pumping or heating processes for example, the bands are removed in just the reverse order in which they appear. This would seem to indicate that in the adsorption process, the low energy levels of higher coordination sites are indeed occupied first (produce higher binding energy) followed by the occupation at high energy levels of less coordination sites (produce weaker chemisorbed CO).

4.1.4 Chemical versus dipole coupling shift [13]

The nature of the chemical shift in $\nu C{\equiv}O$ stretching frequency shows an interesting feature of two physical processes in particular which are thought to be responsible for these shifts.

a) The chemical shift is dependent both in amplitude and sign on the nature of the substrate. For example, the existing data for CO adsorption on several metals show that as the CO coverage increases, a substantial downward frequency shifts occur on Cu, upward shift on Pt and large upward frequency shift on Pd.

b) The chemical shift is CO coverage dependent. The shift in the frequency of a vibrational band with coverage provides an additional measure of the interadsorbate interaction. Therefore the frequency shift with coverage is commonly found to have two components.

i. The first component is a static shift caused by chemical changes induced in an adsorbate by neighbouring molecules. This effect involves the changing in electronic distribution between the metal and the different parts of the adsorbed molecule as the coverage or the surface potential is changed. This chemical shift can shift the band either to lower or to higher frequency depending on the details of the interactions in the system under studies.

ii. The second component is a dynamic shift, which is due to direct electromagnetic interactions between the adsorbates (major contribution) and also through the metal (minor) known as dipole-dipole coupling effect. This is a coupling between the vibrating dipoles of the adsorbed molecules; each molecule experiences an oscillatory electric field, which is a sum of the incident optical field and that due to the surrounding vibrating dipoles. The dynamic dipole-coupling shift, on the other hand, always induces a shift to higher frequency with increasing coverage [14].

On polycrystalline Cu (evaporated film in particular), consisting of microcrystallites of various orientations, so that the surface consists of a collection of microscopic high-index crystal faces, the infrared bands for CO lie in the frequency range of approximately 2090 - 2110 cm^{-1} so that an ensemble of such faces could show a broad band. Low index surfaces on the other hand give bands at appreciably lower frequency at 2076 cm^{-1} on Cu(111) and at 2080 cm^{-1} on Cu(100) [15]. Frequency shifts with coverage occur on both single crystal surfaces but are very small and may be of either sign. Dipole coupling is expected to cause an upward frequency shift with respect to the surface coverage. Chemical effects, such as competition for the electrons involved in synergetic σ and π–bonding, may cause shifts of either sign. Therefore it is very difficult to predict the magnitude of these shifts, which may be determined by isotopic decoupling. By varying the composition from a dilute mixture of ^{12}CO and ^{13}CO to pure ^{12}CO, it is possible to demonstrate a significant shift in frequency as the coverage increases arising from coupling interactions rather than chemical effects, which would be independent of isotopic composition [15, 16].

The static chemical rationale for an upward frequency shift with coverage may be less appropriate for the noble metals such as Cu(111) [17], Au and Ag [18] in which π-back bonding is believed to be far less appropriate. On silver for instant, a negative chemical shift (a shift to lower frequency with increasing coverage), dominates a positive dynamic shift. A large part of the chemical shift could be attributed to the influence of the local work function on the bonding of the CO without any interaction through the metal

and the dynamic chemical shift was well described by a dipole-coupling model [13]. Hollins and Pritchard [15] offered an alternative explanation of adsorbed CO behaviour on Cu where the predominant effects is due to CO 5σ bonding to the metal in which the π-back bonding is assumed to be unimportant on Cu. Due to the 5σ orbital having some anti-bonding character with respect to the CO bond, an increased coverage leads to decreasing donation of 5σ electrons to the dative bond formed with the metal so that the CO bond will weaken with increasing coverage, leading to the downward frequency shift. Neither of these arguments gives any clear picture of the range of the chemical effect, or of the nature of the competition for metal *d* electrons or CO 5σ electrons with coverage. However if an argument is based only on the effect of CO 5σ electrons, one might expect the weakening of the CO bond to be directly linked to a similar continuous weakening of the metal-carbon bond, which is not found experimentally.

Woodruff and Hayden [14] gave an alternative explanation based on the fact that the existence, or otherwise, of π back bonding depends on the relative energies of the Fermi level and the CO 2π anti-bonding level and requires no explicit consideration of the metal *d* electrons. Studies using cluster calculations [19, 20] showed that due to the interaction of CO with the metal, the CO 2π anti-bonding energy level splits into two states, anti-bonding ($2\pi_a$) and bonding ($2\pi_b$) character relative to the metal-CO bond. The bonding character ($2\pi_b$) is shown in Figure 4.3. In the ground state the $2\pi_a$ level lies well above the Fermi level (~2-3 eV) while the $2\pi_b$ lies close to the metal Fermi level; its exact position is

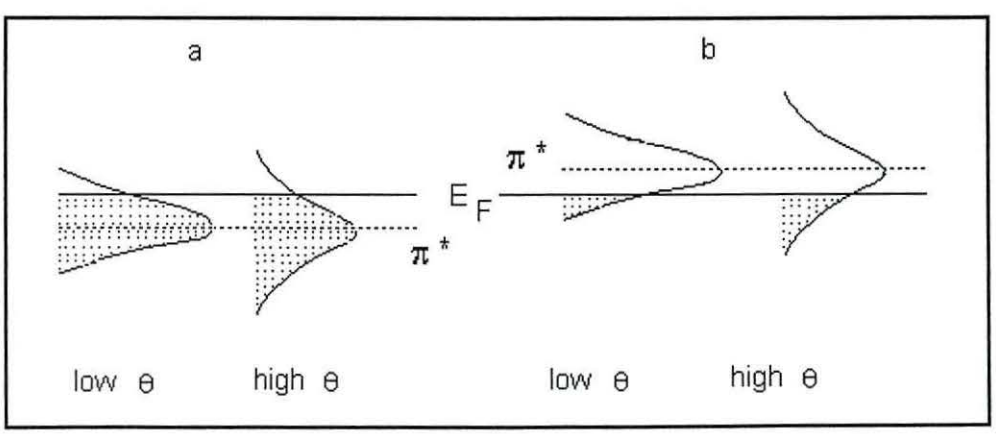

Figure 4.3: Schematic diagram showing the variation in occupation of the broadened of CO $2\pi_b$ state for the cases in which this state lies (a) below and (b) above the Fermi level (E_F) of the metal [14].

sensitive to the method of calculation but as it is interacting with the metal band states, one expects some broadening in any case due to changes in energy level. This partly broadened level is either slightly below or slightly above the Fermi level. If the broadening is sufficient, some partial filling of the state will occur in either case. This is then the π back bonding contribution, which can evidently couple to s-p states at the Fermi level if no *d* states are available. Therefore in the case of increasing coverage, the 2π levels on the CO molecules are exceedingly diffuse and will overlap even at quite low coverage. This overlap leads to a broadening of the 2π states into two-dimensional surface bands whose width reflects the degree of overlap. This broadening of the $2\pi_b$ level leads to a significant change in the occupation of the level. There are two important features where;

a) If its central position lies below the Fermi energy, E_F, then it becomes less filled (Figure 4.3a). This effectively depicts the usual Blyholder argument of decreasing π back bonding with coverage and an associated frequency increase with coverage (suitable explanation for transition metal case, such as Pd).

b) If its central position is above E_F, it becomes more filled. It provides a potential explanation for the downward chemical shift on noble metal such as Cu(111), Ag and Au where in these metals; the back bonding is relatively unimportant.

However in this model, the argument is based effectively on a through space interaction rather than a through metal one, where the actual change in anti-bonding character arises from the shift of metal electrons. Nevertheless this model is consistent with the conventional wisdom that back bonding is important, in any transitions metal.

In conclusion, although many studies on the adsorption of CO on Cu have been reported by Hayden and coworkers [14, 17, 21, 22], Hollins and coworkers [15, 16, 23], Seki and coworkers [24, 25], Hori and coworkers [26-29] and on evaporated film and polycrystalline copper by Eischen *et al.* [30], Pritchard [23, 31, 32], Little [33], Hair [34], Hori *et al.* [28] and the latest report by Hernandez and Kalaji [35], a concordant conclusion about the exact mechanism for CO interaction on polycrystalline copper surfaces is still unclear. Furthermore in the present study, the main product of the electrochemical reduction of carbon dioxide is adsorbed CO. Therefore it is important to study the CO adsorption behaviour on polycrystalline copper to gain more insight into the mechanism of CO_2 reduction. In this chapter, the adsorption of CO on polycrystalline copper electrode was investigated in phosphate buffered solution. The electrochemical behaviour and the

spectroscopic properties of the adsorbed CO on Cu were investigated as a function of polarisation potential (E_{pol}), polarisation time ($T_{hold\ min}$), applied starting potential (E_{ASP}), CO surface coverage, pH and temperature.

4.2 Experimental

The experimental details for the electrochemistry and the spectroscopic studies have been discussed in detail in Chapter II.

4.3 Results and discussion

4.3.1 Cyclic voltammetric

The voltammetric response of Cu in CO and N_2 saturated phosphate buffer solution at 0.01 V/s is shown in Figure 4.4 and similar to that reported in the literature [35]. In N_2 saturated solution, the formation of copper oxides and hydroxides is evident on the forward sweep (Fig 4.4a). On the reverse sweep, the reduction of such species is observed around –0.15 V. When the solution was saturated with CO, two reduction waves are observed, C_1 and C_2 at –0.145 V and –0.25 V respectively. The onset of hydrogen evolution is shifted

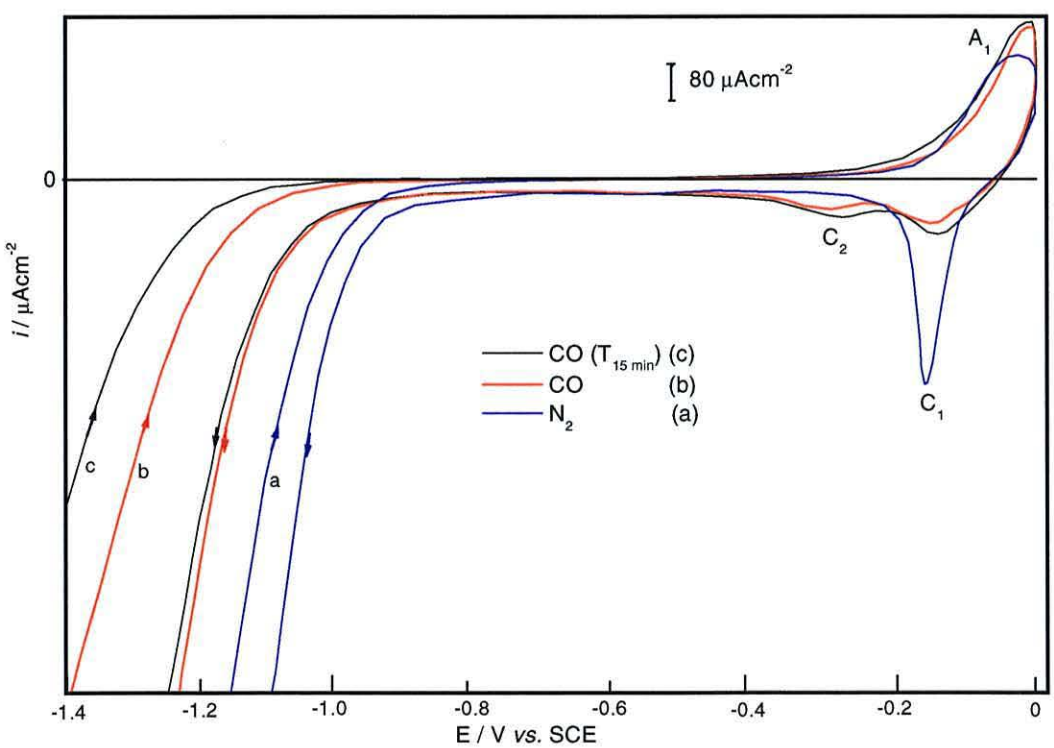

Figure 4.4: Voltammogram of copper at ν= 0.05 Vs^{-1} in (a) N_2 and (b) CO-saturated buffered phosphate solution (pH 6.8) and (c) CO-saturated with polarised electrode at E_{pol} = -1.4 V for 15 min at 18 °C.

cathodically upon saturation with CO (Fig 4.4b). The data clearly indicate that CO has a profound influence on the electrochemical behaviour of Cu. When the electrode was polarised at –1.4 V for 15 min prior the voltammogram measurement, the onset of hydrogen evolution is further shifted cathodically (Fig 4.4c). It might due to the effect of the adsorption of CO on the surface and will be discussed in detail spectroscopically in other section. The rest of the chapter deals with the studies carried out at lower sweep rates and analysis of the dependence of the adsorption of CO as a function of potential, time and pH in order to clarify this interaction.

Figure 4.5 shows of the effect of positive limit on the voltammetric behaviour of Cu in a CO-saturated solution. At least two redox couples can be observed: A_2/C_2 at –0.120/ -0.245 and A_1/C_1 at –0.1/-0.098 V. The voltammograms were recorded at 10 mV/s which clearly indicates that the reduction in slow sweep rate results in a better resolution of the redox peaks (compared to Figure 4.4). The first couple, A_2/C_2 is most likely to be associated with the oxidation of Cu to Cu(I) and the subsequent formation of the oxides or hydroxide of Cu(I) and their corresponding reduction. However the discussion below will show that CO is also involved at these potentials.

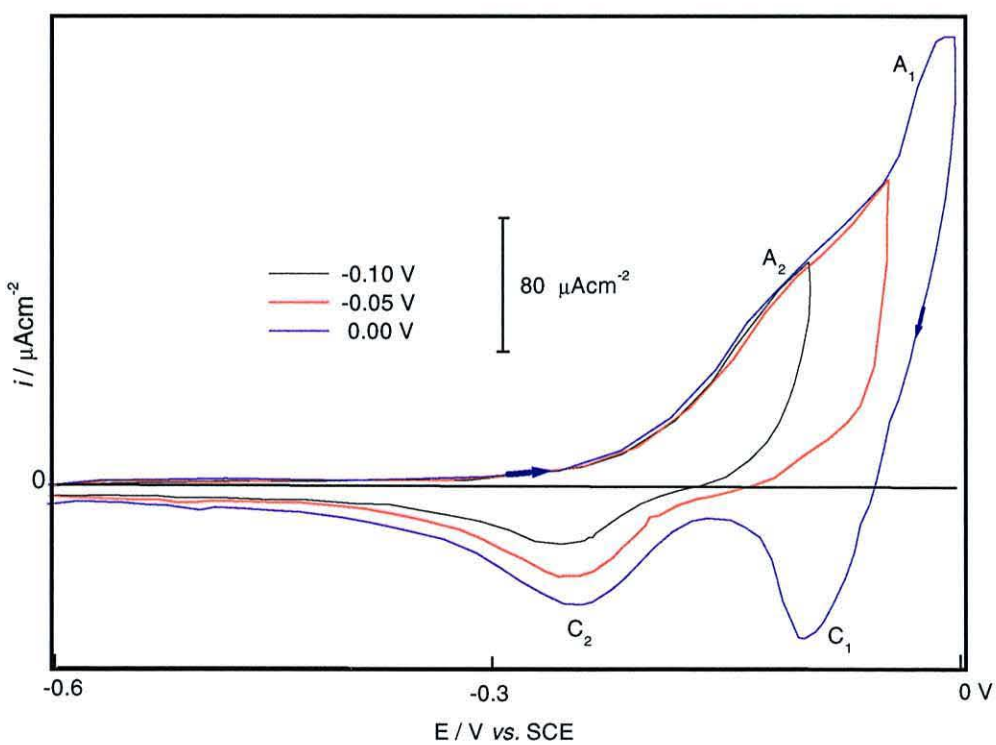

Figure 4.5: Voltammogram of copper at ν= 0.01 Vs^{-1} in CO-saturated buffered phosphate solution at 18 ^{0}C with different anodic potential limit.

A_1/C_1 on the other hand, corresponds to the oxidation of the surface Cu(I) to Cu(II) and the reduction back to Cu(I). Further evidence for this can be obtained when analysing the voltammograms at a very slow sweeps rate, 1 mV/s. Figure 4.6 shows that the voltammogram of the degassed solution is similar to that obtained at faster sweep rates. However, for the CO saturated solution, the ratio of the anodic current density relative to the N_2-saturated solution is much higher at low sweep rates. The charge consumed during the oxidation process at 1 mV/s when the solution is saturated with CO is at least 4 times larger than the N_2-saturated solution.

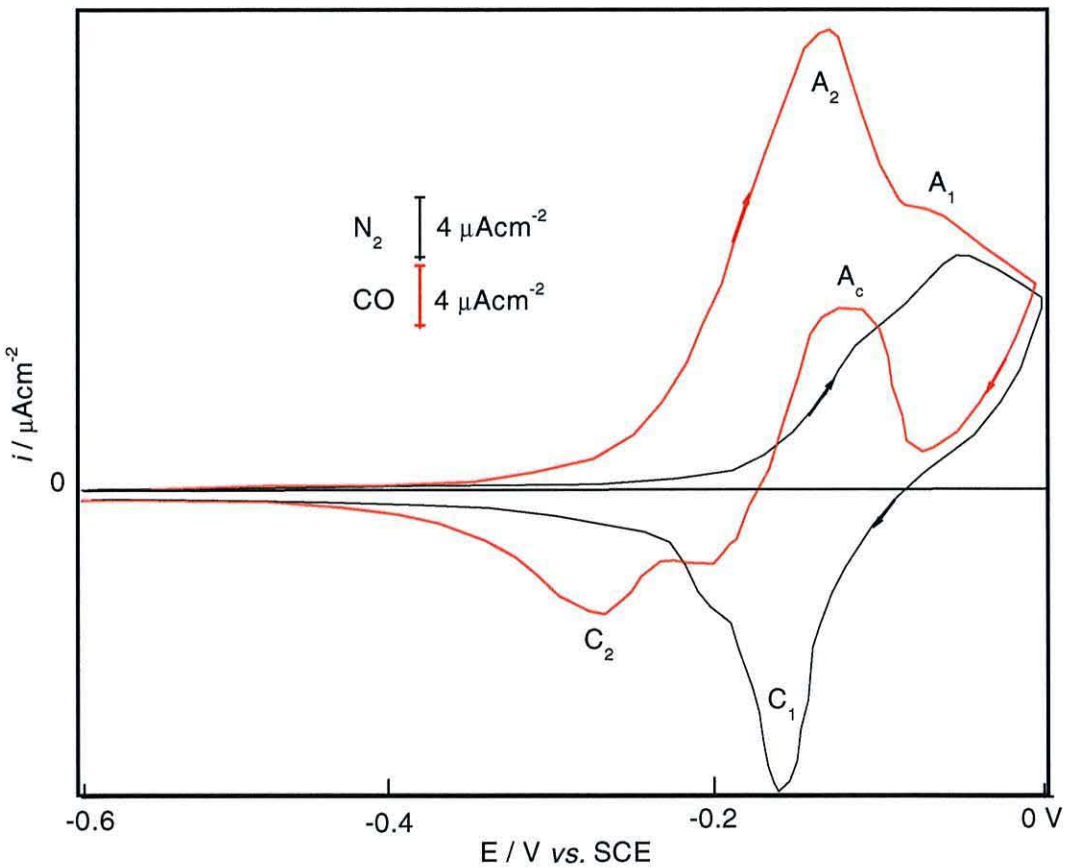

Figure 4.6: Voltammogram of copper at ν= 0.001 Vs^{-1} in N_2 (black) and CO (red) saturated buffered phosphate solution (pH 6.8) at 18 °C.

Another interesting feature is that the anodic current is observed during the negative sweep (A_c) which was also observed by Hernandez and Kalaji [35]. Dragowska *et al.* [36, 37] observed a similar behaviour when copper surfaces were corroded in solutions containing chloride anions. The authors attributed this to the dissolution of the metal. Hernandez and Kalaji showed using spectroscopic and chronoamperometric measurements

that the anodic current on the negatives sweep coincides with the formation of Cu(I) carbonyl species either by direct reaction of CO with Cu(I) or by the reductive reaction of CO with Cu(II) species. However, the authors failed to observe any adsorbed linear bonded CO on Cu in the potential range 0 to –1.15 V. On the other hand, the results presented in Chapter III indicate that the appearance of adsorbed linear bonded CO in CO_2-saturated solution can only be observed if the potential is polarised for a minimum of 10 minutes at values more negative than –1.1 V. Hence, similar experimental procedure as those utilised in Chapter III, were repeated for CO saturated solutions in order to ascertain the origin of the bands observed during the reduction of CO_2.

4.3.2 *In situ* FTIR

4.3.2.1 Linearly bonded adsorbed CO, Cu-CO_L

In this set of experiments, the solution was first degassed with N_2 for 30 minutes in order to remove oxygen and CO_2. After that, the solution was saturated with CO (bubbling 15 min), the electrode was then introduced into the solution and a potential, applied starting potential, E_{ASP}, was applied. Spectral collection was performed after the observed current had stabilised which normally took 30 s. The potential was then stepped in 0.1 V increments to –0.7 V as shown in Scheme A in Figure 4.7. Values for E_{ASP} ranged from

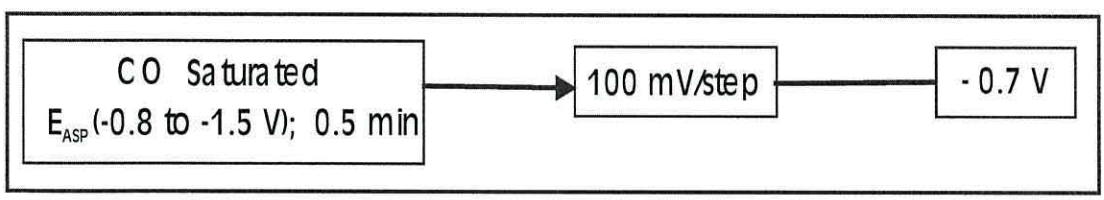

Figure 4.7: Scheme A used to evaluate the adsorption of CO on Cu.

-0.8 V to -1.5 V. Figure 4.8 shows the results obtained from 14 sets of experiments. The first set, Figure 4.8 (a_1-a_7) show the spectra obtained from ^{12}CO-saturated solutions. Each spectrum was calculated by subtracting the spectrum obtained at –0.8 V (reference spectrum at E_{ref} = -0.8 V) in each set, from the spectrum collected at E_{ASP}. A monopolar band is observed at 2085 cm^{-1} (at –1.2 V) that shifts with potential to 2078 cm^{-1} at –1.5 V. This band is neither observed in N_2-saturated solution under the same conditions nor in ^{12}CO-saturated solution when *s*-polarised radiation was used. From the surface selection rules, it is clear that the species responsible for this absorption is an adsorbed species and as expected it is assigned to linear bonded CO, Cu-$^{12}CO_L$. The band position is in

agreement with νC≡O stretching frequency of adsorbed CO on Cu, which lies in the frequency range of 1990 to 2100 cm^{-1} for linearly adsorbed CO on thin Cu films [28, 38, 39] and on Cu(100) at 2070 to 2090 cm^{-1} [17, 40]. The adsorption of CO must be responsible for the observed negative shifts in the onset of HER as indicated by voltammogram in Figure 4.4.

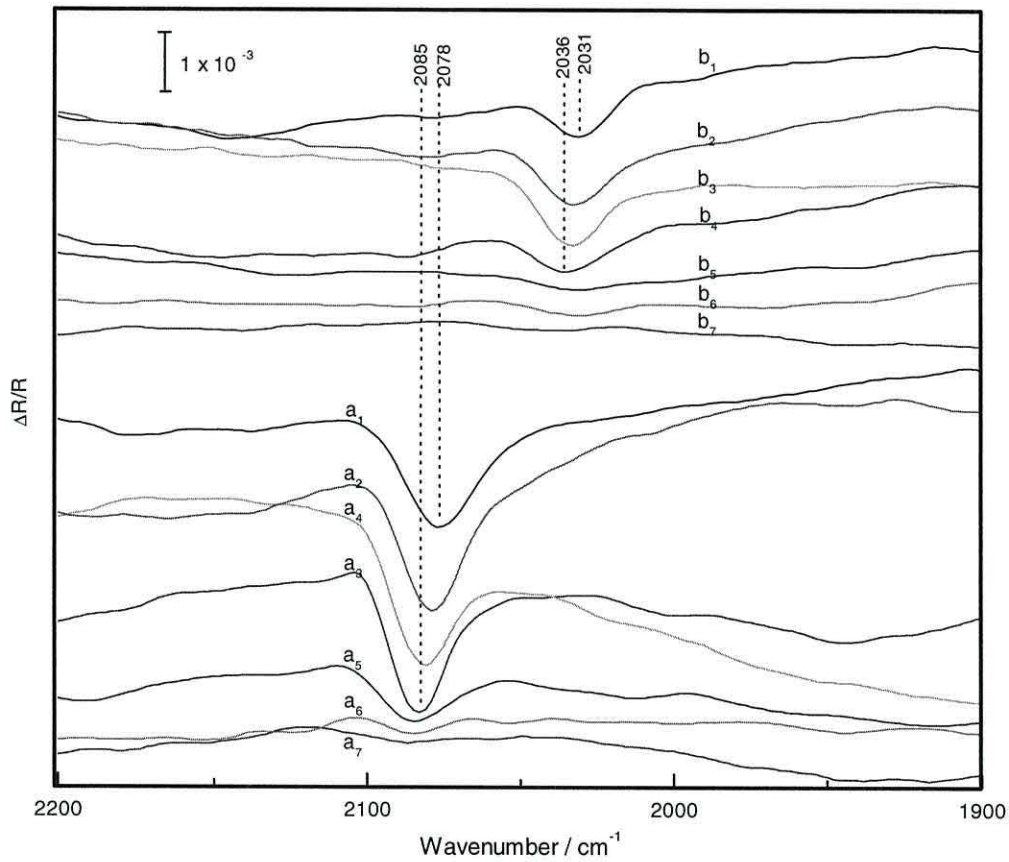

Figure 4.8: SNIFTIR spectra obtained from a ^{12}CO (a_1- a_7) and ^{13}CO-saturated (b_1-b_7) buffered phosphate solution at each E_{ASP} at 0 °C. Spectra shown are at (1) E_{ASP} = -1.5 V to (7) E_{ASP} = -0.9 V. The spectra are normalised relative to E_{ref} = -0.8 V of each set.

The other spectra shown in Figure 4.8 (b_1-b_7) were obtained when ^{13}CO was used. The other experimental conditions were the same as those used with ^{12}CO. Linear bonded ^{13}CO, Cu-$^{13}CO_L$ is observed at 2036 cm^{-1} (at –1.2 V) and shifted to 2031 cm^{-1} (at –1.5 V Figure 4.8 b_7). The frequency shift with potential is clearly due to the same phenomenon as with ^{12}CO. The isotopic frequency shift (49 cm^{-1}) is due to the differences in the reduced mass of the molecule [41, 42]. Again this is well in agreement with other reports on ^{13}CO isotopic labelling effect for adsorbed ^{13}CO on Cu(111) and Cu(110) where the band appears at 2030 cm^{-1} [23, 43] and on other metal such as Pt(111) at 2035 cm^{-1} [44,

45]. The potential-dependent frequency shift was around 15 cm^{-1}/V. Pritchard and Sims [39] reported that the stretching frequency of adsorbed CO on Cu does not exhibit a large shift with coverage and potential because the chemical and dipole coupling shifts (which have the opposite effect on the frequency) are nearly the same. Nevertheless, the results obtained here show a red shift with increasing negative potential. This can be explained in terms of the partial cancellation of the blue coupling shift and the red chemical shift, as suggested by Woodruf and Hayden [14] and by Woodruf *et al.* [21].

4.3.2.1.1 The amount of Cu-CO_L as a function of potential and concentration

Figure 4.9 shows the integrated peak area for the bands observed from experiments carried out under the same condition as those used to produce the spectra in Figure 4.7a, except that the CO bubbling time was varied. One set of data was obtained for short bubbling time (3 min, black curve) and the other set was obtained at long bubbling time (30 min, red curve). It is clear from the red curve that for CO saturated solutions, the amount of CO adsorbed linearly at the surface, increases as the initial applied potential, E_{ASP}, is changed

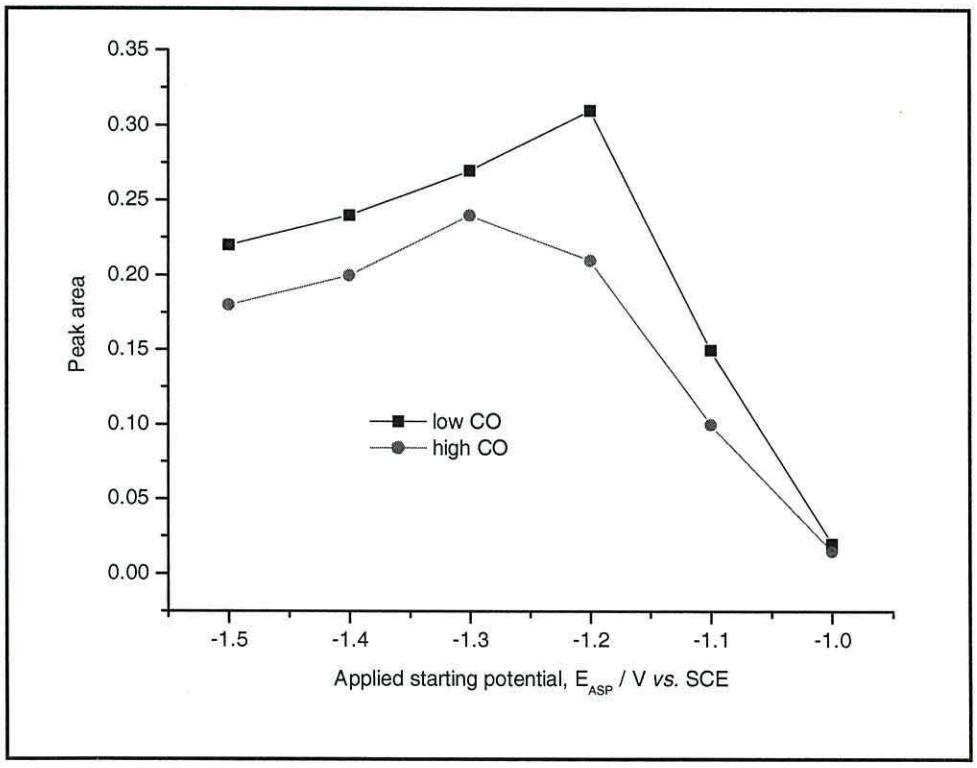

Figure 4.9: Integrated peak area of Cu-CO_L at E_{ASP} as the SNIFTIR spectra are normalised relative to E_{ref} = -0.8 V at each set.

from –1.5 V to –1.3 V, after which it decreases rapidly. It is important to point out at this stage that the analysis has been done when E_{ASP} was varied and not when the initial was stepped to different potentials. The later situation will be discussed later. Unexpectedly, when the concentration of CO was decreased (3 min bubbling time), the amount of linear bonded CO increased compared to the saturated solution. This indicates that for linearly bonded CO is inversely proportional to the concentration of CO in solution. Figure 4.10 shows a comparison between the spectrum obtained at E_{ASP} = -1.3 V (Fig 4.10a) and the spectra obtained at –1.3 V after E_{ASP} was set at –1.4 V (Fig 4.10b) and –1.5 V (Fig 4.10c). The spectra clearly show that the amount of linearly bonded CO at –1.3 V decreases if E_{ASP} was more negative than –1.3 V. A new absorbance is observed, when the data is treated in this way, at around 1945 cm^{-1}. Its intensity is at its highest when

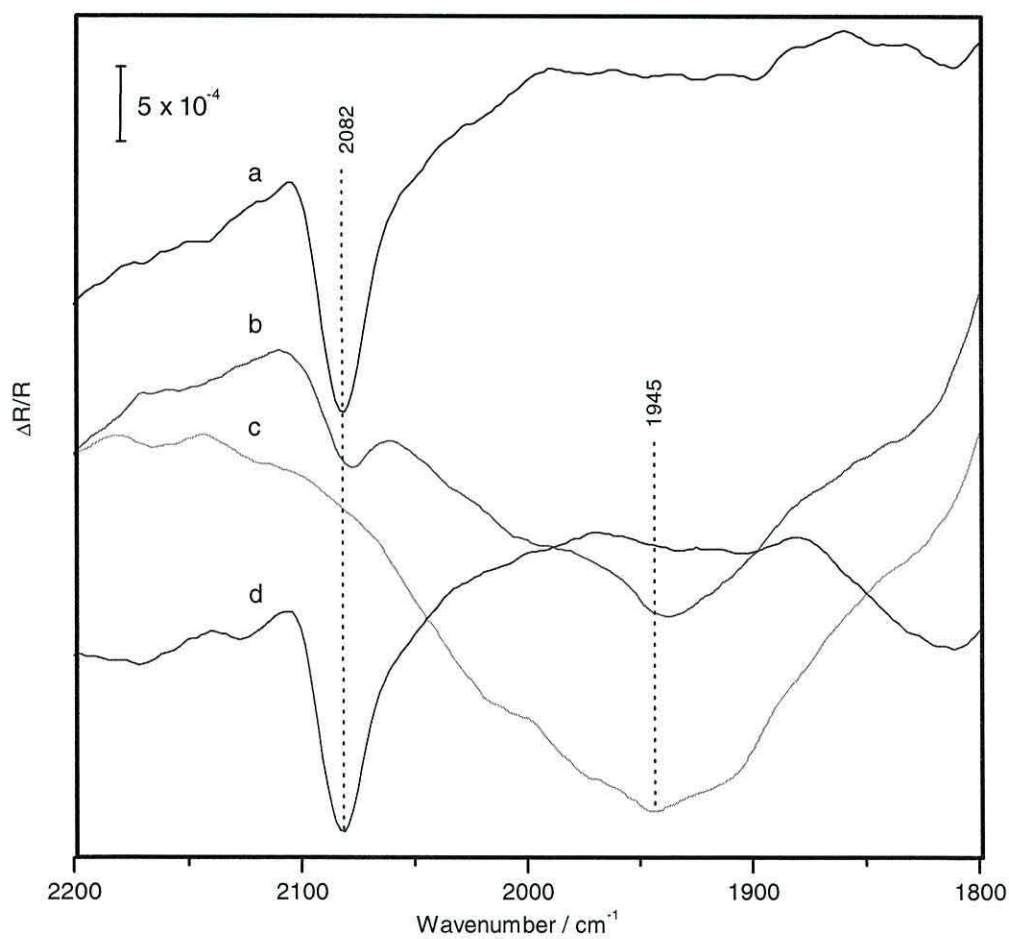

Figure 4.10: Comparison of the Cu-CO_L at –1.3 V obtained from different E_{ASP} values, (a) E_{ASP} = -1.3 V, (b) E_{ASP} = -1.4 V, (c) E_{ASP} = -1.5 V and (d) another E_{ASP} = -1.3 V, as the spectra are normalised relative to E_{ref} = -0.8 V of each sets.

E_{ASP} = -1.5 V and completely disappears at E_{ASP} = -1.3 V. It is very tempting to assign this absorbance to Cu-H which is reported to be at 1940 cm^{-1} [46]. It has been postulated that at negative potentials, metallic copper is formed according to the following equation [47-51];

$$Cu(OH)_{ad} + e^- \leftrightharpoons Cu + OH^-$$

Others suggested [52] the formation of a hydrogen adsorbate;

$$Cu + H_2O + e^- \leftrightharpoons CuH_{ad} + OH^-$$

Therefore in the work reported here, it may be concluded that after the reduction of the surface hydroxide layer, Cu-H can be produced in competition with CO adsorption.
At potentials more negative than –1.3 V, Cu-H can be produced and compete with the adsorption of CO on the clean surface. However, this conclusion does not fully explain the following observation. As the potential is stepped from E_{ASP} = -1.5 V to –1.3 V no Cu-CO_L is observed at –1.3 V. However if the potential is stepped from E_{ASP} = -1.4 V to –1.3 V, a small Cu-CO_L band is observed. The main difference in the experiment is the time taken to reach –1.3 V. Evidence will be provided in the next section dealing with bridge bonded CO to show that the effect of polarisation time is to increase CO surface coverage, θ_{CO} and hence lead to the transformation to bridge bonded CO. The influence of the concentration of dissolved CO on θ_{CO} will be also discussed in that section.

4.3.2.2 Anion effect on the adsorption of CO

The presence of anions such as hydroxide, carbonate and phosphate in solution might cause competition for the adsorption sites as the electrode surface is polarised. The competition for the adsorption sites between pre-adsorbed anions and CO has been reported [53]. Huber *et al.* rationalised the competition for the adsorption site by the charge transfer process, which occurs within desorption of pre-adsorbed anion and the adsorption of CO. Koga *et al.* suggested that the competitive adsorption of CO on Cu(100) and Cu(111) with adsorbed anions such as carbonates and monobasic phosphates occurred at potentials near or below the potential zero charge (pzc) [54]. CO displaces specifically adsorbed anions, $H_2PO_4^-$ at a certain potential below pzc, and in turn it is reversibly displaced by the anions when the potential is reversed at nearly the same potential [29]. The same argument might explain the behaviour of CO adsorption on polycrystalline copper surface. Figure 4.11 (the full spectrum of that shown in Figure 4.8a) shows the appearance of a band at 3660 cm^{-1} at potentials of –0.9 V, where an adsorbed CO is not observed (Fig 4.11g). At potentials where CO adsorbs on the surface

from –1.0 to –1.5 V, the band disappears. The band at 3660 cm^{-1} can be assigned as νOH, the stretching frequency of adsorbed surface hydroxide [55, 56]. Hartinger *et al.* reported the remarkable observation that a Cu(OH) surface species, $Cu(OH)_{ad}$ is formed upon cathodic reduction of Cu at potentials negative to the Cu(I) oxide voltammetric wave. The

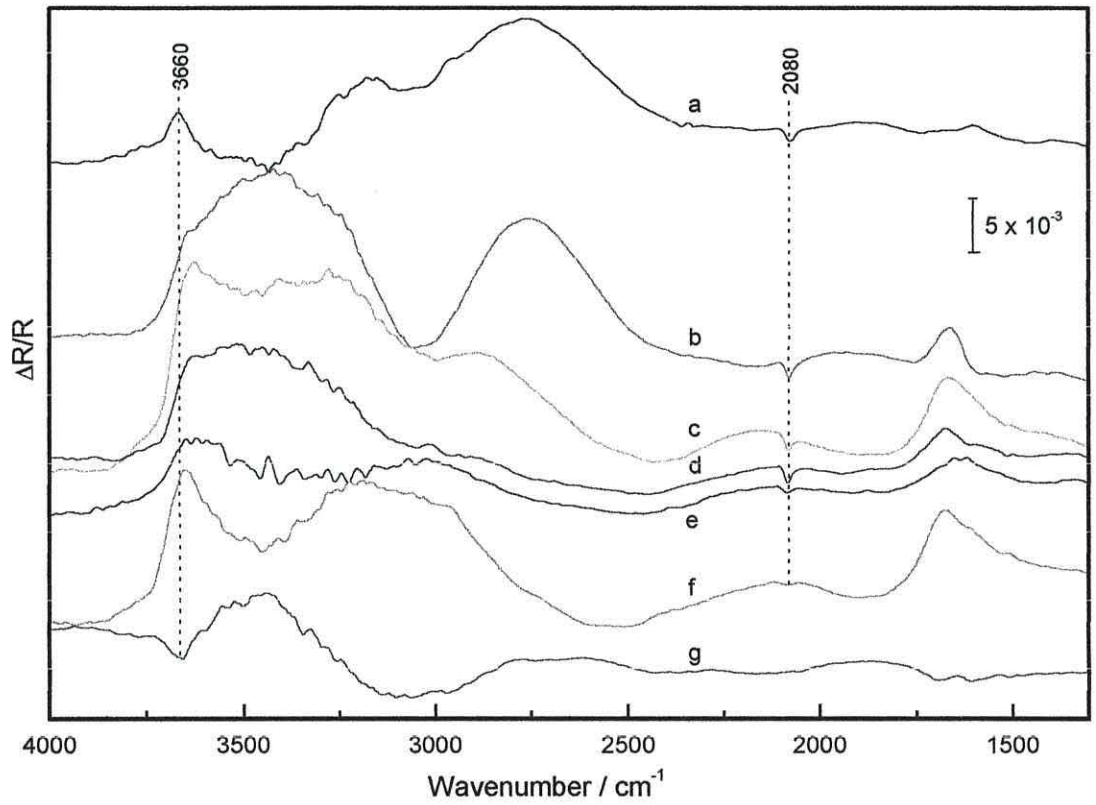

Figure 4.11: SNIFTIR spectra of a ^{12}CO-saturated buffered phosphate solution at each E_{ASP} at 0 °C. Spectra shown are at (a) $E_{ASP} = -1.5$ V to (g) $E_{ASP} = -0.9$ V; normalised relative to –0.8 V of each set.

authors explained this in terms of the reaction of surface oxygen with water or protons as follows:

$$Cu(O)_{ad} + H^+ + e^- \leftrightharpoons Cu(OH)_{surf} \quad (1)$$

$$Cu(O)_{ad} + H_2O + e^- \leftrightharpoons Cu(OH)_{surf} + OH^- \quad (2)$$

Moreover it has been reported that a decrease in adsorbed CO band intensity on platinum can be attributed to a decrease in adsorbed CO coverage, which is induced by hydroxyl adsorption [57]. Therefore the adsorption of CO may be hampered by the surface hydroxide and will not take place until this layer is reduced. However once the surface is reduced, adsorbed hydrogen may also be formed.

4.3.2.3 Bridge-bonded adsorbed CO, Cu-CO_B

As already mentioned, the adsorption of CO on metal surfaces has been reported to occur at a variety of binding sites, namely on atop/terminal/linear and multiple/bridge binding sites. The results discussed so far show that immediately after the application of a cathodic potential, CO is adsorbed as Cu-CO_L. Several reports suggested that the preference for the binding sites depends on the CO surface coverage, θ_{CO} [58 - 62] and the applied potential [63]. In this section the surface coverage was varied by varying the polarisation potential, the polarisation time or by changing the concentration of CO in solution.

Figure 4.12 shows the SNIFTIR spectra observed when the potential was stepped in 0.1 V increments from –1.4 V to 0 V and back to –1.4 V. For the sake of clarity, the figure shows the spectra at 0.2 V increments. The potential was initially held at –1.4 V for

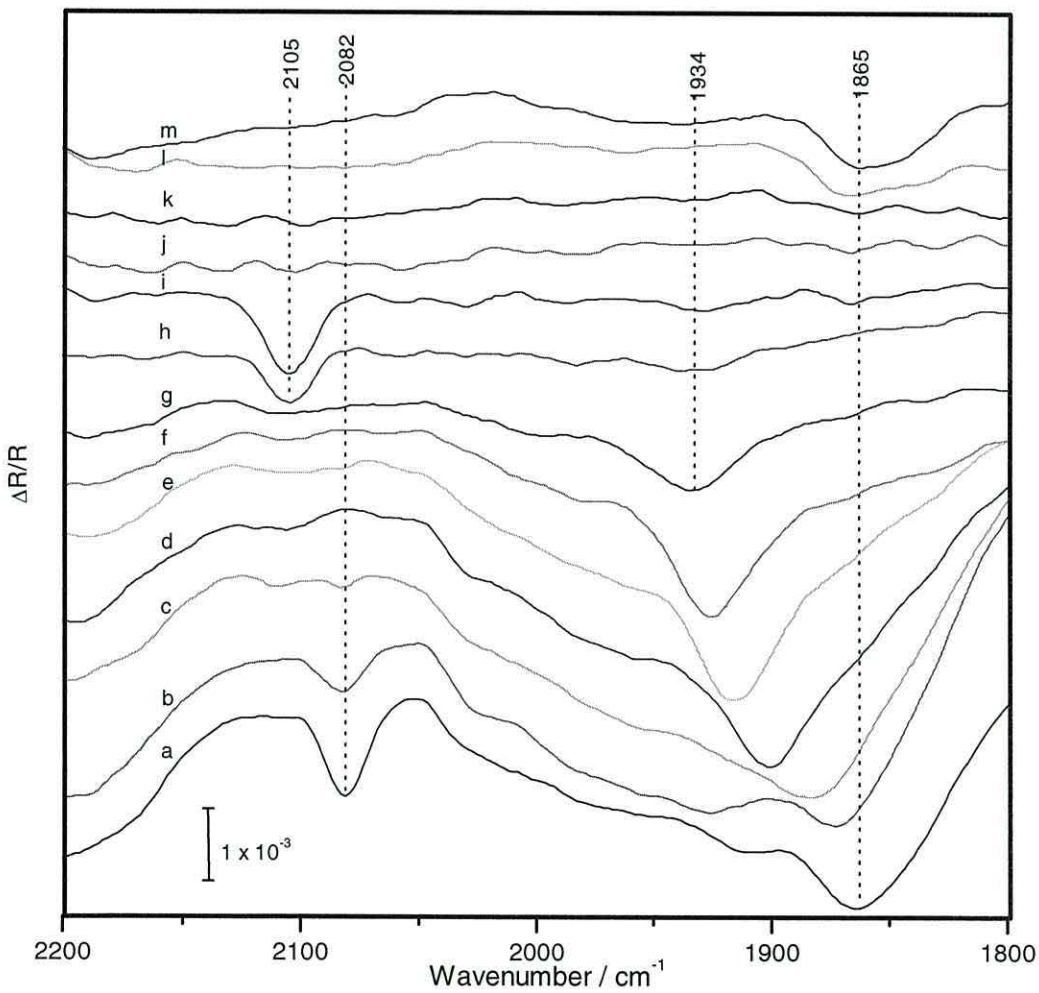

Figure 4.12: SNIFTIR spectra obtained from ^{12}CO-saturated buffered phosphate solution after electrode polarisation at E_{pol} = –1.4 V for 15 min. Spectra shown from (a) –1.4 V to (h) 0 V and back to (m) –1.2 V of reverse sweep in 0.2 V/step; normalised relative to spectrum obtained at –0.4 V (reverse sweep).

15 min before any spectra collection, as of Scheme B in Figure 4.13. Therefore the experimental conditions were similar to those used to obtain the cyclic voltammogram shown in Figure 4.4c (page 113). The spectra were normalised relative to the spectrum

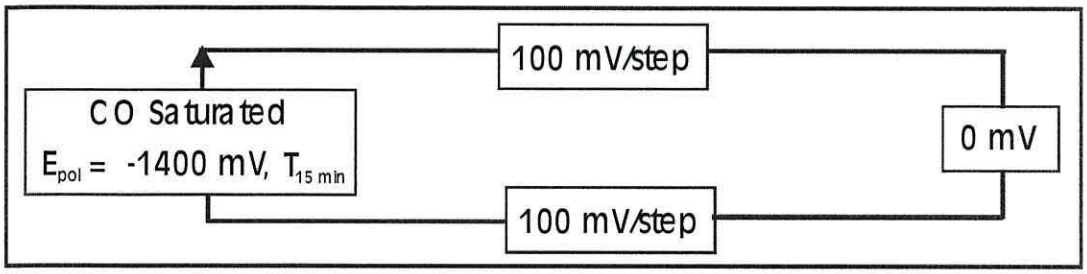

Figure 4.13: Scheme B used to evaluate the adsorption of CO on Cu.

obtained at –0.4 V on the reverse sweep, which is the potential at which the reduction of the surface occurs. At –1.4 V (Fig 4.12a), the negative band at 2082 and 1865 cm^{-1} are due to linear bonded and bridge bonded CO, Cu-$^{12}CO_B$ respectively. The latter band was briefly discussed in Chapter III and its assignment is in agreement with values reported in the literature [35, 63-65). Linear bonded CO was not observed after the potential has been stepped to less negative potentials beyond –1.0 V (Fig 4.12c) and throughout the reverse sweep.

On the other hand, bridge bonded CO undergoes a frequency shift with potential of 58 cm^{-1}/V. At 0 V (Fig 4.12h), the surface is oxidised and a new band appears at 2015 cm^{-1} which has previously mentioned, is due to the formation of Cu(I)-CO. On the reverse sweep, the spectral region shown is featureless until a potential of –1.0 V (Fig 4.12 l) is reached, when bridge bonded CO starts to reappear. When the same procedure was repeated using ^{13}CO, the spectral features shown in Figure 4.14 are the same as those observed with ^{12}CO except for isotopic shift in the bands associated with Cu-$^{13}CO_L$, Cu-$^{13}CO_B$ and Cu(I)-^{13}CO which shift to 2028 cm^{-1}, 1817 cm^{-1} (frequency shift with potential 50 cm^{-1} /V) and 2058 cm^{-1} respectively. The shift in Cu-$^{13}CO_B$ is well in agreement with other isotopic labelling effects for adsorbed bridge-bonded ^{13}CO on other metal such as Pt(111) at 1820 cm^{-1} [44, 66] which shifts by about 50 cm^{-1}. As far as the present study is concerned the present value at 1817 cm^{-1} and 2058 cm^{-1} is the first ever reported isotopic shifts of adsorbed bridge-bonded ^{13}CO, Cu-$^{13}CO_B$ and copper(I)-carbonyl, Cu(I)-^{13}CO at polycrystalline copper. When the same procedure was repeated in D_2O, no new bands were observed except for those associated with D_2O. It is worth noting that the Cu-CO_L, Cu-CO_B and Cu(I)-CO band intensities are higher in D_2O solutions of phosphate or

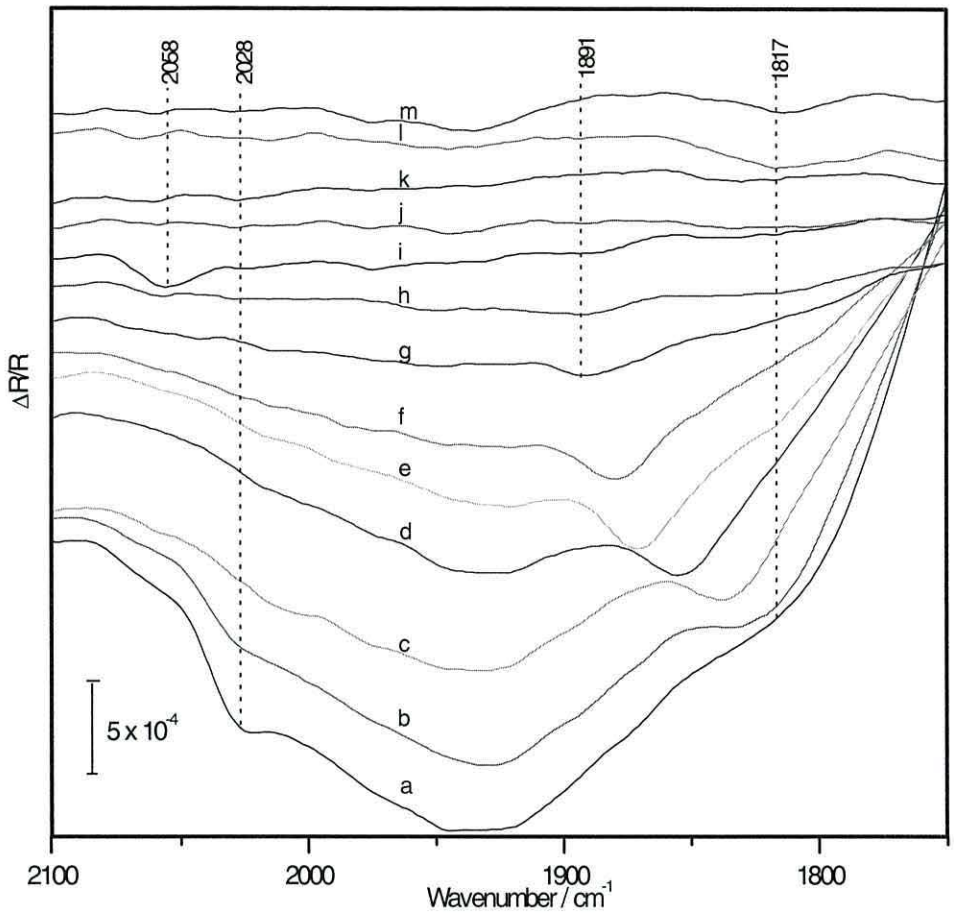

Figure 4.14: SNIFTIR spectra obtained from ^{13}CO-saturated buffered phosphate solution after electrode polarisation at $E_{pol} = -1.4$ V for 15 min. Spectra shown from (a) –1.4 V to (h) 0 V and back to (m) –1.2 V of reverse sweep in 0.2 V/step; normalised relative to spectrum obtained at –0.4 V (reverse sweep).

deuterated phosphate compared to those in H_2O. An increment of about 10 % in peak area of adsorbed CO occurs in D_2O-deuterated phosphate solution (spectra not shown). Anderson [67] reported that there was an increase of about 35% in total intensity of CO_2 in D_2O compared to that in H_2O whereas Ben-Naim [68] has reported about 10% enhanced solubility of argon gas in D_2O due to the high "degree of crystallinity". The same observation was made in the present study indicating higher band intensity/peak area of adsorbed CO in deuterated phosphate/D_2O solutions due to increase solubility of CO in D_2O compared to H_2O.

The data clearly show that there exist at least three different forms of CO at the surface of Cu; stabilities seem to be dependent on the applied potential. The interconversion between different forms of adsorbed CO, especially linearly adsorbed CO

(CO_L) and bridged adsorbed CO (CO_B), has been observed at several metals and this transformation was rationalised in terms of the steric repulsive strain between adjacent CO molecules at high values of θ_{CO}. Zou *et al.* [60] reported that the adsorption of CO on Pd(110), Pd(111) and Pt(111) where νC≡O band shifted from single low frequency at 1810 cm^{-1} (3-fold hollow) at low levels of CO, to a mixture of bands at 1810 and 1930 cm^{-1} (2-fold) at low coverage of $\theta_{CO} = 0.4$. At θ_{CO} in between 0.4 to 0.75, the band is further shifted to a single dominant band at 1960 cm^{-1} (atop). Their finding clearly shows that the CO binding site is shifted from 3-fold to atop/linear binding sites as a function of CO surface coverage, θ_{CO}. Raval *et al.* on the other hand reported that adsorbed CO changed the binding sites in Cu(111) from linear ($\theta_{CO} = 0.33$) to tilted linear ($\theta_{CO} = 0.33 - 0.44$) and finally to a mixture of both linear and bridged species as θ_{CO} increases to above 0.5 [65]. In order to investigate the influence of θ_{CO} on this interconversion, a series of experiments were performed at a fixed $E_{pol} = -1.4$ V. The electrode was introduced into a N_2-saturated solution and held at open circuit potential. Carbon monoxide was then bubbled into solution for 1 min. A potential of –1.4 V was then applied for varying periods of time or holding time, $T_{hold\ min}$, and the electrode was pushed against the IR transparent window after which spectral collection was performed. The potential was then stepped in 0.1 V increments to –0.7 V following Scheme C in Figure 4.15. The electrode was then removed from solution, electropolished and reintroduced into a N_2 saturated solution. CO was bubbled for the same period of time and the electrode polarised for a longer period of time, $2T_{hold\ min}$, pressed against the IR window and then the spectra were collected. The procedure was repeated for different polarisation time, e.g. t_{15} to t_{20}.

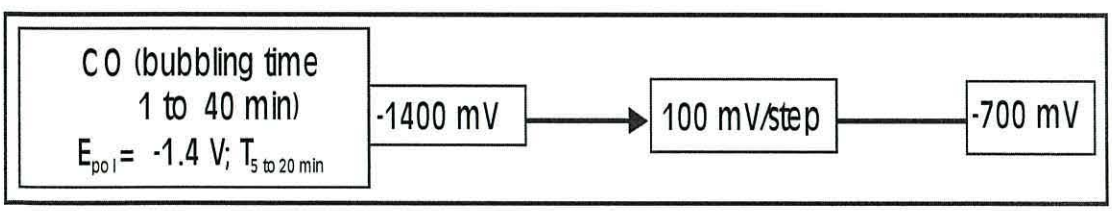

Figure 4.15: Scheme C used to evaluate the adsorption of CO on Cu

Figure 4.16A shows the SNIFTIR spectra at –0.8 V, normalised relative to –1.4 V, obtained when the bubbling time of CO was 1 min and $T_{hold\ min}$ varied up to 20 min. The spectra show that after 5 min of polarisation time (Fig 4.16At_5), CO_L is replaced by CO_B. As t_x increases, CO_B shifts to higher frequencies (Fig 4.16At_{20}). Increasing the

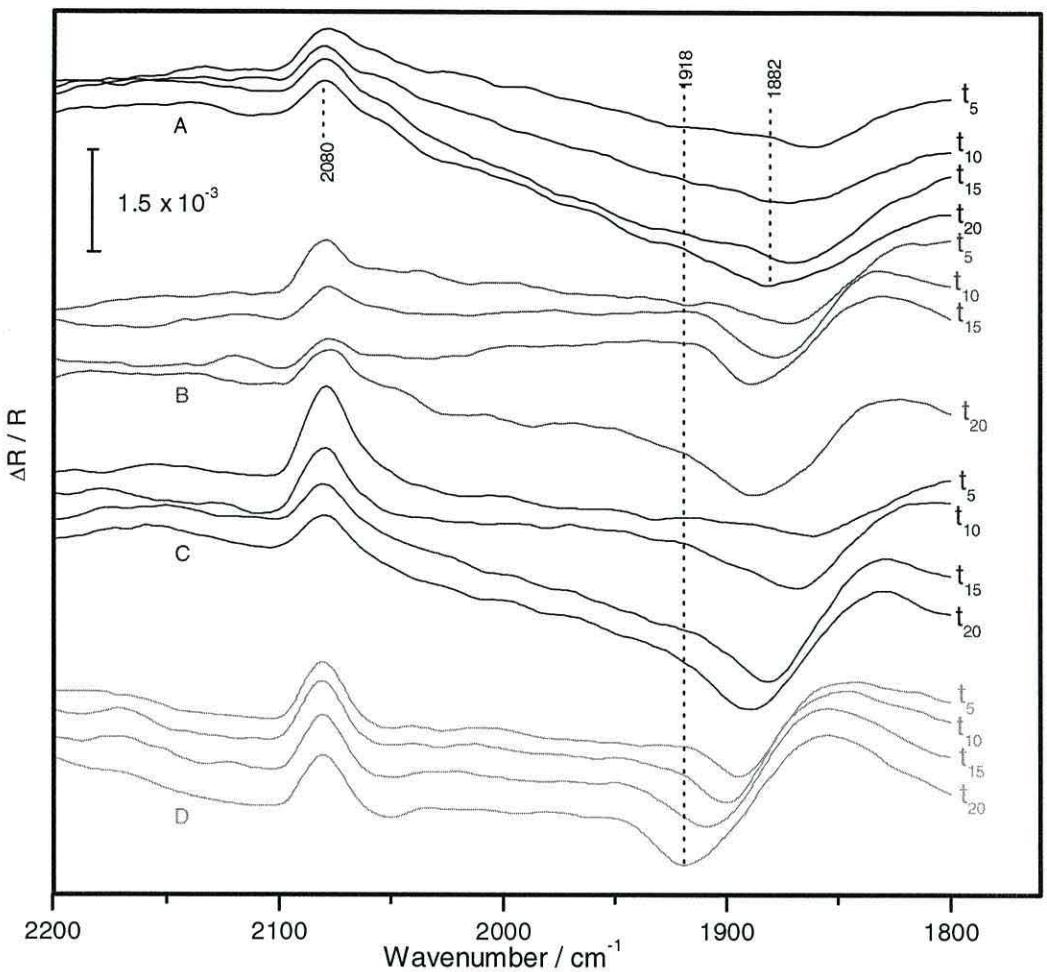

Figure 4.16: SNIFTIR spectra at –0.8 V obtained from different CO concentration/CO bubbling time; A (1 min), B (3 min), C (15 min) and D (40 min) in buffered phosphate solution. The electrode was polarised at E_{pol} = –1.4 V for different holding time; t_5 (T_{hold} = 5 min), t_{10} (T_{hold} = 10 min), t_{15} (T_{hold} = 15 min) and t_{20} (T_{hold} = 20 min). Spectra are normalised relative to spectrum obtained at –1.4 V of each set.

concentration of CO by bubbling for 3 min has the same effect on CO_L/CO_B conversion (Fig 4.16B). However the increased intensity of the CO_L band (positive band at 2080 cm^{-1}) indicate that more CO_L is present at the surface under these conditions (E_{pol} = -1.4 V, bubbling time = 3 min) compared to the same potential but at a CO bubbling time of 1 min. Furthermore, the intensity of CO_B is higher at 3 min bubbling time of CO and the band further shifts to higher wavenumbers. The same trend is observed for varying bubbling times (10, 15, 20, 25, 30, 40 min; for the sake of clarity only the 15 and 40 min experiments are shown); however the amount of CO_L starts to decrease after 15 min of bubbling time, even though the amount of CO_B continues to increase. The reason for the

apparent reduction in the amount of CO_L is possibly due to the molecules moving into a tilted position. As mentioned earlier, Raval *et al.* [65] reported that adsorbed CO shifts from linear to tilted linear as θ_{CO} increases. As *p*-polarised radiation probes vibrations, which have a dipole moment perpendicular to the surface, a tilt in CO_L results in a decreased vector of the dipole moment which is perpendicular to the surface, hence the decrease in the CO_L peak area with bubbling time. Figure 4.17 shows the influence of bubbling time on the CO_L peak area. The integrated peak area at –1.4 V is normalised relative to the highest value of 10 min bubbling time (0.37). The conversion of CO_L to CO_B is best examined looking at Fig 4.16C ($t_{bubbling}$ = 15 min) which shows that the amount of CO_L decreases whereas CO_B increases with holding time. This implies that as the θ_{CO} increases (due to an increase in the amount of CO in solution and the increased holding time), CO_B is preferentially formed. This indicates that the preference of the adsorbed CO binding site on the polycrystalline copper electrode is at linearly binding site follow by multiple binding site of bridge bonded. This might due to the preference of the Cu/CO orbital interaction. The bonding process in adsorbed CO on Cu involves the interaction between the overlap of copper *d* orbital and the highest occupied CO 5σ orbital [69]. Persson *et al.* reported that the orbital overlap between the copper-5σ orbital

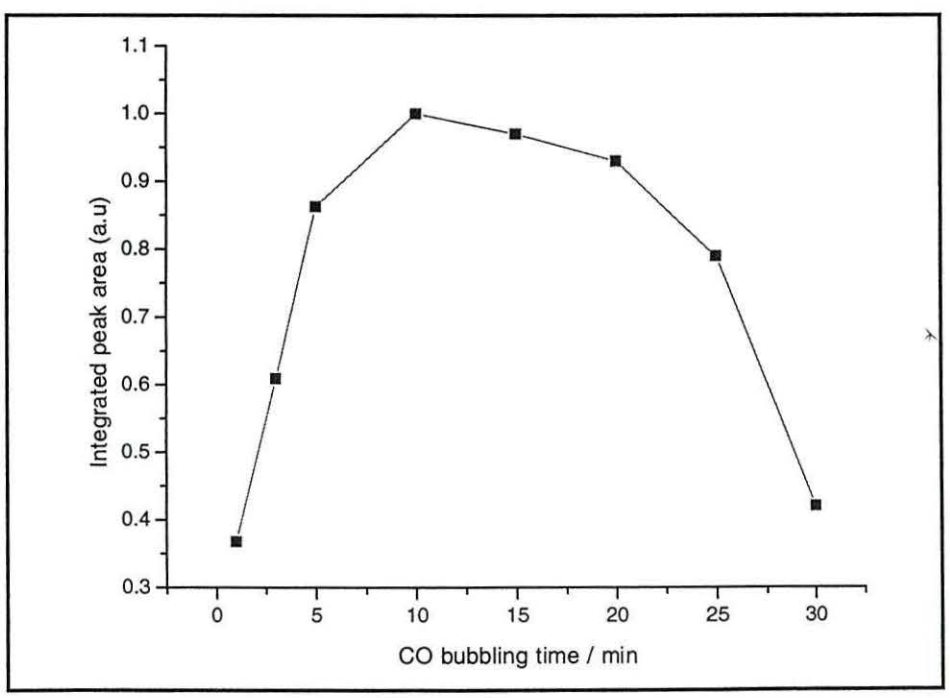

Figure 4.17: Integrated peak area of CO_L at –1.4 V versus CO concentration/CO bubbling time in buffered phosphate solution. SNIFTIR spectra are normalised relative to spectrum obtained at –0.8 V for each set.

interactions is larger in linear bonded and smaller in bridge bonded bonding. Therefore energetically the linear bonded site is a preference adsorption site and will be occupied first followed by the bridge-bonded site, with increasing CO coverage. The Cu-5σ orbital interaction is believed to be more important compared to other possible orbital interaction such as the copper-2π* orbital. At longer polarisation time, CO_L rearranged and adsorbed at bridge binding site, possibly induced by the change of the electronic energy levels [63, 70] as the orbital interaction of Cu-5σ decreases, as the CO coverage increases. The frequency shift to higher wavenumbers in the CO_B brought about by increased holding and bubbling times can be partly explained in terms of the repulsive strain among the adjacent neighbouring CO_B molecules. To reduce the steric strain effect of this repulsive force, a shift of binding sites toward other possible defect 2-fold binding sites such as 2-fold step or 2-fold terrace binding sites might occur. Therefore an increase in θ_{CO} may result in the formation of more CO_B at step or terrace binding site, thus increasing the band frequency position due to these defect binding sites producing stronger CO bonding compared to normal bonding sites due to their more unsaturated or lower coordination binding sites [71, 72]. It has been found that adsorbed molecules at step sites do indeed exhibit different frequency from those on terraces, for instant. Copper step sites give rise to bands at about 15 cm^{-1} higher than those of terrace sites [23, 43, 73, 74]. Therefore increasing the CO concentration (increase θ_{CO}) gives rise to higher CO_B band frequency, from 1882 cm^{-1} (1 minute of CO bubbling time) to 1918 cm^{-1} (40 minute of CO bubbling time). In addition, this frequency shift can also be explained by classical π-back donation where a decrease in back donation to CO antibonding orbital occurs as θ_{CO} increases due to high competition for metal d electrons, thus increasing the $\nu C{\equiv}O$ stretching frequency. Increases in θ_{CO} also leads in dipole-dipole coupling interaction among the adjacent neighbouring CO molecules, thus increases the $\nu C{\equiv}O$ stretching frequency [75].

4.3.3 Stability of CO_L, CO_B and Cu(I)-CO

The bond strength, in particular of adsorbed intermediate species, is relatively important to their reactivity. If the bonding between an adsorbed intermediate and the electrode is strong, it will affect the intermediate reactivity by slowing down the next step in the reaction. A weaker bond on the other hand might lead to higher reactivity. A typical example of this is the hydrogen evolution reaction in which the rate and mechanism of gas evolution depends on the metal-H bond strength. Physical evacuation processes is one of

the ways to evaluate the CO adsorbed bond strength on copper surfaces (mainly in UHV studies). Purging the adsorbed CO from the electrode surface by an inert gas is another way of achieving this in electrochemical systems. Experiments were carried out by polarising the electrode surface at E_{adm} of –1.4 V for 15 minute in CO-saturated phosphate buffered solutions to form both linearly and bridge bonded adsorbed CO. The spectra were recorded as the potential is stepped down to –0.8 V in 0.1 V/step as shown in Scheme D in Figure 4.18. The electrode was lifted from the window and the potential was then slowly brought back to the initial E_{adm} of -1.4 V to restore both CO_L and CO_B. The solution was then purged with N_2 gas for 30 minutes to remove any CO from the solution and then the spectra were recorded as the potential is stepped down to –0.8 V as before.

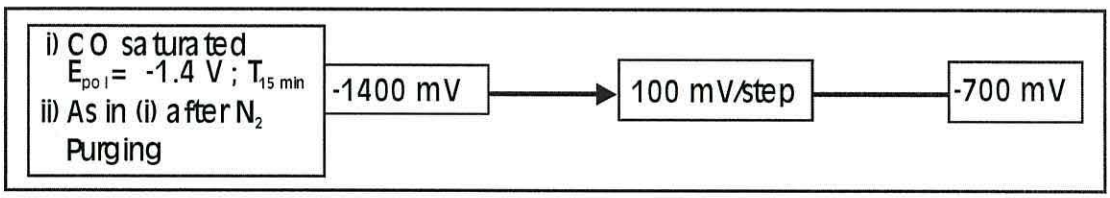

Figure 4.18: Scheme D used to evaluate the adsorption of CO on Cu

Figure 4.19 shows the SNIFTIR spectra for both sets of experiments; (a) CO saturated and (b) N_2 saturated. The spectra are normalised relative to spectrum obtained at –1.4 V. The figure shows positive going band for CO_L at 2081 cm^{-1} and negative going band for CO_B at 1870 cm^{-1} for the CO-saturated solution before N_2 purging (spectrum a_1 to a_6), and total disappearance of the CO_L band and the retention of CO_B band at 1870 cm^{-1} after the N_2 purging (spectrum b_1 to b_6). The results indicate that CO_L is completely removed from Cu through the N_2 purging process whereas CO_B remains unchanged. This indicates that CO_L is weakly adsorbed at Cu. This is in agreement with its relatively low dissociation energy of 30 kJ/mol (CuCO cluster system) as reported by Schwerdfteger and Bowmaker [76]. They suggested that Cu-CO interaction is best described as combination of dispersion, donor-acceptor (charge transfer) and repulsive interactions. Furthermore this is well in agreement with other values of the binding energies of CuCO and Cu_2CO clusters calculated at about 25.1 kJ/mol and 104.6 kJ/mol respectively [77, 78]. The difference in bond stability is also supported by the fact that CO_L only appears in a small potential range from –1.5 to –1.0 V and CO_B can be observed over a wider potential range from –1.5 V to –0.1 V (Figure 4.12 and 4.14). The increase in stability of CO_B compared to CO_L can be ascribed to the strengthening of bonding between Cu and CO by the

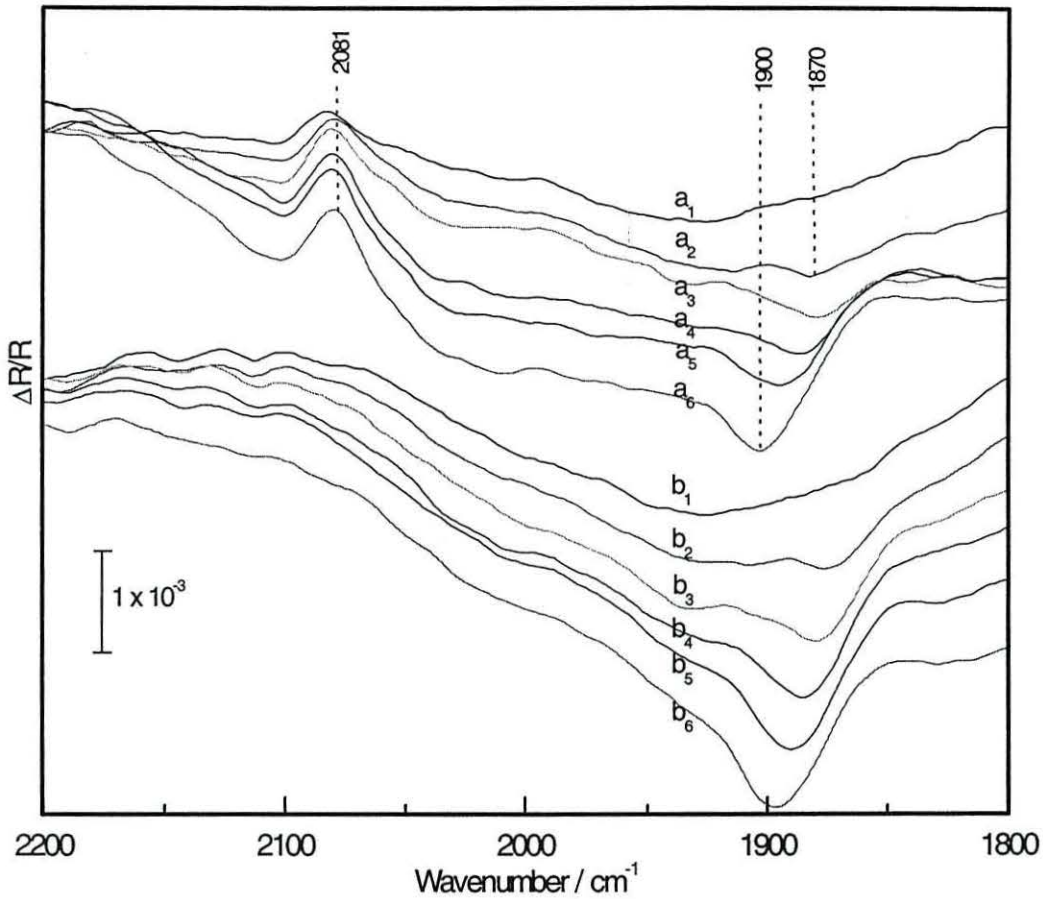

Figure 4.19: SNIFTIRS spectra obtained from CO-saturated buffered phosphate solution (A) before and (B) after N_2 purging. Spectra shown are from (1) –1.3 V to (6) –0.8 V; normalised relative to –1.4 V.

increase of the π back donation of the *d* metal electrons into the $2\pi^*$ orbital through the two Cu-C bonds. The ease of CO_L removal from the surface by N_2 purging may suggest that it is weakly bonded or it might only physisorbed on Cu surface.

It is worth noting that after the N_2 purging process, CO_B remains unaffected and if the potential is further stepped down more positive potentials; the band at 2107 cm^{-1} appears at –0.1 V (Figure 4.20). This suggests that since the measurements were performed in the N_2 environment, the appearance of Cu(I)-CO must come from the only CO source available in the system, which is CO_B. This indicates that the interconversion of CO_B to Cu(I)-CO indeed occurs at the positive potential and further reconfirms that CO_B is converted to Cu(I)-CO at anodic potential. Figure 4.21 shows a "summary" of the stability of CO_L (A_1 and B_1), CO_B (A_2 and B_2) and Cu(I)-CO (A_3 and B_3). The stability of CO_L, CO_B and Cu(I)-CO was also examined using a flow cell. As expected, Cu(I)-CO was

removed from the thin layer during such experiments. Surprisingly, no CO_L was observed during the imposition of a flow regime.

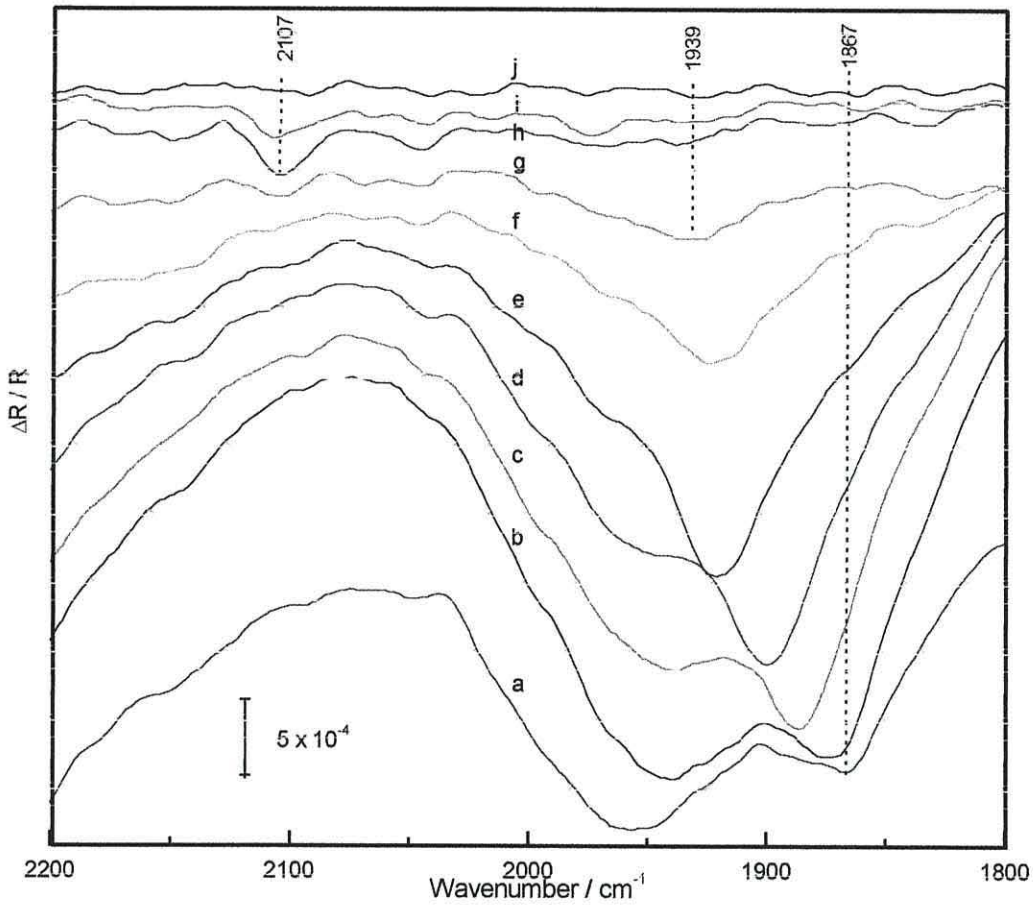

Figure 4.20: SNIFTIRS spectra obtained after N_2-purged buffered phosphate solution of polarised electrode at –1.4 V for 15 minutes in CO-saturated solution. Spectra shown from (a) –1.4 V to (h) 0 V in 0.2 V/step, (i) –0.1 V and (j) –0.2 V of reverse sweep; normalised relative to 0.4 V (reverse sweep).

4.3.4 The influence of temperature on the formation of CO_L, CO_B and Cu(I)-CO

Multiplicity of binding sites on the electrode surface can be roughly characterised by the $\nu C{\equiv}O$ stretching frequency. However the adsorption of CO at specific binding sites on metal surfaces can be varied with the nature of the surface, the physical condition such as smoothness and roughness, the degree of the crystallinity, the CO pressure and coverage as well as the temperature. The relative intensities of the CO band at a specific frequency vary mainly with CO coverage and temperature. Moreover, adsorbed CO can be removed from the surface by pumping or evacuation with or without heating process. Camplin *et al.* [79] reported the adsorption of CO at cryogenic temperatures on Cu(100) where the

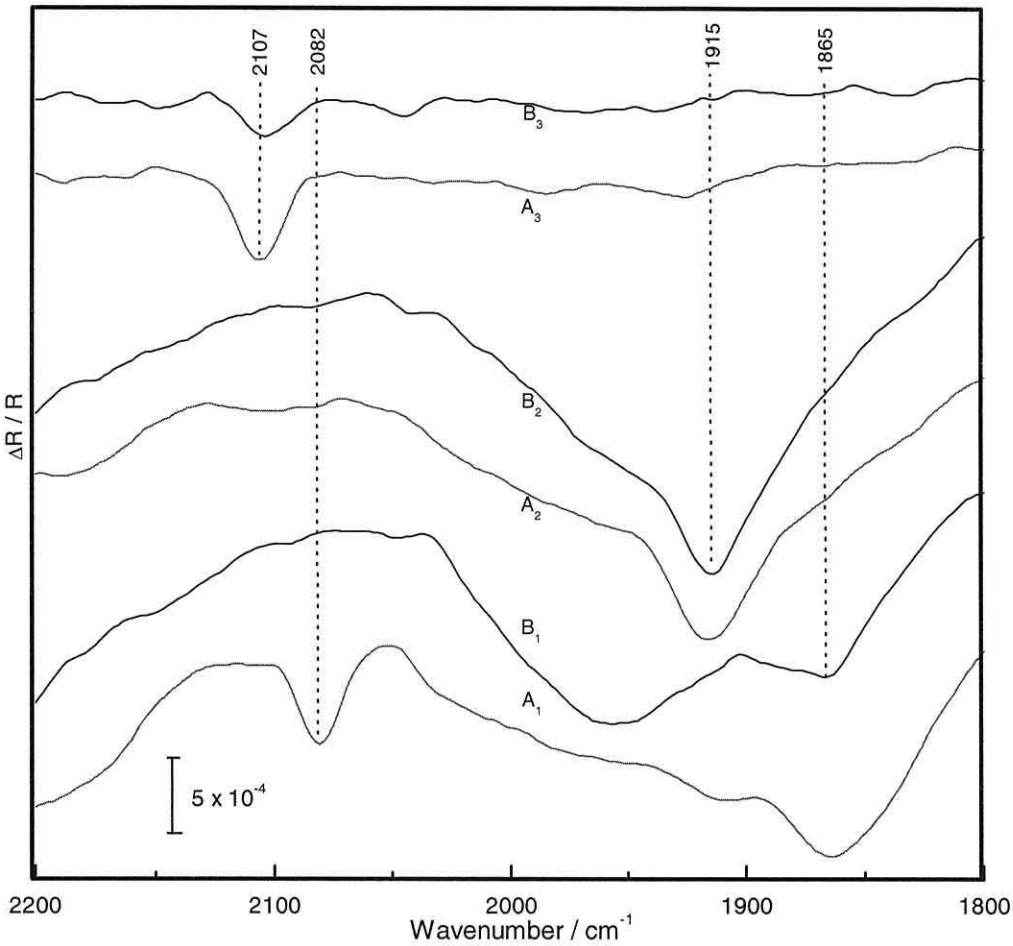

Figure 4.21: SNIFTIR spectra obtained from (A) before and (B) after N_2-purged buffered phosphate solution. Spectra shown are at –1.4 V (A_1 and B_1), –0.7 V (A_2 and B_2) and –0.1 V (A_3 and B_3), normalised relative to –0.4 V (reverse sweep).

adsorption of CO_L is affected by temperature and θ_{CO}. At a low temperature of 23 K, the chemisorbed species at 2083 cm^{-1} is observed with 2 L CO exposure and an extra band for physisorbed species at 2138 cm^{-1} is observed at the same temperature with 4 L CO exposure. [The CO exposure is measured in Langmuirs, L where 1 L is equal to 10^6 Torr/s and 1 Torr is equal to 133.3 Pa]. By increasing the temperature to 40 K, the physisorbed CO band disappeared. In order to investigate the temperature dependency of the CO adsorption on the polycrystalline copper electrode, experiments were carried out at different temperatures from 0 to 20 ^{0}C. The spectra were measured as the electrode potential was stepped from –1.4 V to –0.8 V; modified Scheme A in Figure 4.7 at different solution temperature. Figure 4.22 shows the SNIFTIR spectra for the appearance of CO_L

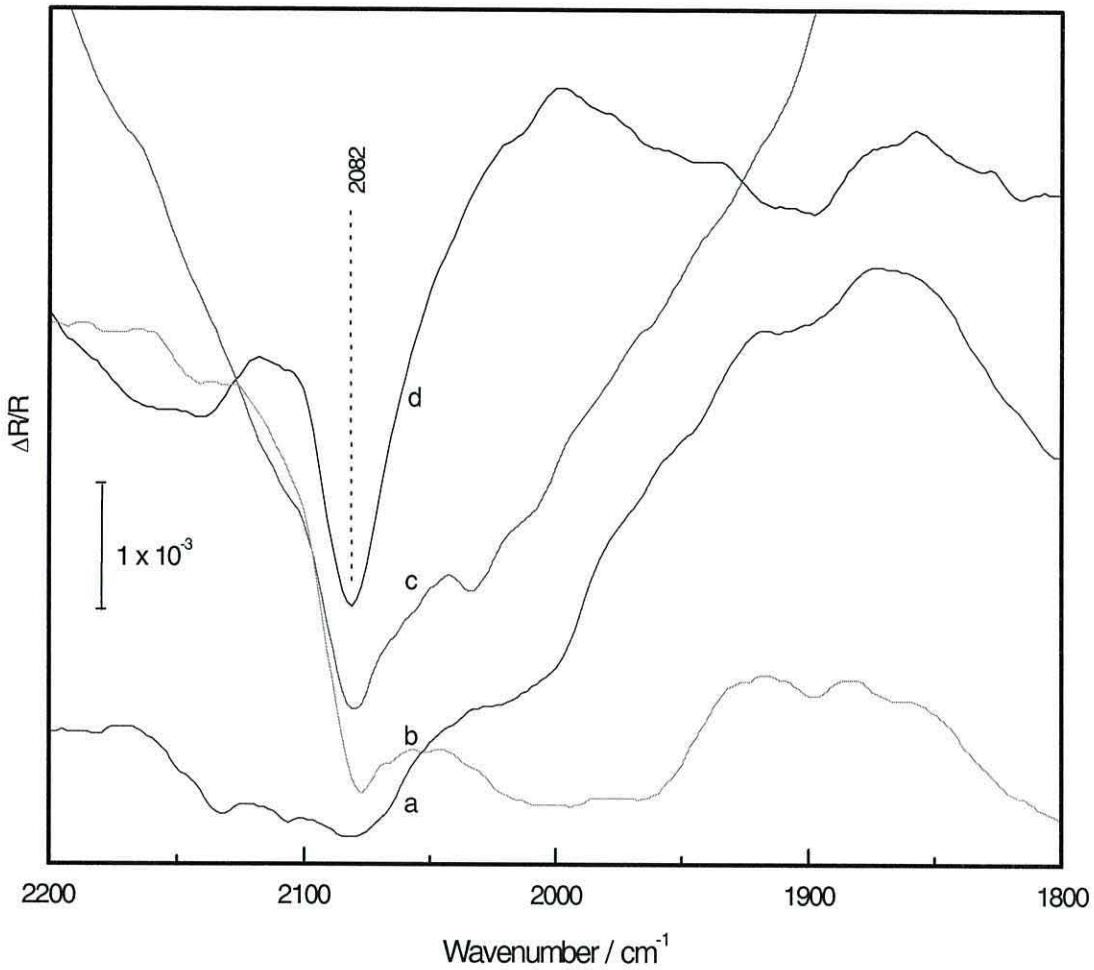

Figure 4.22: SNIFTIR spectra at –1.4 V obtained from CO-saturated buffered phosphate solution at different temperature. Spectra shown are obtained at (a) 18 ^{0}C, (b) 10 ^{0}C, (c) 5 ^{0}C and (d) 0 ^{0}C; normalised relative to –0.8 V of each set.

at 2082 cm^{-1} at –1.4 V at different temperatures. The spectra are normalised relative to -0.8 V of each set. The band at 2082 cm^{-1} appears only at low temperatures (0 ^{o}, 5 ^{o} and 10 ^{o}C) but not at higher temperatures (>18 ^{o}C). This clearly shows that the formation of CO_L on Cu is temperature dependent. This explains that why the previous studies at room temperature failed to observed CO_L on Cu [35]. The adsorption of CO at linear binding sites can only occur at low temperatures due to the effect of the energy transfer between the neighbouring CO molecules and between the CO molecules with copper surfaces. This is consistent with the fact that at low temperatures, the low coordination sites (with slightly higher adsorption energy) are stabilised [74], and thus increasing the chance of orbital overlap in CO_L and consequently its formation is favoured at low temperature.

Inversely at high temperatures, the high coordination sites are stabilised thus no CO_L is observed.

On the other hand the formation of bridge bonded CO, CO_B can be observed at low temperatures (Figure 4.12 and 4.14) and at temperature as high as 80 ^{0}C as in CO_2 saturated solution of Chapter III (Figure 3.30, page 95). The formation of bridging species at high temperature is due to the presence of stable high coordination sites which are stabilised at high temperature. The results show that both adsorbed CO species exist at low temperature but bridge-bonded CO can exist at high temperatures. This is well in agreement with report by Rao *et al.* [80] where on polycrystalline transition metal surfaces the low coordination sites are stabilised at low temperatures (80-120 K), whereas at high temperatures (270-300 K) the higher coordination sites are stabilised. At high temperatures, facile interconversion from lower to higher coordination sites (slightly lower adsorption energy) is aided by the population of the soft frustrated translation as the temperature increases. An increase in higher coordination sites occupation causes a decrease in the $\nu C{\equiv}O$ stretching frequency. The effect of the temperature in facile binding sites in the present study is in agreement with reports by Hayden *et al.* [17] for Cu(111) and for Pt(111) [59].

4.3.5 The influence of pH on the formation of CO_L, CO_B and Cu(I)-CO

In the previous chapter, the reduction of CO_2 was observed to optimally occur at a pH value of 6.8. Figure 4.23 shows the integrated peak areas of CO_L (at –14 V), CO_B (at –0.7 V) and Cu(I)-CO (at 0 V) obtained at different pH values. The SNIFTIR spectra are normalised relative to the spectrum recorded at –0.4 V during the cathodic sweep. The integrated peak area were normalised by the highest values {0.37 for CO_L, 0.24 for CO_B and 0.21 for Cu(I)-CO}; all of which were obtained at pH 6.8. The fact that the optimum pH for the reduction of CO_2 to CO and for the adsorption of CO at Cu is 6.8 may be misleading if one is to assume that both processes are, in their own accord, solely pH dependent. It is more likely that the pH influences the characteristics of the surface and other competing reactions. At low pH values, the adsorption of CO is disfavoured by the hydrogen evolution reaction. At high pH values, the electrode is very likely to be covered by hydroxides which are very difficult to remove even at very negative potentials. Hence, at neutral pH, H_2 evolution is shifted to potentials where it will not dominate CO adsorption, but sufficient enough to reduce the surface.

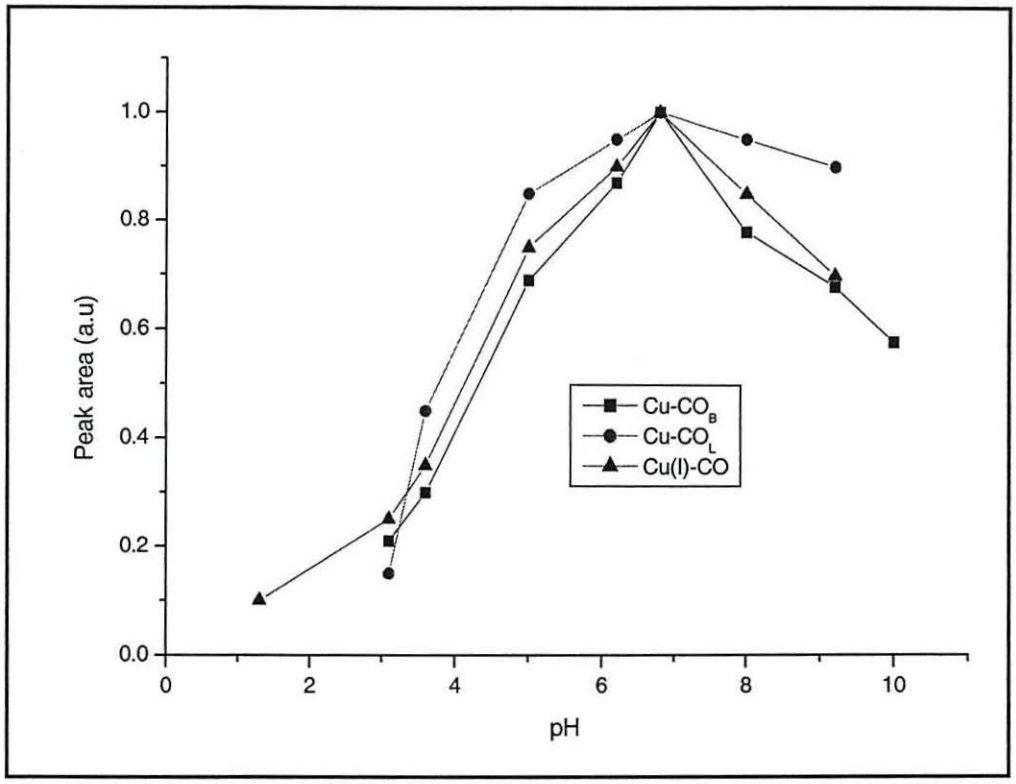

Figure 4.23: Integrated peak area of adsorbed linear-bonded CO, CO_L at –1.4 V, bridge-bonded CO, CO_B at –0.7 V and copper(I) carbonyl at 0 V correspond to pH of the solution.

4.4 Conclusion

The results show that the adsorption of CO on polycrystalline occurs at two different types of binding sites linearly bonded CO, CO_L and bridge bonded CO, CO_B. No higher 3-fold hollow multiple bonded CO was observed under the experimental conditions. The main problem to overcome is the removal of the pre-adsorbed anions, especially hydroxide from the surface due its competing reaction with the adsorption of CO. Polarising the surface at high cathodic potential is one way of removal the pre-adsorbed anions. The appearance of an adsorbed CO and its preference adsorption site on copper are applied potential and its polarisation time, T_{hold}, CO concentration, CO surface coverage, θ_{CO} and temperature. The results show that the adsorption of CO process depends on the state of the copper surface either without or with polarisation process. The results can be simplified as follows: CO_L appears immediately after the surface is polarised with the starting applied potential, E_{ASP} at high negative potential. It appears in a small potentials range from –1.5 to –1.0 V. CO_B on the other hand, appears as a function of polarisation time, T_{hold} at high negative potential or polarisation potential E_{pol}. It appears in a wider potential range, from –1.5 to –0.1 V. The interconversion from CO_L to CO_B in the thin layer can take place as a

function of polarisation time. The interconversion of CO_B to Cu(I)-CO occurs at anodic potential region where the oxidation of copper to copper (I) occurs. On the way back of the reverse sweep, CO_B reappears begin at potential of –1.0 V. The formation of adsorbed CO_L and CO_B cycle and copper(I) carbonyl on polycrystalline copper can be illustrated as follows (Figure 4.24);

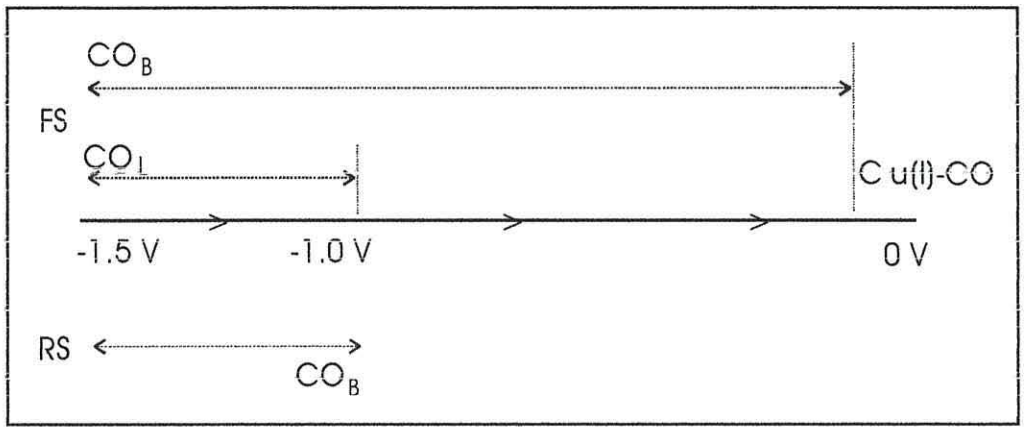

Figure 4.24: The sequence of the formation of adsorbed CO and Cu(I)-CO on copper corresponds to the applied potential. FS is a forward sweep from –1.5 V to 0 V and RS is a corresponding reverse sweep.

The formation of CO_L is a result from a weak interaction between CO and Cu. It can be removed from the copper surface by an inert gas purging process. On the other hand, the formation of CO_B is due to a strong interaction of CO on copper surfaces (chemisorbed) and is unaffected by the gas purging process. The formation of Cu(I)-CO at more positive potential on the other hand involves the reaction of CO with oxidised copper either through direct interaction of CO and Cu(I) or with reduced Cu(II).

4.5 References

1 F.A. Cotton and G. Wilkinson, "*Advanced Inorganic Chemistry*", 5th Ed., John Wiley & Sons, N. York (1985)

2 R. Hoffman, "*Solids and Surfaces: a chemist's view of bonding in extended structures*" Acadenmic Press, N. York (1980)

3 R.R. Ford in "*Advances in Catalysis*," Vol. 21, D.E. Eley, H. Pines and P.B. Weisz (eds.), Acadenmic Press, N. York (1980)

4 R. Maruca, T. Kusuma, V. Hicks and A. Companion, *Surf. Sci.*, 236 (1990) 210

5 G. Blyholder and M.C. Allen, *J. Am. Chem. Soc.*, 91 (1969) 3158

6 G. Blyholder, *J. Phys. Chem.,* 68 (1964) 2772

7 J.H.B. Chenier, C.A. Hampson, J.A. Howard and B. Mile, *J. Phys. Chem.,* 93 (1989) 114

8 C.W. Bauschilcher, *J. Chem. Phys.,* 101 (1994) 3250

9 A.A. Davydov, "*Infrared Spectroscopy of Adsorbed Species on the Surface of Transition Metal Oxides*", C.H. Rochester (Ed.), John Wiley & Sons, New Yorks, (1990)

10 R.P Eischens, S.A.Francis and W.A.Pliskin, *J. Phys. Chem.*, 60 (1956) 194

11 P.W. Selwood, "*Adsorption and collective paramagnetic*" Academic Press, N.York., (1962)

12 R. Suhrmann, *Z.Electrochem.,* 60 (1956) 804

13 P. Dumas, R.G. Tobin and P.L. Richards, *Surf. Sci.,* 171 (1986) 579

14 D.P Woodruff and B.E. Hayden, *Surf. Sci.,* 123(1982) 397

15 P. Hollins and J. Pritchard, *Vibrational Spectroscopy of Adsorbates*, Series in "Chemical Physics", vol. 15, Chp. 8, (1980)

16 P. Hollins and J. Pritchard, *Surf. Sci.*, 134 (1983) 91

17 B.E. Hayden, K Kretzschmar and A.M. Bradshaw, *Surf. Sci.*, 155 (1985) 553

18 P. Dumas, R.G. Tobin and P.L. Richards, *Surf. Sci.*, 171 (1986) 555

19 C.R. Brundle, P.S. Bagus, D. Manzel and K. Hermann, *Phys. Rev.,* B24 (1981) 7041

20 R.P. Messner, S.H. Larmson and D.R. Salahub, *Phys. Rev.,* B25 (1982) 3576

21 D.P. Woodruff, B.E. Hayden, K. Prince and A.M. Bradshaw, *Surf. Sci.*, 123 (1982) 397

22 B E. Hayden and A.W. Bradshaw, *Surf. Sci.*, 125 (1983) 787

23 P. Hollins, K.J. Davies and J. Pritchard, *Surf. Sci.*, 138 (1984) 75

24 H. Seki, *IBM J. Res. Develop.,* 37 (1993) 227

25 K.A.B. Lee, K. Kunimatsu, J.G. Gordon, W.G. Golden and H. Seki, *J. Electrochem. Soc.,* 134 (1987) 1679

26 Y. Hori, A. Murata and Y. Yoshinami, *J. Chem. Soc. Faraday Trans.,* 87 (1991) 125

27 Y. Hori, O. Koga, Y. Watanabe and T. Matsumo, *Electrochim. Acta*, 44 (1998) 1389

28 Y. Hori, O. Koga, H. Yamazuki and T. Matsuo, *Electrochim. Acta*, 40 (1995) 2617

29 Y. Hori, H.Wakebe, T. Tsukamoto and O. Koga, *Surf. Sci.*, 335 (1995) 258

30 R.P. Eischen, W.A.Pliskin and S.A.Francis, *J. Chem. Phys.,* 22 (1954) 1786

31 J. Prtichard, *J. Chem. Soc. Chem. Comn.,* (1962) 437

32 M.A. Chesters, J. Pritchard and M.L. Sims, *J. Chem. Soc., Chem. Comm.,* 1454 (1970)

33 L.H. Little, "*Infrared Spectra of Adsorbed Species*", Academic Press, New York, (1966)

34 M.L. Hair, "*Infrared spectroscopy in surface science*", Marcel Dekker, Inc., New York (1967)

35 R.M. Hernandez and M. Kalaji, *J. Electroanal. Chem.,* 238 (1997) 5323

36 M. Dogrowska, L. Brossard and H. Menard, *J. Electrochem. Soc.,* 139 (1992) 39

37 M. Dogrowska, L. Brossard and H. Menard, *J. Electrochem. Soc.,* 139 (1992) 2789

38 Y. Hori, A. Murata, T. Tsukamoto, H. Wakebe, O. Koga and H. Yamazaki, *Electrochim. Acta.,* 39 (1994) 2495

39 J. Pritchard and M.L. Sims, *Trans. Farady. Soc.,* 66 (1970) 427

40 K. Horn, M. Hussian and J. Pritchard, *Surf. Sci.,* 63 (1977) 244

41 F. Stoop, F.J.C.M. Toolenor and V. Poniec, *J. Chem. Soc.,* (1981) 1024

42 S. Pinchas and I. Laulicht, "*Infrared Spectra of Labelled Compounds*", Academic Press, London, (1971)

43 P. Dumas, R.G. Tobin and P.L. Richards, *Surf. Sci.*, 173 (1987) 79

44 M.W. Severson, C. Stuhlmann, I. Villegas and M.J. Weber, *J. Chem. Phys.,* 103 (1995) 9832

45 C.S. Kim, W.J. Tornquist and C. Korzeniewski, *J. Chem. Phys*., 101 (1994) 9113

46 G. Herzberg, "*Molecular Spectra and Molecular Structure*", Vol 1, 2nd Ed. Van Nostrand, N. York (1945)

47 J. Ambrose, R.G. Barradas and D.W. Shoesmith, *J. Electroanal. Chem.,* 47 (1973) 65

48 M.R. Gennero de Chialvo, S.L. Marchiano and A.J. Arvia, *J. Appl. Electrochem.,* 14 (1984) 165

49 M.R. Gennero de Chialvo, J.O. Zerbino, S.L. Marchiano and A.J. Arvia, *J. Appl. Electrochem.,* 16 (1986) 517

50 J.M.M. Droog, C.A. Alderliesten, P.T. Alderliesten and G.A. Bootsma, *J. Electroanal. Chem.,* 112 (1980) 387

51 C.H. Pyun and S.M. Park, *J. Electrochem. Soc.,* 133 (1986) 2024

52 D. Armstrong, N.A. Hampson and R.J. Latham, *J. Electroanal. Chem.,* 23 (1969) 361

53 H. Huber, E.P. Kundig, M. Moskovits and G.A. Ozin, *J. Am. Chem. Soc.,* 97 (1975) 2097

54 O. Koga, T. Matsuo, N. Hoshi and Y. Hori, *Electrochim. Acta*, 44 (1998) 903

55 S. Hartinger, B. Petting and K. Doblhofer, *J. Electroanal. Chem.,* 397 (1995) 335

56 L.D. Burke, M.J.G. Ahern and T.G. Ryan, *J. Electrochem. Soc.,* 137 (1990) 553

57 M.R. Mucalo and R.P. Cooney, *J. Chem. Soc. Faraday Trans.,* 87 (1991) 1221

58 S.C. Chang and M.J. Weaver, *J. Phys. Chem.,* 94 (1990) 5095

59 S.C. Chang, X. Jiang, J.D. Roth and M.J. Weaver, *J. Phys. Chem.,* 95 (1991) 5378

60 S.Z. Zou, R. Gomez and M.J. Weaver, *J. Electroanal. Chem.,* 474 (1999) 155

61 S.Z. Zou, Y. Ho and M.J. Weaver, *J. Electochem. Soc.,* 139 (1992) 147

62 C. Tang, S.Z. Zou, S.C. Chang and M.J. Weaver, *J. Electroanal. Chem.,* 467 (1999) 92

63 F. Kitamura, M. Takahashi and M. Ito, *J. Phys. Chem.,* 92 (1988) 3320

64 C.M. Truong, J.A. Rodriguez and D.W. Goodman, *Surf. Sci. Lett.*, 271 (1992) L385

65 R. Raval, S.F. Parker, M. E. Pemble, P. Hollins, J. Pritchard and M.A. Chesters, *Surf. Sci.*, 203 (1988) 353

66 M.J. Weaver, *Surf. Sci.*, 437 (1999) 215

67 G.R Anderson, *J. Phys. Chem.,* 81 (1977) 273

68 A. Ben-Naim, *J. Chem. Phys.,* 42 (1965) 1512

69 B.N.J. Persson, M. Tushaus and A.M. Bradshaw, *J. Chem. Phys.,* 92 (1990) 5034

70 H. Ogasawara, J. Inukai and M. Ito, *Chem. Phys. Let.,* 198 (1992) 389

71 J.P. Biberian and M.A.Van Hove, *Surf. Sci.*, 138 (1984) 361

72 C. Ruggiero and P. Hollins, *J. Chem. Soc., Faraday Trans*., 92 (1996) 4829

73 J. Pritchard, T. Catterick and R.K.Gupta, *Surf. Sci*., 53 (1975) 1

74 E. Borguet and H-L. Dai, *J. Chem. Phys*., 101 (1994) 9080

75 J-W. He, W.K. Kuhn, L-W.H. Leung and D.W. Goodman, *J. Chem. Phys*., 93 (1990) 7463

76 P. Schwerdftfeger and G.A. Bowmaker, *J. Chem. Phys*., 100 (1994) 4487

77 M.A. Blitz, S.A. Mitchell and P.A. Hackett, *J. Phys. Chem.,* 95 (1991) 8719

78 R. Fournier, *J. Chem. Phys*., 102 (1995) 5396

79 J.P. Camplin, J.C. Cook and E.M. McCash, *J. Chem. Soc. Faraddy Trans*., 91 (1995) 3563

80 C.N.R. Rao. P.V. Kamath, K.Prabhakaran and M.S. Hegde, *Can. J. Chem*., 63 (1985) 1780

CHAPTER V

Electrochemical Impedance Spectroscopy of CO_2 Reduction on copper

5.1 Introduction.

The advent of computerised data acquisition and the availability of nonlinear least-squares (NLLS) data analysis programs have increased considerably the use of impedance techniques [1, 2]. Impedance Spectroscopy is an ac technique that has developed rapidly over a decade. It is a powerful method for the investigation of many processes, which may involve in several steps occurring at different rates. It has been used to characterise a wide range of materials, from measuring the dielectric properties of plastics to monitoring the water content of constructional concrete and analysing the curing process of adhesives. In electrochemistry, Electrochemical Impedance Spectroscopy (EIS) can be used in the study of corrosion, since it can be used *in situ,* to investigate the rate of degradation and the mechanism of corrosion in metals [3, 4]. Moreover it is also particularly useful in assessing the performance of corrosion inhibitors of coating materials such as polymers, resins and synthetic plastic and even self assembled monolayers of organic or inorganic chemicals on metal surfaces [5-7].

Basically, the method concerns the choice of an equivalent circuit to model the electrical response of an electrochemical cell over a wide frequency range and the analysis of the measured impedance to estimate the circuit elements, which are directly, related to the electrochemical parameters of the system. In order to model the behaviour of materials examined by EIS, equivalent circuit models are devised which mimic the time constants of the reactions in terms of resistance, R and capacitance, C. This is known as RC circuits series. The use of equivalent circuits is particularly important in the EIS analysis of metal corrosion and pitting, where information on the capacitance of the metal and sample used is needed. Indeed EIS is particularly useful for the study of catalyst electrodes such as in the electrochemical reduction of carbon dioxide since it gives information on the kinetics and the mechanism of the charge transfer and the mass transport in such systems [8]. The use of EIS in conjunction with cyclic voltammetry is recognised as the standard procedure necessary to evaluate electrochemical systems [9]. In electrocatalysis, the EIS responses of

catalyst electrodes are similar; however, upon detailed analysis of the data, different capacitance and resistance values associated with the charge transfer and the mass transport of the active material can be obtained. The charge-transfer resistance, the ion-diffusion coefficient, double layer capacitance and redox capacitance are the important electrochemical parameters of such electrochemical systems studied.

5.2 Theory of Electrochemical Impedance Spectroscopy [10]

EIS determines the dielectric response of a system when a variable frequency ac voltage is applied to it. The response can be analysed in terms of the ability of the system to store and transfer charge; *i.e.* its capacitance and conductance. The applied ac voltage and the resultant ac current are measured giving an impedance spectrum over a frequency range. The spectrum gives information on the electrochemical mechanism that is taking place within the system; each reaction operates within a certain frequency domain thus giving a detailed analysis of the system. An important factor that makes EIS so appealing is that the applied small voltage perturbation does not damage the sample. The technique is also very sensitive to small changes in behaviour of the sample. To determine the dielectric response, a small amplitude sinusoidal voltage is superimposed on the dc voltage applied to the sample. This sine wave produces a polarisation; *e.g.* within the double layer a fluctuating ac voltage induces ion redistribution within the double layer yielding a full description of its nature [11].

The resultant output signal is a shifted sine wave that has a different phase and amplitude to the input (Figure 5.1). The response of an electrical circuit in response to an ac voltage is commonly represented as impedance (Z) where Z = V/I. For simplicity, Z is

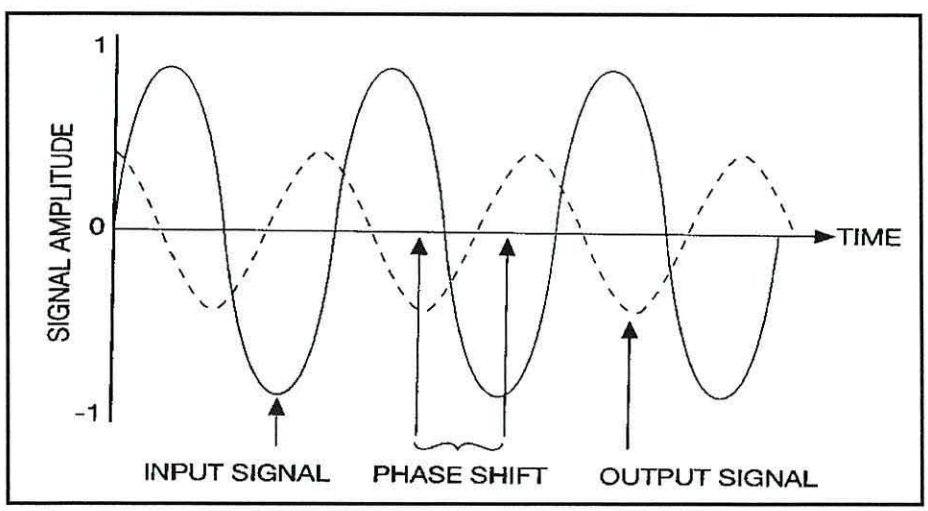

Figure 5.1: The input and output ac signal [10]

often considered as a value that describes how the passage of current is impeded by a system. Thus measuring the ratio of the applied voltage to the resultant current gives the impedance Z. The real and imaginary components of Z are represented by Z' and Z" respectively. The response y(t) of a linear system to a sine wave perturbation x(t), can be described as follows:

Input $x(t) = A \sin \omega t$ where ω is the angular frequency ($2\pi f$)

Output $y(t) = B \sin (\omega t + \phi)$ where ϕ is the phase shift.

A transfer function (T) may be defined as:

$T(\omega) = |T\omega| e^{j\phi}$ where $|T\omega| = B/A$

If x(t) is a current and y(t) a voltage then $|T\omega|$ is an impedance value.

However, if x(t) is a voltage and y(t) a current then $|T\omega|$ is an admittance value.

Therefore, the impedance $Z(\omega)$ of a system can be described as follows:

$Z(\omega) = |Z\omega| e^{j\phi}$ (polar co-ordinates)

or $Z(\omega) = R_e Z + j\, I_m Z \equiv Z' + Z''$ (complex Cartesian co-ordinates) where R_e and I_m are the real and imaginary components and j is complex notation or imaginary number ($j = \sqrt{-1}$) respectively.

It is important to note the following relationships between Z' and Z":

$$|Z|^2 = (Z')^2 + (Z'')^2$$

also $\phi = \text{Arc tan}\,(Z'/Z'')$

and $Z' = |Z| \cos \phi$, $Z'' = |Z| \sin \phi$.

EIS data are usually plotted as complex Cartesian co-ordinates (Z" *vs.* Z') [12]. It represents the impedance plot in which the 90^0 out-of-phase 'quadrature' or imaginary part of the impedance is plotted against the real part of the measured impedance (i.e. that in phase with the impressed electrochemical cell). Plotting the variation of $|Z|$ and ϕ with frequency is known as a Bode plot. Furthermore, data can also be displayed as admittance (Y) where $Y(\omega) = Z^{-1}(\omega)$. By measuring the phase shift over a range of frequencies, information can be gathered on the reaction mechanism, since different types of reactions have different relaxation frequencies [13]. These separate regions can be easily distinguished when plotted as Cartesian co-ordinates. The plot can then be analysed using equivalent circuits. The elements used in simple equivalent circuits are shown in Figure 5.2 together with their impedance response in the Cartesian complex plane and in the Bode plane. It is also possible to use these elements to construct an equivalent circuit that

mimics the response of an electrochemical reaction [15]. In an electrochemical cell the double-layer capacitance closely resembles a pure capacitance hence it is represented in

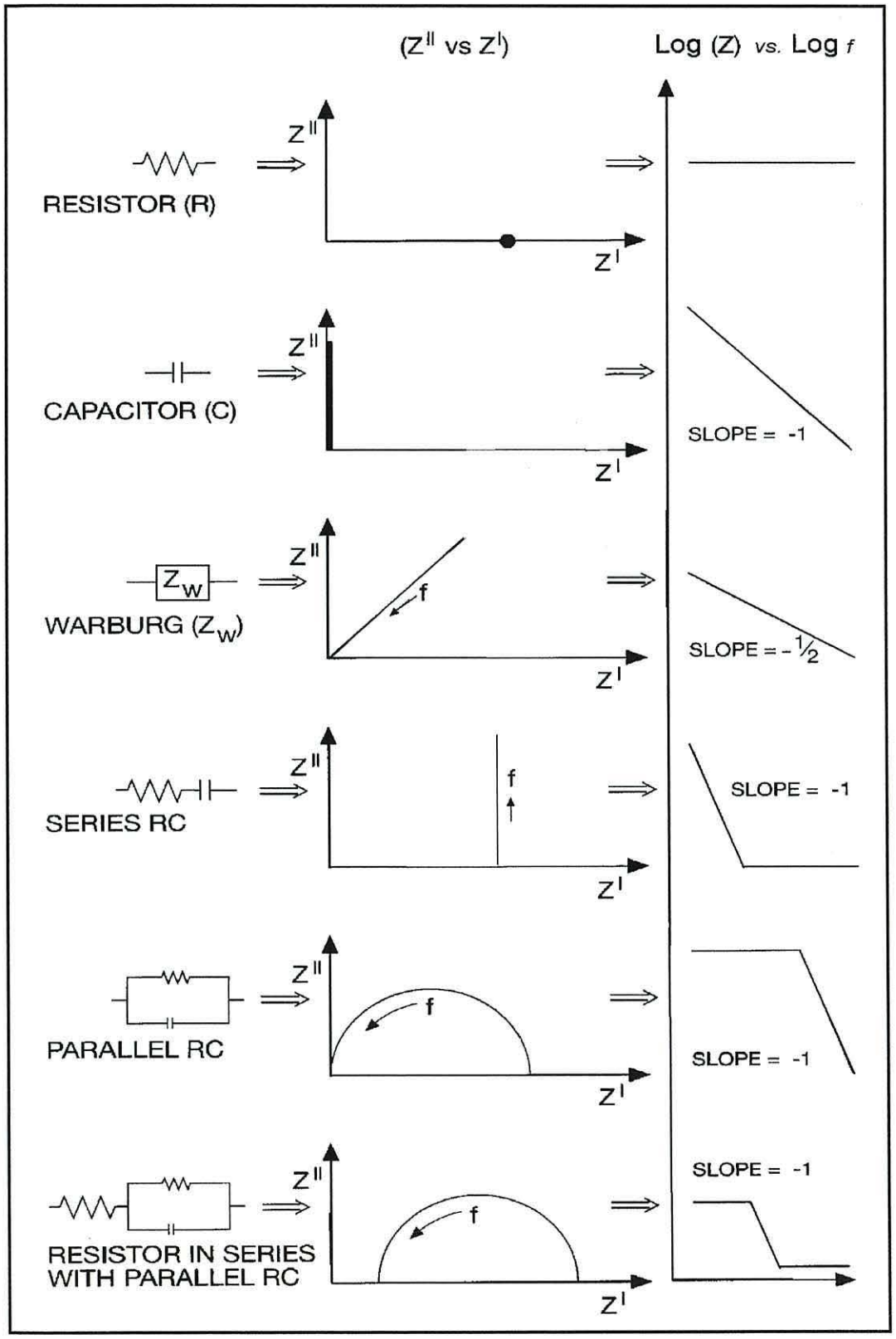

Figure 5.2: EIS response of various circuit elements in the Cartesian complex plane and in the Bode plane [14].

the equivalent circuit by C_{dl}. Finally, since the current must pass through the solution, an element R_Ω representing the uncompensated solution resistance is inserted as a series element [16]. It is important to remember that the Faradaic impedance can be considered in various ways. The simplest way is to describe it as a combination of the pure resistive element R_{ct} (charge transfer resistance) in series with another general impedance element Z_W (the Warburg impedance representing mass transport). However, unlike R_Ω and C_{dl} the Faradaic impedance or capacitance arising from charging of the double layer is not an ideal circuit element since its value is frequency dependent.

A simple equivalent circuit, which represents an ideal electrochemical system, is shown in Figure 5.3, which is known as Randel circuit model.

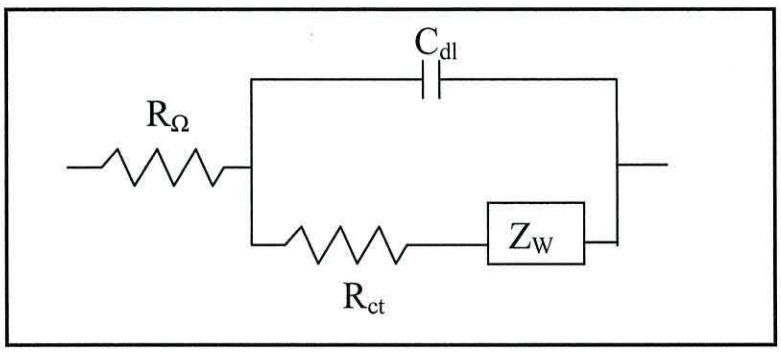

Figure 5.3: Randles circuit that represents an ideal electrochemical system [16]

The typical impedance response of such an equivalent circuit is shown in Figure 5.4. Therefore, it is possible to account for the behaviour of the system at high and low frequencies using the following equations:

At low frequencies $\omega \longrightarrow 0$

$$Z' = R_\Omega + R_{ct} + \sigma\omega^{-1/2} \qquad \text{.....} \quad 5.1$$

$$Z'' = \sigma\omega^{-1/2} + 2\sigma^2 C_{dl} \qquad \text{.....} \quad 5.2$$

where σ is a constant dependant on the concentration of the materials in solution.

Substituting 5.1 in 5.2 gives:

$$Z'' = Z' - R_\Omega - R_{ct} + 2\sigma^2 C_{dl} \qquad \text{.....} \quad 5.3$$

This is in the format of a straight line ($y = mx + c$) where the intercept on the Z' axis is $R_\Omega + R_{ct} - 2\sigma^2 C_{dl}$.

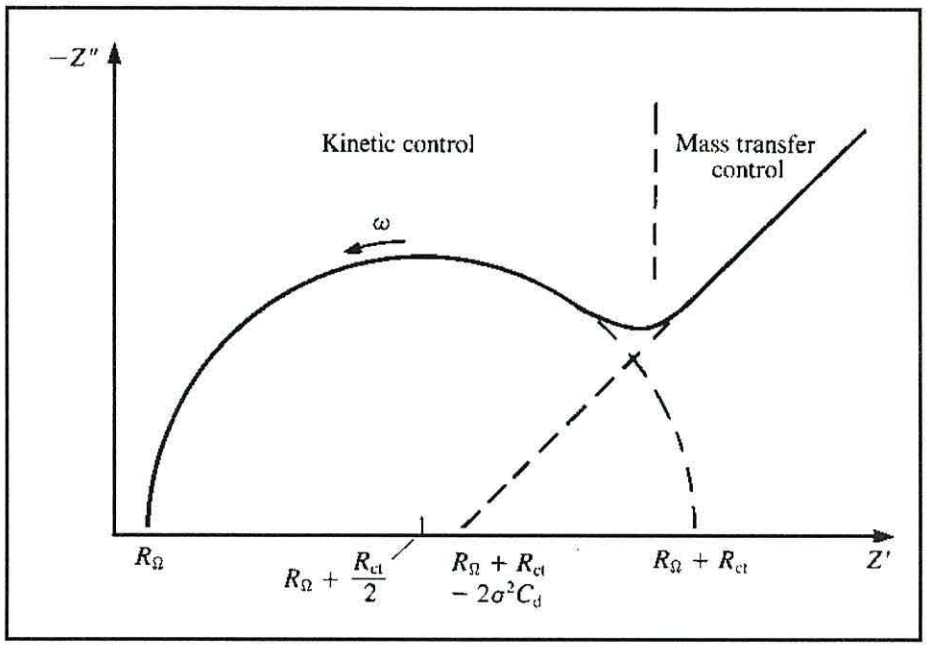

Figure 5.4. Complex impedance plot of an electrochemical system [10]

At high frequencies where $\omega \longrightarrow \infty$

$$Z' = R_\Omega + \frac{R_{ct}}{1 + \omega^2 R_{ct}^2 C_{dl}^2} \quad \text{..... 5.4}$$

$$Z'' = \frac{\omega R_{ct}^2 C_{dl}}{1 + \omega^2 R_{ct}^2 C_{dl}^2} \quad \text{..... 5.5}$$

Therefore:

$$(R_{ct} / 2)^2 = [Z' - R_\Omega - R_{ct} / 2]^2 + (Z'')^2 = (R_{ct} / 2)^2$$

The above is the equation of a circle where the centre is $R_\Omega + R_{ct}/2$ and the radius is $R_{ct} / 2$. The intercept of the low frequency line and the dimensions of the semicircle have an important role in the analysis of impedance data as illustrated in Figure 5.4. The plot displays the semicircle and straight-line regions that correspond to kinetically controlled and diffusion controlled processes, respectively. It should be noted that in the ideal case where the reaction is kinetically controlled a full semicircle is observed.

It should also be noted that there is some controversy over the interpretation of the Warburg impedance (Z_W) [17]; in some cases it is considered as a diffusion process and in other cases as migration. Thus impedance poses a challenge in the representation of the data accurately with a particular arrangement of passive current elements, such as resistors and capacitors, in order to describe the microscopic processes that occur in the system. However, it is important for theoreticians to explain the electric current passing in an

adsorbate layer in terms of the chemical and electrical microstructure of the electrode-adsorbate-solution interface [18].

For simplicity, experimental workers usually prefer the modified Randles circuit, whereas theoretical workers adopt the transmission line model. For this reason the majority of impedance studies on electrocatalyst have been modelled based on a Randles circuit [19]. However, the importance of understanding the complex analysis from the basic equations and the transmission line model should not be forgotten.

On polycrystalline metals surfaces, which are normally heterogeneous, the interfacial origin arises from the surface causing anomalous frequency dispersion [20] where the impedance of the electrode reaction deviates from purely capacitive behaviour. In this case, to fit the experimental data to an equivalent circuit model containing, a constant phase element, CPE, should be used [21, 22]. The impedance-containing CPE (Z_{CPE}) has been used extensively to model rough or porous surfaces electrode [23, 24] and for oxide/hydroxide passivation layers/films formations [25 - 27]. In general the Z_{CPE} has been successfully used to obtain a better fit for experimental data on the formation of anodic passivation film on zirconium in a neutral solution [28] and the adsorption of specifically adsorbing anion on rough capacitive electrodes [21].

In simple electrochemicals system such as the immersion of copper electrode in an electrolyte solution, it is possible to simulate the behaviour of the electrode in its environment using simple Randle equivalent circuit as shown in Figure 5.5.

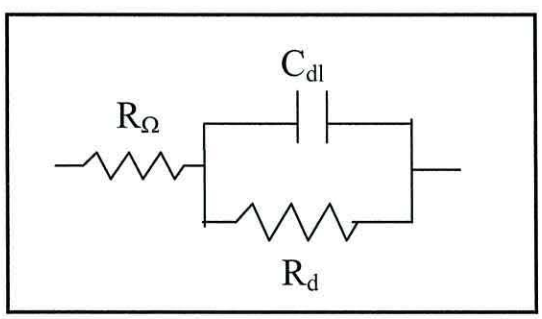

Figure 5.5: An equivalent circuit for the immersion of electrode in electrolyte [16]

The circuit consists of one resistor, R_Ω representing the resistance of the electrolyte solution. R_Ω will be in series with all the interfacial terms, e.g. with a second resistor, R_d, and a CPE including C_{dl}. Therefore the overall impedance of this electrochemical system could be represented as,

$$Z = R_\Omega + [R_d^{-1} + (jw)^n C_{dl}]^{-1}$$

For an ideal electrode, the CPE is a pure capacitor, C_{dl} represents the double-layer capacitance, and n is equal to unity. However in most cases the overall relation as the above is preferred and n may be lower than 1 due to the inhomogeneity of the electrode surfaces. Brug *et al.* [22] calculated the average double-layer capacitance values of an irregular surface, C_o where it can be estimated from C_{dl},

$$C_{dl}^{-1} = C_o^n (R_\Omega^{-1} + R_d^{-1})^{1-n}$$

The anodic behaviour of copper encompasses several well-defined reaction phenomena such as active dissolution, passivation layer, active-passive transition and formation of bulk oxides. Anodic copper corrosion or/and dissolution behaviour either as a pure cathodic electrode or alloy has been investigated [29-33]. Copper electrodissolution in slightly acidic solution for instance, showed that the adsorption of chloride plays an importance rôle in anodic mass transport process. The formation of sub-monolayer of copper species such as adsorbed $CuCl_{ads}$, deposition of a layer of CuCl and finally diffusion through the copper chloride layer have been shown as major steps for the anodic copper corrosion behaviour in sodium chloride solution [29] and in sodium sulphate through the formation and the diffusion of copper sulphate respectively [28]. The electrochemical impedance behaviour of copper for the electrochemical reduction of carbon dioxide is rarely investigated. Nevertheless Friebe *at al.* [8] reported that the poisoning of the copper electrode during the reduction of CO_2 due to the formation of an irreversible adsorbate on the surface. Therefore the adsorbate reacts as a blocking layer that lowers the electron transfer in the double layer and thus leads to a decrease of the surface conductance. Apparently the adsorption and charge transfer process effects in the Helmholtz double-layer play an importance rôle in the efficiency of carbon dioxide reduction. These effects cannot be investigated using only cyclic voltammetric and infrared spectroscopy. However EIS measurements are very sensitive to surface reactions such as an adsorption and desorption of species from the electrode surfaces. To get a better insight into the electrochemical reduction of carbon dioxide reaction and the adsorption of specifically adsorbed anion and reduction products, EIS were used as a complementary method to investigate the reduction of CO_2.

5.3 Experimental

The instrument used for measuring electrochemical impedance over a wide range of frequencies is called a Frequency Response Analyser (FRA). The technique measures one frequency range at a time and relies on a computational technique called sine wave correlation to determine the complex frequency response. By sweeping the frequency range a response spectrum is produced. The complex results are then handled by data processing computer programme, which can output the results in various forms, *e.g.* complex plane, bode and admittance.

The FRA used in this study was a Solatron 1170 FRA connected to an electrochemical interface. The FRA was interfaced to a PC *via* an IEEE card (using a "visual basic" programme) and the data was handled using the Solatron impedance data handling software Zview incorporating the MacDonald fitting programme based on the LEVM 6.0 software. The EIS was carried out in a three electrodes cell; using the cell set-up as that was described in Chapter II (page 52). A polycrystalline Cu disc working electrode (0.8 mm diameter) was employed in phosphate buffered solution. The counter electrode employed was a platinum foil and the reference electrode was a SCE. An ac signal with peak-to-peak amplitude of 0.01 V and a frequency range of 0.1 Hz to 10 kHz was applied. The frequency was stepped in a logarithmic sweep mode measuring ten points per decade. The dc bias from high cathodic potential (-1.5 V to 0 V in 0.1 V per step) was applied to the system *via* a potentiostat and before taking measurements the system was allowed to rest at the selected potential for one minute. The electrode was then characterised in N_2-, CO_2- and CO-saturated phosphate buffered solution by CV and then by EIS. The real (Z') and imaginary (Z'') component of the impedance obtained experimentally were analysed and fitted using the complex nonlinear least-squares (CNLLS) from the Zview software incorporating the MacDonald fitting programme or using the 'EQUIVCRT' program by Boukamp [34] from which the parameters were determined.

5.4 Results and discussions

The discussion will be focused on the electrochemical behaviour of copper electrode in phosphate buffered solution through their charge transfer resistance and double-layer capacitance at the onset of the hydrogen evolution region, which coincides with the reduction of the CO_2 and the adsorption of CO region and also particular emphasis on the

anodic passivation layer formation and diffusion of Cu(I)-CO species at anodic potential regions will be made.

5.4.1 N_2-saturated buffered phosphate solution

In general the impedance of the copper electrode in phosphate buffered solution can be divided into three regions according to the applied dc potential. The respective cyclic voltammogram regions of copper in phosphate buffered solution are shown in Figure 5.6. The impedance response of the copper electrode in phosphate buffered solution in region I (hydrogen evolution region) is shown in Figure 5.7. It shows small semicircles dominating at high frequency, HF and straight line at low frequency, LF. At these potentials region, hydrogen evolution is expected to occur. The impedance plot for hydrogen evolution reaction exhibits a semicircle, which indicates that this reaction is under a charge-transfer

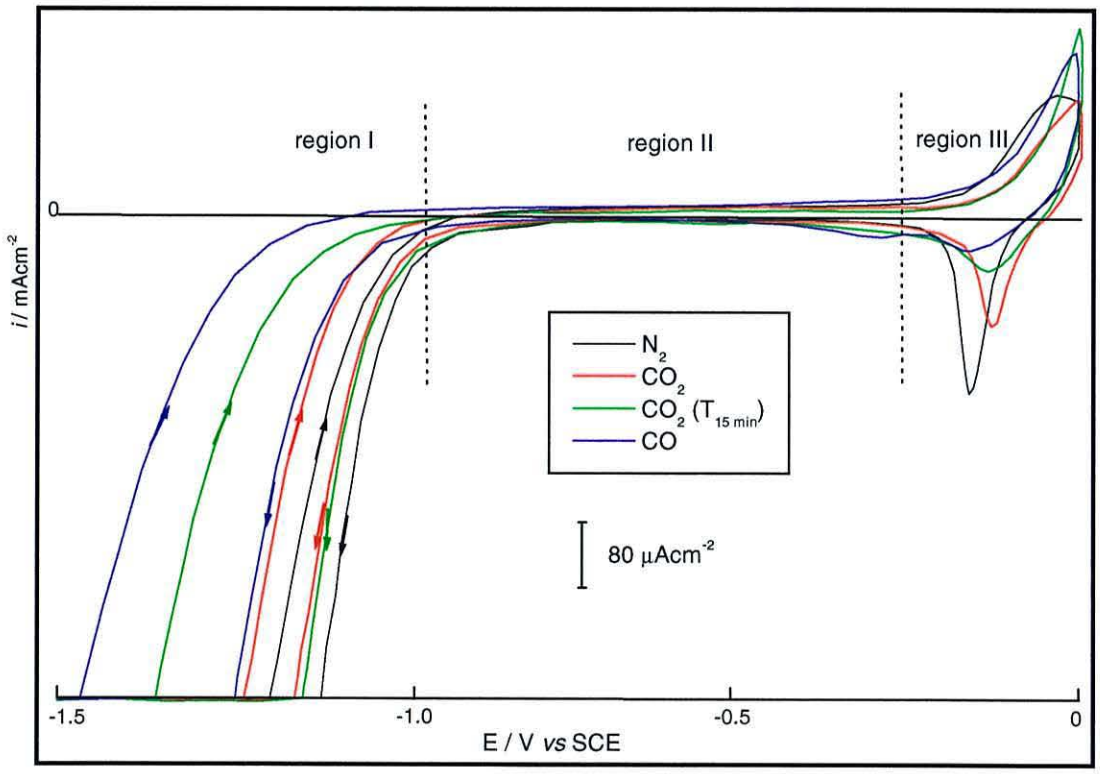

Figure 5.6: Cyclic voltammogram of copper in buffered phosphate solution at $\nu = 0.05\ Vs^{-1}$.

control [35]. In general HF semicircle represents the time constant charge transfer and double-layer capacitance of the system [21]. As expected in an electrochemical cell, the double-layer capacitance closely resembles a pure capacitance, hence, it is represented in

the equivalent circuit by C_{dl} and a pure resistive element, represented by charge transfer resistance, R_{ct} where these impedance parameters are in parallel to each others. The response in Figure 5.7 can be modelled using simple equivalent circuit as shown in Figure 5.3. By fitting the HF semicircle, the charge transfer resistance, R_{ct} for the hydrogen

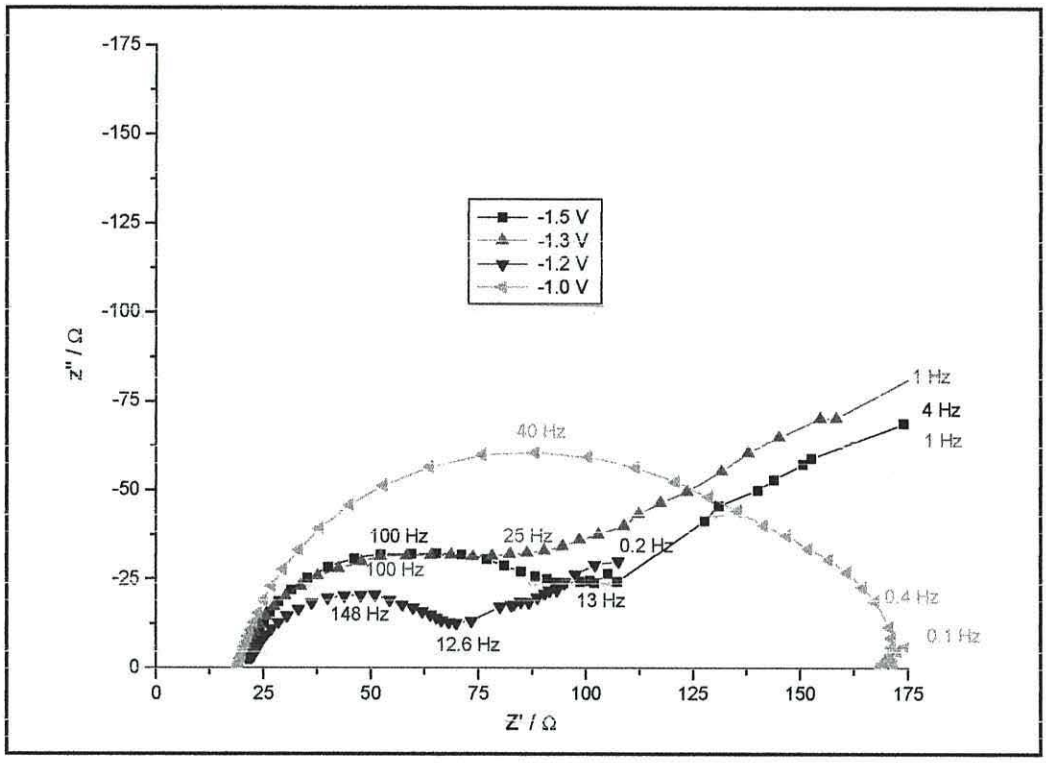

Figure 5.7: EIS of copper electrode in N_2-saturated buffered phosphate solution. Potential bias at –1.5 V, -1.3 V, -1.2 V and –1.0 V.

evolution reaction can be calculated at about 85 Ω or 169 Ωcm^{-2} at –1.5 V. This is close to the value of 133 Ωcm^{-2} of HER at –1.2 V for stainless steel in carbonate solution [35]. Since the current must pass through the solution, an element R_Ω representing the uncompensated solution resistance is inserted as a series element in the equivalent circuit. This analysis yields the following values as shown in Table 5.1.

Potential / V	R_Ω / Ω	R_{ct} / Ω	C_{dl} / μF
-1.5	20.3	84.8	50.8
-1.4	17.5	72.6	53.9
-1.3	19.0	70.6	93.1
-1.2	20.6	56.4	116.2
-1.1	17.7	59.4	92.0
-1.0	19.2	140.7	49.8

Table 5.1: The values obtained from NLLS fitting of EIS spectra from Figure 5.7

At the potential region of HER the electrode is expected to exhibit Warburg impedance element, Z_W at LF region [35, 36]. In the case where the Z_W value is 0, the faradaic impedance is reduced to a simple charge transfer resistance. The impedance spectra in the present study show the semicircle behaviour at HF and a straight line at LF. Therefore the Z_W impedance representing the mass transport in LF region should be incorporated in the equivalent circuit. As expected during HER, protons are initially reduced to form an adsorbed hydrogen atom on the metal surface, followed by the electrochemical desorption of hydrogen and/or the chemical desorption by the recombination of the adsorbed H atoms [37, 38]. Thus the impedance responses in these potentials region can be modelled by a modified Randle type equivalent circuit, which represents the electrochemical system as shown in Figure 5.3 with constant phase element, CPE in series with the solution resistance, R_Ω and parallel with the R_{ct} [39, 40].

By extrapolating the LF straight line, which indicates an almost pure capacitive behaviour, the capacitance in LF region can be measured at 5.8 mF and the resistance associated with it can be estimated at 7.5 Ω at –1.5 V. The pure capacitive behaviour at other potentials is shown in Table 5.2.

Potential / V	R_p / Ω	C_p / mF
-1.4	7.9	3.7
-1.3	6.9	3.2
-1.2	4.5	10.8
-1.1	7.2	69.8

Table 5.2: The values obtained from NLLS fitting of LF regions.

Drowgoska *et al.* reported that Z_W can be used as a general impedance element indicative of the mass or vacancies transfer through the oxide film [35]. However in these HER potentials region, the diffusion of oxide film is unlikely to occur from freshly electropolished electrode. Beside desorption of adsorbed hydrogen, desorption or diffusion of specifically preadsorbed anions is likely to occur in these potentials region. As shown by the *in situ* infrared studies in Chapter IV, the diffusion of preadsorbed anion of PO_4^{3-} and hydroxide might dominate the process in this region compared to the diffusion of preadsorbed hydrogen. If this is the case, as expected during the HER process, desorption of preadsorbed hydroxide and phosphate (PO_4^{3-}) from the electrode surface contributes significantly to the total impedance, as indicated by Z_W. Indeed the C_p value observed is higher than the C_{dl}.

As the potential is stepped to –1.4 V and –1.3 V, the HF semicircle becomes smaller but the LF lines remains similar to that observed at –1.5 V. Small HF semicircle at these potentials may be due to the influence of the desorption of preadsorbed anion from the electrode surface, thus increasing the conductivity. Good conductivity of the electrode surfaces exhibits low resistance and high capacitance values [41, 42]. At –1.2 V and –1.1 V, PO_4^{3-} is produced to a lesser extent on the surface as the potential become less negative, thus its adsorption become insignificant. This might indicate the lower resistivity or higher capacitivity. Indeed at –1.0 V, the LF Warburg impedance disappears leaving only a large HF semicircle, indicating that the Faradaic impedance is reduced to a simple charge transfer resistance. However the semicircle size increases at –1.0 V indicating a high impedance with high resistance and low capacitance. This indicates that readsorption of some anion starts to occur on the surface, thus reducing the capacitivity of the electrode surface. Adsorption of monobasic phosphate, $H_2PO_4^-$ might occur at this potential, as PO_4^{3-} is no longer present, as shown by IR spectra (Figure 3.10, pg 74).

Figure 5.8 shows the impedance responses in the potential regions II (-0.9 V to –0.2 V) which exhibit higher impedance values. As the potential is made less negative, the HF semicircle predominates and the semicircle size increases and becomes flattened. No LF impedance is observed. Depressed semicircle behaviour has been known to occur at an electrode/solution interface associated with a roughened electrode [21]. Pajkossy reported that the "capacitance dispersion" with depressed semicircle impedance is not totally due to the interfacial origin, it also contributed from the specific anion adsorption at double layer region [20]. This adsorption phenomenon is believed to occur in the present study indicated by depressed/flattened semicircles in these potentials region. It might indicate that the specific adsorption of $H_2PO_4^-$ anion occurs at these double layers region. As shown in the CV (Figure 5.6), the cathodic current becomes zero at the baseline current at these potentials. Moreover it has been reported from the isotopic labelling ^{32}P ortho-phosphoric acid that $H_2PO_4^-$ has a greater adsorbility than the multiple charged anions [43]. The response in Figure 5.8 can be modelled by using simple Randles type equivalent circuit as shown in Figure 5.5 with R_{ct} is in parallel with R_{Ω}. This analysis yields the following values (Table 5.3):

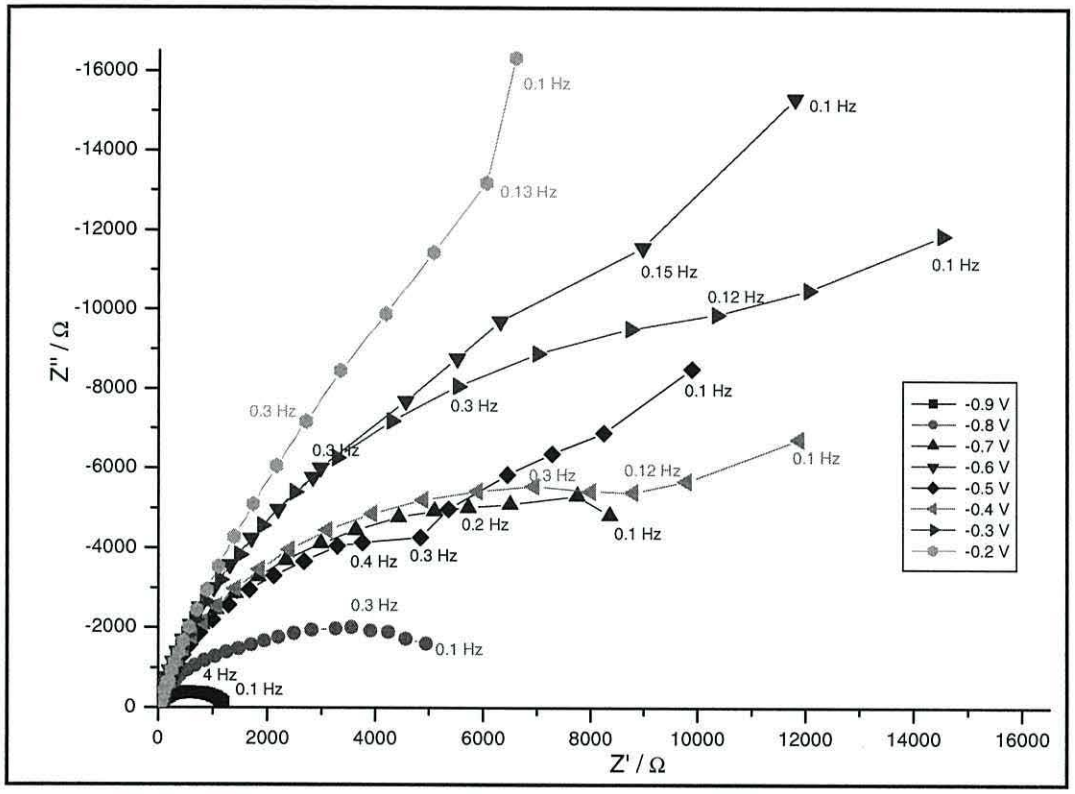

Figure 5.8: EIS of copper in N_2-saturated buffered phosphate solution. Spectra shown are from potential bias of –0.9 V to –0.2 V.

Potential / V	R_Ω / Ω	R_{ct} / Ω	C_{dl} / μF
-0.9	19.5	936	56.1
-0.8	19.6	3308	47.2
-0.7	20.0	11200	56.0
-0.6	19.6	22400	49.1
-0.5	19	10200	52.0
-0.4	18.8	12800	44.8
-0.3	18.6	22400	44.6
-0.2	18.3	56500	68.4

Table 5.3: Impedance parameters values obtained from Randles equivalent circuit fitting of EIS spectra in Figure 5.8

The adsorption of anions causes more resistance at the surface as shown by tremendous increase of the R_{ct}. The adsorption of $H_2PO_4^-$ from phosphate buffered solution has been reported by Hori *et al.* [44] to occur below the potential zero charge, pzc between –0.8 V to –0.3 V on Cu(100) surfaces. Large increase in resistivity from 11.2 kΩ at –0.7 V to 22.4 kΩ at –0.6 V might due to the adsorption of hydroxides on the surface as the potential reaches the pzc value of –0.6 V. An increase in current density due to an adsorption of

hydroxides and/or oxides is observed at this potential region as shown in voltammogram of Figure 5.6 at high resolution (CV not shown). The resistivity of the surface becomes highest at –0.2 V. At these potential the copper surface tends to oxidise. This is the stage where a mixture of the copper oxide or hydroxide layer [45] and a film of anions fully cover the electrode surface [46] and in turn the resistivity of the electrode increases dramatically.

In region III, the potential below –0.2 to 0 V, the impedance values decrease compared to the impedance value in region II, as shown in Figure 5.9. The same compressed HF semicircle is observed. This response can be modelled using the same equivalent circuit as Figure 5.5. The analysis of the EIS spectra yields impedance with low R_{ct} and higher capacitance, C_{dl} compared to the impedance values at potential region II as shown below in Table 5.4.

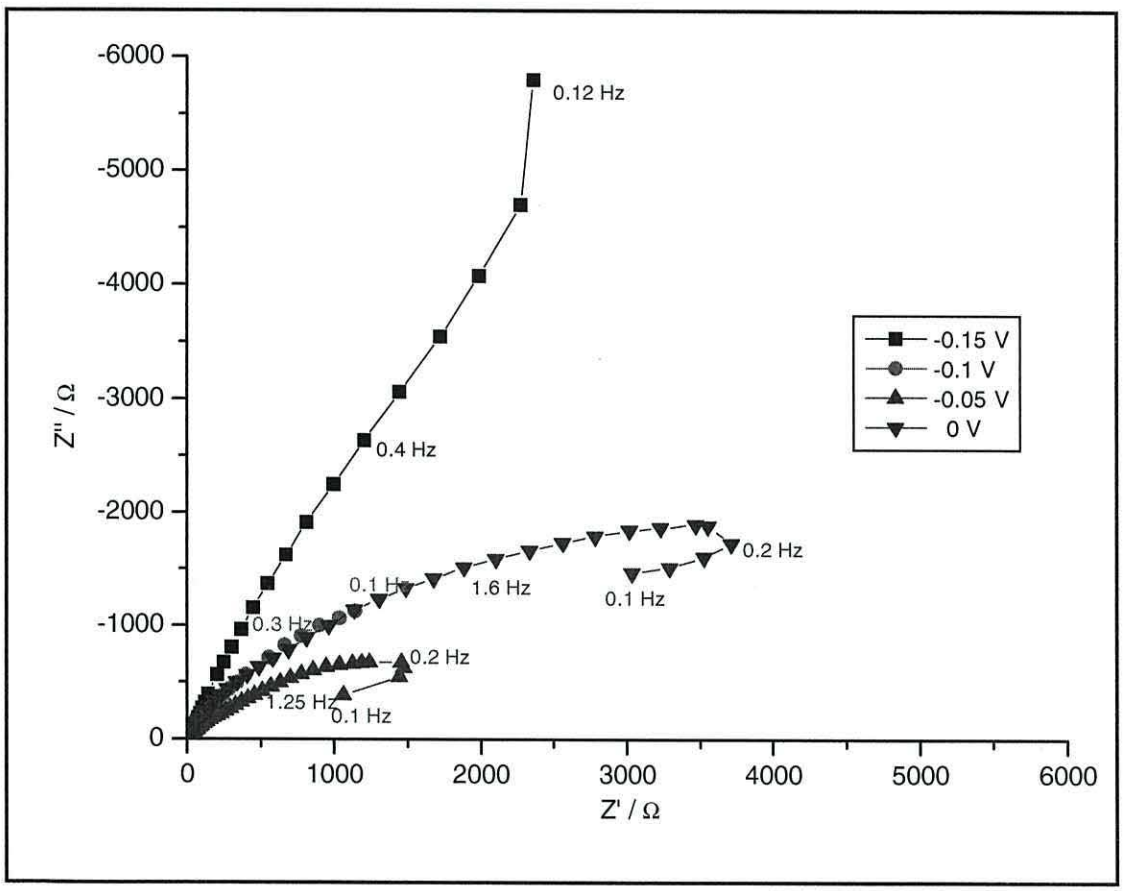

Figure 5.9: EIS of copper in N_2-saturated buffered phosphate solution; spectra shown from –0.15 V to 0 V.

Potential / V	R_Ω / Ω	R_{ct} / Ω	C_{dl} / μF
-0.15	19.0	28700	193
-0.1	18.7	4040	519
-0.05	17.8	2551	578
0.0	17.9	1806	230

Table 5.4: Impedance parameters values obtained from EIS spectra of Figure 5.9.

It is interesting to note that the resistivity reduces dramatically and the capacitance becomes highest in these potentials region. This is due to the removal of the blocking layer of the oxide film from the surface due to the formation of soluble copper species, possibly through the formation of copper phosphate. The formation of soluble copper species in sodium chloride solution at these potentials has been reported as $CuCl_2$ [29] and $Cu_2(OH)_3Cl$ [50]. The semicircle becomes more depressed at these potentials which is due to a combination of surface roughness as a result of the surface oxidation and blocking from copper oxides. Blocking feature can be shown by the appearance of a small inductive loop at LF [29]. However no Warburg impedance, Z_W is observed at these potential region, indicating a diffusion process of soluble copper species, which occur through the oxide layer as has been reported in many electrode surfaces such as copper alloy [29], stainless steel [36] and RuO_2 [37].

5.4.2 CO_2-saturated buffered phosphate solution

In general the same impedance responses were obtained for CO_2 compared to N_2-saturated solutions. The differences between them at particular potentials are only in the values of R_{ct} and C_{dl} values. CO_2-saturated solution within the potential region from –1.5 V to –1.0 V show larger HF semicircles compared to N_2-saturated solution (Figure 5.10). Moreover the HF semicircle in CO_2-saturated solution is dominant with a very weak LF Warburg impedance. This indicates that the adsorption of anions of hydroxide and phosphate (PO_4^{3-}) is less in extent for CO_2-saturated solution, thus less diffusion of these anions in the spectra is observed. In this potential region, processes such as the reduction of CO_2 to CO and other products, the adsorptions of CO as linearly bonded, CO_L and hydrogen evolution reaction are expected to occur. All these reactions occur *via* a charge transfer process in which a HF semicircle is expected.

In general the size of the HF semicircle increases in CO_2-saturated solutions compared to that N_2-saturated solution at the same potential except at –1.5 V where hydrogen evolution is enhanced at this potential in solution of CO_2. The adsorption of CO

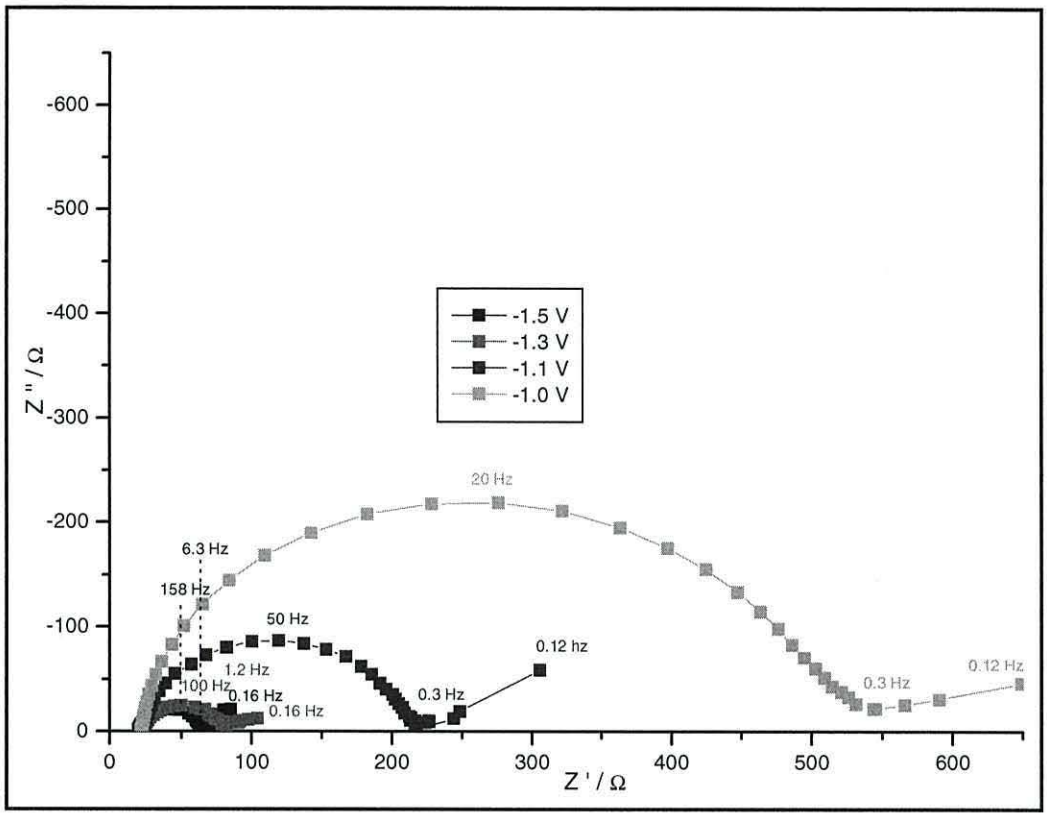

Figure 5.10: EIS of copper in CO_2-saturated buffered phosphate solution. Spectra shown from –1.5 V to –1.1 V in 0.2 V per step and at –1.0 V.

is expected to occur at this potential. However HER is enhanced as the solution pH is reduced by about 0.6 pH unit in CO_2-saturated solutions. A large semicircle observed at HF and a weak LF straight line, indicate that the charge-transfer resistance becomes dominant. At –1.1 V for example, the R_{ct} increases to 188 Ω from 65 Ω at –1.3 V. The EIS responses at –1.1 V in N_2 and CO_2 saturated solutions are shown in Figure 5.11 for comparison. Large increment of this value compared to the N_2-saturated solution (59.4 Ω) for the same potential at –1.1 V, might be due to the adsorption of CO. When the electrode was polarised for 15 min at –1.5 V, {CO_2 ($T_{15\ min}$)} prior the collection of EIS data, the semicircle is larger than when the potential was not held for any period of time. Again simple Randel equivalent circuit as in Figure 5.5 can model the responses in Figure 5.11. Table 5.5 shows the impedance values calculated from CO_2 saturated solution without and with electrode polarization, CO_2 ($T_{15\ min}$) for comparison (spectra not shown). The R_{ct} value of the polarised surface at –1.1 V increases to 568 Ω from 123 Ω at –1.3 V. This indicates that more adsorbates are present at the electrode surface as the electrode is polarised. The adsorption of CO occurs extensively as the electrode surface is polarised at high cathodic potential where more CO_2 is reduced to CO, and consequently CO adsorbed

as bridge-bonded CO, CO_B. This is in agreement with the *in situ* IR measurement as was discussed earlier in Chapter III.

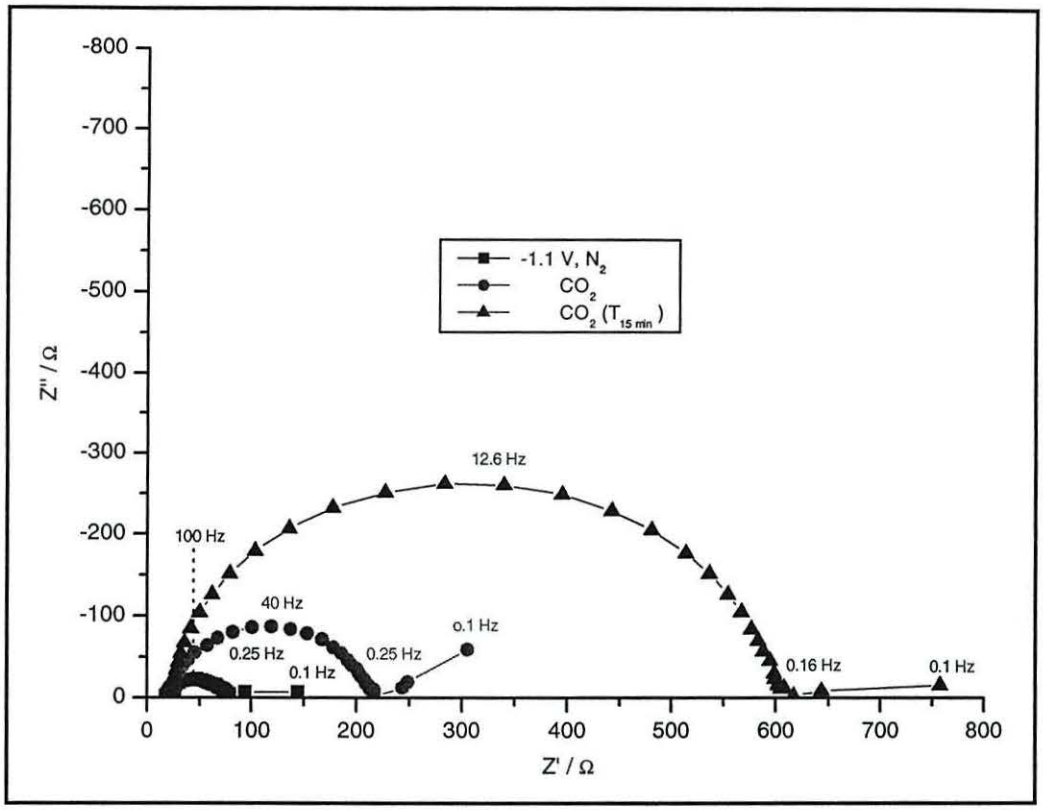

Figure 5.11: EIS response for N_2 and CO_2-saturated buffered phosphate solution at -1.1 V.

Potential / V	R_Ω / Ω		R_{ct} / Ω		C_{dl} / μF	
	CO_2	$CO_2(T_{15\,min})$	CO_2	$CO_2(T_{15\,min})$	CO_2	$CO_2(T_{15\,min})$
-1.5	20	22	46	43	35.6	31.1
-1.3	21	21	65	123	64.2	26.2
-1.1	20	21	188	568	28.2	22.9
-1.0	21	20	478	1530	24.0	21.6

Table 5.5: Impedance parameters values obtained from EIS spectra of CO_2-saturated solution of Figure 5.11 and for polarised surface (some spectra not shown)

As the potential is made less negative, the semicircle size increases and becomes depressed in shape as was observed in N_2-saturated solutions. The EIS response at potential region from –0.8 to –0.15 V is shown in Figure 5.12. The adsorption of specifically adsorbed anion on the electrode surface causes an increase in resistivity. The same observation is made on polarised surface electrodes with larger HF depressed semicircle (Figure 5.13). The R_{ct} values are generally higher for polarised surfaces due to

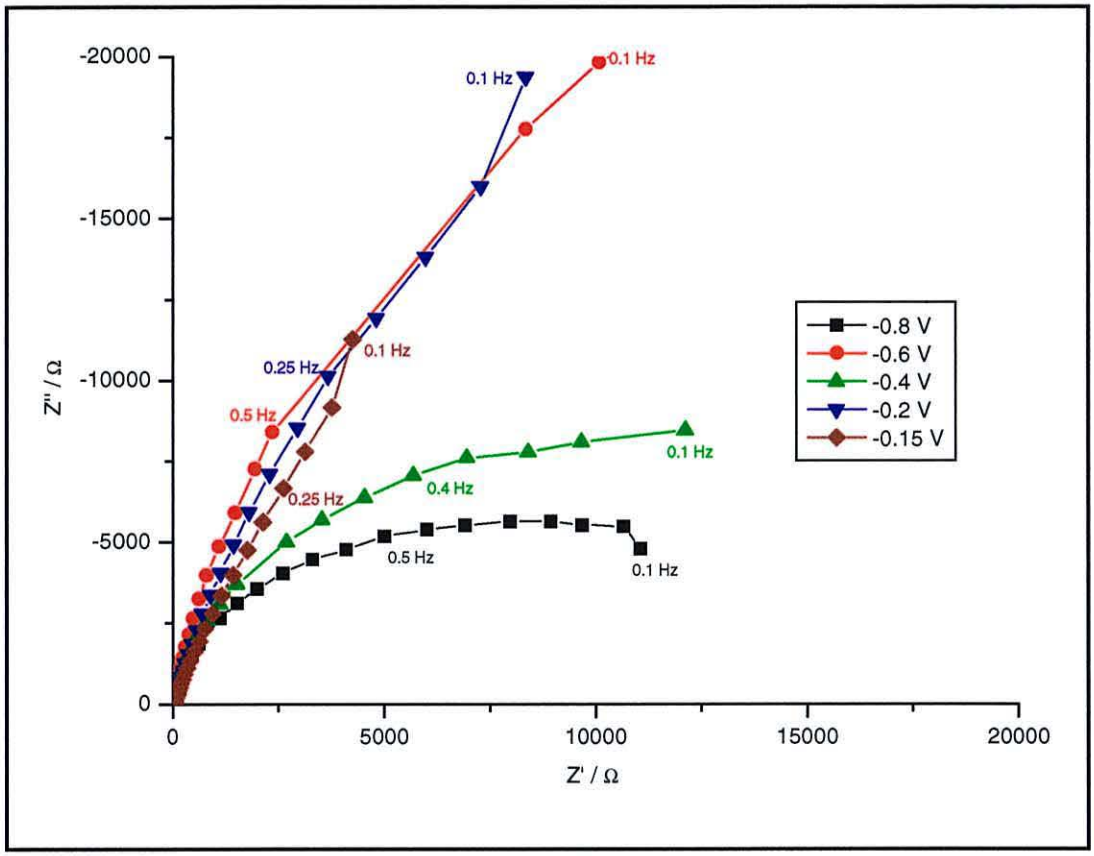

Figure 5.12: EIS of copper in CO_2-saturated buffered phosphate solution.

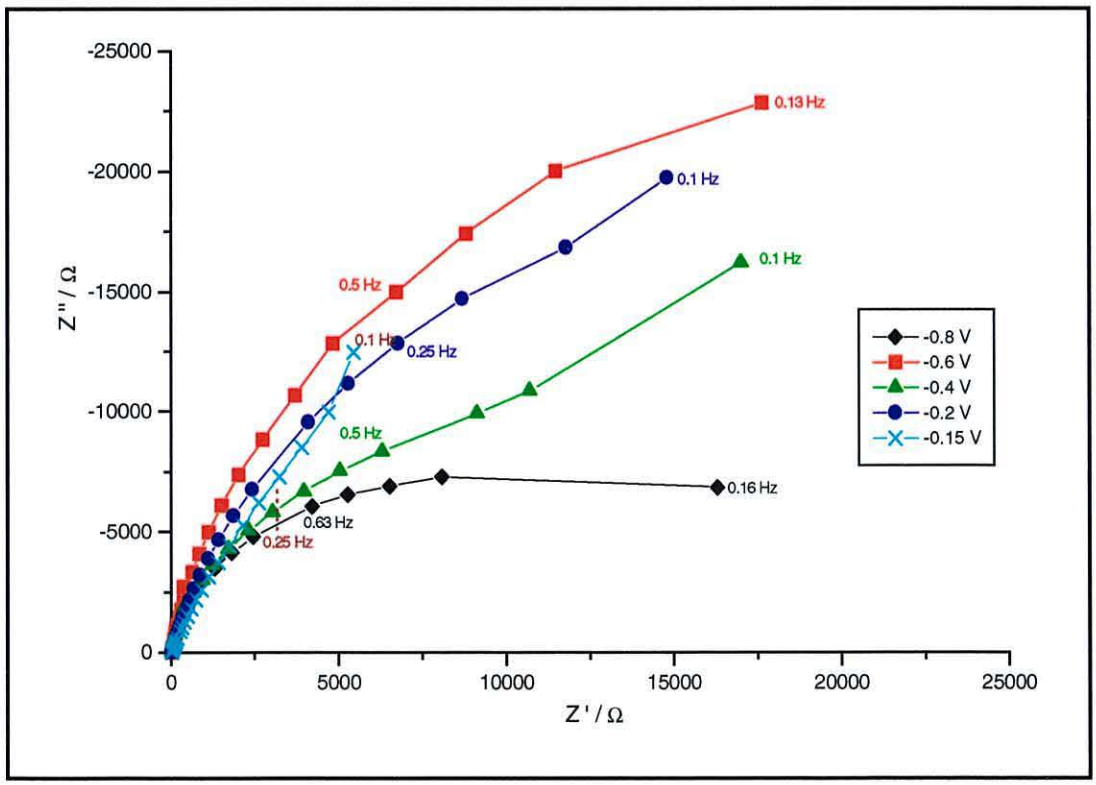

Figure 5.13: EIS of copper in CO_2-saturated buffered phosphate solution when the electrode was polarised at –1.5 V for 15 min prior to any measurement

the adsorption of CO on the electrode surface. The impedance values calculated from the Randal equivalent circuit are shown in Table 5.6 for comparison. It is worth noting that the dramatic change in resistivity in this region occurred at –0.6 V is observed for both N_2 and CO_2 saturated solutions, which may be due to hydroxide adsorption at the pzc.

Potential / V	R_Ω / Ω		R_{ct} / Ω		C_{dl} / μF	
	CO_2	$CO_2(T_{15\ min})$	CO_2	$CO_2(T_{15\ min})$	CO_2	$CO_2(T_{15\ min})$
-0.8	21	22	12630	15232	34.4	23.5
-0.6	20	21	54300	55900	36.1	29.2
-0.4	20	22	17400	19000	35.8	29.7
-0.2	20	23	63000	56500	47.2	57.6
-0.15	19	23	60400	54600	70.7	97.1

Table 5.6: The impedance values obtained from Figure 5.12 and Figure 5.13.

At more anodic potentials where the copper surface is oxidised, the impedance reduces while maintaining the depressed semicircle at high frequencies (Figure 5.14 and 5.15). Again the inductive loops are observed at LF at –0.05 and 0 V for both CO_2 solutions (electrode nonpolarised and polarised). It indicates that the blocking feature from oxidised copper still occurs.

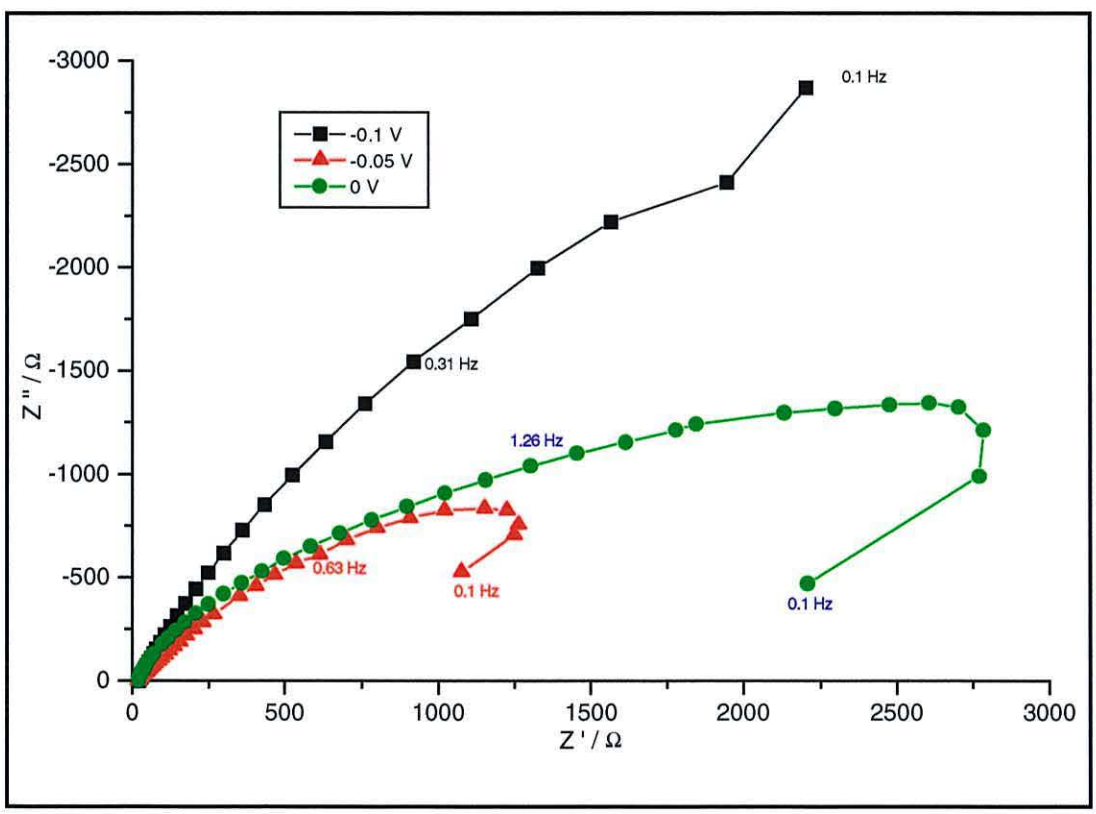

Figure 5.14: EIS of copper in CO_2-saturated buffered phosphate solution

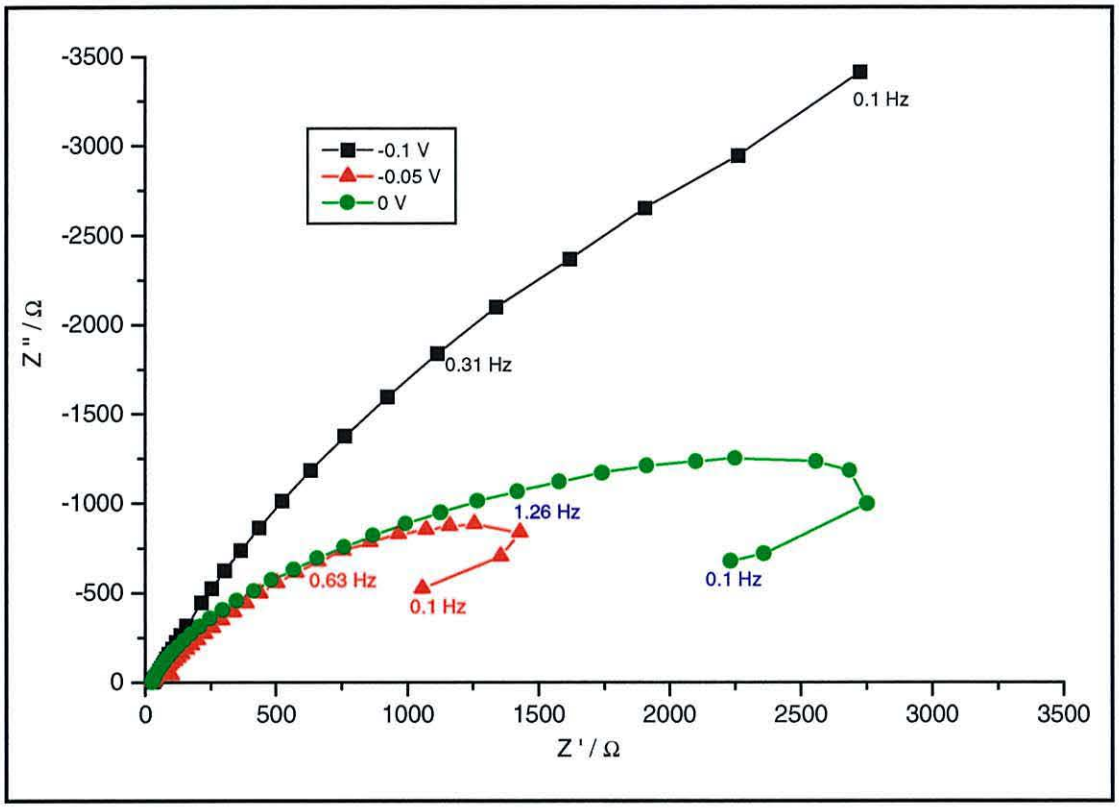

Figure 5.15: EIS of copper in CO_2-saturated buffered phosphate solution when the electrode was polarised at –1.5 V for 15 min prior to any measurement

The calculated impedance parameters obtained from Figure 5.14 and 5.15 are shown in Table 5.7.

Potential / V	R_Ω / Ω		R_{ct} / Ω		C_{dl} / μF	
	CO_2	$CO_2(T_{15\ min})$	CO_2	$CO_2(T_{15\ min})$	CO_2	$CO_2(T_{15\ min})$
-0.1	21	23	10500	14200	306	266
-0.05	18	22	3490	4360	343	340
0	19	21	3224	3346	66.2	75.6

Table 5.7: The impedance values obtained from Figure 5.14 and 5.15.

The R_{ct} exhibits the highest value at –0.2 and –0.15 V then reduces as the potential become more anodic. The C_{dl} on the other hand, exhibits highest value at 0.05 V and then reduce at 0 V. It seems that the blocking from oxidised copper, probably copper(I) species, increases at –0.2 to –0.15 V which is the potential where the optimum anodic peak appears in the voltammogram. As the potential is made more positive, copper(II) species is produced, the resistivity reduces while the conductivity increases.

5.4.3 CO-saturated buffered phosphate solution

The EIS response in CO-saturated phosphate buffered solution at high cathodic potentials, -1.1 V is shown in Figure 5.16. It shows only a HF semicircle. This indicates that the HER is depressed in CO-saturated solution as shown by the voltammogram in Figure 5.6. No LF impedance is observed. The response in Figure 5.16 can be modelled using equivalent circuit as in Figure 5.5. The analysis yields R_{ct} = 107 Ω and C_{dl} = 151 μF at –1.1 V and R_{ct} = 411 Ω and C_{dl} = 127 μF at –1.0 V. Higher R_{ct} and C_{dl} values at –1.1 V compared to N_2-saturated solution indicate that the adsorption of CO on the copper surface occurs in CO-saturated buffered phosphate solution. This is in agreement with the SNIFTIR spectra in Chapter IV. At –1.0 V, the impedance increases with R_{ct} about 4 times, whereas slight change in conductivity. This coincides with the potential when CO_B replaces CO_L. CO_B is more strongly bonded to the surface.

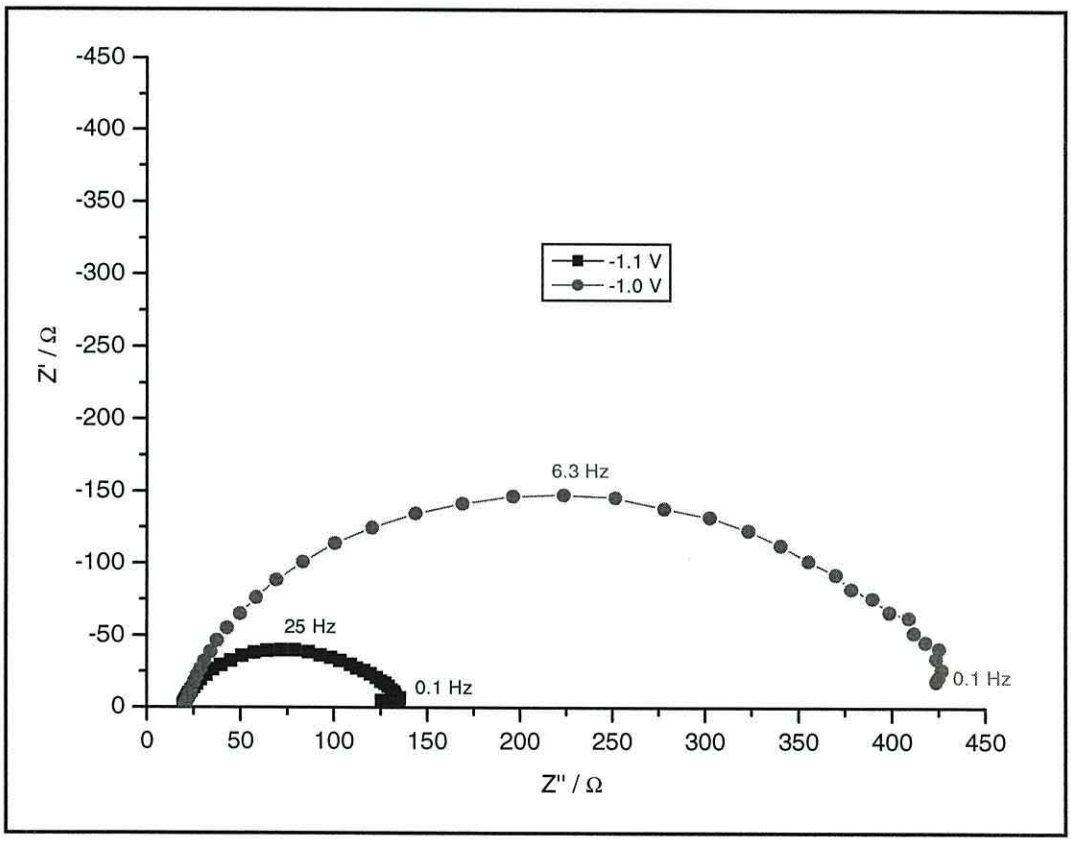

Figure 5.16: EIS of copper in CO-saturated buffered phosphate solution

As the potential is made less negative, the HF semicircle increases and becomes depressed in shape as expected as shown in Figure 5.17. The analysis using the same equivalent circuit yields impedance parameters as in Table 5.8.

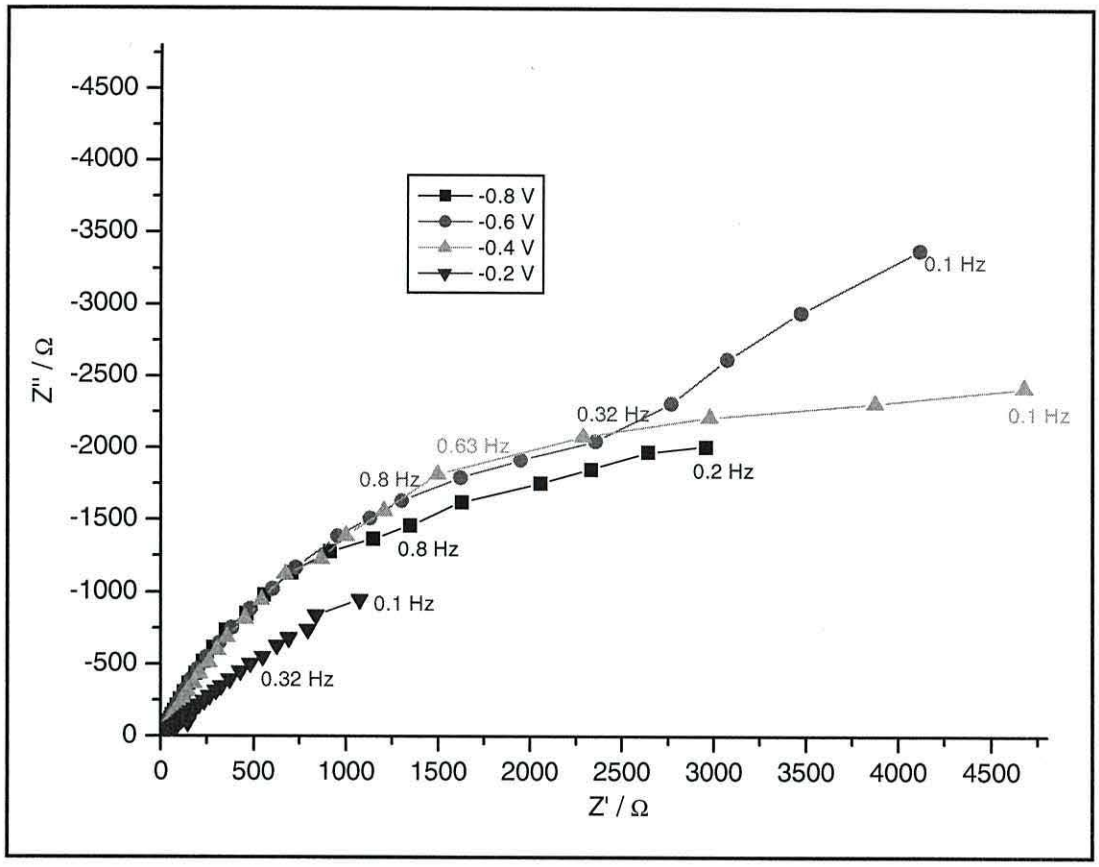

Figure 5.17: EIS of copper in CO-saturated buffered phosphate solution

Potential / V	R_{ct} / Ω	C_{dl} / μF
-0.8	4201.3	94.9
-0.6	5019.9	97.8
-0.4	6193.7	115.5
-0.2	6094.0	796.1

Table 5.8: The R_{ct} and C_{dl} estimated for EIS responses in Figure 5.17

As expected the highest R_{ct} values are observed in these potentials region where the adsorption of electrolyte anion occurs on the electrode surface. However the R_{ct} values are lower compared to N_2-saturated solution. It indicates that the adsorption of CO is competing with the specifically adsorbed anions. Indeed at –0.2 V, the impedance is near purely capacitive.

The EIS response at more anodic potentials is shown in Figure 5.18 where HF semicircle and LF impedance are clearly observed especially at –0.05 and 0 V. Therefore the response in Figure 5.18 can be modelled using equivalent circuit as in Figure 5.3 with incorporating the Warburg impedance.

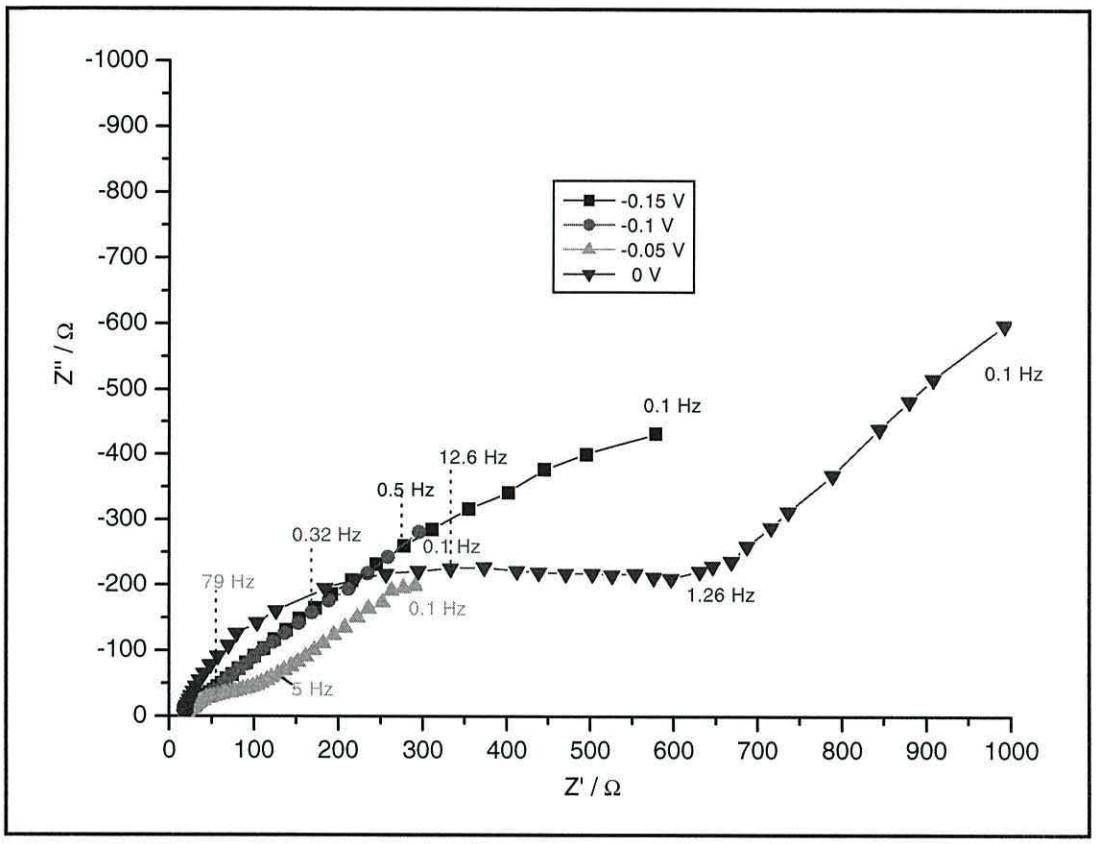

Figure 5.18: EIS of copper in CO-saturated buffered phosphate solution

The fitting analysis yields values R_{ct} = 2673.9 Ω and C_{dl} = 1.48 mF for –0.15 V and R_{ct} = 1244.5 Ω and C_{dl} = 3.17 mF at 0.1 V. The more anodic the potential is, the more Warburg impedance characteristic appears for –0.05 V and 0 V. The LF straight-line fitting yields pseudocapacitance, C_p = 3.35 mF and 3.75 mF and R_p = 5.76 Ω and 7.65 Ω for –0.05 V and 0 V respectively. The pseudocapacitance might rise from the diffusion of soluble copper(I)-carbonyl which has been shown to exist at these potential by infrared spectra studies. This is in agreement that the low frequency linear portion is generally related to a Nernst diffusion process of soluble or insoluble metal species to the bulk solution [47, 48]. HF semicircle, on the other hand, indicates the copper redox process where Cu(I) is oxidised to Cu(II) species.

5.4.4 Impedance behaviour of CO_2 reduction

Figure 5.19 shows plots of the calculated values for R_{ct} as a function of potentials for CO, N_2 and CO_2 saturated solutions. In addition it also contains values for CO_2 solution when the potential was polarised at –1.5 V for 15 min prior to data collection. The R_{ct} increases

from –0.8 V to –0.6 V and reduce back at –0.4 V. The R_{ct} value increases from 3.3 kΩ (-0.8 V) to 22.4 kΩ (-0.6 V) and reduces to 12.8 kΩ (-0.4 V) for N_2-saturated solution whereas the R_{ct} increases from 12.6 kΩ (-0.8 V) to 54.3 kΩ (-0.6 V) and reduces back to 17.4 kΩ (-0.4 V) for CO_2-saturated solution. The results indicate that another adsorbate layer is formed on the electrode surface at this potential which is close to the pzc for Cu [44]. The formation of oxide or hydroxide copper(I) is more likely to occur as shown by the very weak shoulder or anodic current on the CV at these potential range. This is consistent with the CV of copper in 0.1 mol dm^{-3} NaOH where the formation of oxide or hydroxide copper(I) has been reported [41, 42, 49, 50] at this potential region.

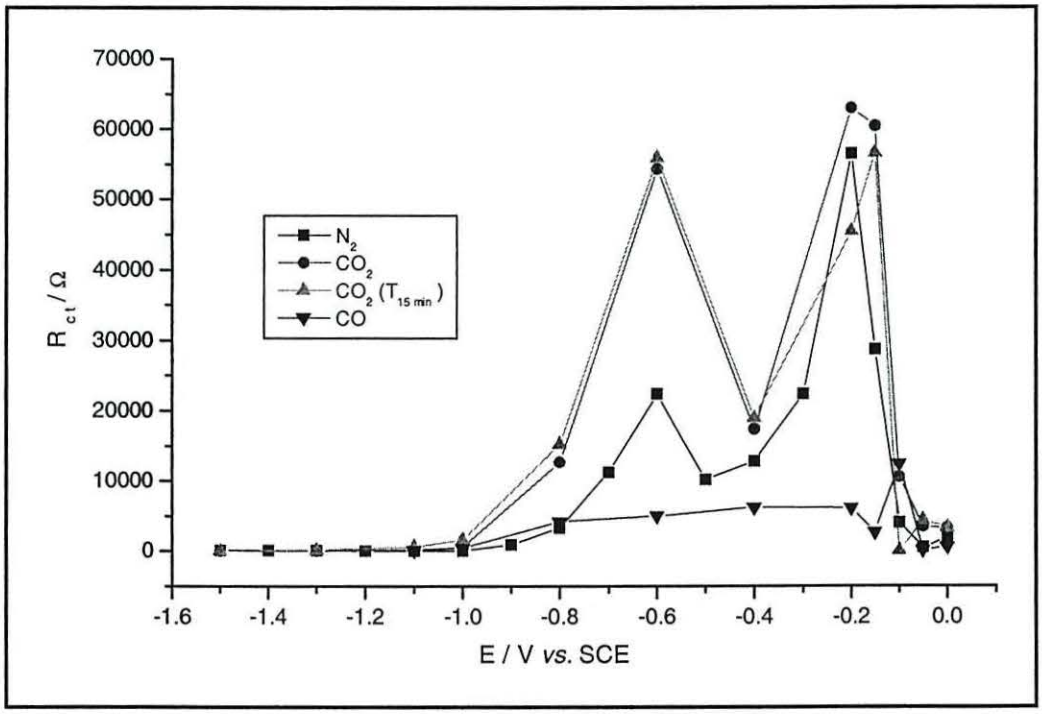

Figure 5.19: The R_{ct} value versus the applied potential

The high value of R_{ct} in CO_2 saturated solutions is brought about by an increase in the amount of HCO_3^- in the double layer. This is consistent with IR data which shows that CO_3^{2-} is converted to HCO_3^- in that potential range as shown in Figure 5.20. The assumption made here is that HCO_3^- is adsorbed at the surface. Unfortunately no evidence is provided by the IR data to confirm the presence of adsorbed HCO_3^-. The highest R_{ct} value is shown at –0.2 V with 56.5 kΩ (for N_2-saturated), at –0.2 V with 63.1 kΩ (for CO_2-saturated), at –0.15 V with 56.6 kΩ (for $CO_2(T_{15\ min})$) and at –0.1 V with 6.1 kΩ (for CO-saturated solution). At these potentials the surface is further oxidised to copper(I) and

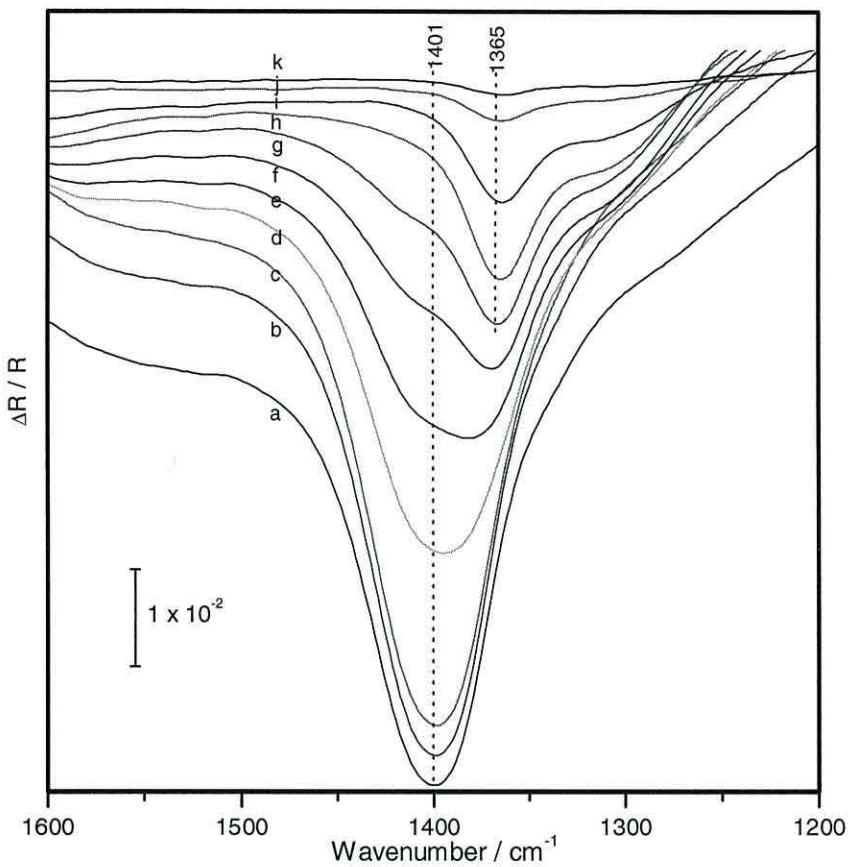

Figure 5.20: SNIFTIR spectra of CO_2-saturated buffered phosphate solutions. Spectra shown from (a) –1.5 V to (d) –0.9 V in 0.2 V increment, (e) –0.8 V to (g) –0.6 V in 0.1 V increment, (h) –0.4 to (j) 0 V in 0.2 V increment of forward sweep and (k) –0.2 V of reverse sweep. E_{ref}= -0.4 V of reverse sweep.

copper(II), thus the oxide film is further blocking the surface and in turn the resistivity of the surface increases. In the potential region III (–0.2 to 0 V), the impedance value decreases with low R_{ct} and higher capacitance, C_{dl} compared to the impedance values of potential at region II. It is interesting to note that the capacitance value becomes highest in these potentials region for all solution (Figure 5.21) where some of the oxide layer is removed from the surface due to the diffusion or deposition of soluble or insoluble copper(II) species, possibly through the formation of copper phosphate and diffusion of copper(I)carbonyl in CO saturated solution. This is in agreement with the literature where the formation of soluble copper(II) species at these potentials region has been reported [29]. Another possibility is that copper surface suffers from pitting process at anodic potential where the surface oxidation occurs at this potential [4, 29, 51].

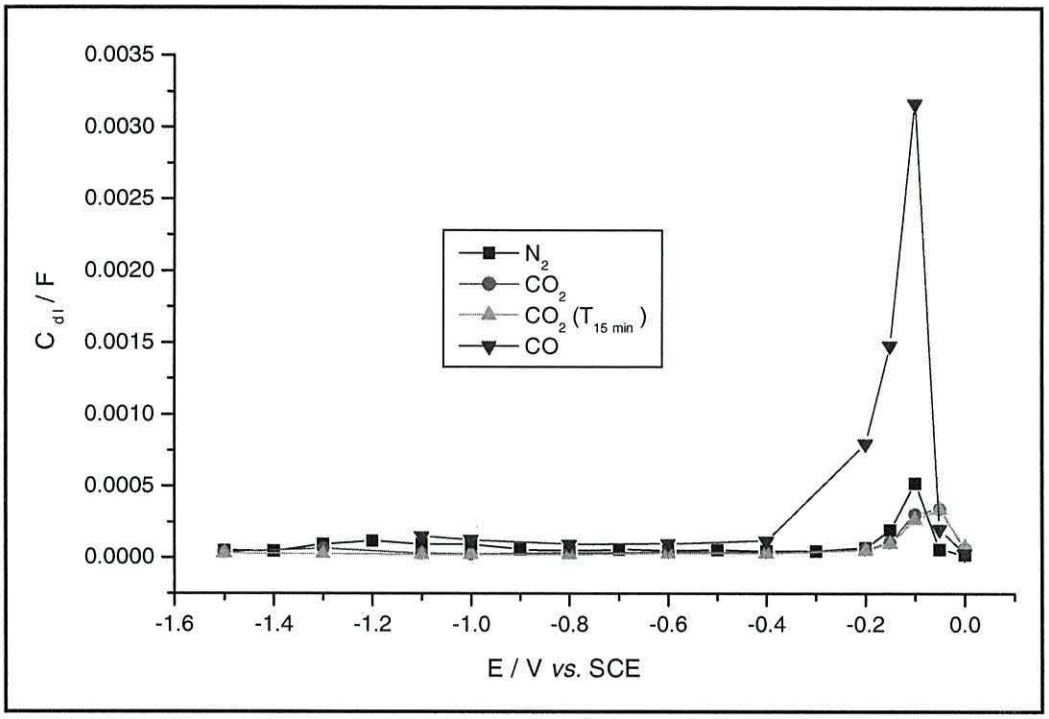

Figure 5.21: The C_{dl} values versus the applied potential

Figure 5.22 shows the scanning electron micrographs for the experiments after which the applied potential was stepped in from –1.5 V to 0 V. The figure shows (a) the deposition of insoluble copper species, (b) pitting at copper surface together with SEM EDAX spectrum of the photo for (c) clean surface and (d) surface with deposit substances. From the EDAX studies, the composition of deposited copper substances contain major elements of phosphorous, potassium and copper, might possibly for insoluble copper(II) potassium phosphate complex like species containing $CuKPO_4$, $CuK_2(HPO_4)_2$, or $Cu_2K_2(H_2PO_4)_4$. However the exact formula structure is not known at this stage. The presence of these deposits confirms the conclusions drawn from the appearance of the inductive loop at LF region as shown in Figure 5.14 and 5.15. As expected copper pitting occurs at more positive potential.

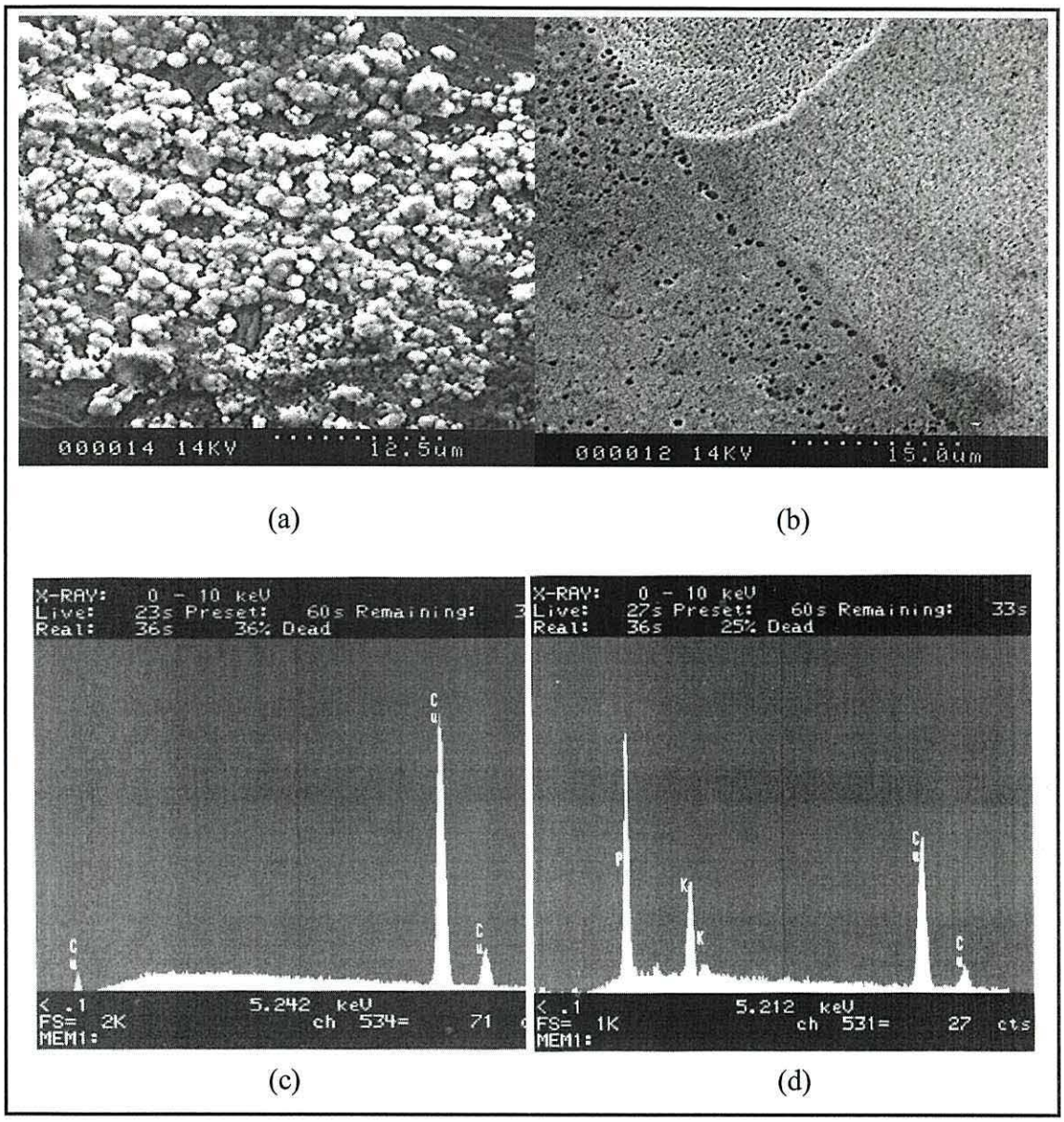

Figure 5.22: SEM micrographs of (a) deposited substance, (b) surface pitting. SEM EDAX of (c) the clean surface and (d) the deposited surface; after the potential was stepped in forward sweep from –1.5 V to 0 V.

5.5 Conclusion

The electrochemical reduction of CO_2 was investigated using electrochemical impedance spectroscopy. The impedance response of the CO_2-saturated solution with prolonged polarisation time shows higher impedance values at most potentials studies compared to CO_2-saturated solution without polarisation and N_2-saturated solutions. This indicates the adsorption of reduced-CO_2 such as adsorbed CO_L and CO_B on the polarised electrode surfaces in agreement with SNIFTIRS studies. It is also worth noting that CO-saturated

solution shows higher capacitance values compared to N_2- and CO_2-saturated solutions for most potentials studied except at more anodic potentials. It indicates that the adsorption of CO on the surface competes with the adsorption of electrolyte anions ($H_2PO_4^-$).

At high cathodic potentials, the adsorption of anions (OH^-, PO_4^{3-}, $H_2PO_4^-$) hampers CO adsorption. However by polarising the electrode, the anions adsorption is depressed. At anodic potentials, the impedance at N_2 and CO_2-saturated are low (high resistance and low capacitance) and high at CO-saturated solution with low resistance and high capacitance. It indicates that high blocking process from anions and oxides or hydroxides copper species occurs in both N_2 and CO_2-saturated solutions. Moreover the deposition of insoluble copper species in both solutions is observed. However this blocking process is depressed in CO-saturated solution. This is well in agreement with the fact that the interaction of CO with copper(I) occurred extensively at this potential region to form soluble copper(I)-carbonyl. C_{dl} is higher at these potentials (-0.3 V to –0.1 V) in CO-saturated solution with estimated values of 1.48 mF to 3.17 mF. This is further pronounced by the appearance of the low-frequency Warburg impedance at CO-saturated solution with estimated pseudocapacitance value about 3.74 mF at 0 V. At this potential region the Warburg impedance should be incorporated into the Randel equivalent circuit.

5.6 References

1 P.A. Christensen and M.A. Hamnett, "*Techniques and Mechanisms in Electrochemistry*", Blackie Academic, N.York (1994)

2 P. Ferloni, M. Mastragostini and L. Meneghello, *Electrochim. Acta*, 41 (1996) 27

3 V.A. Alves, L.A. da Silva and J.F.C. Boodts, *J. Appl. Electrochem.*, 28 (1998) 899

4 R. Buchheit, *J. Appl. Electrochem.*, 28 (1998) 503

5 M. M. Hukovic, R. Babic, Z. Grubac and S. Brinic, *J. Appl. Electrochem.*, 26 (1996) 443

6 A. El-Sayed, *J. Appl. Electrochem.*, 27 (1997) 193

7 K.Bandyopadhyay, K. Vijayamohann, G.S. Shekhawat and R.P. Gupta, *J. Electroanal. Chem.*, 447 (1998) 11

8 P. Friebe, P. Bogdanoff, N. A. Vante and H. Tributsch, *J. Catalysis*, 168 (1997) 374

9 C.M.A. Brett and A.M.O. Brett, "*Electrochemistry: Principal, methods and applications*", Oxford University Press, N. York, (1993)

10 R. Greef, R. Peat, L.M. Peter, D. Pletcher and J. Robinson, "*Instrumental Methods in Electrochemistry*", Elvis Horwood, N. York, (1990)

11 J. R. Macdonald (Ed.), "*Impedance Spectroscopy*", Wiley and Sons, N. York (1987)

12 D.E. Smith, *Electroanal. Chem.*, A.J. Bard, (Ed.), Dekker, N.York (1970)

13 M. Sluyters-Rehbach and J.H. Sluyters, *Electroanal. Chem.*, A.J. Bard, (Ed.), Dekker, N.York (1970)

14 C. Gabrielli, "*Identification of Electrochemical Processes by Frequency Response Analysis*", Solatron Instruments, Morris Bros. Ltd, UK. (1980)

15 A. Jimenez-Morales, J.C. Galvan, R. Rodriguez and J.J. de Damborenea, *J. Appl. Electrochem.,* 27 (1997) 550

16 J E B Randles, *Disc. Faraday Soc.,* 1 (1947) 11

17 P G Pickup and X Ren, *Faraday Trans.,* 89 (1993) 321

18 G. Williams, Ph.D thesis, University of Wales, Bangor (2000)

19 H.P. Argawal, "*Modern Aspects of Electrochemistry*", Plenum Press, N. York (1989)

20 T.Pajkossy, *J. Electroanal. Chem.,* 364 (1994) 111

21 B.W. Johnson, D.C. Read, P. Christensen, A. Hamnett and R.D. Armstrong, *J. Electroanal. Chem.,* 364 (1994) 103

22 G.J. Brug, A.L.G. van den Eeden, M. Sluyters-Rehabach and J.H. Sluyters, *J. Electroanal. Chem.,* 176 (1984) 275

23 J.R. Macdonald and D.R. Franceschetti, in "*Impedance Spectroscopy, Emphasing Solids Materials and Systems*", J.R. Macdonald, (Ed.), J. Wiley & Sons, New York (1987)

24 A. Sakharova, L. Nyikos and Y. Pleskov, *Electrochim. Acta*, 37 (1992) 973

25 U. Rammelt and G. Reinhard, *Electrochim. Acta*, 40 (1995) 505

26 M. J. Esplandiu, E.M. Patrito and V. A. Macagno, *J. Electroanal. Chem.,* 353 (1993) 161

27 M. J. Esplandiu, E.M. Patrito and V. A. Macagno, *Electrochim. Acta*, 40 (1995) 809

28 J. Bradwell and M.C.H McKubre, *Electrochim. Acta*, 36 (1991) 647

29 A.V. Benedetti, P.T.A. Sumodjo, K. Nobe, P.L. Cabot and W.G. Proud, *Electrochim. Acta*, 40 (1995) 2657

30 S. Magaino, *Electrochim. Acta*, 42 (1997) 377

31 C. Alemany, J.P. Diard, B.L. Gorrec and C. Montella, *Electrochim. Acta*, 41 (1996) 1483

32 A. Jardy, A.L.L Molin, M. Keddam and H. Takenoutt, *Electrochim. Acta*, 37 (1992) 2195

33 A. Nishikata, Y. Ichihara and T. Tsuru, *Electrochim. Acta*, 41 (1996) 1057

34 B.A. Boukamp, "*Equivalents Circuit*" (EQUIVRT – PAS), version 4.51, University of Twente (1989)

35 M. Drogowska, H. Menard, A. Lasia and L. Brossard, *J. Appl. Electrochem.,* 26 (1996) 1169

36 M. Saaken, P.J.vanDuin, A.C.P. Ligtuver and D. Schanel, *J. Power Source*, 47 (1993) 129

37 N. Spataru, J.G. LeHelloco and R. Durand, *J. Appl. Electrochem.,* 26 (1996) 397

38 T. Dobrev, C. Cachet and R. Wiart, *J. Appl. Electrochem.,* 28 (1998) 1195

39 X. Cheng, G. Li, E.A. Eneer, B. Vermaire, H.G. Parks and S. Raghavan, *J. Electrochem. Soc.,* 145 (1998) 352

40 S. Gudic, J. Radosevic and M. Kliskic, *J. Appl. Electrochem.,* 26 (1996) 1027

41 Y. Feng, W-K. Teo, K-S. Siow, Z. Gao, K.L. Tan and A-K. Hsieh, *J. Electrochem. Soc.*, 144 (1997) 55

42 Y. Feng, W-K. Teo, K-S. Siow, Z. Gao, K.L. Tan and A-K. Hsieh, *Corros. Sci.,* 38 (1996) 369

43 M.W. Hsiao, R.R. Adzic and E.B. Yeager, *J. Electrochem. Soc.,* 143 (1996) 759

44 Y.Hori, O. Koga, Y. Watanabe and T. Matsuo, *Electrochim. Acta*, 44 (1998) 1389

45 G.E. Cavigliasso, M.J. Esplandiu and V.A. Macagno, *J. Appl. Electrochem.,* 28 (1998) 1213

46 P.C. Searson and X.G. Zhang, *Electrochim. Acta*, 36 (1991) 499

47 C. Deslouis and B. Tribollet, *J. Appl. Electrochem.,* 16 (1988) 374

48 O.E. Barcia, O. R. Mattos, N. Pebere and T. Tribollet, *J. Electrochem. Soc.,* 140 (1993) 2825

49 J.C. Becerra, R.C. Salvarezz and A.J. Arvia, *Electrochim. Acta*, 33 (1988) 613

50 C.H. Pyun and S.M. Park, *J. Electrochem. Soc.,* 133 (1986) 2024

51 Y. Feng, W.K. Teo, K.S. Siong, K.L. Tan and A.K. Hsieh, *Corr. Sci.,* 38 (1996) 369

General conclusions and recommendations

It has been shown that the reduction of carbon dioxide on polycrystalline copper in both hydrogen carbonate and phosphate buffered solutions occurs when the electrode was polarised at high negative potentials for prolonged periods of time at neutral pH. The use of low pH solutions does not favour the CO_2 reduction since the pH of the solution predominantly controls the Cu surface condition and the competing reactions that may occur during the reduction process. Therefore the use of buffer solutions such as buffered phosphate solutions that can provide not only better pH control in the diffuse double layer condition, but also a source of protons without inducing the inconvenient formation of hydroxyl ions from the hydrolysis of water. It is known that hydroxyl ions are produced in most of the reduction reactions carried out at high negative potentials in aqueous solution; the removal of such pre-adsorbed ions is a key step before the reduction of CO_2 can be proceeds. One of the ways to achieve this is by the polarising the Cu electrode at a specific cathodic potential for prolonged periods of time. However, care must be taken to avoid further adsorption and accumulation of anions during the polarisation. An alternative way to increase the Faradaic efficiency of this process can be achieved by anodic pulse techniques. Furthermore the use of a flow cell is the best alternative method to overcome this problem by allowing the removal of the excess hydroxyl ions produced during HER process and anions which produced at potentials where the reduction of CO_2 occurs; both of which are competing processes.

At low θ_{CO}, reduced-CO_2 adsorbs in both linearly bonded, CO_L and bridge-bonded, CO_B where CO_L being the predominant species. However at high θ_{CO}, CO_B appears predominantly due to its thermodynamically stable structure. As the CO coverage increases by polarisation at higher negative E_{pol} and prolonged polarisation time, CO_L transforms to CO_B. Under the experimental conditions, CO_2 is electrochemically reduced in phosphate buffered solution at a wide pH range from 2.5 to 9.2 and a wide range of temperatures from 0 to 80 ^{0}C. CO_B exists with prolonged polarisation process and appears at wider potential range from -1.5 V to -0.1 V and is not affected by continuous CO_2 bubbling or N_2 purging process where the band intensity increases with high negative potential and polarisation time. On the other hand, CO_L appears immediately within

smaller potential range from -1.5 to -1.0 V and disappears with bubbling or N_2 purging process. It indicates that CO_B is thermodynamically stable compared to CO_L, probably exists as chemisorbed species on copper surface whereas CO_L is weakly adsorbed on the polycrystalline copper, possibly as physisorbed species. It is plausible to suggest from the results obtained that an intermediate reactive species involved in the CO_2 electrochemical reduction process is CO_L as an intermediate with short lifetime, which depresses HER at the potential where the reduction of CO_2 occurs whereas CO_B may be the product responsible for poisoning the electrode, thus reducing the efficiency of the reduction process.

The impedance response of the CO_2-saturated solution with prolonged polarisation time show higher impedance values at most potentials studied compared to CO_2-saturated solution without polarisation and N_2-saturated solutions. Furthermore the CO-saturated solution shows higher capacitance values compared to N_2- and CO_2-saturated solutions for most potentials studied except at more anodic potentials. It indicates that the adsorption of CO on the surface competes with the adsorption of pre-adsorbed hydroxides and electrolyte anions. This confirms that the adsorption of reduced-CO_2 either as CO_L or CO_B occurs on the polarised electrode surfaces and in agreement with SNIFTIRS studies.
At high negative potentials, the preadsorption of anions (OH^-, PO_4^{3-}, $H_2PO_4^-$) hampers CO adsorption. However by polarising the electrode, the anions adsorption is depressed and allows the adsorption of CO to take place. At anodic potentials, high blocking process from oxide copper and deposited copper species at N_2-and CO_2-saturated solution occurred and high rate of soluble copper diffusion at CO-saturated solution were observed. It is believed that a different anodic process occurs at different conditions, especially involved the reaction of reduced-CO_2 or CO with oxidised copper. This coincides with the fact that the interaction of CO with copper(I) occurs extensively at this potential region to form soluble copper(I)-carbonyl. Further phase formation at this potential region should be carried out by X-ray diffraction spectroscopy to gain further insight the electrocatalytic behaviour of oxidised copper.

As has been shown, copper is very sensitive to the environment in which it is used, and its treatment is of fundamental importance; a slight variation in its surface history and pre-treatment leads generally to unpredictable electrochemical behaviour. Much of the structure of the surface under the conditions employed during the present work remains the object of active research by many groups. Thus studies employing others techniques such as the Electrochemical Quartz Micro-Balance, Raman spectroscopy, X-ray spectroscopy,

Electron Energy Loss spectroscopy and a surface probe microscopy techniques, along with the use of the single crystal electrodes should be performed in order to gain more insight the details of the polycrystalline structure and its interaction with supporting electrolyte and the electroactive species produced during the reduction of CO_2.

The use of SNIFTIRS and electrochemical impedance for the study of the reduction of CO_2 in the present condition has successfully allowed the acquisition of useful information about the processes occurring in the diffuse double layer and at the surface of the electrode during the reduction of CO_2 process. However the interferences caused by strong absorbance of the supporting electrolyte and water must be reduced in order to inquire more information buried underneath. This can be achieved by improvement of the acquisition method such as time resolved spectra and by using novel interpretation of algorithms and data treatment such as two dimensional infrared correlation methods.